THESES

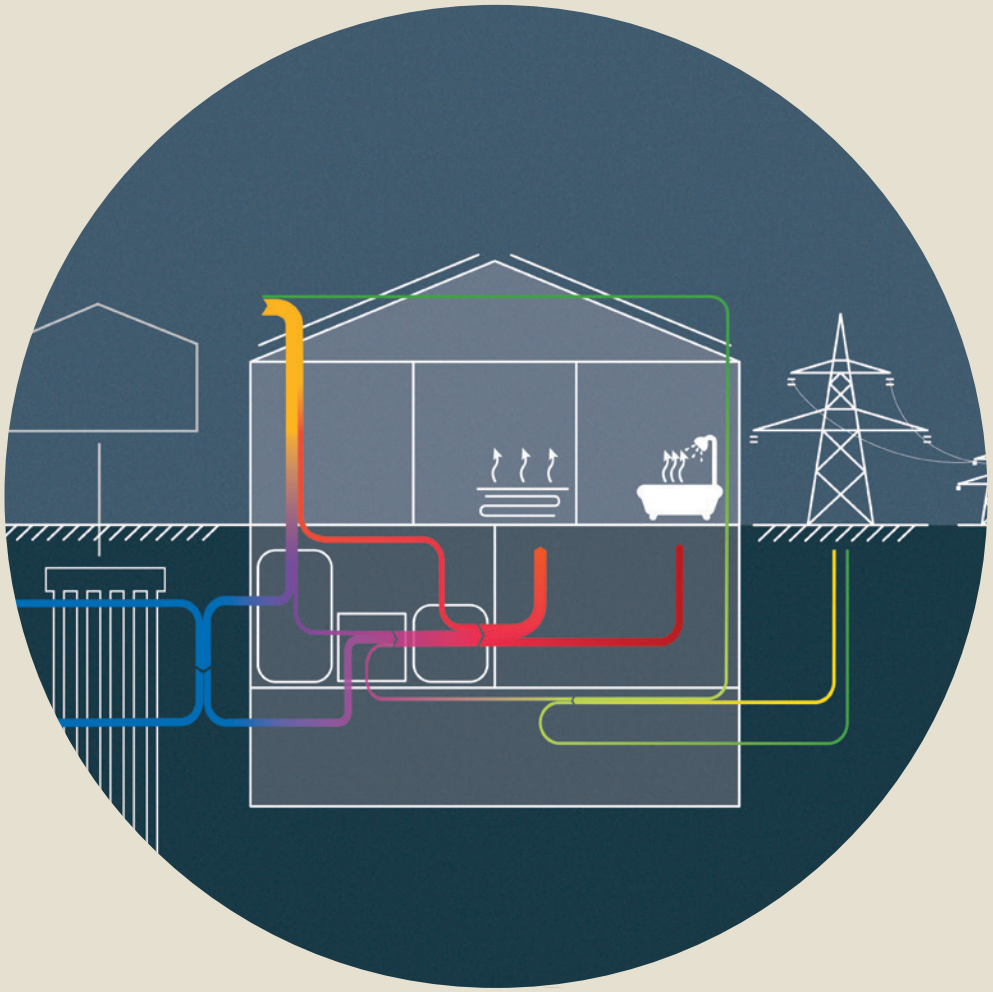

Mechanical Engineering

Karl Martin Heissler

5th Generation District Heating Networks

Potentials for Reducing CO_2-Emissions and Increasing the Share of Renewable Energies in Residential Districts

TUM.University Press

Munich School of Engineering
Technical University of Munich

5th Generation District Heating Networks

Potentials for Reducing CO_2-Emissions and Increasing the Share of Renewable Energies in Residential Districts

Karl Martin Heißler

Vollständiger Abdruck der von der Munich School of Engineering der Technischen Universität München zur Erlangung des akademischen Grades eines Doktor-Ingenieurs (Dr.-Ing.) genehmigten Dissertation.

Vorsitzender:

Prof. Dr.-Ing. Frank Petzold

Prüfer der Dissertation:

1. Prof. Dipl.-Ing. Thomas Auer
2. Prof. Dr.-Ing. Werner Lang

Die Dissertation wurde am 16.11.2020 bei der Technischen Universität München eingereicht und durch die Munich School of Engineering am 04.05.2021 angenommen.

The German National Library has registered this publication in the German National Bibliography. Detailed bibliographic data are available on the Internet at https://portal.dnb.de.

Imprint

1. Edition

Layout design and typesetting: Karl Martin Heissler
Cover design: Caroline Ennemoser
Cover illustration: Karl Martin Heissler, edited by Caroline Ennemoser

TUM.University Press
Technical University of Munich
Arcisstrasse 21
80333 Munich

DOI: 10.14459/2021md1577768
ISBN printed edition: 978-3-95884-071-3

www.tum.de

Für meine Familie
Für Dorothee

Abstract

State-of-the-art district heating networks operate at temperature levels well above ambient temperature. The main trends of recent years towards more efficient district heating networks are a reduction in flow temperatures, minimization of heat losses and increased input of renewable heat into the networks. For these measures networks at very low temperature levels offer significant advantages: the low temperature difference to the surroundings reduces thermal losses and the network in combination with a seasonal storage is able to absorb, shift, and store low-temperature renewable heat or waste heat within a district.

This work investigates the viability and the energy efficiency potentials of a district heating network at very low temperature levels. A district with urban density in Munich, Germany, serves as example. For the investigation a thermo-hydraulic grid model is developed, which connects different building models to a district-wide co-simulation model. The simulation model of a traditional district heating network serves as a reference.

Focus of the investigation is the influence of different demand scenarios, network typologies, heat densities and heat sources on network performance and district emissions, supplemented by an economic analysis of selected network typologies.

The simulation results show a large potential for reducing fossil energy demand: to supply the same quarter, the district heating network at very low temperature levels requires 11% of the non-renewable primary energy required by the traditional district heating network. In addition, thermal losses are reduced to 45% and CO_2 emissions to 31% of the emissions of the traditional network.

This demonstrates the effects of a successful integration of renewable energies into a local heating supply and illustrates the positive impact of a local use of solar and waste heat sources on the performance, energy demand and emissions of the network. In combination with a reduction in demand, district heating networks at very low temperature levels can make a valuable contribution to global efforts to reduce CO_2 emissions and energy demand.

Kurzfassung

Heutige Fernwärmenetze arbeiten mit Temperaturen die deutlich über der Umgebungstemperatur liegen. Haupttrends der letzten Jahre hin zu effizienteren Fernwärmenetzen sind eine Absenkung der Vorlauftemperaturen, eine Verringerung der Wärmeverluste und ein verstärktes Einspeisen erneuerbarer Wärme in die Netze. Hierfür bieten Wärmenetze auf sehr niedrigem Temperaturniveau erhebliche Vorteile: die geringe Temperaturdifferenz zur Umgebung reduziert die Wärmeverluste und das Wärmenetz ermöglicht in Kombination mit einem saisonalen Speicher, erneuerbare Niedertemperaturwärme oder Abwärme aufzunehmen, zu verschieben und zu speichern.

Diese Arbeit untersucht die Machbarkeit und die Energieeffizienzpotenziale eines Wärmenetzes auf sehr niedrigem Temperaturniveau exemplarisch für ein Wohnquartier mit städtischer Dichte in München. Für die Untersuchung wird ein thermohydraulisches Netzmodell entwickelt das verschiedene Gebäudemodelle zu einem quartiersweiten Co-Simulationsmodell verbindet. Als Referenz dient ein Simulationsmodell eines traditionellen Fernwärmenetzes.

Im Mittelpunkt der Untersuchung steht der Einfluss verschiedener Nachfrageszenarien, Netztypologien, Wärmedichten und Wärmequellen auf die Leistung des Netzes und die Emissionen des Quartiers, ergänzt durch eine Wirtschaftlichkeitsanalyse ausgewählter Netztypologien.

Die Simulationsergebnisse zeigen ein großes Potenzial zur Verringerung des fossilen Energiebedarfs: für die Versorgung desselben Quartiers benötigt das Wärmenetz mit sehr niedrigem Temperaturniveau 11% der nicht erneuerbaren Primärenergie, die für das traditionelle Fernwärmenetz erforderlich ist. Außerdem werden die Wärmeverluste auf 45% der Verluste des traditionellen Netzes und die CO_2-Emissionen auf nur 31% der Emissionen des traditionellen Netzes reduziert.

Dies demonstriert die Auswirkungen einer erfolgreichen Integration erneuerbarer Energien in die Nahwärmeversorgung und verdeutlicht die positiven Effekte einer lokalen Nutzung von Solar- und Abwärmequellen auf Leistung, Energiebedarf und Emissionen des Wärmenetzes. In Kombination mit einer Verringerung der Nachfrage können Wärmenetze auf sehr niedrigem Temperaturniveau einen wertvollen Beitrag zu den globalen Bemühungen der Verringerung von CO_2-Emissionen und Energiebedarf leisten.

Table of Contents

List of Abbreviations

5GDHCN	5th Generation District Heating and Cooling Network
Abs	Section (Absatz)
BCVTB	Building Controls Virtual Test Bed
BEHG	Fuel Emission Trading Act (Brennstoffemissionshandelsgesetz)
BSD Socket	Berkeley Software Distribution Socket
BSI	Building Simulation Interface
BSM	Building Services Model
CO_2	Carbon Dioxide
COP	Coefficient of Performance
DH	District Heating
DHN	District Heating Network
DHW	Domestic Hot Water
DIW	German Institute for Economic Research
EEWärmeG	Renewable Energies Heating Act (Erneuerbare-Energien-Wärmegesetz)
FAR	Floor Area Ratio
GEA	German Environment Agency (Umweltbundesamt)
GFG	German Federal Government
HVAC	Heating, Ventilation and Air Conditioning
HW	Heating Water
IDA ICE	IDA Indoor Climate and Energy
IF	Insulation Factor
IWEC	International Weather for Energy Calculations

KSG	Federal Climate Protection Act (Klimaschutzgesetz)
LTDHN	Low Temperature District Heating Network
MCC	Mercator Research Institute on Global Commons and Climate Change
MFH	Multi Family House
Mio.	Million
MWh	Megawatt Hour
NLD	Networks with Large Pipe Diameter
NSD	Networks with Small Pipe Diameter
NSF	Network Scaling Factor
NSM	Network and Storage Model
PIK	Potsdam Institute for Climate Impact Research
PSF	Pipe Scaling Factor
PV	Photovoltaic
PVT	Photovoltaic-thermal
SFH	Single Family House
STN	Solar-thermal Network
TCP/IP	Transmission Control Protocol/Internet Protocol
TE	Total Energy
TS	Temperature Sensor
TWh	Terawatt Hour
ULTDHN	Ultra-low Temperature District Heating Network
VAT	Value Added Tax
WHN	Waste Heat Network
WSHP	Water Source Heat Pump

List of Symbols

Latin Symbols

Symbol	Description	Unit
A_N	Annuity of the Total Annual Payments	€/a
$A_{N,B}$	Annuity of Operation-Related Costs	€/a
$A_{N,E}$	Annuity of Proceeds	€/a
$A_{N,K}$	Annuity of Capital Costs	€/a
$A_{N,S}$	Annuity of Miscellaneous Costs	€/a
$A_{N,V}$	Annuity of Demand-Related Costs	€/a
ANF	Annuity Factor	1/a
b_B	Price-Dynamic Cash Value Factor for Operation-Related Costs	-
b_E	Price-Dynamic Cash Value Factor for Proceeds	-
b_I	Price-Dynamic Cash Value Factor for Maintenance costs	-
b_k	Price-Dynamic Cash Value Factor for Capital Costs	-
b_S	Price-Dynamic Cash Value Factor for Miscellaneous Costs	-
b_v	Price-Dynamic Cash Value Factor for Demand-Related Costs	-
c_{ground}	Specific Heat Capacity of the Ground	kJ/kg.K
c_{H_2O}	Specific Heat Capacity of Water	kJ/kg.K
E_{sol}	Total Solar Input	kJ; MWh
K_{WG}	Minimum Cost of Heat Production for the Observation Period	€
l_{net}	Network Length	m
m	Mass	t; kg
m_{dot}	Mass Flow	kg/s
m_{dot_actual}	Actual Mass Flow	kg/s
$m_{dot\_actual\_byp}$	Actual Bypass Mass Flow	kg/s

m_{dot_DHW}	Domestic Hot Water Load Mass Flow	kg/s
m_{dot_HW}	Heating Water Load Mass Flow	kg/s
m_{dot_set}	Set Value of Mass Flow	kg/s
$m_{dot\_set\_cold}$	Set Value of Mass Flow Cold	kg/s
$m_{dot\_set\_warm}$	Set Value of Mass Flow Warm	kg/s
$P_{el\_pump\_1}$	Electric Power Pump 1	W
$P_{el\_pump\_2}$	Electric Power Pump 2	W
q	Interest Rate Factor	-
q_{net}	Heat-load Density	kWh/m.a
Q_{DHN}	Heat Input in the District Heating Network	kJ; MWh
Q_{DHW}	Domestic Hot Water Heat Demand	kJ; MWh
Q_{dot_DHW}	Domestic Hot Water Heat Load	kJ; MWh
Q_{dot_HW}	Heating Water Heat Load	kJ; MWh
Q_{el}	Heat from Electricity Demand W_{el}	kJ; MWh
Q_{HP}	Low Thermal Heat for Heat Pump Operation	kJ; MWh
Q_{HP_tot}	Total Heat Output of the Heat Pump	kJ; MWh
Q_{HW}	Heating Water Heat Demand	kJ; MWh
Q_{loss}	Total Energy Loss	kJ; MWh
Q_{loss_calc}	Calculatory Energy Loss	kJ; MWh
Q_{loss_net}	Thermal Energy Loss of the Network	kJ; MWh
Q_{loss_stor}	Thermal Energy Loss of the Storage	kJ; MWh
Q_{net_c}	Heat Transferred into 5GDHCN	kJ; MWh
Q_{net_h}	Heat Transferred from 5GDHCN	kJ; MWh
Q_{NRE}	Renewable Energy	kJ; MWh
Q_{RE}	Non-Renewable Energy	kJ; MWh
Q_{ST}	Total Solar-thermal Heat Gains	kJ; MWh
Q_{ST_dir}	Direct Solar-thermal Heat Gains	kJ; MWh

$Q_{ST\_dir\_exp}$	Expected Direct Solar-thermal Heat Gains	kJ; MWh
Q_{ST_indir}	Indirect Solar-thermal Heat Gains	kJ; MWh
$Q_{ST\_indir\_exp}$	Expected Indirect Solar-thermal Heat Gains	kJ; MWh
$Q_{ST\_indir\_HP}$	Indirect Solar-thermal Heat Gains used locally by Heat Pump	kJ; MWh
Q_{total}	System-Wide Heat Input, Sum of Q_{ST} and Q_{waste}	kJ; MWh
$Q_{transported}$	Heat Transported, Sum of Q_{net_h} and Q_{net_c}	kJ; MWh
Q_{use}	Useful Energy, Sum of Q_{HW} and Q_{DHW}	kJ; MWh
Q_{w}	Annual Heat Demand	kJ; MWh
Q_{waste}	Total Waste Heat Input	kJ; MWh
t	Observation Period	a
T	Temperature	°C;K
T_{12_c}	Temperature of Building 12 Cold Line	°C
T_{12_c24}	Temperature of Building 12 Cold Line 24 Hour Moving Average	°C
T_{12_h}	Temperature of Building 12 Hot Line	°C
T_{12_h24}	Temperature of Building 12 Hot Line 24 Hour Moving Average	°C
T_{a}	Outer Pipe Wall Temperature	°C
T_{flow_cold}	Flow Temperature Cold	°C
T_{flow_warm}	Flow Temperature Warm	°C
T_{fluid}	Fluid Temperature	°C
T_{ground}	Ground Temperature	°C
T_{i}	Inner Pipe Wall Temperature	°C
T_{m}	Average Monthly Ground Temperature	°C
T_{main}	Water Main Temperature	°C
T_{max}	Maximum Temperature	°C
T_{mean}	Mean Temperature	°C
T_{min}	Minimum Temperature	°C
T_{net_c}	Network Temperature Cold Line	°C

T_{net_c24}	Network Temperature Cold Line 24 Hour Moving Average	°C
T_{net_h}	Network Temperature Hot Line	°C
T_{net_h24}	Network Temperature Hot Line 24 Hour Moving Average	°C
T_{return}	Return Temperature	°C
T_{set}	Set Temperature	°C
T_{tap}	Domestic Hot Water Set Temperature	°C
V_{mov}	Total Volume of Fluid Transported	m^3
W_{aux}	Auxiliary Heater Electric Energy Demand	kJ; MWh
W_{DHW}	Domestic Hot Water Heating Electric Energy Demand	kJ; MWh
W_{el}	Total Electric Energy Demand	kJ; MWh
W_{grid}	Electric Energy obtained from Public Distribution Network	kJ; MWh
W_{HP}	Heat Pump Electric Energy Demand	kJ; MWh
W_{pump}	Electric Pump Energy Demand	kJ; MWh
$W_{pump\_c\_h}$	Pump Energy Demand for Pump Direction form Cold to Hot	kJ; MWh
$W_{pump\_h\_c}$	Pump Energy Demand for Pump Direction form Hot to Cold	kJ; MWh
W_{pump_red}	Pump Energy Reduction Potential	kJ; MWh
W_{PV_gain}	Photovoltaic Energy Gains	kJ; MWh
W_{PV_grid}	Excess Photovoltaic Energy fed into Public Distribution Network	kJ; MWh
W_{PV_use}	Photovoltaic Energy Gains Locally Used	kJ; MWh
y_{byp}	Control Value of Bypass	-
y_{dir}	Control Value of Direction of Flow	-
y_{set}	Control Value of Mass Flow	-

Greek Symbols

Symbol	Description	Unit
ΔT	Temperature Difference	K
ΔT_{cum}	Cumulative Temperature Difference	K
ΔT_{DHW}	Domestic Hot Water Temperature Difference	K
ΔT_{HW}	Heating Water Temperature Difference	K
λ_{ground}	Thermal Conductivity of the Ground	W/m.K
$\lambda_{insulation}$	Thermal Conductivity of the Insulation	W/m.K

1. Introduction

Humankind's effect on the balance of greenhouse gases within the earth's atmosphere is drastic and the resulting man-made global warming is accelerating. With the Paris Agreement of 2015, 195 nations have agreed upon and ratified contractually binding obligations to keep the increase of man-made global warming below 2°C, if possible below 1.5°C in relation to pre-industrial levels (United Nations 2015).

To comply with the contractual obligations of the Paris Agreement, the government of the Federal Republic of Germany agreed in their Climate Action Plan 2050 on the reduction of Carbon Dioxide (CO_2) emissions in 6 different sectors. In the Building sector the aim is to reduce the emissions of CO_2-equivalents from 209 Mio. t CO_2-equivalents in 1990 to 70 to 72 Mio. t CO_2-equivalent in 2030. In the Energy Industry sector the aim is to reduce the emissions of CO_2 equivalents from 466 Mio. t CO_2-equivalents in 1990 to 175 to 183 Mio. t CO_2-equivalent in 2030. Combined, these two reduction goals equal reductions in CO_2 emissions until 2030 of up to 62% in relation to the 1990 values. (BMU 2016)

In the Climate Action Programme 2030, which is part of the strategy to meet the targets of the Climate Action Plan 2050, the government of the Federal Republic of Germany among other measures describes its goals to set a CO_2 price, to subsidise energy-saving measures in building refurbishment, to subsidise e-mobility and to reduce value added tax (VAT) on public transport (Bundesregierung 2019).

To meet these goals the Federal Climate Protection Act (KSG) and the Fuel Emission Trading Act (BEHG) have been passed by German parliament in 2019. The latter sets the legal framework for a national emissions trading system to price fossil greenhouse gas emissions (§ 1 BEHG). The former sets the reduction goal of greenhouse gas emissions to 55% in 2030 in relation to the 1990 values (§3 Abs. 1 KSG) and defines the six sectors of the Climate Action Plan 2050, with the Building and Energy Industry sectors among them, as the sectors of greenhouse gas emission reduction (§ 4 Abs. 1 KSG).

One means of reducing greenhouse gas emissions in the Building and Energy Industry sectors, as set by § 4 Abs. 1 KSG, is the reduction of the combustion of fuels through the reduction of heat demand, system losses, or alternative energy systems not based on fuel combustion. One fourth of the end energy consumption (651 TWh) in Germany

is caused by private households of which 84% are used for domestic heat supply, with 69% for heating water (HW) and 15% for domestic hot water (DHW) production, mainly provided through the combustion of natural gas or mineral oil (Umweltbundesamt 2018). Consequently the urban quarter, where many different building types are supplied by various energy systems delivering heat, electricity, natural gas or a combination of the aforementioned, is a field with great reduction potential.

Historically houses are heated by fossil fuels, which when combusted, provide heat and combustion products. Local combustion, however, can be inefficient and dangerous and produces significantly more atmospheric pollution than a centralised, controlled combustion environment. A trend which potentially saves fuel and increases user comfort and safety is to reduce combustion-based heating in urban areas and supply the heat to the users via a district heating network (DHN) from a central combustion plant. (Lund et al. 2014)

However, most heat sources of DHNs in operation today are still combustion-based, resulting in large amounts of greenhouse gas emissions for heat production. For 2017 the heat supply of DHNs in Germany was produced to 47% by the combustion of natural gas, 28% by the combustion of hard coal and lignite, 14% by the combustion of waste, 7% by renewable, and 4% by other fossil sources (Destatis 2018). At the same time, especially in dense urban areas, large amounts of heat are discarded into the environment via air conditioning and cooling processes with great effort and energy input.

This available waste heat, heat from solar irradiation, and ambient heat could be recycled and reused for heating, rendering the additional combustion of fossil fuels redundant. Therefore the idea of this work is to investigate the greenhouse gas reduction potential of a heat supply system for urban quarters, not based on combustion, and examine its ecological, technological and economic limitations.

1.1. District Heating

The idea of centrally heating a fluid, distributing it and using it to supply the surrounding buildings for heating and DHW can be traced back to Roman times. In Pompeii open trenches served as supply lines for hot water distribution to houses and baths. As early as the 14th century, wooden pipes were used in Chaudes Aigues, France, to distribute geothermal heat to individual houses by laterals branching off from one main line. (Bloomquist 2001)

Several centuries later between 1880 and 1930, steam-based district heating (DH) systems were installed in the US and Europe as well, which were succeeded until the 1970s by the second generation of district heating systems based on hot pressurized water above 100 °C (Figure 1-1). Further improving system efficiency, a third generation of DH systems, also based on pressurized water, but below 100 °C, was implemented from the 1970s on. The historic trend of continuously decreasing temperatures still continued and led to the fourth generation of DH with networks at supply temperature levels of 50 °C to 60 °C. (Lund et al. 2014)

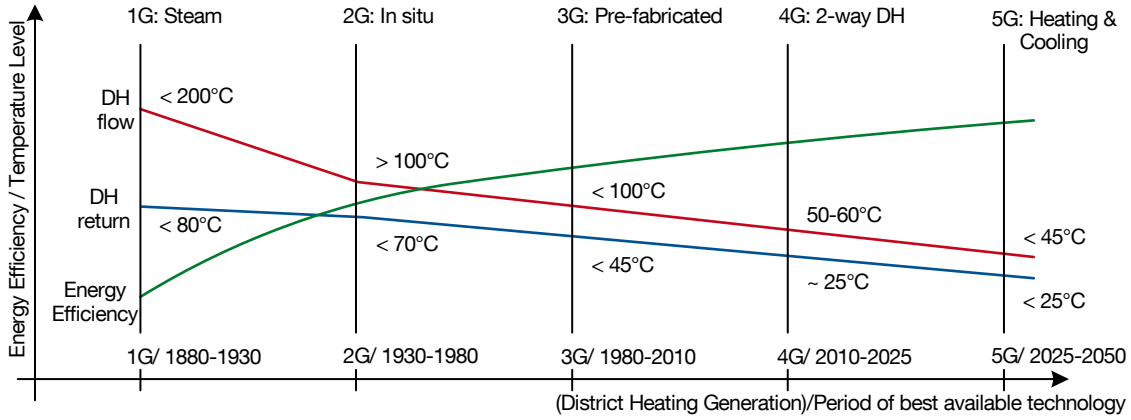

Figure 1-1: Development of District Heating from 1880 on (Lund et al. 2014; Thorsen et al. 2018; Buffa et al. 2019)

The idea of further decreasing network temperature levels to a range between 45 °C and 5 °C is driven by the energy potential becoming available at even lower network temperatures: otherwise unused or discarded heat, such as waste heat, low temperature solar heat or ambient heat, becomes the heat source. However, such low temperature levels of a network can only be reached and maintained through a low-temperature demand and supply structure with low-temperature heating and low-temperature DHW systems in the connected buildings on one side, and the integration of low-temperature heat sources, e.g. renewable and waste heat sources, on the other side.

1.2. Problem Statement and Objective, Hypothesis

Decreasing the network temperatures not only reduces thermal losses but also leads to lower energy densities of the heat carrier, which in turn leads to higher mass flows in a network when keeping the heat demand constant, resulting in a higher pump energy demand. Additionally, compared to traditional DHNs, further investment in heat pumps, storage capacities and heat collectors is required.

However, the continuing trend of decreasing DHNs temperatures also aims at making unexploited energy efficiency potentials accessible by

- a utilization or recycling of low-temperature heat from waste heat or renewable heat sources
- reduced thermal losses during transport of the heat carrier due to small temperature differences to the surroundings
- enabling a free spatial and temporal shift of heat in the network and the seasonal storage
- enabling the propagation of water/water ground-coupled heat pumps to areas without geothermal potential
- enabling a direct exchange of heat between buildings, especially different building types
- sharing the high investment costs for seasonal storage and infrastructure between all users, reducing the individual financial burden

These possible advantages and disadvantages of this low-temperature system show the field of tension this work examines. With the overall goal of reducing CO_2 emissions of the energy supply structure, a cross-linking and development of currently unused low-temperature heat sources could be a major contribution to a significant reduction of CO_2 emissions in the building sector. The main research question is:

Can the benefits mentioned above outweigh the additional effort, ecologically, technologically and economically and if so, what are the boundary conditions under which a DHN at very low temperature levels can do so?

Therefore, the aim of this work is to develop a model capable of dynamically simulating the heat flow within a district, equipped with a DHN at very low temperature levels, with detailed modelling of the hydraulic network, to provide a basis for the identification of energy efficiency potentials of districts through the use of DHNs at ultra-low temperature levels. In a case study the model is applied to a residential district. On the basis of a parametric analysis, the range of efficiency potentials is pointed out, with special focus on the pump energy demand of the network. Based on the information of the case study, economic and energetic feasibility are examined, researching the possibility of a CO_2-neutral heat supply of a residential district.

Therefore the hypothesis of this work is:

A district heating network at low temperature levels with seasonal heat storage is able to provide a CO_2-neutral heat supply in residential districts with urban density.

1.3. Research Approach

The approach chosen in this work follows a standard problem-solving approach. The initial statement of the research question and hypothesis of this work (1.2) is followed by an analysis of the state of the art in technology and modelling of thermal networks at very low temperatures (2). Current approaches as well as software used on related research questions are examined in 2.1 and 2.2.

Chapter 3 describes the methodology and the development of the simulation models used in this work. In the subsequent chapter the simulation itself is examined in detail: 4.1 and 4.2 introduce a case study which is used to test the simulation models in several scenarios. The scenarios described in 4.3 include a baseline version which is used as reference. From this baseline the other scenarios and simulation models are derived. 4.4 presents the simulation results of the various scenarios described in 4.3. 4.5 additionally presents the simulation results of a study previously conducted which investigated further scenarios. Based on the simulation results a cost and profitability analysis is conducted in chapter 5 to evaluate the economic aspects of the technology at hand.

A discussion of the results obtained through simulation (4) and profitability analysis (5) in the light of the research question and hypothesis (6) is followed by the conclusion and outlook (7) on further potentials of the technology examined.

2. State of the Art

Not counting the early use of geothermal heat (see 1.1), the development of DHNs historically was driven by safety concerns. Heat distribution systems were installed to minimize the local risk of fire (Bloomquist 2001) and boiler explosions and were mainly based on steam as the heat carrier (Lund et al. 2014). The high steam temperatures led to significant heat losses and major accidents (Lund et al. 2014). Today, some steam-based networks are still used (Manhattan, Paris) while others have been replaced (Munich, Copenhagen, Salzburg, Hamburg) by systems using pressurized hot water as the heat carrier (Lund et al. 2014).

In more recent times the further development and expansion of DHNs was driven by the need to improve public health and reduce pollution caused by the omnipresent combustion of fossil fuels in Europe's inner cities. Today, German municipalities are authorized to impel building owners to connect to DHNs for climate and resource protection purposes, based on the German Renewable Energies Heating Act (§ 16 EEWärmeG, revised by Article 9 of the Act of 10/20/2015 (BGBl. I p. 1722)) in combination with state legislation (BVerwG, Decision of 9/8/2016). Today the reinvention of DH to use lower temperatures and decentralized structures is driven by the goal of further improving their efficiency and reducing CO_2 emissions of the building sector.

2.1. Technology

Unlike conventional DHNs, DHNs at low temperature levels do not have standards regarding layout, control strategy or labeling yet. This section gives a short summary of the established labels, layout types and the different modes of operation possible. (Heissler et al. 2017b)

From a thermodynamic point of view the energy of a system can be divided into an anergetic part and an exergetic part. Reference temperature for this division is the ambient temperature of the surroundings of the system. The exergetic part, or exergy of the system, is the maximum amount of work which can be performed by the system until the system reaches thermal equilibrium with the surroundings. Once equilibrium is reached, the system has no exergy. The anergetic part, or anergy of the system, is

the share of energy of the system which cannot perform any work regarding the surroundings. (Perrot 1998), (Heissler et al. 2017b)

It follows (Perrot 1998):

$$Energy = Anergy + Exergy \tag{2-1}$$

Based on their exploitation of heat sources with low temperatures relative to the surroundings (low exergetic share), this type of network is often called “Anergy Network” (“Anergienetz”) whether the network is an open ground-water network (IBC Energie Wasser Chur 2014), a closed network supplied by renewables (Vetterli et al. 2017), or one supplied by waste heat (Lauber IWISA AG 2008). Other commonly used designations are “low-exergy network” (“Low-Exergy-Netz”) (Bolle 2015), “cold district heating” (“kalte Nahwärme”) (Sulzer and Hangartner 2014), “cold long-distance heating” (“kalte Fernwärme”) (Sulzer and Hangartner 2014), (Schmidt and Schurig 2013), “low temperature network” (“Niedertemperaturnetz”) (Stadtwerke München 2015; Schluck et al. 2015) or “low temperature district heating network” (Christiansen et al. 2014). (Heissler et al. 2017b)

As mentioned above a variety of designations are used and lead to ambiguity and lack of clarity. A comparison of the labels used, based on the supply temperatures, shows no systematic approach. Sulzer applies the label “Anergy Network” to networks with flow temperatures between 8 °C and 18 °C (Sulzer 2011), but uses “cold district heating” synonymously (Sulzer and Hangartner 2014). Caratsch also uses the label “cold district heating”, although for networks with flow temperatures below 60 °C (Caratsch et al. 2015), while Schmidt uses the label “cold long-distance heating” for flow temperatures between 15 °C and 20 °C (Schmidt and Schurig 2013). (Heissler et al. 2017b)

The use of the label “low temperature network” and “low temperature district heating network” (LTDHN) also varies significantly. Lund et al. (2014) apply this to future grids with supply temperatures of 50 °C, Christiansen et al. (2014) to networks with supply temperatures from 50 °C to 55 °C, while the municipal energy supplier of Munich applies it to networks with supply temperatures of 60 °C (Stadtwerke München 2015) and Schluck et al. (2015) apply it to networks with operating temperatures from 8 °C to 20 °C. Previously the label was in use for supply temperatures ranging from 70 °C in winter to 60 °C in summer (Christiansen et al. 2014).

For networks with yet lower temperatures than that of LTDHNs, the label “ultra-low temperature district heating network” (ULTDHN) has been coined, but, similarly to the label LTDHN, not defined clearly. Yang et al. (2016) use it for networks with supply temperatures below 50 °C as well as for networks with a supply temperature range from 35 °C to 45 °C (Yang and Svendsen 2017), Ommen et al. (2017) defined a supply temperature range from 35 °C to 50 °C while Østergaard and Svendsen (2017) defined a supply temperature range from 30 °C to 50 °C. Østergaard and Svendsen (2017) describe them also as the next step, referring to the continuous reduction of temperatures of DHNs over the last few centuries as well as the trend of decentralization.

Also acknowledging the confusion of labelling, Buffa et al. (2019) have advocated the use of Fifth Generation District Heating and Cooling Network (5GDHCN) as a label which unifies the different definitions. They provide the following definition of a 5GDHCN:

> “A 5GDHC network is a thermal energy supply grid that uses water or brine as a carrier medium and hybrid substations with Water Source Heat Pumps (WSHP). It operates at temperatures so close to the ground that it is not suitable for direct heating purpose. The low temperature of the carrier medium gives the opportunity to exploit directly industrial and urban excess heat and the use of renewable heat sources at low thermal exergy content. [..]” (Buffa et al. 2019)

Since the definition of Buffa et al. (2019) is very precise and capable of unifying the different labels in circulation, the label used in this work is Fifth Generation District Heating and Cooling Network (5GDHCN).

2.1.1. Fifth Generation District Heating and Cooling Networks

5GDHCNs are networks at very low temperature levels close to ambient temperature (see 2.1). At these temperature levels in the network, recycled heat from waste heat sources or renewable heat from geothermal or solar-thermal heat sources can be easily integrated into the network (Lund et al. 2014). Heat transfer losses are also minimized due to the low temperature differences to the surroundings. The low temperature levels facilitate an efficient, network-wide, decentralized use of WSHPs for HW supply while reducing the need for individual investments in stand-alone heat sources. Another major benefit compared to traditional DHNs is that it is not necessary to regulate network temperature to service the least efficient building in the circuit, since every building can exercise individual temperature control via its heat pump.

Following traditional DHN types, Sulzer and Hangartner (2014) distinguish the networks through the numbers of pipes used (Heissler et al. 2017b):

- 1-pipe system: a heat carrier is transported via one single supply pipe. After heat extraction the heat carrier is disposed of to the surroundings (for example, leaching to groundwater) (Sulzer and Hangartner 2014). This approach is commonly used for groundwater networks.

- 2-pipe system: The most widely used type of heating network transports a heat carrier via one supply pipe to the consumer. After heat extraction a return pipe transports the depleted heat carrier back to the heat source. This traditional approach is mostly used in traditional unidirectional, directed networks (Figure 2-1, top left).

- 3-pipe system: Two pipes serve as flow and return pipes. The set temperature of the third pipe is significantly higher or lower than the set temperature of the other two pipes and therefore can be used for direct cooling/heating (Sulzer and Hangartner 2014). Another control strategy uses the third pipe as an additional variable flow or return pipe: during summer as a direct feed pipe for solar heat and as a second flow pipe during winter (Technisches Handbuch Fernwärme 2009).

- 4-pipe system: a heat carrier is transported via two flow and two return pipes on different temperature levels and can be used directly via heat exchangers or indirectly via WSHPs for heating, cooling or DHW preparation (Sulzer and Hangartner 2014).

Another classification (Sulzer and Hangartner 2014) is a distinction of networks specifying energy flow (uni- or bidirectional) and heat carrier flow (directed or undirected) (Figure 2-1)(Sulzer and Hangartner 2014; Heissler et al. 2017b):

- *Unidirectional, directed networks* are the most common type of heating networks. One centralized heat source supplies the network via a central pumping station which defines a pressure difference between flow and return line, resulting in a mass flow dependent on the flow resistance of the system. Energy flow and heat carrier flow have the same direction (Figure 2-1, top left).

- *Unidirectional, undirected networks* are also very common. In contrast to the directed networks the heat carrier flow is undirected, which can be the result of

multiple heat sources and pumping stations. The momentary flow direction of the heat carrier is dependent on the momentary supply and demand (Figure 2-1, bottom left).

- In *bidirectional, directed networks* the network can simultaneously serve as heat source and heat sink. In combination with a directed heat carrier flow, the return temperature is a mixing temperature which, depending on the momentary thermal demand, is lowered or increased by the central heat source/heat sink (Figure 2-1, top right).

- *Bidirectional, undirected networks* enable each user to meet the momentary heat or cold demand by drawing from one line of the network while simultaneously feeding the resulting return heat or cold into the other line of the network, preventing temperature mixing losses. The interaction of the decentralized pumps results in a cumulative pressure difference leading to an undirected heat carrier flow within the network (Figure 2-1, bottom right).

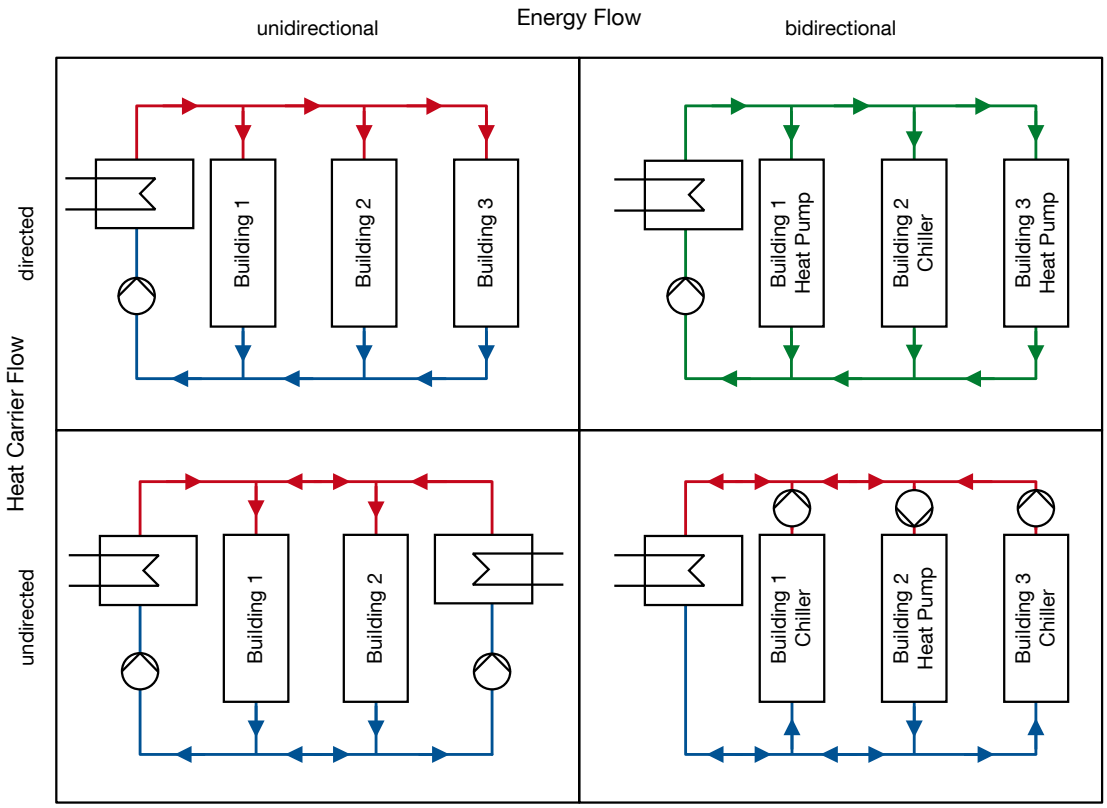

Figure 2-1: Network typology (Heissler et al. 2017b; Sulzer and Hangartner 2014)

Similar to traditional DHNs (Nussbaumer 2017), 5GDHCN types can also be divided into two main network types: star and meshed networks, with the subtypes line network and ring network.

Ring and meshed DHNs are often the result of an ongoing development process over several years or decades, with subsequent additions and changes to the existing structure, often starting from line networks or small star networks (Nussbaumer 2017). Since there is no data available on the growth of 5GDHCNs over time, a similar development to DHNs for 5GDHCNs is assumed.

2.1.2. Supply and Demand

The low temperatures of 5GDHCNs allow an input of heat at temperature levels between the current network temperature and a maximum input temperature of 45 °C (see 2.1). The types and sizes of heat sources implemented affect the network layout and the storage requirements: while large continuous heat sources (for example, waste heat processes) require few or no storage capacities in the network, highly volatile heat sources such as solar-thermal collectors require large storage capacities to ensure a stable heat supply over the course of one year.

The heat supplied from the network to the buildings is used for heating purposes and DHW production. WSHPs in the connected buildings raise the temperature level to supply heating and DHW production systems. Since heat pump performance is closely linked to the temperature gain a heat pump has to provide, low temperature heating and low temperature DHW production and distribution systems are required in combination with 5GDHCNs.

Traditional 4-pipe in-house distribution systems are set up with separate loops for heating and DHW distribution. Compared to the former, novel 2-pipe distribution systems offer significant advantages: reduced in-house distribution losses due to shorter total pipe lengths, and simpler installations, systems engineering, control and integration of solar heat. (Mercker and Arnold 2017)

However, the aim of low temperature DHW production systems, to provide DHW at low temperature levels, collides with scientific findings regarding the prevention of Legionella. According to Codony et al. (2002) and Alary and Joly (1991), low DHW temperatures, DHW stagnation and sediment accumulation promote a proliferation of Legionella. Addressing this problem, the German codes of practice for drinking water installations (DIN 1988-200) require a DHW temperature of 60 °C or higher in DHW systems with circulation and water volume above 3 L. Exempt of this regulation are DHW systems with decentralized continuous-flow heating, if the water volume in the pipes does not exceed 3 L (DIN 1988-200).

Yang et al. (2016) also discuss and evaluate different methods of DHW preparation in combination with 5GDHCNs and conclude that decentralized substations combining a high efficiency heat exchanger and an in-line electric heater offer better energetic and economic performances than decentralized substations with storage tanks or micro heat pumps. Mercker and Arnold (2017) also emphasize hygienically advantageous in-line electric heating for the production of DHW.

Considering gravity-driven and steam-based heating systems and their requirement of high supply temperatures, supply temperatures for space heating have decreased continuously. At the same time, building standards and energy prices have increased, leading to the development of low temperature heating systems for space heating of low-energy buildings. Today, supply temperature levels of 40 °C (Brand and Svendsen 2013) or even lower (Schmidt et al. 2017) for floor heating, radiant panel heating or thermal activation of building structures are state of the art. For existing buildings, there are state of the art retrofit solutions available: for example, low-temperature radiators, which also allow supply temperatures as low as 45 °C (Kermi GmbH 2016) or even below 40 °C (Cosmo GmbH 2016) after thermal improvement of the buildings, making them fit for use in 5GDHCNs.

2.1.3. Transport and Storage

Traditionally DHNs are set up with flow temperatures above 70 °C (Sulzer 2011). Due to the temperature differences to the surroundings the losses during transport of the heat carrier are significant. The heat losses of German state-of-the art DHNs range from 8% to 18% with average losses of 13% of the heat input of the network (Pfnür et al. 2016). Additional exergetic losses occur at the heating plant due to the temperature differences between combustion process and heat carrier. Also, the exergetic losses caused by the user through the necessity of reducing the DHW to a maximum temperature of 60 °C add further to the total losses. The exergy content of the primary energy carrier is therefore gradually, over the whole process of production and distribution in a traditional DHN, converted to anergy (not counting a possible co-generation of electricity). (Heissler et al. 2017b)

5GDHCNs follow the opposite approach: comparatively high mass flows in the network at low temperature levels are lifted by WSHPs to the temperature levels required in the buildings, exactly where and when they are required (Sulzer and Hangartner 2014), (Heissler et al. 2017a). This requires additional effort and investment (heat pumps, pipe diameters, seasonal storage, etc.) compared to traditional DHNs. How-

ever, previous research in this field sees a potential reduction of up to 25% of the thermal losses of the network (Bestenlehner et al. 2014) or even up to 60% of the exergetic losses (Sulzer 2011).

An integral part of any 5GDHCN not permanently supplied by a large heat source is a thermal storage. Depending on the volatility and size of the heat source, the requirements for the thermal storage vary. Figure 2-2 shows the seasonal variation of the solar irradiation available at a middle-European location opposed with the seasonal variation of the building energy demand. During the winter months a low solar irradiation is met by a high building energy demand. In the summer months, the opposite occurs: a high solar irradiation is met by a very low building energy demand. Here, a seasonal storage can compensate for the imbalance by shifting the surplus solar gains of the summer months into the winter months when they are needed.

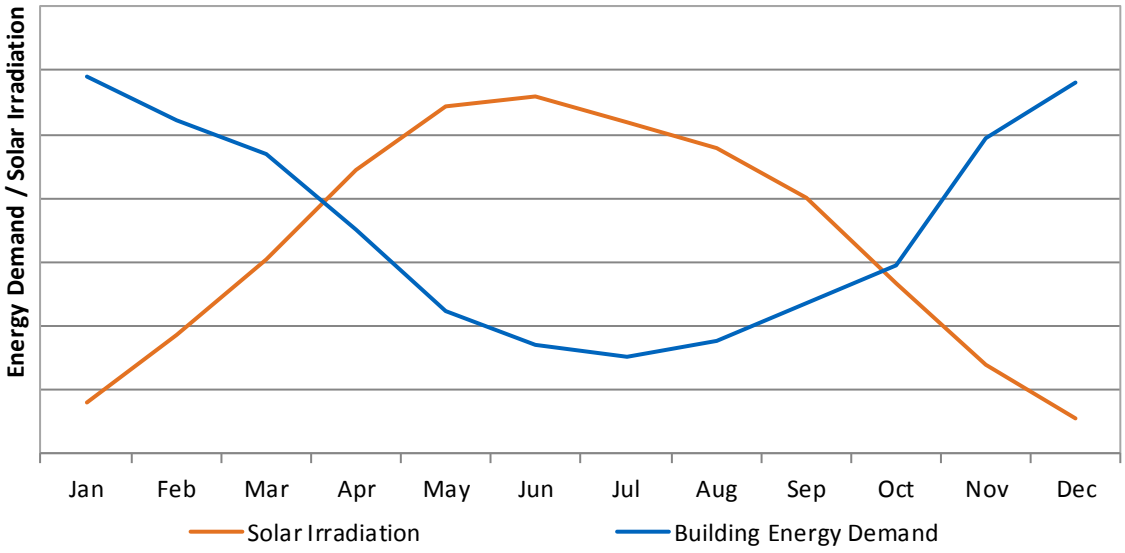

Figure 2-2: Seasonal imbalance of solar irradiation and building energy demand

In combination with a 5GDHCN supplied by solar heat only, a thermal storage must have the heat capacity to be able to shift the excess solar heat gains of summer into the winter months. Traditional hot water thermal storage concepts range between 4 °C and 95 °C (Krames 2013). Due to the low temperature levels of the 5GDHCN, the maximum thermal spread utilizable for sensible heat storage is the temperature difference between the highest temperature of the warm line of 45 °C (see 2.1) and the lowest temperature of the cold line of 0 °C. With a constant specific heat capacity this limited temperature range doubles the thermal storage mass required for storing the same amount of sensible heat (Weber 2007).

For high storage capacity requirements and a thermally limited usable temperature range, two options exist: increased storage size or increased heat capacity.

Through an increased storage size more mass can be thermally activated, resulting in higher storage capacities. This also leads to more expensive storage systems, depending on scalability and type of storage. Some types of thermal storage systems scale more easily and are easier to expand in later stages (for example, borefield heat exchangers), while others are easier to construct (for example, pit heat storage units). (Novo et al. 2010)

Increasing the heat capacity can be achieved by using substances for thermal storage that undergo a phase change from solid to liquid within the thermal range required. The total amount of storable thermal energy is increased by the latent energy required for the phase change. Ice storage systems use this phenomenon (Viessmann Eis-Energiespeicher GmbH 2017).

The type of seasonal heat storage defines the thermal behaviour in general and at the thermal extremes. Depending on the type of storage, the thermal ranges are set by physical boundaries (boiling, freezing) or systemic boundaries, defined by the connected systems or networks. Commonly used seasonal heat storage systems are hot water storage units (Dallmayer et al. 2010), borefield heat exchangers (Sibbitt et al. 2012), pit heat storage units (Novo et al. 2010), aquifer heat storage units (Holstenkamp et al. 2017) and ice storage units (Carbonell et al. 2016). Considering the abovementioned points, seasonal heat storages for use in 5GDHCNs are required to provide

- good temperature maintenance at long storage periods,
- high thermal inertia,
- high storage capacity,
- few insulation requirements,
- easy scalability,
- easy construction,
- and operational temperatures in 5GDHCN range.

A comparison of existing 5GDHCNs with seasonal storage units (2.1.4) shows that a vast majority of seasonal storage systems chosen are borefield heat exchangers.

2.1.4. Existing 5GDHCNs

This section presents 5GDHCNs which are already in use or are currently under construction (Table 2-1). The review shows that there are a notably high number of systems already implemented in Switzerland. One reason for this accumulation might be a high interest of the Swiss Federal Office of Energy in a further development of heat supply systems at low temperature levels (Caratsch et al. 2015). The systems displayed here mostly tap non-depletable heat sources. Therefore, most of the systems do not address one of the major challenges, the seasonal shift of heat. The 5GDHCN of the Suurstoffi quarter, the Richti quarter and the Sedrun network do address this challenge and solve it by using borefield heat exchangers. (Heissler et al. 2017b)

Table 2-1: Overview of existing or planned 5GDHCNs

Name	Country	Heat source	Seasonal storage	Heat pumps	Source
Drake Landing Solar Community, Okotoks	CAN	Solar, Gas	+	-	(Sibbitt et al. 2012)
Visp-West, Visp	CH	Waste heat	-	+	(Sulzer 2011; Caratsch et al. 2015; Lauber IWISA AG 2008)
ETH Zürich Höngger-berg, Zürich	CH	Waste heat, Ground	+	+	(Amstein + Walthert 2010; Maurer Hartmann 2013; ETH Zürich 2015)
Suurstoffi Quarter, Rotkreuz	CH	Solar	+	+	(Vetterli et al. 2017)
Solar Settlement Ohrberg, Emmerthal	GER	Ambient heat, Solar	-	+	(Vanoli et al. 1997)
Neckarpark, Stuttgart	GER	Waste heat, Cogeneration	-	+	(BINE Informationsdienst 2015)
Anergy Network Sedrun, Tujetsch	CH	Solar	+	+	(Energi Alpina 2015, 2016; Pajarola 2017)
Rheinfels Quarter, Chur	CH	Ground, Co-generation	-	+	(Spescha 2014; IBC Energie Wasser Chur 2014; Swisspower AG 2014)
Richti Quarter, Wallisellen	CH	Waste heat, Gas	+	+	(Amstein + Walthert 2015)
Vordere Viehweide, Wüstenrot	GER	Ground	-	+	(Pietruschka 2016)

Drake Landing Solar Community, Okotoks, CAN

The DH system of Drake Landing (Figure 2-3) supplies 52 houses with solar-thermal heat all year. 2293 m² solar-thermal collectors, located on detached garages next to each house (small orange squares), are connected to the community's Energy Centre. Two short-term storage tanks receive the heat and transfer it to the building circuits (blue lines) or the Borehole Thermal Energy Storage (orange octagon) consisting of 144 boreholes each with a depth of 35m. The building circuits, four parallel branches of a 2-pipe unidirectional, directed network, run with flow temperatures of 37 - 55 °C and provide the energy for space heating of the buildings. Independently installed solar DHW systems with two extra solar-thermal collectors and gas-fired water heaters secure the supply with DHW. (Sibbitt et al. 2012)

Figure 2-3: Topology of the network in Okotoks, Canada (Mesquita et al.; Open Street Map Foundation 2019)

Visp-West, Visp, CH

In Visp-West an Anergy Network (Figure 2-4, blue line) uses the industrial waste heat of the Lonza AG, disposed in a canal of cooling water. Water from the canal (10 °C - 18 °C) is pumped through a flat plate heat exchanger and heats a secondary circuit, a directed, bidirectional network. Decentralized heat pumps connected to the network supply the adjacent buildings with heat. Since the average supply temperature is 16 °C, the network can also be used for direct cooling. The system does not have a seasonal storage, since the heat supplied by the canal is available all year. (Sulzer 2011; Caratsch et al. 2015; Lauber IWISA AG 2008; Heissler et al. 2017b)

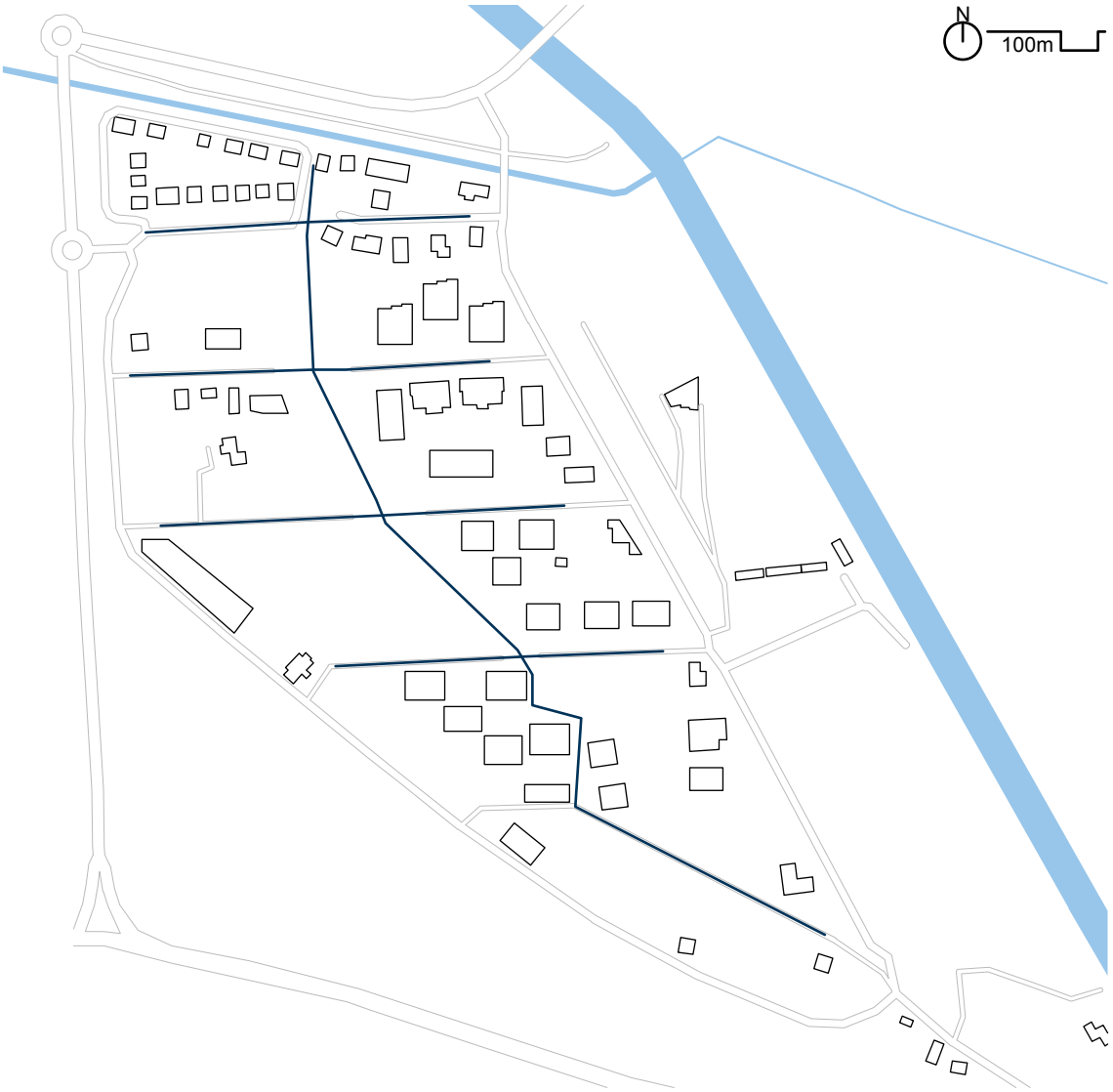

Figure 2-4: Topology of the Anergy Network in Visp-West, Switzerland (Lauber IWISA AG 2008; Open Street Map Foundation 2019)

ETH Zürich Hönggerberg, Zürich, CH

The bidirectional, undirected network (blue line) of ETH Zürich (Figure 2-5) at the Hönggerberg site consists of three lines: a cold and a warm line and an additional line for free cooling. Heat source and heat storage of the network are borehole heat exchangers (orange areas) with 100-200 boreholes each, with a depth of up to 200 m. Heat and cooling stations as part of the network regulate the mass flow and raise the temperature level provided by the borehole heat exchanger to supply temperature level. The network is currently under construction. It is expected for the network to provide 100% of the heating and 80% of the cooling demand in 2025. (Amstein + Walthert 2010; Maurer Hartmann 2013; ETH Zürich 2015; Heissler et al. 2017b)

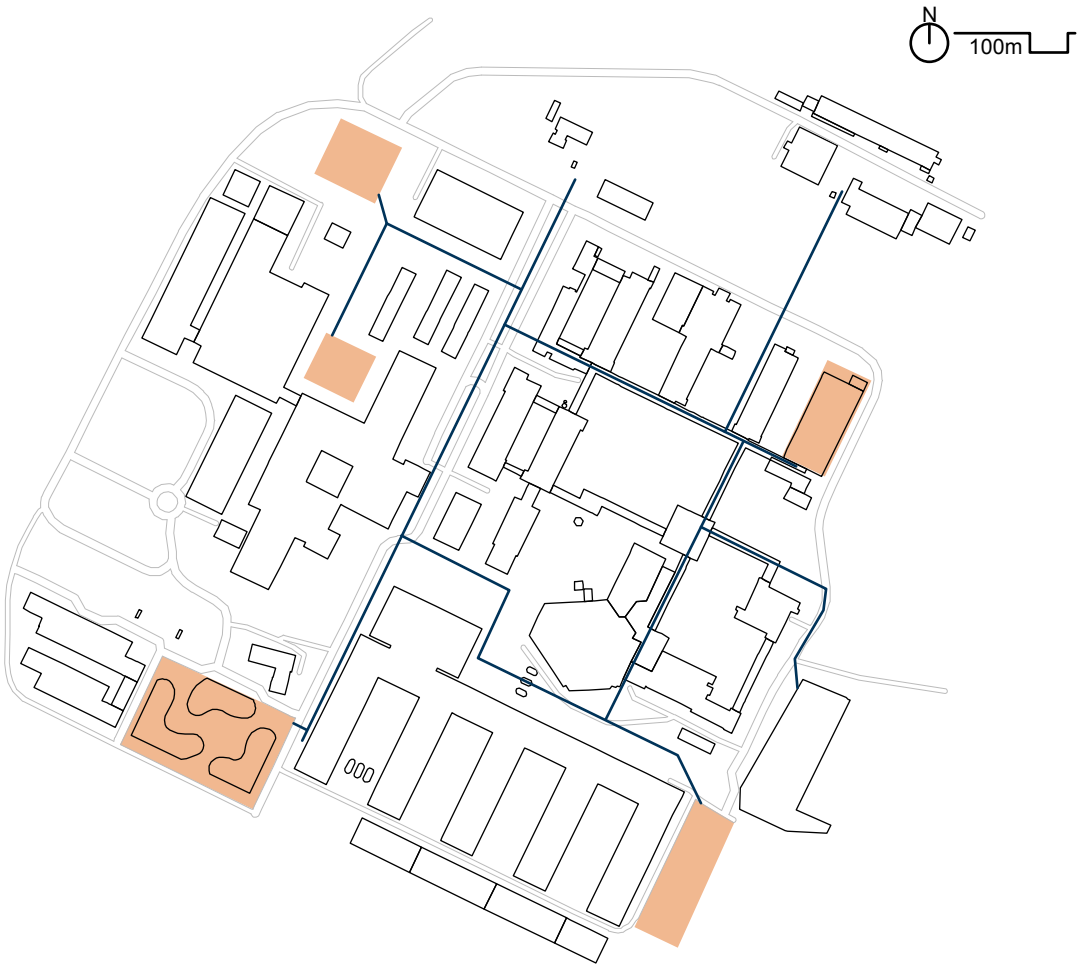

Figure 2-5: Topology of the network in Zurich, Switzerland (Amstein + Walthert 2010; Lauber IWISA AG; ETH Zürich 2015; Open Street Map Foundation 2019)

Suurstoffi Quarter, Rotkreuz, CH

Since summer 2010 a new quarter including an Anergy Network for heat and cold supply (blue line) is under construction at the site of a former oxygen production plant in Rotkreuz, Switzerland (Figure 2-6). The first of three construction phases of the two-line, bidirectional, and undirected network was completed and put into operation in June 2012. About 400 boreholes of a borehole heat exchanger (orange area) serve as heat storage and heat source of decentralized heat pumps and as heat sinks for direct cooling, regenerating the ground. The project showed a thermal imbalance of the network with more heat taken from the network than being put in. From December 2013 to April 2015, a pellet boiler and an auxiliary heater for DHW were installed to prevent a further cooling of the network. Since 2014, additional photovoltaic-thermal (PVT) collectors have been installed to add more heat to the Anergy Network. (Vetterli et al. 2017; Heissler et al. 2017b)

Figure 2-6: Topology of the Anergy Network in Rotkreuz, Switzerland (Vetterli et al. 2017; Open Street Map Foundation 2019)

Solar Settlement at Ohrberg, Emmerthal, GER

The solar settlement at Ohrberg (Figure 2-7), built from 1997-2001, uses water from the river Weser (5 °C to 20 °C) as a heat source of the primary side of its heating network. One central pumping station equipped with a heat pump raises the temperature to 12 °C on average, which is the average temperature level of the directed, unidirectional secondary circuit (blue line). This circuit supplies the decentralized heat pumps in the buildings. Solar collectors are used for DHW preparation support. A use of waste heat or a heat exchange between the buildings is not a property of the system. (Vanoli et al. 1997; Heissler et al. 2017b)

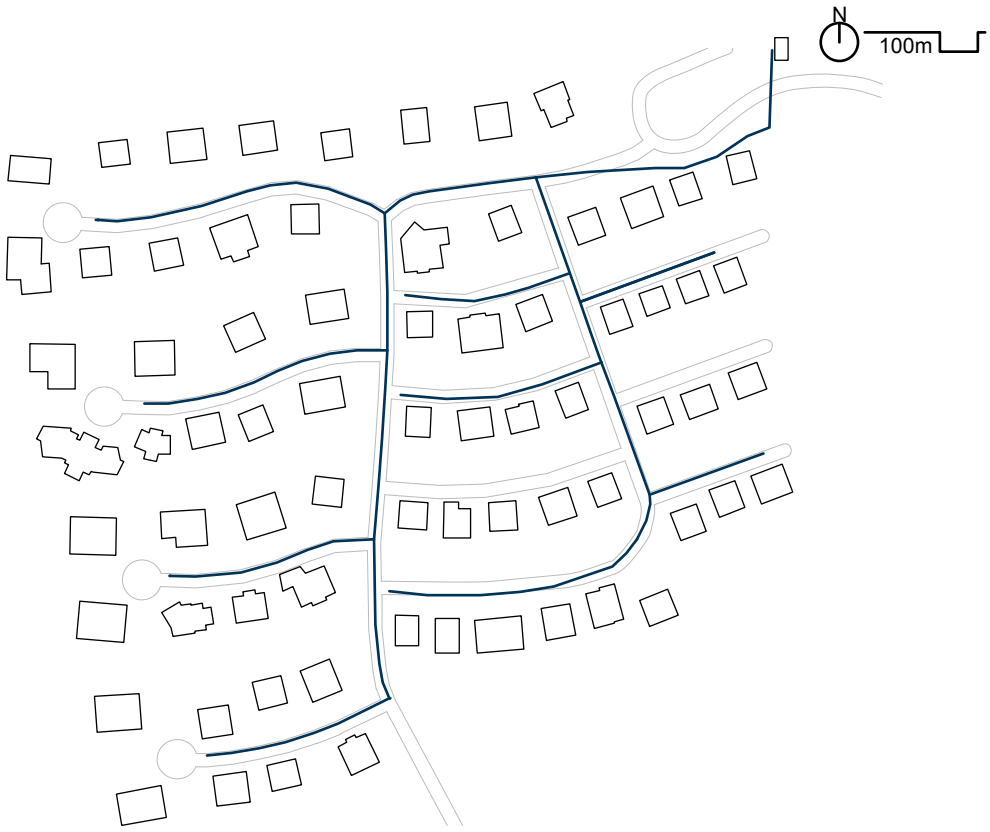

Figure 2-7: Topology of the network in Emmerthal, Germany (Vanoli et al. 1997; Behnisch 2018; Open Street Map Foundation 2019)

Neckarpark, Stuttgart, GER

Using the area formerly occupied by the freight depot Bad Cannstatt, a new city quarter “Neckarpark” is being built. Energy efficient buildings with different types of usage are under construction and will be supplied by a 4-line network (Figure 2-8). Heat source of the heating line of the network is a waste water heat exchanger (orange line), which supplies the primary side of a heat pump. The heat pump feeds the flow of the low temperature heating line with a temperature of 30 °C. The flow of the DHW heating line is supplied independently by a cogeneration unit. (BINE Informationsdienst 2015; Forschungsinitiative EnergiewendeBauen 2017; Heissler et al. 2017b)

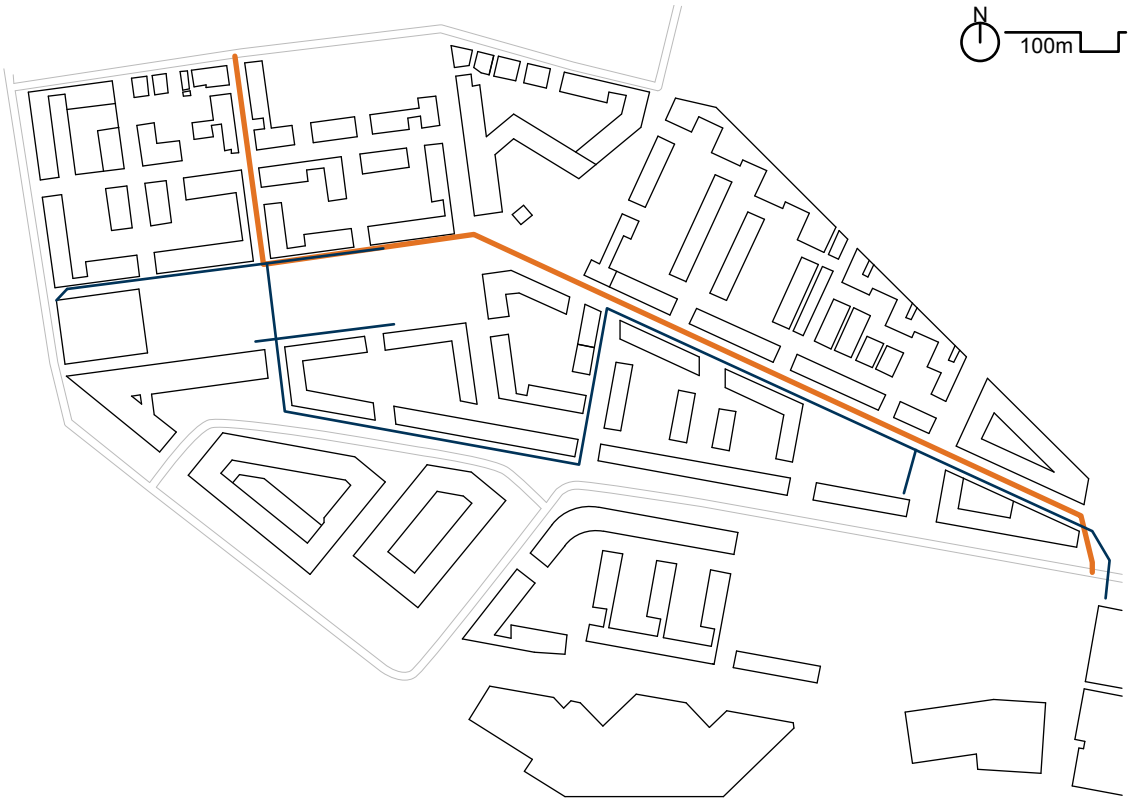

Figure 2-8: Topology of the network in Stuttgart, Germany (Forschungsinitiative EnergiewendeBauen 2017; Open Street Map Foundation 2019)

Anergy Network Sedrun, Tujetsch, CH

The heat source of the 5GDHCN (Figure 2-9, blue line) of the Swiss village Tujetsch is the 75 boreholes of a borefield heat exchanger (orange area). The network supplies the heat pumps in municipal buildings such as a local gym, a town hall, and a school, as well as privately owned buildings with low temperature heat at a temperature level of 10 °C to 12 °C. The borehole heat exchanger is regenerated by PVT collectors. (Energi Alpina 2015, 2016; Pajarola 2017; Heissler et al. 2017b)

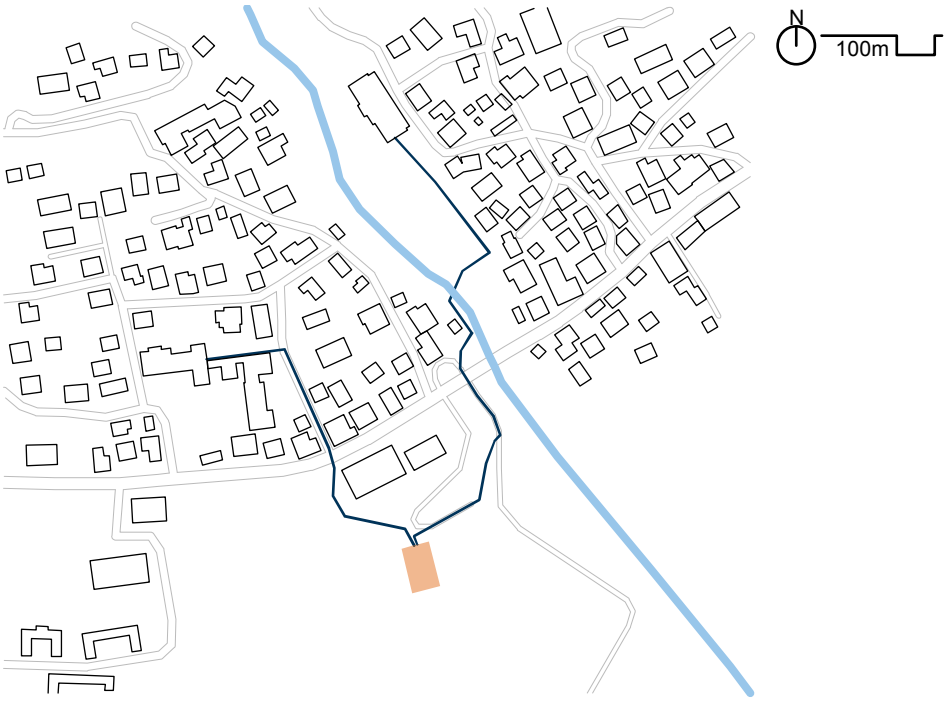

Figure 2-9: Topology of the network in Sedrun, Switzerland (Energi Alpina 2016; Open Street Map Foundation 2019)

Rheinfels Quarter, Chur, CH

With its dense and mixed existing development, the Rheinfels quarter at Chur has a HW, DHW and cooling demand. In 2013 a former drinking water pump plant was reactivated to be part of an Anergy Network (Figure 2-10, blue line). The heat source of the network is a ground water heat exchanger combined with a pellet boiler and a cogeneration unit (orange square). The network supplies the decentralized heat pumps of about 200 households with a flow temperature of 6 °C – 16 °C. The return temperature varies between 2 °C and 25 °C. (Spescha 2014; IBC Energie Wasser Chur 2014; Swisspower AG 2014; Heissler et al. 2017b)

Figure 2-10: Topology of the network in Chur, Switzerland (IBC Energie Wasser Chur 2014; Open Street Map Foundation 2019)

Richti Quarter, Wallisellen, CH

At the site of the former Richti quarter in Wallisellen, a mixed-use quarter was constructed with the aim to meet the requirements of the 2000W-society vision. A 2-line Anergy Network with temperatures between 8 °C and 22 °C serves as a heating and cooling network (Figure 2-11, blue line). The heat source during heating season is a borefield heat exchanger (orange area) with 220 boreholes, each with a length of 225 m. The network supplies decentralized substations with heat pumps in the adjacent buildings. To maximize the network's cooling capacity for summer, the aim is to reach a temperature level of 8 °C on the flow side and 4 °C on the return side at the end of the heating period. The dense layout of the boreholes limits their capacity for natural regeneration. Thus, waste heat from a computer centre, space cooling, and compression refrigeration machines are used to regenerate the borehole heat exchanger. At the end of the summer period the highest temperature level of the Anergy Network is about 25 °C. Special features are the decentralized substations with decentralized pumps, reducing the auxiliary electrical energy demand. The DHW demand is covered by two-stage heat pumps or independent gas boilers. (Amstein + Walthert 2015; Heissler et al. 2017b)

Figure 2-11: Topology of the network in Wallisellen, Switzerland (Amstein + Walthert 2015; Open Street Map Foundation 2019)

Plus-Energy Settlement “Vordere Viehweide”, Wüstenrot, GER

The Plus-Energy Settlement “Vordere Viehweide” of the village Wüstenrot is supplied by a “cold heating network” (Figure 2-12, blue line). The heat source is a horizontal earth collector field (orange areas) below agricultural land. The average temperature of the undisturbed ground is 10-12 °C. Decentralized heat pumps in the buildings connected to the network raise the heating temperature level to 35 °C. The network is also used to cool the buildings during summer. (Pietruschka 2016; Heissler et al. 2017b)

Figure 2-12: Topology of the network in Wüstenrot, Germany (Pietruschka 2016; Open Street Map Foundation 2019)

2.2. Software

The modelling and simulation of 5GDHCNs requires powerful modelling tools capable of accurately and flexibly mapping networks, storage, heat sources, heat sinks and building services. The most important requirements are:

- hydraulic modelling with dynamic pressure resistances and capacity for flow reversal
- a dynamic heat exchange between the network and its surrounding ground
- a dynamic seasonal heat storage model and a flexible building services model
- dynamic pump simulation models based on performance maps
- a flexible integration of heat sources and heat sinks
- a modular setup of model parts with dynamic data exchange

There are a variety of modelling and simulation tools of DHNs which mainly focus on optimizing the network design regarding cost or strategic network development (Robbi 2013). Also previous works aim to examine the performance of 5GDHCNs. Doetsch and Bargel (2009) examine different network temperatures and their resulting exergetic efficiencies and conclude the thermodynamically ideal temperature difference between feed and return line in heating networks is 10 to 15 K. In previous works on 5GDHCNs, Kräuchi and Kolb (2012) built a network model in IDA ICE (EQUA Simulation AB 2018) with additional in-house developed elements, modelled and programmed in the neutral model format (Kräuchi et al. 2014) also used by Schluck et al. (2015) to compare the exergetic efficiency of unidirectional and bidirectional networks. They stress the economic, exergetic and electric advantages of bidirectional low temperature networks (Schluck et al. 2015). Bestenlehner et al. (2014) compare a groundwater-based 5GDHCN with traditional DHNs using TRNSYS (Klein et al. 1976), while Carli et al. (2014) use the combination of TRNSYS and Earth Energy Designer (Blocon AB 2018) to analyse the energetic and economic performance of a district-wide heating and cooling system based on a ground source heat pump. Robbi (2013) uses TRNSYS-TUD (Perschk 2012), an in-house development of TU Dresden based on TRNSYS for an analysis of DHNs under full and part load conditions. Zarin Pass et al. (2018) analysed the thermodynamic behaviour of bidirectional district heating and cooling networks using the Modelica-based environment Dymola (Dassault Systèmes) in combination with the open source Modelica Buildings library (Wetter et al. 2014). Vivian et al. (2018) based their cost evaluation of heat from 5GDHCNs on simulations performed with TRNSYS, while Bünning et al. (2018) also used Dymola in combination with the Modelica Buildings library as well as Python (Python Software Foundation 2018) for their comparison and optimization of LTDHNs with agent-based control.

A comparison by Crawley et al. (2008) for building systems modelling tools identified TRNSYS, among 20 tools, to be the simulation tool with the most heating, ventilation and air conditioning (HVAC) and renewable energy system components. Nageler et al. (2018) also emphasize the large component library of TRNSYS, as well as a simple integration of measurement-based weather data and the option for co-simulation with other tools such as Dymola or EnergyPlus via Building Controls Virtual Test Bed (BCVTB). The most promising software for achieving the research objectives as stated in 1.2 are the simulation programs TRNSYS, Dymola and BCVTB which are introduced below.

2.2.1. TRNSYS

TRNSYS is a software environment that was originally developed at the Solar Energy Laboratory at the University of Wisconsin, Madison (Klein et al. 1976) for simulating the behaviour of solar energy systems. Graphically based, the software enables general modelling and simulation of transient systems, e.g. thermal energy systems or electrical energy systems. TRNSYS comes with a standard library of about 150 system component models. Additional libraries with specific functionalities e.g. geothermal, cogeneration or HVAC equipment components are commercially available. Written in Fortran, the functionalities of TRNSYS can be extended either by modifying existing TRNSYS components or by writing additional new components. (TESS 2018)

The TRNSYS software package is comprised of the programs TRNSYS Studio, TRNBuild, TRNEXE, TRNEdit and TRNSYS3d. TRNSYS Studio (Figure 2-13) is the graphical front-end of TRNSYS in which the user graphically models a simulation problem using library components and defining the relations between them. The SketchUp plugin TRNSYS3d is used for the creation of multi-zone building envelopes which are assigned with building properties by using TRNBuild as an interface. TRNEXE is the core of TRNSYS, solving the equations and creating data output in form of output files or plots. TRNEdit allows the user to manually edit TRNSYS input files and is not part of the internal standard TRNSYS workflow. (University of Wisconsin, Madison 2017; Transsolar Energietechnik GmbH 2014)

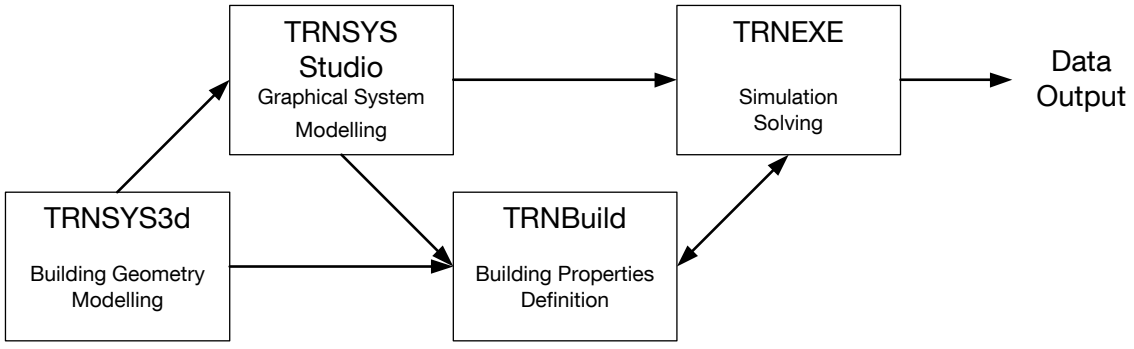

Figure 2-13: Internal TRNSYS workflow (Transsolar Energietechnik GmbH 2014)

2.2.2. DYMOLA

The simulation and modelling environment Dymola (Dassault Systèmes), originally developed by Dynasim AB, is a software which enables modelling and simulation in various fields of engineering, e.g. vehicle development, flight simulation, energy and power systems and electronic systems (Bausch-Gall 2012). Dymola is an acronym for "Dynamic Modeling Laboratory" (Elmqvist 2014). It uses Modelica, "a non-proprietary,

object-oriented, equation based language to conveniently model complex physical systems containing, e.g., mechanical, electrical, electronic, hydraulic, thermal, control, electric power or process-oriented subcomponents" (Modelica Association 2015).

The aim of the language Modelica is to enable the user to model and simulate systems which are constructed from components of diverse fields of engineering, combining mechanical, electrical, thermal, hydraulic, pneumatic and control theory. The combination of object-oriented and equation based modelling rooted in a formal, standardized modelling language facilitates a reuse of modelling knowledge and an easy exchange of models. (Bausch-Gall 2012)

This is promoted by the Modelica Association which maintains and advances Modelica as well as the open Modelica Standard Library, containing a great variety of blocks, components and models (Bausch-Gall 2012). Additionally there are various commercial and open source libraries, providing models and components for specific modelling and simulation problems: for example, the Modelica Buildings library (Wetter et al. 2014), the AixLib library (Müller et al. 2016), or the IDEAS library (Baetens et al. 2012).

Addressing a simulation problem with Dymola follows a standard workflow consisting of the steps modelling, translation and simulation (Figure 2-14). During the modelling step, the user sets up the simulation model using either a graphical or a textual approach for the definition of the model components and the relations between them. The translation step flattens, sorts and optimizes the simulation model, after which the C-code is generated and compiled. In the simulation step the model is executed and the results are post-processed for display and data output. (Fish 2017; Bausch-Gall 2012)

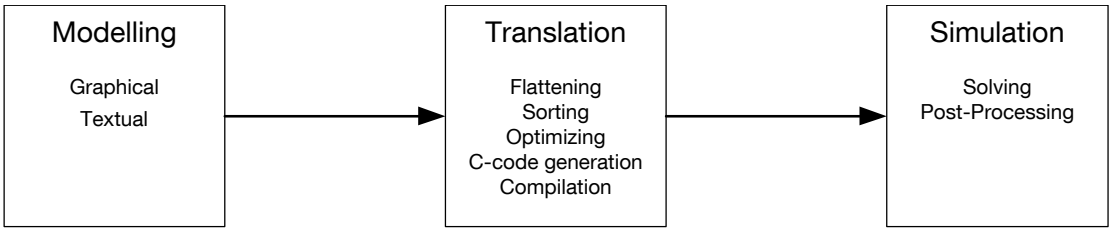

Figure 2-14: Internal Dymola workflow (Bausch-Gall 2012)

2.2.3. BCVTB

The open-source software environment BCVTB enables a co-simulation of separate, different simulation programs by coupling them and providing a method of data exchange between them during the time integration (Wetter 2011). It was developed at Lawrence Berkeley National Laboratory and is based on Ptolemy II, an actor-oriented open-source software environment for heterogeneous systems developed at the University of California, Berkeley (Brooks et al. 2008).

Complex building systems with a variety of functions often cannot be analysed by one single simulation program, since each program is designed to model and solve specific types of problems. The idea behind BCVTB is to enable the coupling of clients (simulation programs with different functionalities) to adequately address each simulation problem with the best fitting program. Ptolemy II as middleware (Figure 2-15, dotted box) links, initiates, synchronizes and stops the clients. (Wetter 2011)

At each synchronization time step the director signals the actors and manages the data exchange between them. Every client is taken care of by an actor, which specifies in a configuration file how to connect to the actor. Following the director's signal, the actors start the simulation programs and servers using the Berkeley Software Distribution Socket (BSD Socket). After reading the configuration file, the simulation program is connected to the actor via a BSD Socket through TCP/IP. The data exchange between simulation program and actor runs through this socket at each synchronization time step. When the final time is reached, Ptolemy II sends each client a flag with a value of 1 indicating the last time step, ending the simulation. (Wetter 2011)

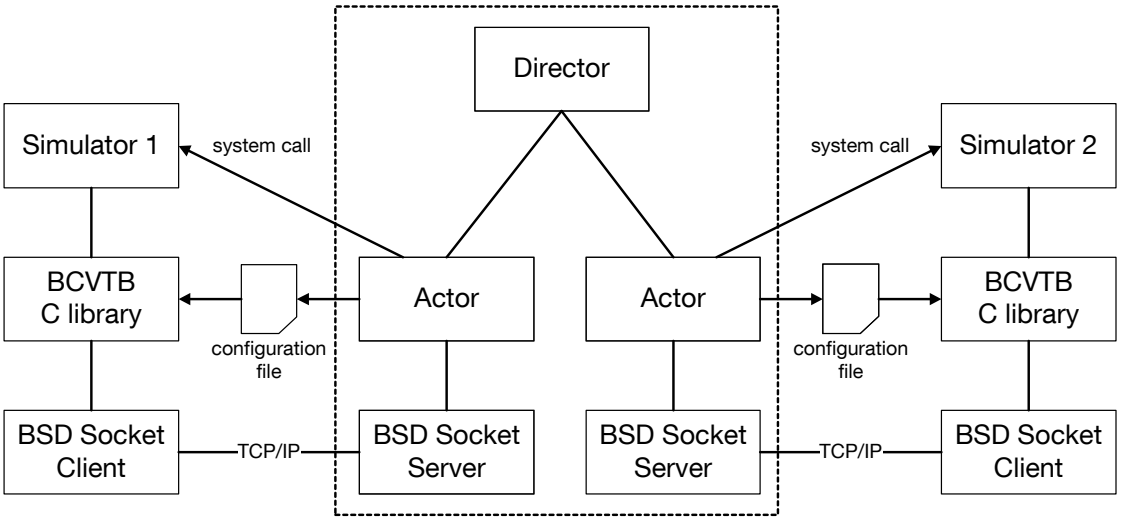

Figure 2-15: Architecture of BCVTB with the middleware Ptolemy II in the dotted box and one client on each side (Wetter 2011)

3. Methodology

Simulation tools are developed to solve specific problems in one specific field. If the boundaries of a problem are expanded, different specific qualities in a simulation tool are needed to find an adequate answer through simulation.

Modelling 5GDHCNs challenges many simulation tools (see 2.2) due to the reversible and highly dynamic flow conditions in the network compared to traditional DHNs (Heissler et al. 2017a). Additionally, detailed building services simulations are needed to provide the network with supply and demand data in high resolution. Factoring in a maximized use of volatile heat sources, very few simulation tools are able to cope with the complete simulation problem as a whole (2.2).

With regard to the complex modelling task of a 5GDHCN, a divisive approach was chosen: splitting the simulation in partial models, with each partial model to be modelled in a simulation environment best fitting to the respective requirements. Prerequisite of such an approach is the ability to enable efficient synchronization and two-way communication during a simulation run between the partial models. Additionally, interfaces in the partial models have to be defined to enable data exchange at given intervals. BCVTB (see 2.2.3) was developed for exactly this purpose: to link different simulation programs to expand the individual simulation capabilities (Wetter 2011).

As laid out in section 2.2 above, commonly used tools for building or systems simulations are either mathematically incapable of solving hydraulic mass flow reversal problems or are severely challenged by them (Heissler et al. 2016). The Modelica-based modelling and simulation environment Dymola (2.2.2), with the open-source modelling libraries Buildings (Wetter et al. 2014) and IDEAS (Baetens et al. 2012), does not have these limitations and was chosen for modelling the hydraulic network and the seasonal storage (Heissler et al. 2017a). The modelling and simulating environment TRNSYS, which is one of the most commonly used tools in building performance simulation and offers a library with a variety of different solar collectors and storage types, was chosen for the building services simulations (Heissler et al. 2017a).

For modelling a 5GDHCN, one basic requirement is model flexibility. In addition to spatial adaptability to different network layouts, the model has to be flexible to system changes, for example in the amount or the types of buildings connected to it. Combined with the complex requirements of the modelling task itself, the approach is to

split the model into three partial models: modelling the heat demand, modelling the building services engineering (TRNSYS), and modelling the network with the seasonal storage (Dymola). Additionally, communication between the models has to be enabled. Therefore a communication model is added (BCVTB). This results in four partial models within one model framework: a Heat Demand Model, a Building Services Model (BSM), an Interlink Zone, and a Network and Storage Model (NSM) (Heissler et al. 2017a). Figure 3-1 displays the layout of the framework and the connections between the partial models.

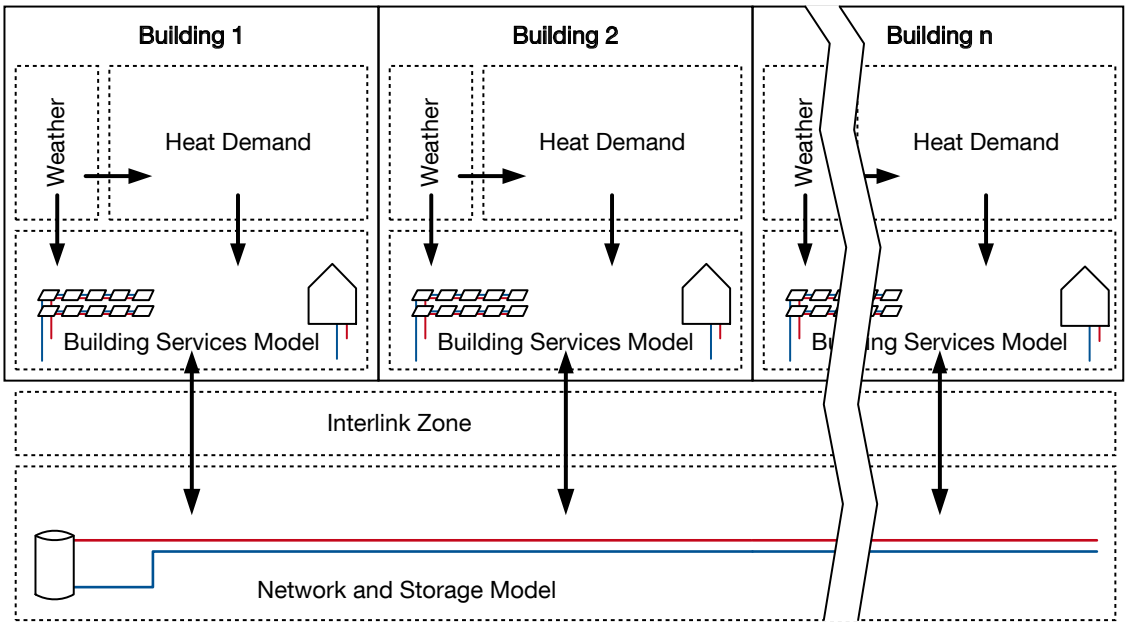

Figure 3-1: Layout of the framework and connection between the partial models (Heissler et al. 2017b)

Every BSM receives minute-based DHW and HW loads from the associated Heat Demand Model. Processed with the weather input and the current network temperatures received from the NSM via the Interlink Zone, each BSM calculates a mass flow to be received from or to be sent to the network to cover the DHW and HW loads. These values are sent via the Interlink Zone to the NSM which acts accordingly. This framework structure allows a simultaneous execution of all BSMs, the Interlink Zone, and the Network and Storage Simulation as Co-Simulation. Since the BSMs decide independently, without higher-level control, to demand heat from or to supply heat to the network, the flow conditions within the 2-line network become bidirectional and undirected. (Heissler et al. 2017b)

3.1. Building Services Model

As previously mentioned in section 2.2, TRNSYS is one of the standard tools in the field of building performance and building services modelling. The BSM constructed in TRNSYS serves the following purposes:

- Supply of the HW and DHW loads
- Gain of thermal and electrical solar energy
- Heat exchange with the 5GDHCN

The model setup of the BSM is based on a standard setup of a solar heat pump system (Braungardt et al. 2013). PVT collectors provide electrical energy and solar heat for direct and indirect use. The PVT collector, the stand-by storage, the buffer storage, the WSHP and the electric heater are the main components of the BSM (Figure 3-2) (Heissler et al. 2017a). The buffer storage and the stand-by storage are supplied with solar heat while the WSHP, the pumps, the auxiliary heater of the stand-by storage, and the electric heater are supplied with solar electricity by the PVT collector. The gap between electric energy demand and supplied solar electricity is filled by electricity from the public distribution network. The heat in the buffer storage is supplied to the WSHP or the 5GDHCN depending on the heat load at the heat pump. The 5GDHCN supplies the heat pump directly in times of low heat supply from the buffer storage.

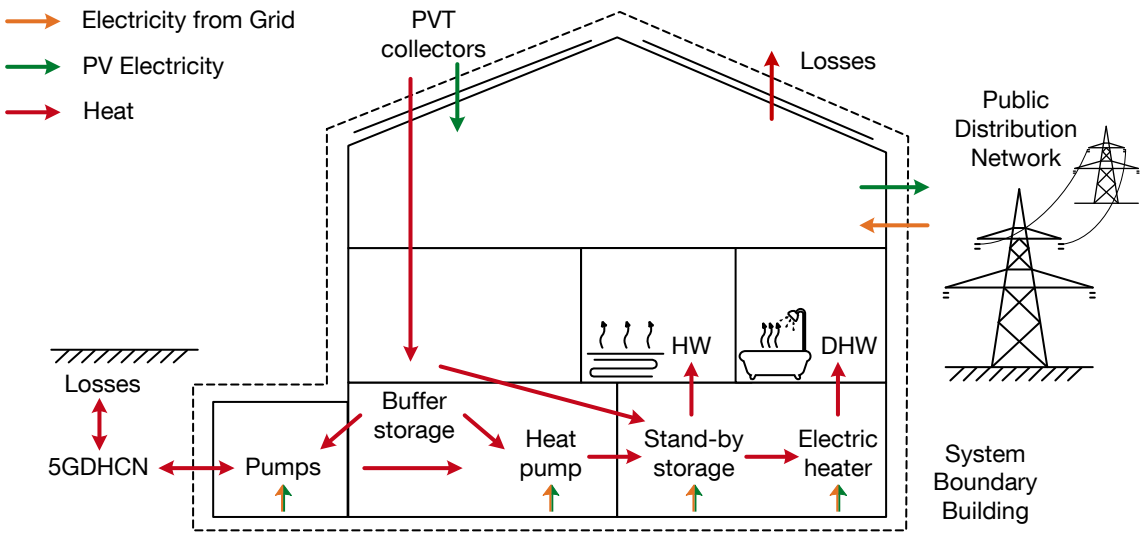

Figure 3-2: System Boundary and main components of the BSM

In addition to the direct solar heat from the PVT collectors, the heat pump supplies the stand-by storage which feeds the heating loop. The DHW demand, mainly covered by

using the heating loop for preheating, is met by decentralized electrical heaters which ensure the keeping of the predefined supply temperature level. (Heissler et al. 2017b)

The BSM also keeps the balance of electric energy gains and demand. Every time step the electric energy demand of the pumps is submitted from the associated Building Simulation Interface (BSI) to its BSM (see also 3.3.2). With the other local electric energy demand of the BSM for heat pumps, auxiliary heaters and decentralized electrical heaters, it is totalled and set against the local electric energy gains from the PVT collectors in this time step. For the yearly balance all time steps with surpluses and all time steps with shortfalls are totalled.

The model structure allows a parametric adaptation of the BSM (collector area, thermal storage sizes, number of heat pumps, etc.) depending on the total heat demand, the maximum heat demand and the heated living space. The BSM consists of four main loops: solar loop, heating loop, secondary heat pump loop, and primary heat pump loop (Figure 3-3). Circulation and storage losses as well as the auxiliary power demand for pumps within the BSM are not considered. The aim of the BSM design is to meet the local heat demand of the building and use the 5GDHCN as a secondary level of thermal storage. (Heissler et al. 2017b)

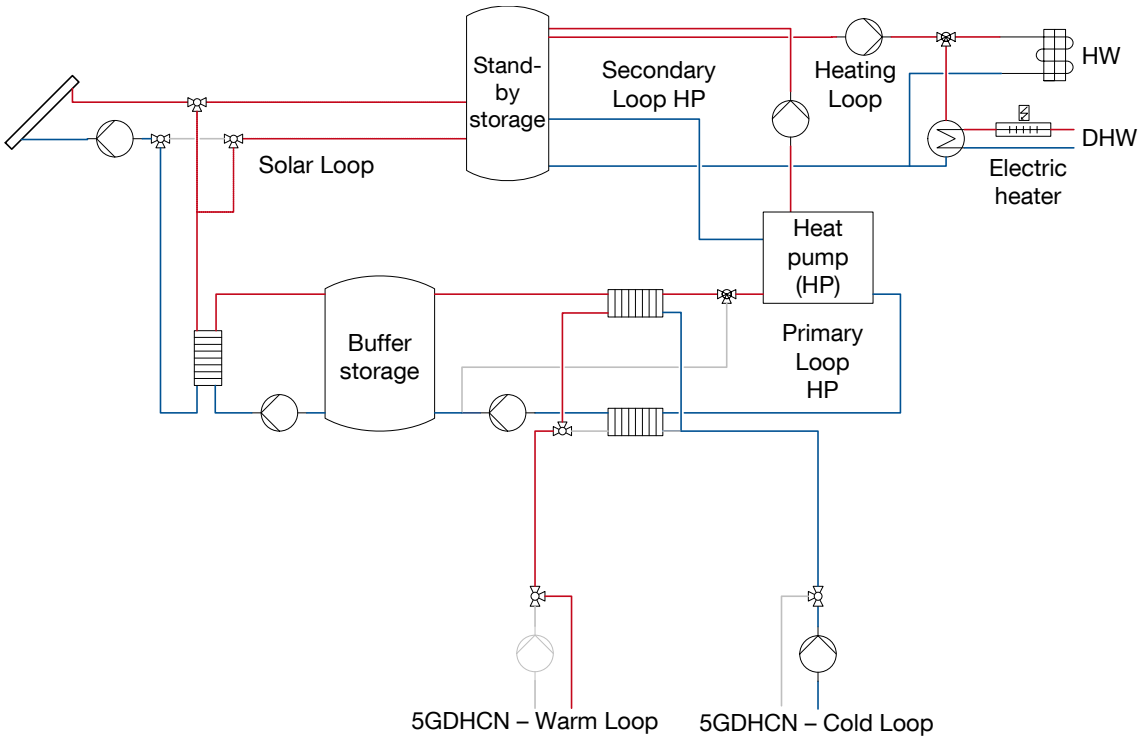

Figure 3-3: BSM schematic 5GDHCN (Heissler et al. 2017a)

3.1.1. Solar Loop

Buffer storage and stand-by storage are connected with the solar collector through the solar loop. The outlet fluid temperature of the collector is controlled by varying the fluid flowrate through the collector depending on the destination of the fluid (buffer storage or stand-by storage). The set temperature (T_{set}) is 50 °C if the stand-by storage is the fluid destination. With the buffer storage as destination of the fluid, T_{set} is defined to be 10 K above the collector inlet temperature with a maximum of 40 °C. (Heissler et al. 2017b)

As described in Heissler et al. (2017b), the implemented controls are:

Seasonal priority: During summertime (April – October) the stand-by storage has charging priority. During wintertime (November – March) the buffer storage is primarily charged, since the collector power during wintertime is not high enough to heat the fluid to the stand-by storage temperature level.

Full stand-by storage: If the stand-by storage is fully charged and it is summertime, the seasonal priority control is overridden and the buffer storage is charged.

Secondary use of return line: If the return line temperature of the stand-by storage during charging is above the lowest temperature level of the buffer storage, the return line is routed through the buffer storage to utilize the residual heat and increase the collector efficiency.

Table B-1 (Appendix) lists the most important TRNSYS types used in the solar loop of the BSM. Listed below are the parameters used in the solar loop of the BSM:

- Collector: azimuth 20°, inclination 35°, cell efficiency 0,1 (for further details see Table B-2)
- Pump: controlled by iterative feedback controller, variable flow rate to meet a set temperature difference (ΔT), maximum flow rate scalable depending on floor space
- Buffer storage: 20-node tank, variable inlet positions, no heat losses
- Stand-by storage: 100-node tank, variable inlet positions, no heat losses
- Array Shading: four rows, collector row separation 2,96 m, collector height 1 m

3.1.2. Heating Loop and Secondary Loop

The stand-by storage supplies the heating loop which covers the heating demand of the building and the preheating demand of the hot water tapping stations (Figure 3-4). The average supply temperature of the heating loop is 45°C. The cold drinking water is locally preheated to about 40 °C through a heat exchanger in the tapping station which is fed by the heating loop (Mercker and Arnold 2017). On top of that an electrical heater raises the temperature to the defined set temperature (T_{tap}) of 45 °C (Zvingilaite et al. 2012; Østergaard and Andersen 2016) or 60 °C, depending on the simulation scenario. Table B-3 lists the most important TRNSYS types used in the heating loop of the BSM.

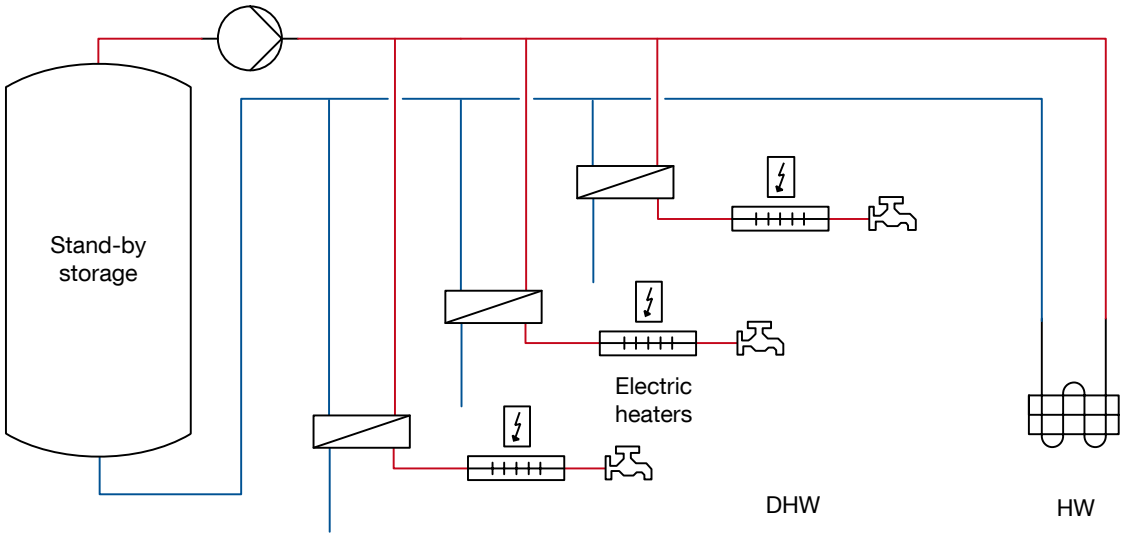

Figure 3-4: Schematic of the heating loop in the BSM

Every simulation time step the HW load (Q_{dot_HW}) and the DHW load (Q_{dot_DHW}) (4.2) are fed to the BSM. Following Weber (2007)

$$\dot{Q} = c_{H_2O} \cdot \dot{m} \cdot \Delta T \qquad (3\text{-}1)$$

the corresponding mass flow (m_{dot}) with the specific heat capacity (c_{H_2O}) and the predefined temperature difference ΔT between flow and return loads are calculated from Q_{dot_HW} and Q_{dot_DHW}. The temperature difference ΔT_{HW} assumed for the HW load is 15 K (Doetsch and Bargel 2009), the temperature difference ΔT_{DHW} for the DHW load is 35 K or 50 K based on the assumption of an average water main temperature (T_{main}) of 10 °C and a defined DHW set temperature T_{tap} of 45 °C or 60 °C.

For meeting the HW load, the stand-by storage is tapped from the top with the HW load mass flow (m_{dot_HW}) by which Q_{dot_HW} is imposed on the stand-by storage. For

meeting the domestic hot water load, the stand-by storage is also tapped from the top with the DHW load mass flow (m_dot_DHW) which is fed to the primary side of a heat exchanger (Figure 3-4). On the secondary side, the heat exchanger is fed with the same mass flow m_dot_DHW with the temperature T_main which is preheated and subsequently raised to tapping temperature T_tap by the electric heater.

Central to the BSM is the stand-by storage. It connects the solar loop, the heating loop, and the secondary loop of the heat pump. If the heat provided by the collector is not sufficient to meet the HW and DHW loads, the heat pump recharges the stand-by storage via the secondary loop. The stand-by storage is a stratified thermal storage tank with five temperature sensors (TS) and five double ports which allow for a stratified charging of the storage (Figure 3-5). The TS are installed at the bottom and the top of the thermal storage (TS1 and TS5) and in steps of fourths (TS2, TS3, TS4) of the storage height. The collector, the heat pump and the auxiliary heater have charging priority in descending order. (Heissler et al. 2017b)

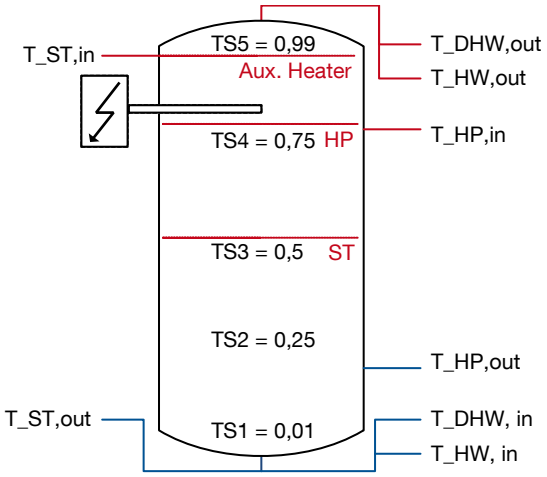

Figure 3-5: Schematic of the stratified stand-by storage with temperature sensor heights (Heissler et al. 2017b)

The controller of the solar loop monitors the temperature at the bottom of the storage (TS1). For temperatures below 45 °C the storage is charged, if allowed by the collector temperatures. Additionally the heat pump charges the stand-by storage at 45.5 °C if the temperature at TS4 (summer) or TS3 (winter) falls below 42.5 °C. If the joint heat supply of collector and heat pump does not suffice and the temperature at TS5 drops below 36 °C, the auxiliary heater heats the highest storage layer (TS5) to 40 °C. (Heissler et al. 2017b)

The TRNSYS types used in the secondary loop are shown in the Appendix in Table B-4.

3.1.3. Primary Loop

The primary loop of the heat pump supplies it with low-temperature heat coming from the buffer storage or the 5GDHCN. The buffer storage, which is a stratified thermal storage, buffers low-temperature solar heat to enable a time-shift supply of the heat pump or a discharge into the 5GDHCN. As mentioned above (3.1.1), the primary charging mode of the solar collector during wintertime is charging the buffer storage. During summertime the return of the stand-by storage is routed through the buffer storage if the temperature level of the return line of the stand-by storage is high enough to allow for an additional use of ultra-low-temperature heat. (Heissler et al. 2017b)

If the buffer storage cannot provide sufficient heat to meet the heat demand of the heat pump, the 5GDHCN provides the additional heat needed. Depending on the momentary temperature level of the network, the heat can be transferred to the primary loop via heat exchangers to the flow or return line of the heat pump. The buffer storage is charged by the solar collector. If the storage reaches a temperature at the bottom of 23 °C (summer) or 31 °C (winter), it is discharged into the warm loop of the 5GDHCN via the primary loop. (Heissler et al. 2017b)

Limiting cases are the overheating or undercooling of the 5GDHCN. For the former, the primary loop is disconnected form the 5GDHCN. The flow to the heat pump is cooled to a maximum temperature of 25 °C through bypassing the buffer storage and re-circling the return of the heat pump and thus preventing an overheating of the heat pump. For the latter, the primary loop is also disconnected from the 5GDHCN. If the buffer storage cannot supply a minimum temperature higher than 4 °C, the pump of the primary loop as well as the heat pump are disabled. This can lead to a cooling down of the stand-by storage temperature and therefore to an activation of the auxiliary heater. (Heissler et al. 2017b)

The TRNSYS types used in the primary loop are listed in Table B-5.

3.2. Interlink Zone

The Interlink Zone, modelled in BCVTB, initiates, links and synchronizes the partial models BSM and NSM in the simulation environments TRNSYS and Dymola and thus enables a Co-Simulation of the partial models. The Interlink Zone only routes and transports the simulation data; the data content of the data transported remains unchanged.

As described in the beginning of chapter 3, the Modelica environment Dymola sends one data vector to BCVTB (Figure 3-6) every data exchange cycle. This vector is comprised of the variables which have to be transported to the BSMs (TRNSYS) (see also 3.3.1). The vector elements are either components of global variables to be distributed to all BSMs (represented by the blue lines in Figure 3-6) or components of local variables only relevant to one of the BSMs. The Interlink Zone deconstructs the received vector into its components, regroups the components according to their destination, and vectorises them again. The newly constructed vectors are sent to the respective BSM and are processed there. (Heissler et al. 2017b)

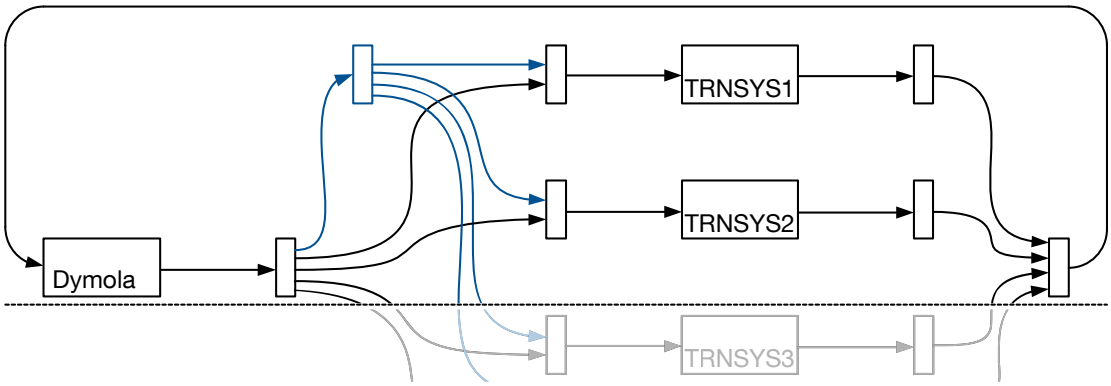

Figure 3-6: BCVTB schematic (Wetter 2011)

In the opposite direction, the data vectors coming from the BSMs are deconstructed at the same time and revectorised to one vector which is sent to Dymola for processing. This data exchange cycle is triggered every minute of simulation time by the Interlink Zone and is matched to the simulation models with the biggest simulation time steps which are the BSMs.

3.3. Network and Storage Model

Based on the state of the art (2.1), the model of the hydraulic network is constructed as a two-line, bidirectional, undirected 5GDHCN. Combined with a seasonal storage capacity, this layout enables the network user to shift low-temperature heat spatially and temporally. With this system surplus, solar heat collected during summertime can be made available and used in winter. (Heissler et al. 2017b)

Figure 3-7 displays an exemplary setup of a two-line, bidirectional, and undirected 5GDHCN with a borehole heat exchanger as seasonal storage.

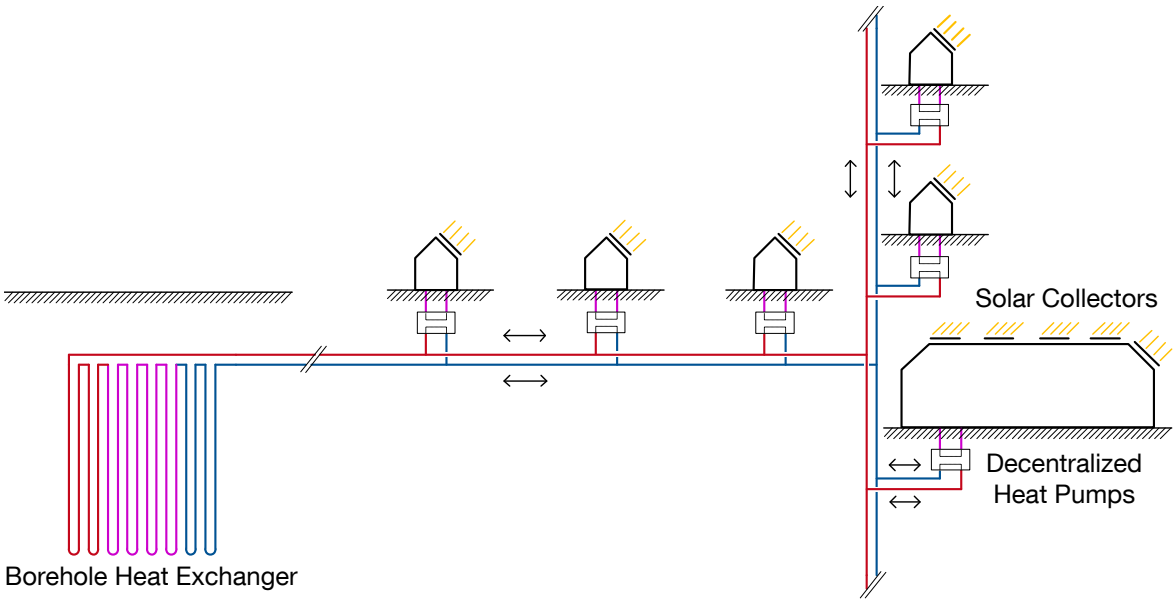

Figure 3-7: 5GDHCN with decentralized heat pumps and a borehole heat exchanger (Heissler et al. 2017b)

The limit to the maximum seasonal transfer of heat is set by the storage capacity of the seasonal storage. Either single buildings or groups of buildings are connected to the network via BSIs. Depending on the time of day or the time of year, each BSI can act as a heat source or a heat sink. If there is a local surplus of heat, the BSI draws the heat transfer fluid from the cold line, transfers the surplus heat into the fluid, and discharges the fluid into the warm line. If there is a local demand for heat, the opposite process occurs (Figure 3-8). (Heissler et al. 2017b)

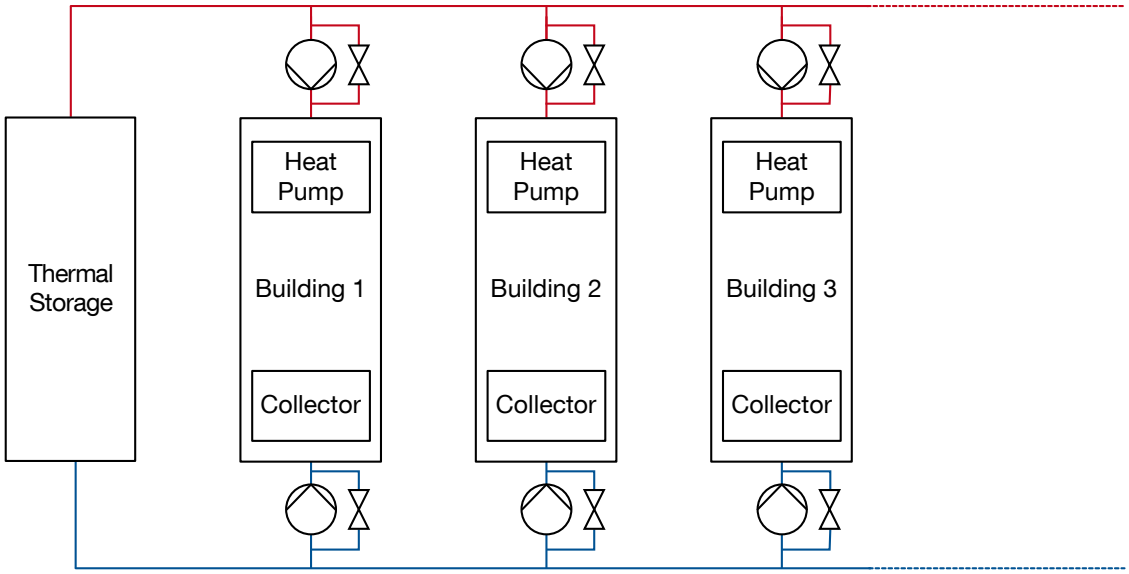

Figure 3-8: Hydraulic setup of a 5GDHCN (Heissler et al. 2017b)

In sum, the amounts of fluid locally transported add up to a pressure difference between the cold and warm lines of the network. The seasonal storage is a hydraulic short circuit between the two lines and facilitates, through compensating the pressure difference, the hydraulic balance. This effect automatically charges or discharges the seasonal storage. Since the flow direction of the fluid within each BSI is only dependent on the respective local energy supply and demand, there is no predefined flow direction in the network. The resulting self-adjusting, complex hydraulic condition is bidirectional and undirected. (Heissler et al. 2017b)

As described in Heissler et al. (2017b), the construction of the NSM within the Modelica environment Dymola is based on components from the IDEAS library (Baetens et al. 2012), the Buildings library (Wetter et al. 2014), and the standard Modelica Library (Modelica Association 2015). The main components of the NSM (Figure 3-9) are

- the BCVTB-Interface (3.3.1),
- the BUS-System (3.3.1),
- the BSIs (3.3.2),
- the Piping Model (3.3.3) and
- the Seasonal Storage (3.3.4).

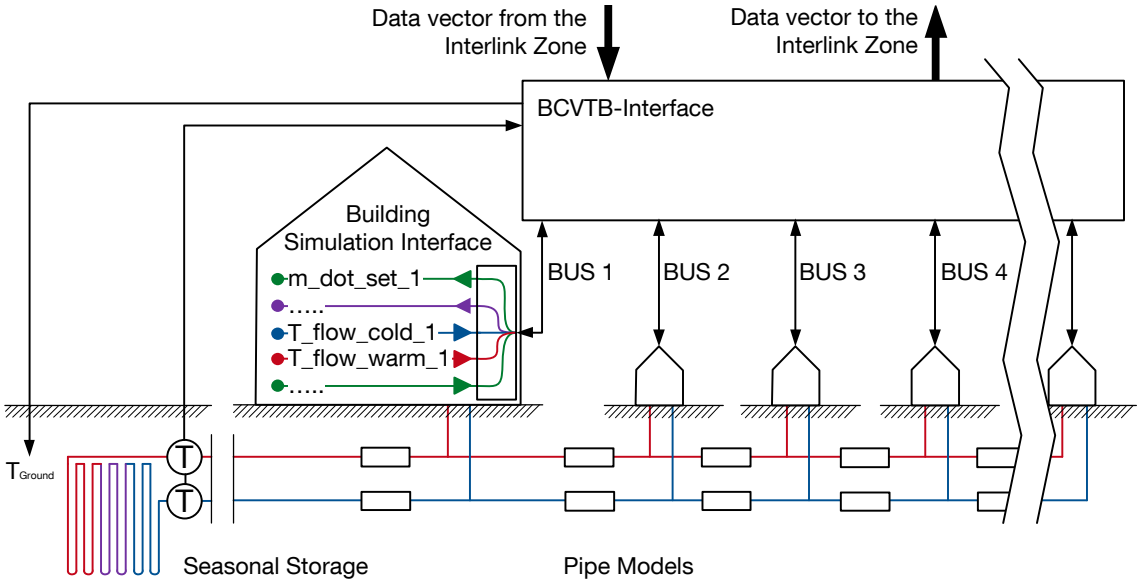

Figure 3-9: NSM schematic BSI (Heissler et al. 2017b)

3.3.1. BCVTB Interface and BUS-System

The BCVTB-Interface, as part of the NSM, processes and routes the incoming and outgoing data vectors as well as the global variables and the data busses (Figure 3-10).

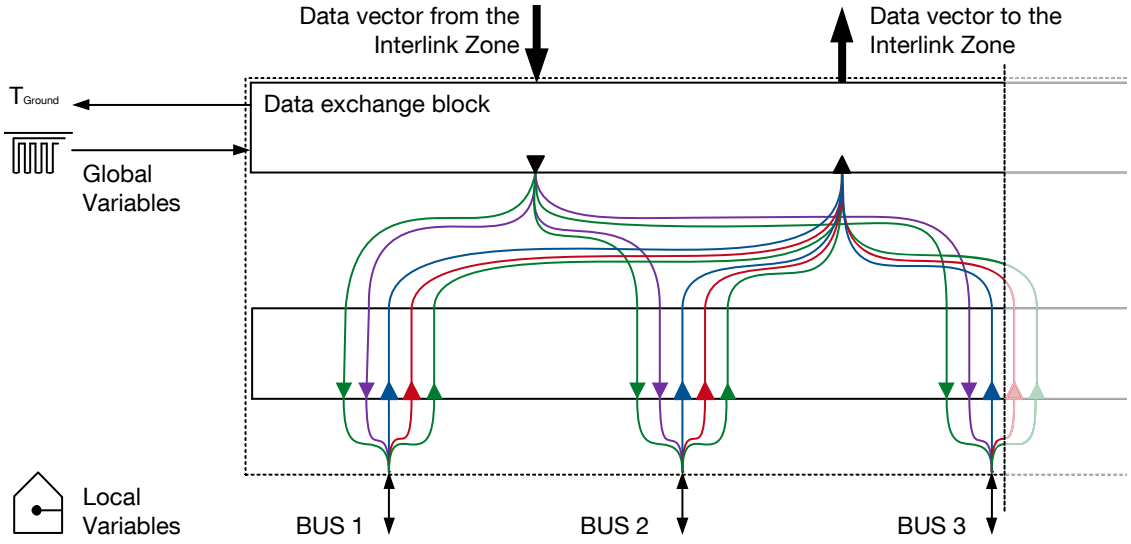

Figure 3-10: Setup of the BCVTB Interface

The Buildings Library (Wetter et al. 2014) contains a configurable data exchange block which enables a data exchange between Dymola and BCVTB. This data exchange block is able to send and receive data vectors from inside the simulation environment Dymola to an external destination (Wetter 2011).

Every data exchange cycle the variables to be sent are combined by the data exchange block to one outgoing data vector which is transmitted to the Interlink Zone in BCVTB. At the same time the incoming data vector is deconstructed into its components by the data exchange block. These components are either local or global variables (see 3.2).

Global variables are defined to be variables which are determined at specific points in any model of the framework, but are relevant to the whole model. Examples are the hot and cold side temperatures of the seasonal storage or the ground temperature (T_{ground}).

Local variables are defined to be variables which are determined locally and are only relevant to the associated model in another part of the framework. Examples are the variables which are exchanged between each BSI and its associated BSM.

The BCVTB-Interface makes the incoming global variables from BCVTB available to the entire NSM. Local variables are routed to the associated data busses by connecting the single components of the particular data bus, according to their direction and position, to the incoming and outgoing data vector. Thus the bus system facilitates an efficient two-way communication of the BCVTB-Interface with each BSI.

3.3.2. Building Simulation Interface

The function of each Building Simulation Interface (BSI) is to connect its associated BSM to the NSM. The BSI applies the simulation values determined in the BSM to the NSM and vice versa. It is not within the range of functions of the available simulation environment TRNSYS to determine the state variable of pressure. Therefore pressure differences are not accounted for within the BSM. Thus the BSI is also an interface between the pressureless simulation in TRNSYS and the pressurized simulation in Dymola.

The two-line network in the NSM is constructed as a closed fluid loop. Changes in pressure are therefore able to travel through the network. Pumps which transport fluid from one line to the other change the network pressure on the suction-side as well as the pressure-side. The resulting interaction of all pumps connected to the network and the occurring pressure differences within the perfused pipes determine the cumulative state of flow of the network (Figure 3-8).

The heat transfer in and out of the network is achieved through countercurrent heat exchangers in the BSIs (Figure 3-11). This way the network and the fluid loops of the buildings are hydraulically separate. Since these heat exchangers only serve the purpose of connecting the two simulation environments TRNSYS and Dymola, but must not have any influence on the amount of heat transferred, they are modelled as ideal heat exchangers with a constant heat exchanger effectiveness of one. The primary sides of the heat exchangers are the sides of the network loops. The flow on both the primary and the secondary side of the heat exchangers is defined by the associated BSM in TRNSYS.

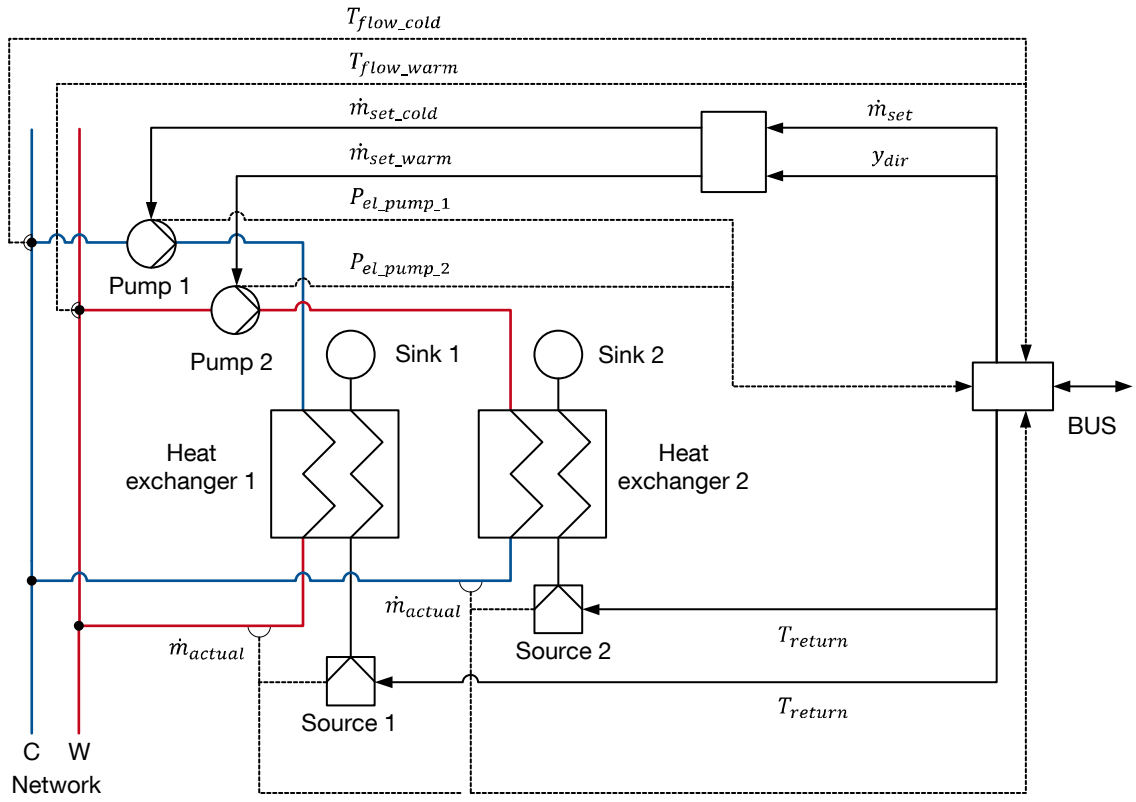

Figure 3-11: Functional schematic of a BSI in the NSM for a simulation of 5GDHCN

As described in the beginning of chapter 3 the BSM determines the set mass flow (m_dot_set) and the direction of the set mass flow (y_dir). It also determines the corresponding return temperature (T_return) based on the flow temperatures of cold (T_flow_cold) and hot line (T_flow_warm), measured at the warm and cold connection point between the BSI to the network, and the flow direction (Figure 3-3). Below the partial steps within one time step are presented:

Pumps 1 and 2 with prescribed mass flow rate define the flow through the primary sides of the heat exchangers. The set values of the pumps (m_dot_set_cold, m_dot_set_warm) are calculated from m_dot_set and y_dir coming from the associated BSM.

A state of control with $m\_dot\_set\_cold > 0$ and $m\_dot\_set\_warm > 0$ simultaneously does not exist.

For $m\_dot\_set\_warm > 0$, fluid from the warm line of the network is pumped through the primary side of heat exchanger 2 into the cold line. At the outlet of heat exchanger 2 the actual mass flow (m_dot_actual) is measured. For $m\_dot\_actual > 0$ source block 2 replicates m_dot_actual with a temperature of T_return and feeds the secondary side of heat exchanger 2.

The fluid model used is a simplified liquid water model with the assumption of incompressibility and constant data (Modelica Association 2015). Since the heat exchangers are modelled as ideal heat exchangers in countercurrent mode, the temperatures between primary and secondary side are fully exchanged, which leads, in combination with the simplified fluid model, to a complete exchange of heat in or out of the hydraulically closed loop of the NSM.

The pumping power of pumps 1 and 2 is determined each time step on the basis of volume flow, pressure difference overcome and efficiency factors for motor and hydraulic efficiency of 0.7 (Wetter et al. 2014; Modelica Association 2015). For determining the pump energy demand, 60 second mean power values are sent to the associated BSM. Table 3-1 lists the signals of the data bus which connects each BSI with the BCVTB Interface.

Table 3-1: Data bus signals of a BSI

Direction TRNSYS → Dymola		Direction Dymola → TRNSYS	
Variable	**Name**	**Variable**	**Name**
Set mass flow	m_dot_set	Actual mass flow	m_dot_actual
Direction of set mass flow	y_dir	Flow temperature (warm)	T_flow_warm
Return temperature	T_return	Flow temperature (cold)	T_flow_cold
		Electric pumping power (pump 1)	$P\_el\_pump\_1$
		Electric pumping power (pump 2)	$P\_el\_pump\_2$

3.3.3. Piping Model

The piping model described by Heissler et al. (2017b) and used in the NSM is based on the structure of commercially available DHN polymer piping (Rehau 2011). The pipe is surrounded by an insulation layer of polyurethane. Since the thickness of the pipe wall (15 mm) is very small compared to the thickness of the pipe insulation (Figure 3-12), a thermal conductivity of 0.03 °W/m.K is assumed for both materials. The ground surrounding the piping is modelled as a layer with a thickness of 1 m with a thermal conductivity (λ_ground) and a specific heat capacity (c_ground). Furthermore, the influence of the heat capacities of pipe and insulation are not taken into account since they are very small compared to the heat capacity of the surrounding ground. Also not accounted for is the reciprocal influence between warm and cold line. Inner boundary condition is the temperature of the fluid (T_fluid). Outer boundary condition is the seasonally fluctuating undisturbed ground temperature T_ground. (Heissler et al. 2017b)

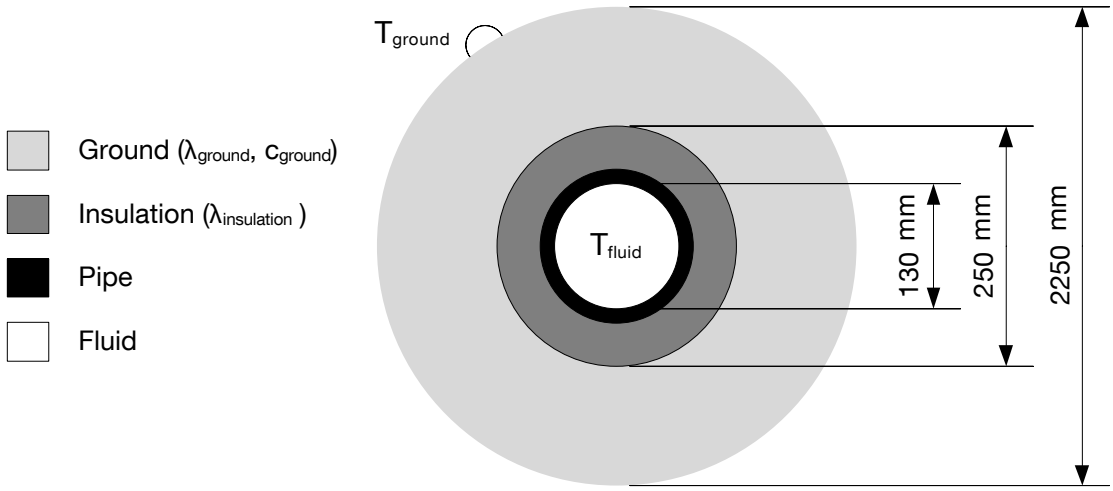

Figure 3-12: Cross-section piping model in mm (not true to scale) (Heissler et al. 2017b)

Assuming no thermal capacity of the hollow pipe and insulation cylinder itself, the heat flow through its wall according to VDI-Wärmeatlas (2002) is defined as:

$$\dot{Q} = \lambda \cdot \frac{2\pi l}{ln\, r_a - ln\, r_i} \cdot (T_i - T_a) \qquad (3\text{-}2)$$

with $T\_i = T\_fluid$ as inner wall temperature, T_a as outer wall temperature of the pipe insulation, λ as thermal conductivity of the wall ($\lambda\_insulation$), l as length, r_i as inner and r_a as outer radius of the hollow cylinder. The heat flow through the pipe wall and the pipe insulation is determined by Equation 3-2.

Analogously, the heat flow through the surrounding ground layer is calculated based on the temperature difference between T_a and undisturbed ground temperature

T_ground. However, here the ground layer not only features a thermal conductivity λ_ground but also a heat capacity c_ground (Figure 3-13). Therefore each simulation time step the heat flux is determined under consideration of the concentric layout and the instationary thermal behaviour caused by the heat capacity of the surrounding ground layer. The thermal conductivity, density and heat capacity of the ground are considered to be constant.

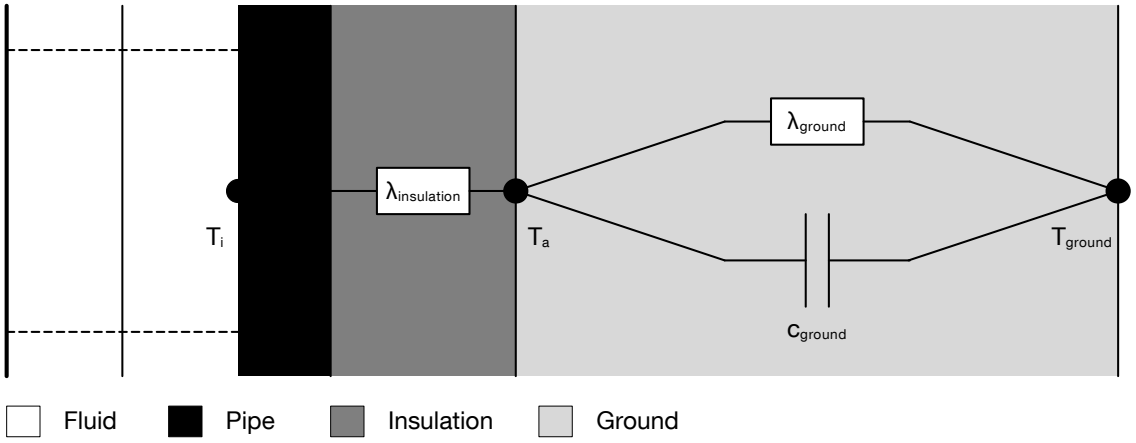

Figure 3-13: Schematic of pipe and ground model

The pressure difference in each pipe segment is calculated each time step on the basis of the actual mass flow through the segment, its length and pipe diameter, with a transition from laminar to turbulent flow at a Reynolds number of 4000, following the pipe model provided in the Modelica Buildings library. (Wetter et al. 2014)

3.3.4. Seasonal Storage

The hydraulic balance between warm and cold lines is established through the seasonal storage (Heissler et al. 2017b) (see Figure 3-8). On the basis of 2.1.3 and 2.1.4, a borefield heat exchanger implemented as a hybrid step response model (Picard and Helsen 2014) is chosen as seasonal storage. The hybrid structure of the model, comprised of a long-term and a short-term model, allows for a high accuracy of long-term as well as short-term simulations. Therefore it is suitable for minute- and year-based simulations (Picard and Helsen 2014). The basic configuration of the borefield heat exchanger is a 8 m*8 m square with a borehole depth of 110 m, 5.5 m distance between the boreholes, and sandstone as surrounding ground. The adaptation of the storage capacity is achieved by a multiplication of the basic configuration, not taking into account resulting additional storage effects. (Heissler et al. 2017b)

3.4. Traditional district heating network model

To enable an evaluation of the performance of 5GDHCNs, a point of reference is required. The point of reference chosen is a traditional DHN similarly modelled to the NSM (3.3). The hydraulic network is constructed as a two-line, unidirectional, directed DHN. Figure 3-14 displays an exemplary setup of such a network.

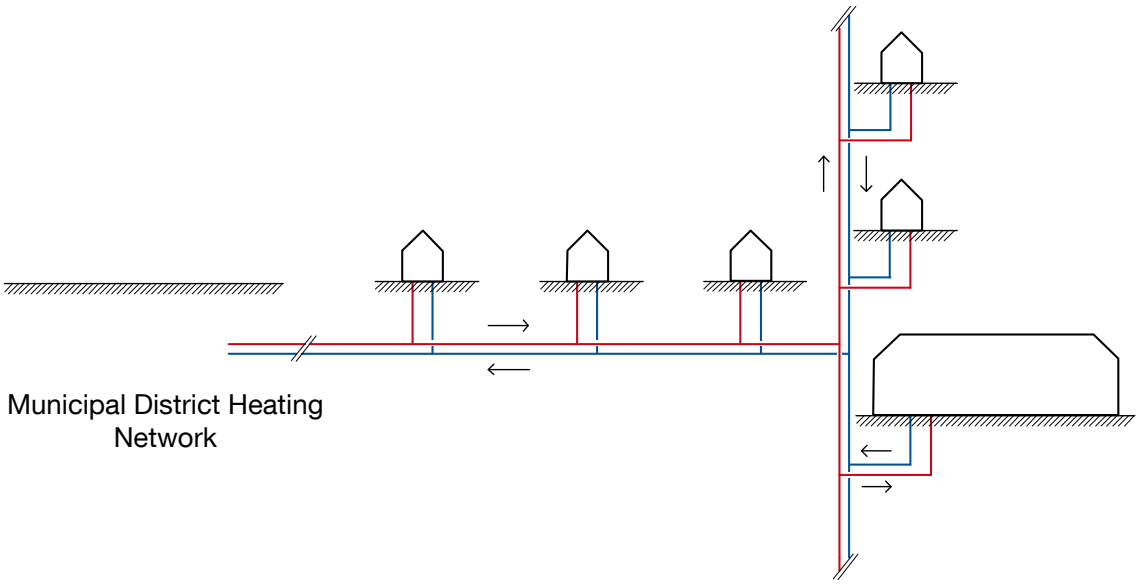

Figure 3-14: Traditional District Heating Network (Heissler et al. 2017b)

Since it is a unidirectional DHN, there is only heat transfer from one central supplier via the network to the buildings. Similar to the model shown in 3.3, single buildings or groups of buildings are connected to the network via DHN-BSIs. Each of these can only act as a heat sink. If there is a local heat demand, the DHN-BSI draws the heat transfer fluid from the warm line, transfers the heat required from the fluid, and discharges the fluid into the cold line. (Heissler et al. 2017b)

One major difference to the NSM described in 3.3 is the pressure setup. In contrast to 3.3, here the pressure difference between supply and return line is created and maintained by central pumps at the heat source (Figure 3-15).

A survey among utility companies (Robbi 2013) found that the upper limit of supply temperatures in DHNs lies between 70 °C and 150 °C with maximum return temperatures between 50 °C and 75 °C. On this basis the temperatures in the model were set at 100 °C as supply temperature, 70 °C as minimum supply temperature, and 65 °C as average return temperature. The pressure difference at the heat source between the warm and cold lines is set at 10 bar.

Especially during the summer months, the heat demand and the masses transported are low. In conjunction with a high temperature difference between fluid and surrounding ground, this leads to increased heat losses and a significant cooling down of the supply side. However, security of supply has to be ensured at all times. Therefore it is common practice to short-circuit the end pieces of the pipes to guarantee a minimum flow turnover and thus a minimum supply temperature at the end of the pipes (Schmirler 6/29/2018). Since the extent of the network examined in this work is very small, a permanent short circuit of the end pieces would render the model invalid and falsify the simulation results. (Heissler et al. 2017b)

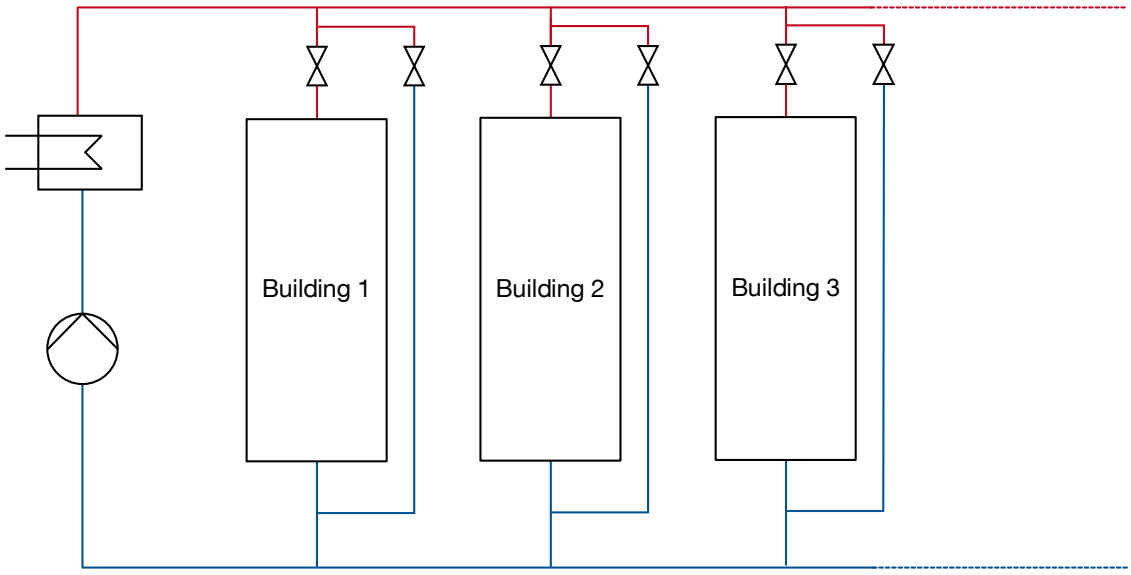

Figure 3-15: Hydaulic setup of a traditional district heating network (Heissler et al. 2017b)

Instead, an approach of controlled short circuits was chosen, where each DHN-BSI maintains a minimum supply temperature by short-circuiting the feed and the return line as soon as the temperature on the supply side drops below 68 °C. A hysteresis control closes the short-circuit valve once a temperature of 72 °C has been reached on the supply side. This ensures 70 °C as the minimum supply temperature at all times.

A similar model structure to the model of the 5GDHCN allows the use of some components described in 3.3:

- the BCVTB-Interface (3.3.1),
- the BUS-System (3.3.1) and
- the Piping Model (3.3.3).

As described above, the pressure difference between the flow and return lines is maintained by central pumps at the heat source. Therefore each DHN-BSI (Figure 3-16) is equipped with two valves which set the mass flow through the building bypass (m_dot_actual_byp, y_byp) (Valve 1) or to the building (y_set) (Valve 2). Each valve is governed by a PID controller which adjusts the control signal to the valve to maintain a requested mass flow. When activated by the hysteresis (Hyst 1), the mass flow through the bypass is set constant at 0.1 kg/s. The mass flow to the building m_dot_set_warm is set by the DHN BSM in TRNSYS.

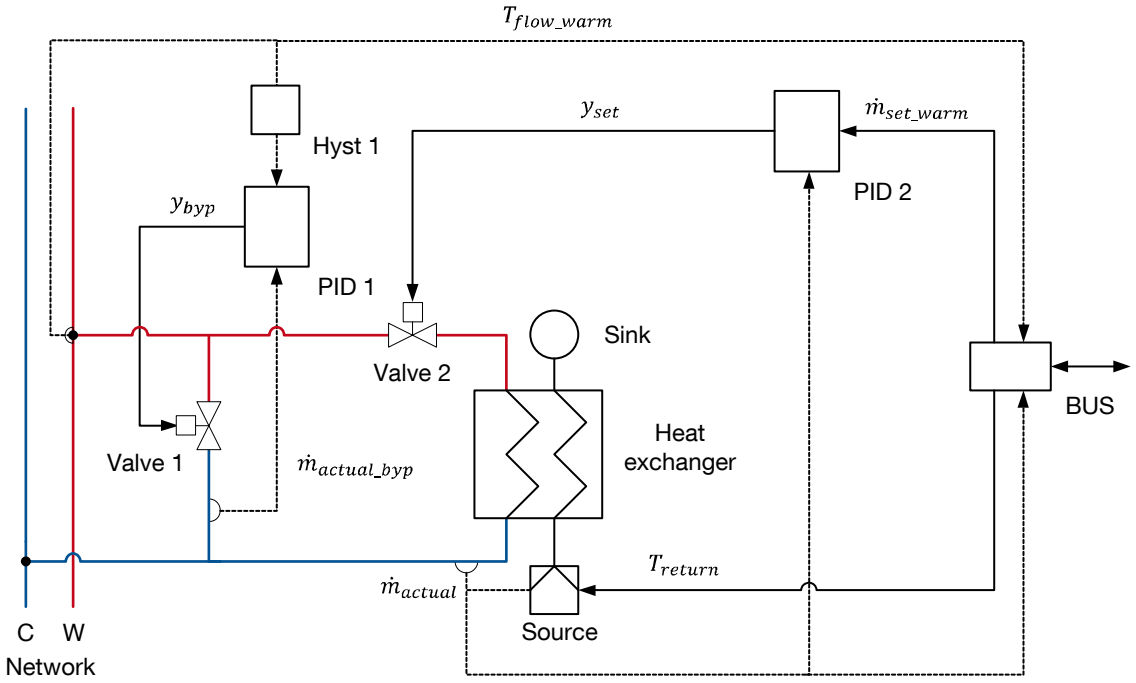

Figure 3-16: Functional schematic of a DHN-BSI

Similar to the model in 3.3.2, the heat transfer out of the network is achieved through one ideal countercurrent heat exchanger in the DHN-BSI (Figure 3-16). For $\mathrm{m\_dot\_set\_warm} > 0$, fluid from the warm line of the network flows via valve 2 through the primary side of the heat exchanger into the cold line. m_dot_actual is measured at the outlet of the heat exchanger. For $\mathrm{m\_dot\_actual} > 0$, the source block replicates m_dot_actual with a temperature of T_return and feeds the secondary side of heat exchanger 2. Thus heat is transferred out of the network.

Also similar to the model in 3.3.2, the fluid model used is a simplified liquid water model with the assumption of incompressibility and constant data (Modelica Association 2015). Since the heat exchanger is modelled as an ideal heat exchanger in countercurrent mode, the temperatures between primary and secondary sides are fully ex-

changed, which leads, in combination with the simplified fluid model, to a complete exchange of heat in or out of the hydraulically closed loop of the DHN model.

Table 3-2 lists the signals of the data bus which connects each DHN-BSI with the BCVTB Interface.

Table 3-2: Data bus signals of a DHN-BSI

Direction TRNSYS → Dymola		Direction Dymola → TRNSYS	
Variable	**Name**	**Variable**	**Name**
set mass flow	m_dot_set_warm	actual mass flow	m_dot_actual
return temperature	T_return	flow temperature (warm)	T_flow_warm

Compared with the BSM (3.1), the DHN BSM, also constructed in TRNSYS, is less complex. Its tasks are limited to the supply of HW and DHW loads through the heating loop and the heat exchange with the DHN. The heating loop is very similar to the heating loop described in 3.1.2, with two major differences:

- The volume of the stand-by storage is 3 m³. It only serves as short-time buffer and is charged from the DHN to maintain a temperature minimum of 50 °C.
- There are no electric heaters, since the DHN ensures a high enough supply temperature at all times.

Table B-6 lists the most important types used in the DHN BSM.

4. Simulation

This chapter introduces the simulation fundamentals: for example, the case study chosen and the different simulation scenarios. On the basis of the location and the boundary conditions, the model framework described above is applied. The focus of the investigation is the behaviour of the 5GDHCNs under different conditions such as different network typologies, heat demand densities, heat sources, or insulation thicknesses of the piping. All simulations are two-year simulations with the second year as the time period in the focus of the investigation to minimize the influence of the initial conditions.

4.1. Case Study: Ecological Model Settlement

In larger German cities, new city quarters in conversion areas are currently under development, conversion areas which were formerly appropriated for official use only. In the eastern part of Munich a 30 hectar area of the former Prince-Eugen barracks is currently under development for 1800 flats. An ecological model settlement of approximately 450 flats is being built in the southern part (Figure 4-1), with an intensified use of wood as raw material. (Heissler et al. 2017b)

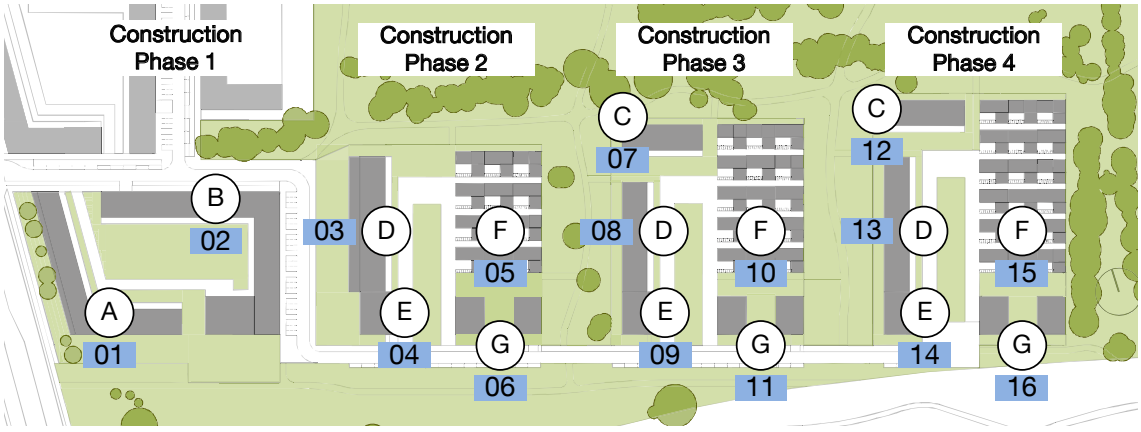

Figure 4-1: Land-use plan (section) of the ecological model settlement with building types (A-G), building numbers (01-16) and construction phases, not to scale, (Heissler et al. 2017b)

The section of the land-use plan of the area (Figure 4-1) displays the plan of development in four construction phases, the associated numbering of the building interfaces, as well as the respective building types. The ecological model settlement is comprised of different urban building types such as point buildings (building types E, G) and block buildings (building types A, B, D), multi-storey residential buildings, and concen-

trated tract housing of single family homes (building types C, F). Table B-7 in Appendix B displays the number of floors and living area per building and construction phase which results in a total Floor Area Ratio (FAR) of 1.34. (Heissler et al. 2017b)

Due to the recency and the typical basic conditions, the envisaged development of the ecological model settlement serves as a case study. On this basis, system characteristics such as energy supply and demand, climatic conditions, and geometric boundary conditions are determined. Based on the topology of the model settlement, not every building is connected to the network with its own building interface. There are no building interfaces 3, 8 and 13. Instead these buildings are “pooled” with the respective adjacent building and are examined as a compound. (Heissler et al. 2017b)

Therefore the building interfaces

- 4, 9 and 14 each supply two multi-family homes
- 5, 10 and 15 each supply 15 single-family homes
- 6, 11 and 16 each supply two multi-family homes

For example, building interface 4 supplies building 3 and 4. The living area, the roof area, the collector area, the volume of the buffer storage, and the volume of the standby storage of building interface 4 are therefore a set of values generated from both buildings’ features (Table B-8). (Heissler et al. 2017b)

The collector area per building is determined proportionally to the ratio of usable floor area of per building, relative to the total usable floor area.

The ecological model settlement is located in the eastern part of Munich. Therefore the weather conditions of Munich, as recorded in the International Weather for Energy Calculation (IWEC) Data (ASHRAE 2001), are used for the case study. Figure 4-2 displays the monthly irradiation as well as minimum, maximum and mean dry bulb temperature.

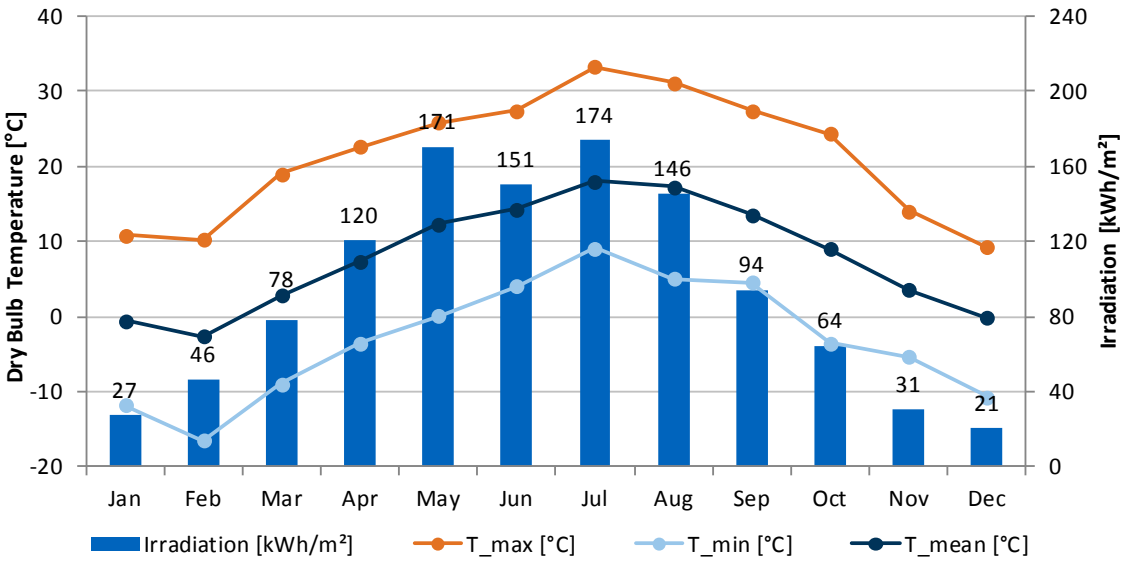

Figure 4-2: Climatic boundary conditions of Munich, Germany (ASHRAE 2001)

Located in the transition area between the maritime humid climatic region dominated by the Atlantic Ocean and the dry continental climatic region, Munich experiences hot summers with temperatures up to 33 °C and cold winters with temperatures as low as -16.5 °C with a monthly irradiation on the horizontal from 21 kWh/m² in December to 174 kWh/m² in August. The total yearly irradiation is 1123 kWh/m²a. (ASHRAE 2001)

The ground in this part of Munich is mainly silt and loess (Bayerisches Landesamt für Umwelt 2013) with a thermal conductivity ranging from 1.1 W/m.K to 3.1 W/m.K, a heat capacity ranging from 0.9 kJ/kg.K to 1.4 kJ/kg.K, and a density ranging from 2000 kg/m³ to 2200 kg/m³ (VDI 4640). Table 4-1 displays the thermal properties of the ground used for the piping model (3.3.3).

Table 4-1: Soil properties Ecological Model Settlement, Munich (VDI 4640)

Parameter	Value	Unit
Thermal conductivity	1.8	W/m.K
Specific heat capacity	1.27	kJ/kg.K

Due to a lack of measured data on long-term ground temperatures for the Munich, T_{ground} is based on average monthly ground temperature (T_m), measured by the Potsdam-Institute for Climate Impact Research from 1895 to 2017 in Potsdam at a depth of 2 m (Potsdam-Institut für Klimafolgenforschung 2018).

According to Hillel (1982), the seasonal fluctuation of a ground temperature $T(t)$ at constant depth can be expressed by a sinusoid function (Equation 4-1).

$$T(t) = A \cdot sin(B \cdot t + C) + D \qquad (4\text{-}1)$$

A periodic regression based on the method of least squares (Linder and Berchtold 1982) allows the fit of the average monthly ground temperature values to a sinusoid function and thus makes an approximation of the seasonally fluctuating undisturbed ground temperature possible. The aim of the periodic regression is the minimization of the sum of the squared residuals $(T_m - T(t))^2$ (Table B-9). The minimum sum identified is 0.67 for the parameters A, B, C and D in Table B-10. From Equation 4-1 follows the approximated temperature function of the undisturbed ground temperature.

$$T_{ground}(t) = 6.45711 \cdot sin(-0.04132 \cdot t - 26.26886) + 10.44180 \qquad (4\text{-}2)$$

Figure 4-3 displays $T_{ground}(t)$ and T_m over the course of one year.

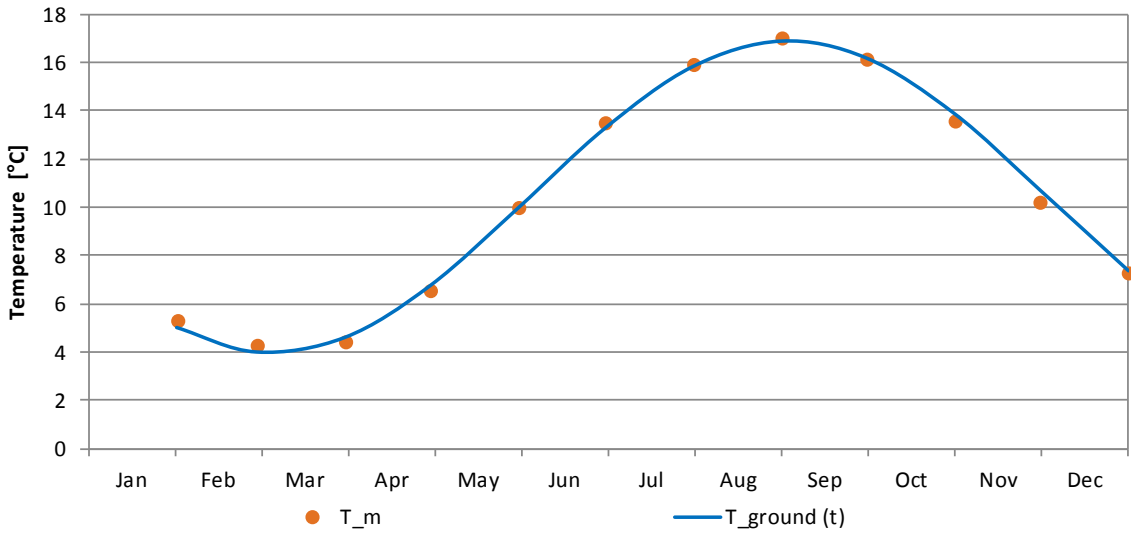

Figure 4-3: Approximated temperature function $T_{ground}(t)$ and average monthly ground temperature T_m at a depth of 2 m (Potsdam-Institut für Klimafolgenforschung 2018)

In this work an installation depth of the network of 2 m is assumed. The ground temperature of other depths is not examined.

4.2. Heating Demand

As described in Chapter 3, prerequisite for analysing the interaction between and the behaviour of the system components are thermal loads as input values to the BSMs. Since the transient behaviour of the buildings themselves is not the focus of the investigation and changes in performance through load variation have to be easily traceable, the loads are determined by a steady-state approach. The basis of this approach is DIN V 4108-6 to determine building–specific energy demands, taking into account the considerable variance of the compactness of the buildings within the mixture of single family homes and multi-story buildings. The loads are calculated on the basis of the quality of the building envelope, the type of construction, the climatic influence, the user behaviour and the composition of the quarter. Via the method of “typical days” of VDI 4655, the yearly heat loads are broken down into loads for every minute of the year. (Heissler et al. 2017b)

Depending on the specific characteristics of location, topology and orientation of the buildings as well as the geometric and physical composition of the building envelope, the heat loads can vary significantly. Following the thematic priority of modelling and simulating a 5GDHCN, extensive variations on the side of the heat demand are not an objective. The focus lies on the transparency and traceability of potential effects. Therefore, the level of thermal energy demand for heating is defined as 23 kWh/m².a for multi-family houses (MFH) and 35 kWh/m².a for single-family houses (SFH) (EnEV, revised by Article 1 of the Ordinance of 11/18/2013 (BGBl. I p. 3951)).

With building envelopes steadily improving and consequently the thermal energy demand for HW generation decreasing, the heat demand for DHW preparation becomes more dominant. Taking into account the variance of user requirements in terms of comfort and DHW temperature and based on VDI 6002, the DHW demand is defined as 30 l/person.d normalized to a tapping temperature of 60 °C resulting in 16 kWh/m².a. In the simulation, the DHW tapping temperatures are adjusted to the actual scenario settings, whilst keeping the total heating demand constant. (Heissler et al. 2017b)

4.3. Scenarios

The simulation framework described in Chapter 3 is able to use a variety of input parameters to simulate the behaviour of different types of 5GDHCNs with distinct features. In this section a baseline scenario and several variations of the baseline case are defined and described. The baseline scenario serves as a point of reference. The features varied in the following sections are:

- Network typology (line, ring and mesh network)
- Network heat-load density
- Feed-in of waste heat
- Network pipe insulation

Furthermore a traditional DHN (described in 3.4) is simulated for comparison and evaluation of the baseline scenario.

The simulations conducted all span a period of two years, to keep the influence of the initial conditions on the simulation results small. Among these influences are the temperatures of all thermal masses in the system, for example thermal storages, heat carriers or the ground layer surrounding the pipes. Also, since a balanced energy use at the seasonal storage is aimed for, the influence of the long-term temperature development of the seasonal storage is minimized.

The photovoltaic cell efficiency at 25 °C of the PVT collectors is set at a conservative value of 0.1 compared to values in literature of 0.15 (Lämmle et al. 2017) to prevent undue electric energy gains and account for the status of development of PVT collectors.

4.3.1. Baseline

The baseline scenario examines a 5GDHCN with line layout and a building heat demand as described in 4.2. Table 4-2 provides an overview of the baseline input parameters.

Table 4-2: Baseline input parameters

Parameter	Value
HW Demand [kWh/m².a]	(MFH: 23; SHF: 35)
DHW Demand [kWh/m².a]	16
DHW supply temperature [°C]	45
Collector Area [m²]	4566
Buffer Storage [l/m²coll]	94
Stand-by Storage [l/m²coll]	43
Volume Borehole Heat Exchanger [m³]	425920
Network Pipe Diameter [m]	0.13

The buildings are equipped with PVT collectors which provide thermal and electrical energy. The network typology of the baseline scenario is a line layout connecting the seasonal storage and the buildings via one main line and several stubs with a total pipe length of 915.1 m. For a detailed overview see the Appendix A, Figure A-1. A schematic overview is provided in Figure 4-4 which displays the layout of the network with the main line at the bottom and the long stubs to the buildings.

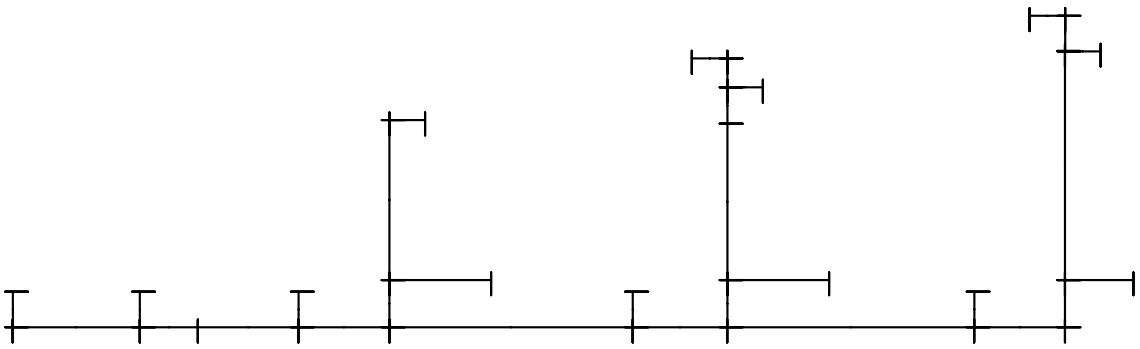

Figure 4-4: Schematic of a line network

Each line end is the position of a building interface. The seasonal storage is, as described in 3.3.4, a borehole heat exchanger.

4.3.2. Network Typology

The scenario Network Typology compares the performance of three different network layouts: line, ring and mesh networks, each additionally with a variation of its pipe diameter. The network typologies examined are a line network as displayed in Figure 4-4 (Figure A-1), a ring network as displayed in Figure 4-5 (Figure A-2), and a mesh network as displayed in Figure 4-6 (Figure A-3). A variation of the network layout results in different pipe surface areas.

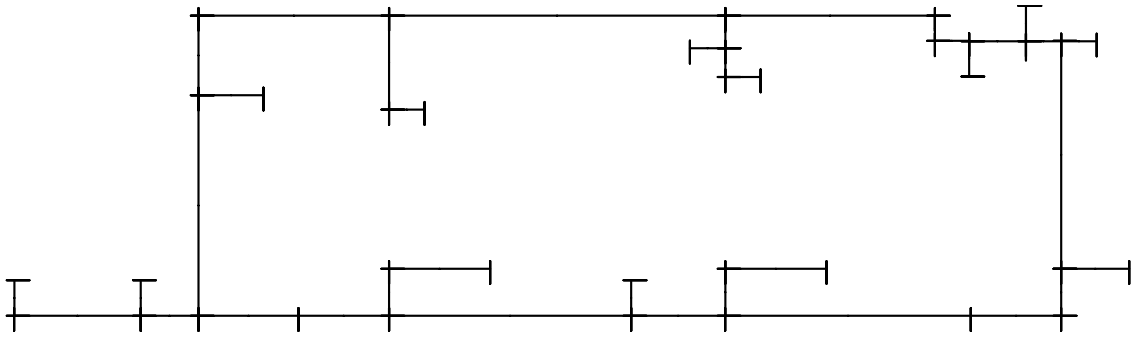

Figure 4-5: Schematic of a ring network

The difference between the ring layout (Figure 4-5) and the line layout of the baseline case is the missing long stubs supplying the building interfaces further away from the main line. Here the buildings interfaces are supplied from the main ring with short stubs resulting in a total pipe length of 1269.8 m. Compared to the line layout, the hydraulics are more complex, since every fluid "package" has two possible ways to get from one point of the ring to another, resulting in a reduced hydraulic resistance.

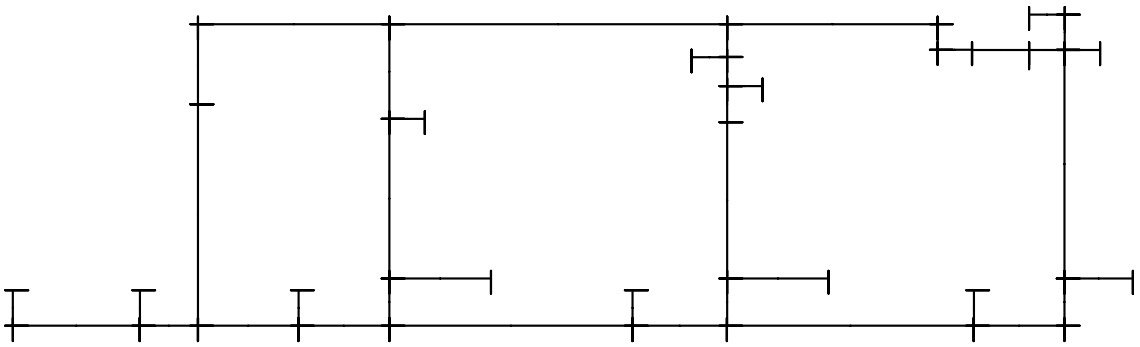

Figure 4-6: Schematic of a mesh network

The mesh layout (Figure 4-6) further increases the complexity of the network model. With the additional connection lines in the inner part of the ring layout, the mesh layout offers several different ways to transport a fluid package from one point of the network to another, which further reduces the hydraulic resistance between the two points. The total pipe length is increased to 1398.8 m. Compared to the line layout, the total

pipe surface areas of ring and mesh layout are significantly higher due to the longer pipe lengths. In addition to the variation of the network layout, the pipe diameter of the network is varied for each network layout. Figure 4-7 displays examples of pipe cross-sections for different pipe diameters. Starting at a pipe scaling factor (PSF) of 1, which represents the pipe diameter of the baseline case (4.3.1), the PSF is successively increased by 25% until a PSF of 2 is reached.

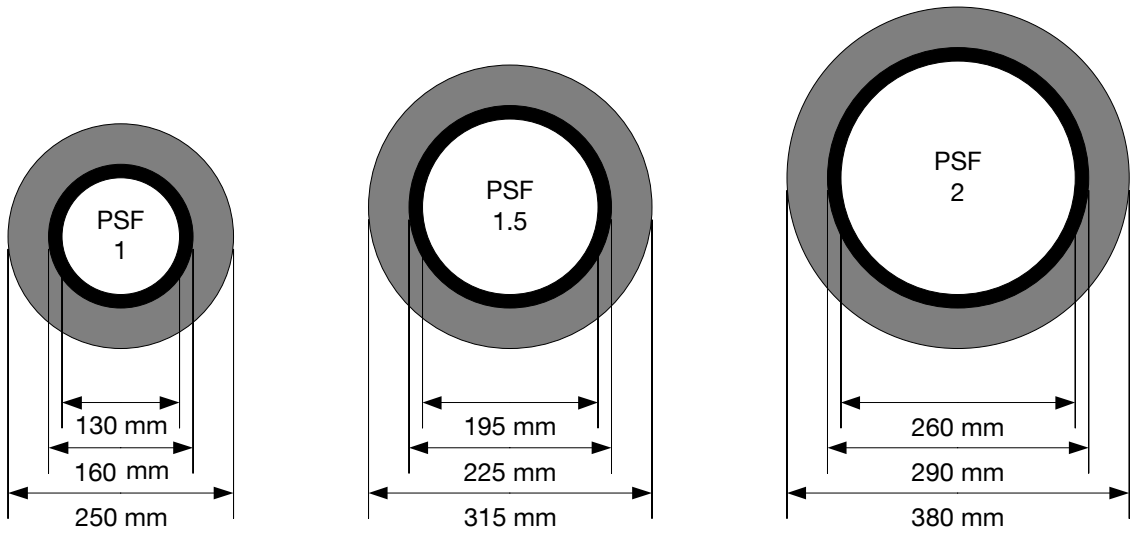

Figure 4-7: Examples of different pipe sizes in mm (not to scale)

As displayed in Table 4-3, this too leads to an increase in pipe surface area compared to the baseline scenario and provides an additional insight into the influence of the hydraulic cross-section in combination with different network layouts. All other simulation parameters (heat demand, weather, etc.) and the distances between the building interfaces are kept constant and identical to the baseline case.

Table 4-3: Pipe surface areas for different PSFs, pipe diameters and network layouts (line, ring, mesh)

		Total pipe surface area [m²]		
PSF	**Pipe Diameter [m]**	**Line**	**Ring**	**Mesh**
1	0.13	373.7	518.6	571.3
1.25	0.16	467.1	648.2	714.1
1.5	0.20	560.5	777.9	856.9
1.75	0.23	654.0	907.5	999.7
2	0.26	747.4	1037.2	1142.6

4.3.3. Network Heat-load Density

This section defines the scenarios to examine the influence of different heat-load densities on the network performance of 5GDHCNs. The baseline case and its boundary conditions (heat demand, network layout, etc.) serve as the basis (4.3.1). Heat transferred from the network to the buildings is defined as Q_{net_h}, while heat transferred into the network is defined as Q_{net_c}. To be able to extract Q_{net_h} from the network, the sum of Q_{net_h} and the total system losses (Q_{loss}) must be supplied to the network, which is Q_{net_c}. Therefore, the heat transported through the network ($Q_{transported}$) is the sum of Q_{net_h} and Q_{net_c}. The heat-load density of the network (q_{net}) is determined by dividing $Q_{transported}$ by the total network length (l_{net}) (Equation 4-3).

$$q_{net} = \frac{Q_{transported}}{l_{net}} \tag{4-3}$$

In opposition to traditional DHNs, $Q_{transported}$ and not the heat demand was chosen as the reference, since 5GDHCNs act as heat source and heat sink. Therefore, the heat is transported twice through the network. The effects of a variation of q_{net} are assessed by keeping the heat demand of the buildings constant while linearly varying the network size (Table 4-2).

Table 4-4: Pipe surface areas for different NSFs, network sizes and pipe diameters

			Total pipe surface area [m²]	
Scenario	NSF [-]	Total Pipe Length [m]	Pipe Diameter 0.13 m	Pipe Diameter 0.26 m
very small	0.5	457.5	186.9	373.7
small (baseline)	1	915	373.7	747.5
medium	1.5	1372.5	560.6	1121.2
large	2	1830	747.5	1494.9
very large	2.5	2287.5	934.3	1868.7
extremely large	4	3660	-	2990

A network scaling factor (NSF) of 0.5 represents half of the total pipe length of the baseline case (457.5 m). The NSF is increased in steps of 0.5 until a factor of 2.5 is reached. Additionally each network size is examined for two different pipe diameters (0.13 m and 0.26 m). A system with a NSF of 4 is also examined.

4.3.4. Feed-in of Waste Heat

In the baseline scenario the thermal energy supplying the system originates solely in the PVT collectors. This section examines the behaviour of 5GDHCNs with various shares of feed-in of waste heat, replacing the solar-thermal input of the buildings. The waste heat source is a pulsating heat source with a period of 30 minutes, a pulse width of 15 minutes, a provided temperature difference of 10 K, and a pulse mass flow defined according to the amount of waste heat input. The total yearly amount of heat input in the 100%-waste-heat case is based on the total yearly solar-thermal input into the system in the baseline case (4.4.1) of 1863.9 MWh. The feed-in of waste heat is increased in steps of 10%. By the percentage the feed-in of waste heat is increased the PVT collector area and the buffer storage size are reduced, compared to the base-line case (Table 4-5).

Table 4-5: Waste heat scenario input parameters

Waste heat input [%]	PVT collector area and buffer storage size [%]	Waste heat input [MWh]	Pulse mass flow [kg/s]
0	100	0.0	0.0000
10	90	186.4	1.0156
20	80	372.8	2.0312
30	70	559.2	3.0468
40	60	745.5	4.0624
50	50	931.9	5.0781
60	40	1118.3	6.0937
70	30	1304.7	7.1093
80	20	1491.1	8.1249
90	10	1677.5	9.1405

The waste heat source is located at the end of the critical path at the outermost point of the 5GDHCN (Figure A-4). The waste heat is assumed to have no environmental impact in terms of CO_2-equivalents, since by definition it is produced and disposed of anyway. However, since the pump of the waste heat source is not necessarily in close proximity to the buildings or the PVT collectors, it is supplied with electric energy from the public distribution network.

4.3.5. Network Pipe Insulation Thickness

Compared to traditional DHNs, one advantage of 5GDHCNs is the reduced thermal losses due to lower temperature differences between pipes and their surroundings. Here we examine the effects of different insulation layer thicknesses on the heat losses and the performance of 5GDHCNs to determine the need for pipe insulation (Figure 4-8). For easier parametric variation, an insulation factor (IF) is used. The thickness of the insulation of the baseline case of 60 mm is defined as an IF of 1. The thicknesses of insulation for IFs from 0.25 to 2 are calculated accordingly (Table 4-6).

Table 4-6: Pipe insulation thickness scenario input parameters

IF [-]	0.25	0.4	0.6	0.8	1	1.2	1.4	1.6	1.8	2
Thickness of pipe insulation [mm]	15	24	36	48	60	72	84	96	108	120

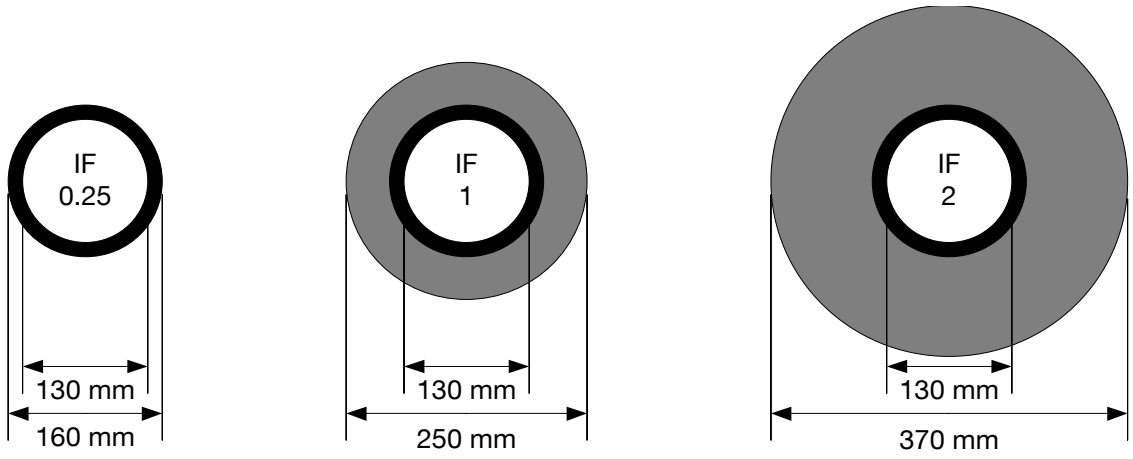

Figure 4-8: Examples of different IFs in mm (not to scale)

4.3.6. Traditional District Heating Network

Since a traditional DHN is not only a technological predecessor but also one of the main competitors of 5GDHCNs, a comparison of the performance of the two aims to point out the differences. With the DHN modelled as described in 3.4, it shares with the 5GDHCN model the input parameters of heat demand, network layout, and total pipe length (4.3.1). The energy source of the network is a larger DHN with an emission factor as found in BMI (2016a) of 0.2614 kg CO_2-equivalent per kWh thermal energy. This includes the emissions for pressure maintenance in the DHN.

4.4. Results

This section displays the results of the simulation scenarios defined in 4.3. All results refer to simulation results of the second year of operations of the respective scenario. All statements refer to the use phase if not otherwise marked or explicitly mentioned. The benchmarks are (Heissler et al. 2017b):

- **Total Energy Turnover**
  The total energy (TE) turnover of the system, the sum of useful energy (Q_{use}) and system losses (Q_{loss}).

- **Useful Energy**
  The useful energy Q_{use} made available to the user, sum of heat for heating (Q_{HW}) and domestic hot water preparation (Q_{DHW}).

- **System Losses**
  The energy lost Q_{loss} to the surroundings of network and storage.

- **Renewable Energy and Non-Renewable Energy**
  The energy input into the system, divided in shares of renewable and non-renewable origin. The electric energy obtained from the public distribution network is 35.12% of renewable origin (BMI 2016b). The heat in the traditional DHN scenario (4.3.6) is 11.1% of renewable origin (BMI 2016a).

- **CO_2-equivalent**
  The CO_2-equivalent of the total energy turnover of the system. It is based on 0.5345 kg CO_2-equivalent per kWh electrical energy obtained from the public distribution network (BMI 2016b) and 0.2614 kg CO_2-equivalent per kWh thermal energy obtained from a DHN (BMI 2016a).

- **Annual Coefficient of System Performance (COP)**
  The annual coefficient of system performance of the 5GDHCN as a whole is defined as the ratio of Q_{use} to the total electrical energy required (W_{el}):

$$COP = \frac{\sum Q_{HW} + \sum Q_{DHW}}{\sum W_{el}} \tag{4-4}$$

  It is not to be confused with the coefficient of performance of the heat pumps.

4.4.1. Baseline

The TE turnover of the baseline case (4.3.1) of 2284 MWh can be divided in 2165 MWh useful energy Q_{use}, the sum of Q_{HW} and Q_{DHW}, and 119 MWh losses (not accounting for the excess electrical energy production of the PVT panels). It can also be divided according to its origin into 89.3% energy from renewable sources (Q_{RE}) and 10.7% energy from non-renewable sources (Q_{NRE}) (Table 4-7). Since the 5GDHCN is fully supplied by energy from renewable sources, with the exception of electrical energy from the public distribution network, its part of non-renewable energy can be traced back to the share of non-renewable energy in the public distribution network. According to Ökobaudat 2016 (BMI 2016b), 64.9% of each kilowatt hour from the public distribution network is of non-renewable origin. With the parameters introduced above this leads to a total CO_2-equivalent of 201.82 t/a or 88.35 g/kWh TE.

Table 4-7: Summary of the simulation results (Baseline)

2284	MWh Total Energy Turnover
consisting of	
2165	MWh Useful Energy
119	MWh Losses
or	
2040	MWh Renewable Energy
244	MWh Non-Renewable Energy
resulting in	
202	t CO_2-equivalent/a
88	g CO_2-equivalent/kWh Total Energy
5.1	annual COP (System)

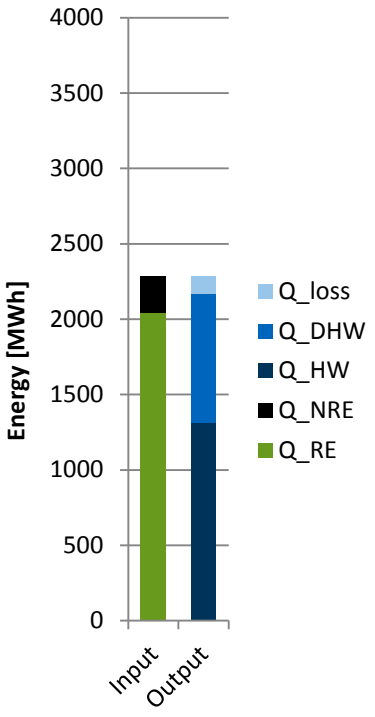

Figure 4-9: Energy In- and Output (Baseline)

Figure 4-9 contrasts the energy input of the system, Q_{RE} and Q_{NRE}, with the energy output Q_{DHW}, Q_{HW} and Q_{loss}, showing that almost all of the useful energy in the baseline case is provided from renewable sources. Q_{loss} consist of thermal losses of the network (Q_{loss_net}), storage losses of the seasonal storage (Q_{loss_stor}), and calculatory losses (Q_{loss_calc}) due to a difference of the total inner energy of the system between start and end of the simulation.

Figure 4-10 shows the monthly HW and DHW demand Q_{HW} and Q_{DHW}. Depending on the time of year, this demand is covered by changing shares of direct solar-thermal heat gains (Q_{ST_dir}), low-temperature heat made available by heat pumps (Q_{HP}), and heat provided by electric heaters (Q_{el}) (Heissler et al. 2017b).

Also visible in Figure 4-10 is the seasonally changing heating demand of the buildings while the DHW demand is nearly constant all year. Bars of supply and demand that are not balanced, for example in the months of May, June, July or August, indicate months with significant losses (also see Figure 4-14).

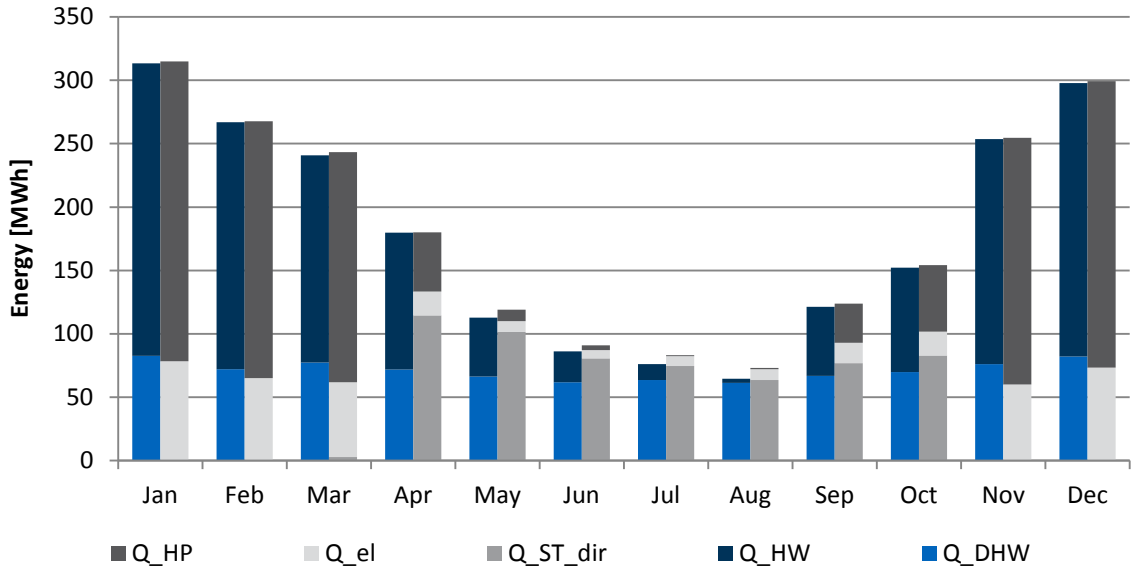

Figure 4-10: Monthly heat balance with DHW and HW demand (Baseline) (Heissler et al. 2017b)

The heat sources of the heat pumps are the 5GDHCN and the buffer storages with low-temperature solar-thermal heat (see Chapter 3). The sum of the electricity demand W_{el} of heat pumps, electric heaters, and pumps turned to heat, is combined to Q_{el}. During the months of April through October the stand-by storages are mainly supplied directly by solar-thermal heat. (Heissler et al. 2017b)

Figure 4-11 displays the total solar energy gains, divided into photovoltaic (PV) (W_{PV_gain}), direct (Q_{ST_dir}), and indirect (Q_{ST_indir}) solar-thermal energy gains. The total solar-thermal gains (Q_{ST}) are the sum of Q_{ST_dir} and Q_{ST_indir}. While Q_{ST_dir} only contributes to the system in the months from April to October (as mentioned above), Q_{ST_indir} and W_{PV_gain} occur all year. Figure 4-11 is complemented by Figure 4-12, showing the heat transfer from (Q_{net_h}) and into (Q_{net_c}) the 5GDHCN, which is mainly determined by the local conjunction of Q_{ST_indir} and the local heat demands (Figure 4-10).

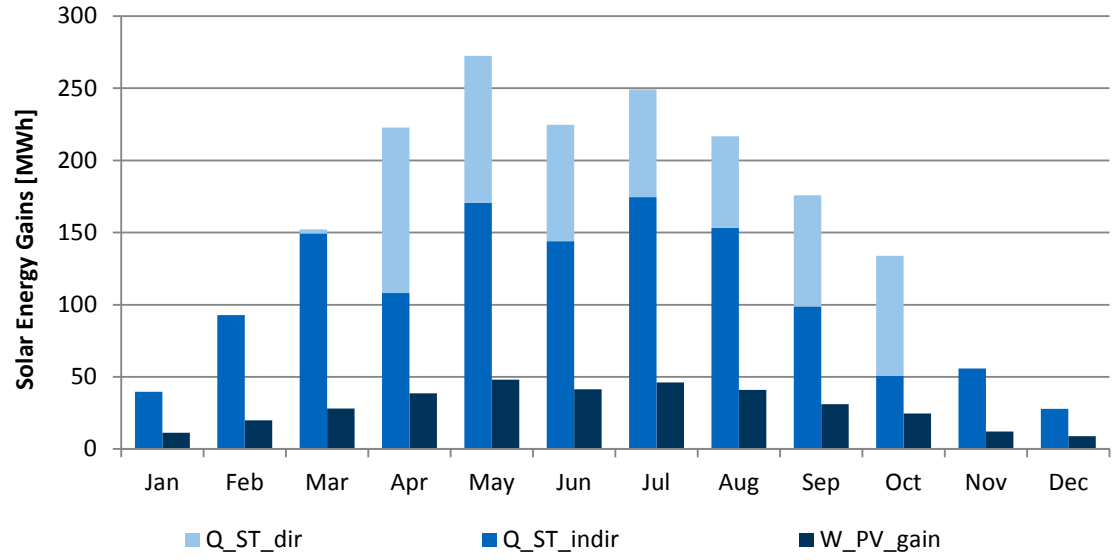

Figure 4-11: Electrical, direct solar-thermal and indirect solar-thermal energy gains of the system on a monthly basis (Baseline)

Noteworthy are the months of April and October (Figure 4-12), which stick out with almost equal amounts of locally gained and locally used heat and therefore very little heat transferred into or out of the 5GDHCN. (Heissler et al. 2017b)

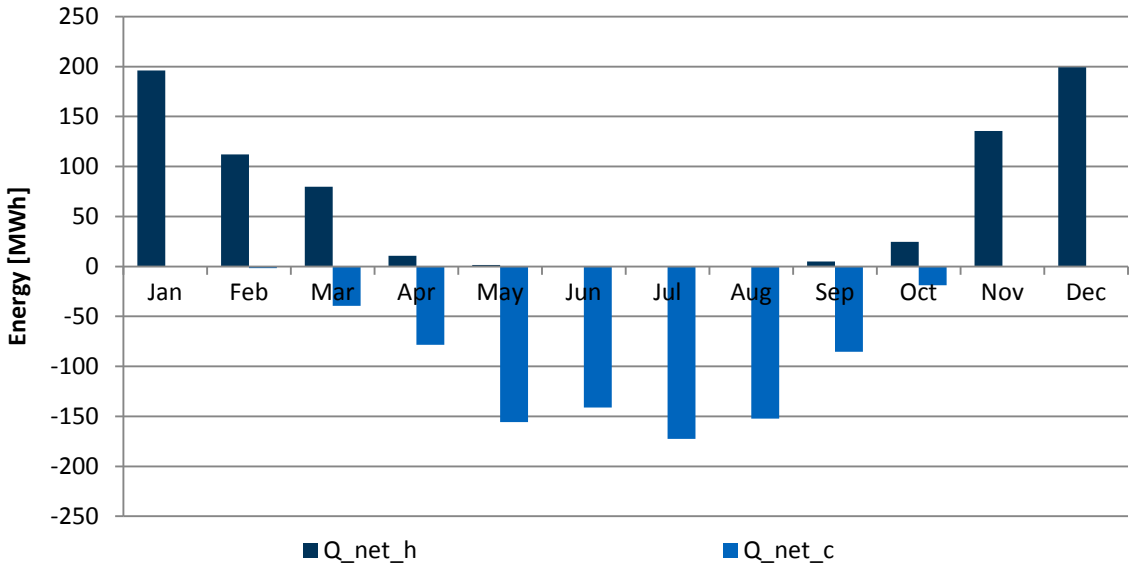

Figure 4-12: Heat transfer from and into the 5GDHCN (Baseline) (Heissler et al. 2017b)

The temperature profiles of the warm and cold lines of the 5GDHCN at the seasonal storage are T_{net_h} and T_{net_c}. For better readability, Figure 4-13 displays the 24h moving averages of T_{net_h} (T_{net_h24}) and T_{net_c} (T_{net_c24}) as well as the undisturbed soil temperature of the surrounding ground (T_{ground}) (see 4.1).

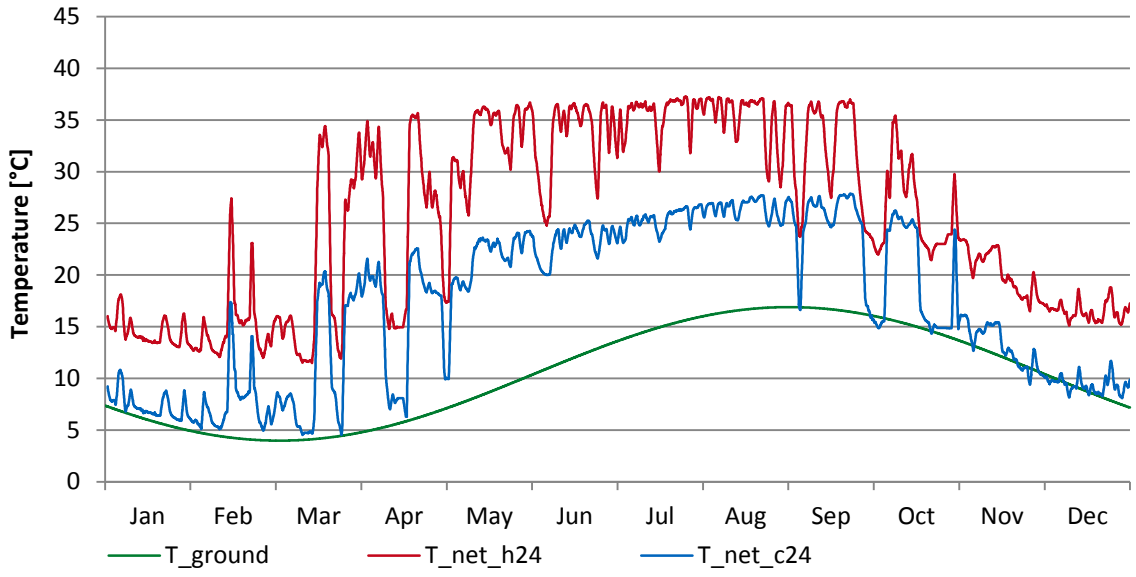

Figure 4-13: High and low temperatures of the 5GDHCN and undisturbed ground temperature (Heissler et al. 2017b)

Noteworthy are the sudden temperature changes indicating a reversal of flow in the network in the months of February, March and April, switching to and from discharging and charging the 5GDHCN. Similar behaviour can be observed in the months of September and October. The temperature ranges from 3.8 °C in March to 39.8 °C in July.

Also contained in this graph is the temperature profile of the seasonal storage. Looking at the line temperatures, bearing in mind the occurring flow reversals in the network and assuming the fluid leaving the seasonal storage carries the average storage temperature, the continuous line in the middle of Figure 4-13 is composed of red and blue parts and shows the temperature of the seasonal storage with a similar seasonal characteristic as the ground temperature.

During the months of November and December the cold line temperature frequently drops below the average ground temperature, leading to “negative losses” and therefore thermal gains of the network. However, combined with the thermal losses of the warm line, Q_{loss_net} during that time is still positive, albeit it is lower than during the rest of the year (Figure 4-14).

Besides the Q_{loss_net} of 45 MWh, Figure 4-14 also shows the electric energy demand of the pumps to transport the fluid through the network (W_{pump}) and the volume of fluid moved through the network (V_{mov}). V_{mov} peaks twice per year, once in December and January and once in July and August.

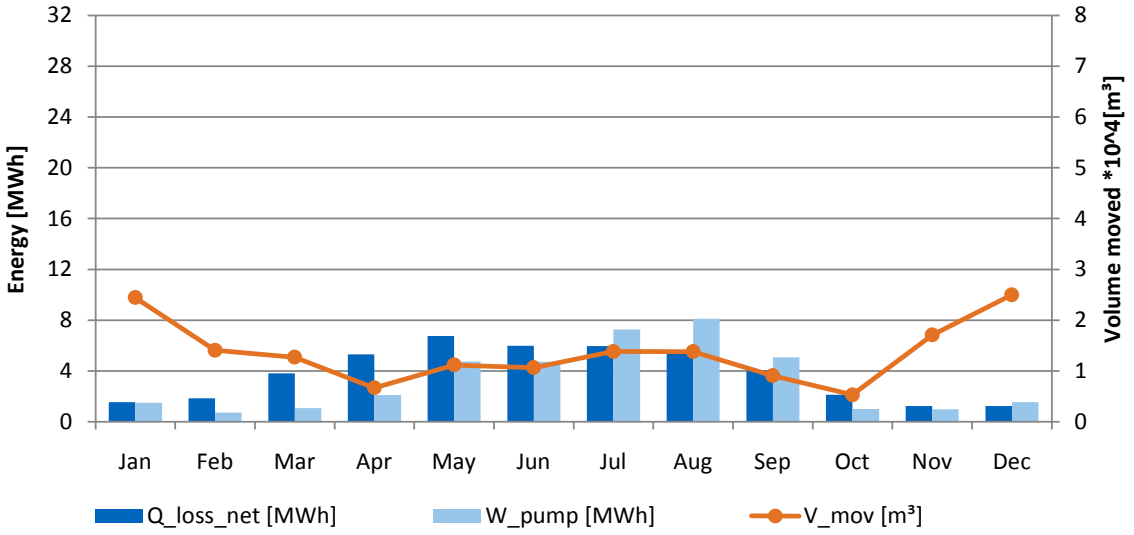

Figure 4-14: Thermal network losses, electric pump energy demand and total volume moved (Baseline)

However, the months with the highest V_{mov} are not the months with the highest W_{pump}. An almost exactly opposite behaviour can be observed: the winter months with the highest V_{mov} are the months with the lowest W_{pump}, and the summer months (especially July and August) are the months with the highest W_{pump}.

The main parameter determining W_{pump} is the pressure loss in the network, which is connected to V_{mov}, but also to the simultaneousness of processes and network lay-out.

In summer, buildings discharge into the network simultaneously, while in winter they charge irregularly. The discharging process into the network is mainly weather dependent (see 3.1) and therefore self-synchronized: when the sun shines, the buffer storages of all buildings are charged. Once the buffer storages are full, they are discharged into the network. This cycle is repeated as long as the sun shines and the local heat demand is lower than the local solar gains. However, the simultaneous discharging leads to high pressure differences between the warm and cold lines of the network and therefore a high W_{pump}.

The charging process is, due to its connection to the user and the different building types, inherently more irregular than the discharging process. It is determined by the heat demand of the heat pumps when charging the stand-by storages (see 3.1). However, since the charging levels of the stand-by storages also change with solar input and alternating HW and DHW demands, and the heat pumps are either supplied centrally from the buffer storages or decentrally from the network, the charging from the network occurs irregularly. This keeps the pressure differences between the warm and

cold lines of the network at low levels, leading to low pump energy demands in the months where charging is the predominant mode. For further analysis and evaluation of W_{pump} see also section 6.1.7.

Q_{loss_net} is highest in the summer months and peaks in May when the temperature difference between ground temperature and average network temperature is highest (Figure 4-14). Compared to the influence of this temperature difference, the influence of V_{mov} on Q_{loss_net} is negligible.

Figure 4-15 displays the mean hourly values of the total pressure at the critical hydraulic path in the warm line (p_{crit}), at the T-junction between building interface 12 and 15.

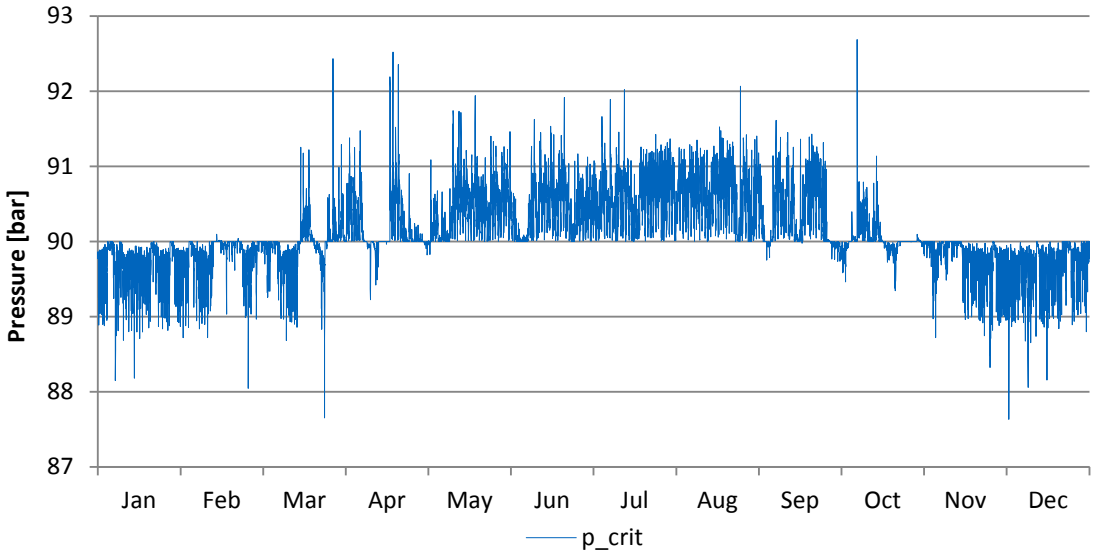

Figure 4-15: Total pressure at the critical path

Since the NSM is extremely sensitive to pressure levels below saturation vapour pressure, a pressure level of 90 bar was chosen as zero level, to rule out any possibility of any single pressure peak reaching saturation vapour pressure. The pressure peaks in Figure 4-15 range from 87.6 bar to 92.7 bar, with an average pressure level in winter of 89.8 bar and in summer of 90.4 bar.

As described in 3.1, the solar collectors modelled are PVT collectors which enable a collection of low temperature heat and electricity at the same time. The monthly electricity production of the PVT collectors W_{PV_gain} is presented in Figure 4-11 and divided (Figure 4-16) into the share of photovoltaic energy actually used by the system (W_{PV_use}) and the excess share of photovoltaic energy (W_{PV_grid}). Figure 4-16 further shows W_{PV_gain} in conjunction with the total monthly electricity demand of the build-

ings. Similar to the seasonal imbalance of heat supply and demand (Figure 4-12) a large imbalance in photovoltaic energy supply and demand can be observed. November, December and January have the highest electricity demand, due to the high electricity demand of the heat pumps (W_{HP}). In these months, W_{PV_gain} from the PVT collectors is negligible. The opposite can be found in the summer months, where W_{PV_gain} is high with little electric energy demand on the other side. Even though the pump energy demand W_{pump} is increased in the summer months (c.f. Figure 4-14), W_{PV_gain} in summer is too high for full local use. The excess energy, W_{PV_grid}, is discharged into the public distribution network.

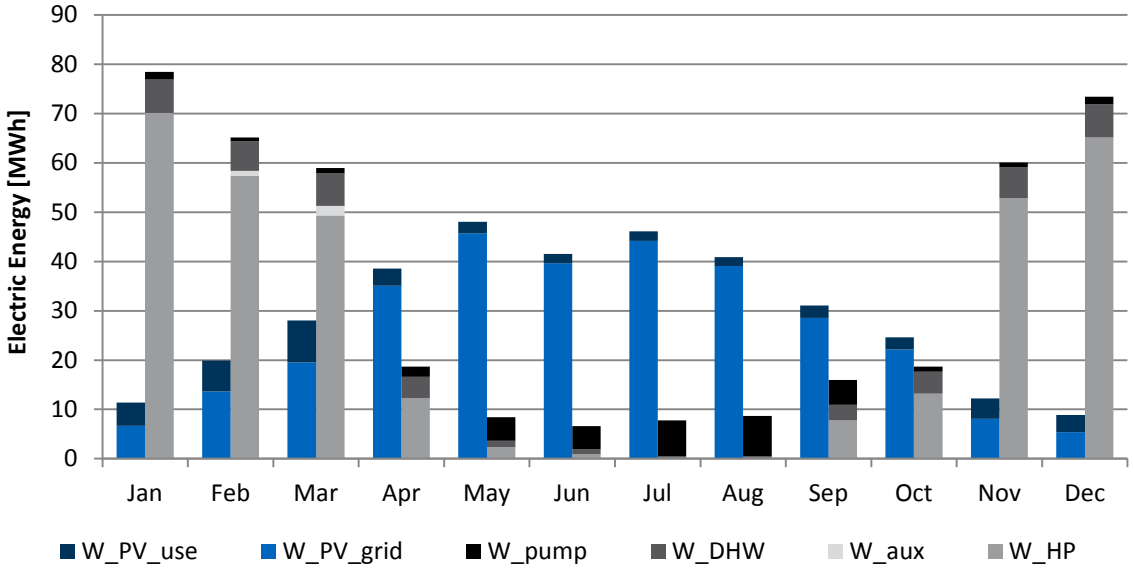

Figure 4-16: Photovoltaic energy supply and electric energy demand (Baseline)

The electricity demand for local DHW heating (W_{DHW}) is also reduced in the summer months when Q_{ST_dir} through the stand-by storages is highest. The lowest electric energy demand comes from the auxiliary heaters of the stand-by storages (W_{Aux}), which only run a few times in the months of February and March when the 5GDHCN is coldest and the heat pumps are therefore not fully able to fill the stand-by storages.

Figure 4-17 displays the energy flows of the baseline case cumulated for all buildings of the district over the time period of one year. The building shown in Figure 4-17 therefore represents all the buildings in the system and serves to visualize the cumulated energy flows between the components of every building in the system at once. In sum the total solar energy collected (E_{sol}) by all PVT collectors in the district is 2214.9 MWh, which can be divided into W_{PV_gain} of 351 MWh and Q_{ST} of 1863.9 MWh. With Q_{ST_dir}, roughly one third (597.8 MWh) of the thermal energy has a

high enough temperature to be used directly in the stand-by storages while the remaining Q_{ST_indir} of 1266.1 MWh is used in the buffer storages.

From the buffer storages $Q_{ST\_indir\_HP}$ of 420.7 MWh serves locally as a feed for the heat pumps while Q_{net_c} of 845.3 MWh is fed into the 5GDHCN via pumps with an electrical energy demand of 33.4 MWh ($W_{pump\_c\_h}$). These 878.7 MWh, as well as 762.5 MWh from the seasonal storage, supply the 5GDHCN. In turn, the 5GDHCN supplies the seasonal storage with 813.1 MWh. The thermal network losses Q_{loss_net} amount to 45.2 MWh. Additional losses are Q_{loss_stor} of 50.6 MWh and Q_{loss_calc} of 23.6 MWh. The remaining 759.4 MWh are fed to the buildings and combined with 5.4 MWh of pumping energy demand ($W_{pump\_h\_c}$). In total, the thermal energy from the network used as a feed for the heat pumps amounts to 764.8 MWh. Combined with the direct feed from the buffer storages and an electricity supply W_{HP} of 331.8 MWh, the heat pumps charge the stand-by storages with a total heat provided by the heat pumps (Q_{HP_tot}) of 1517.2 MWh. From there, 1312.6 MWh are used for heating to meet Q_{HW}. A further 805.2 MWh from the stand-by storages are combined with W_{DHW} of 47.2 MWh through the electric heaters, to provide Q_{DHW} of 852.4 MWh in form of DHW at the specified temperature setpoint.

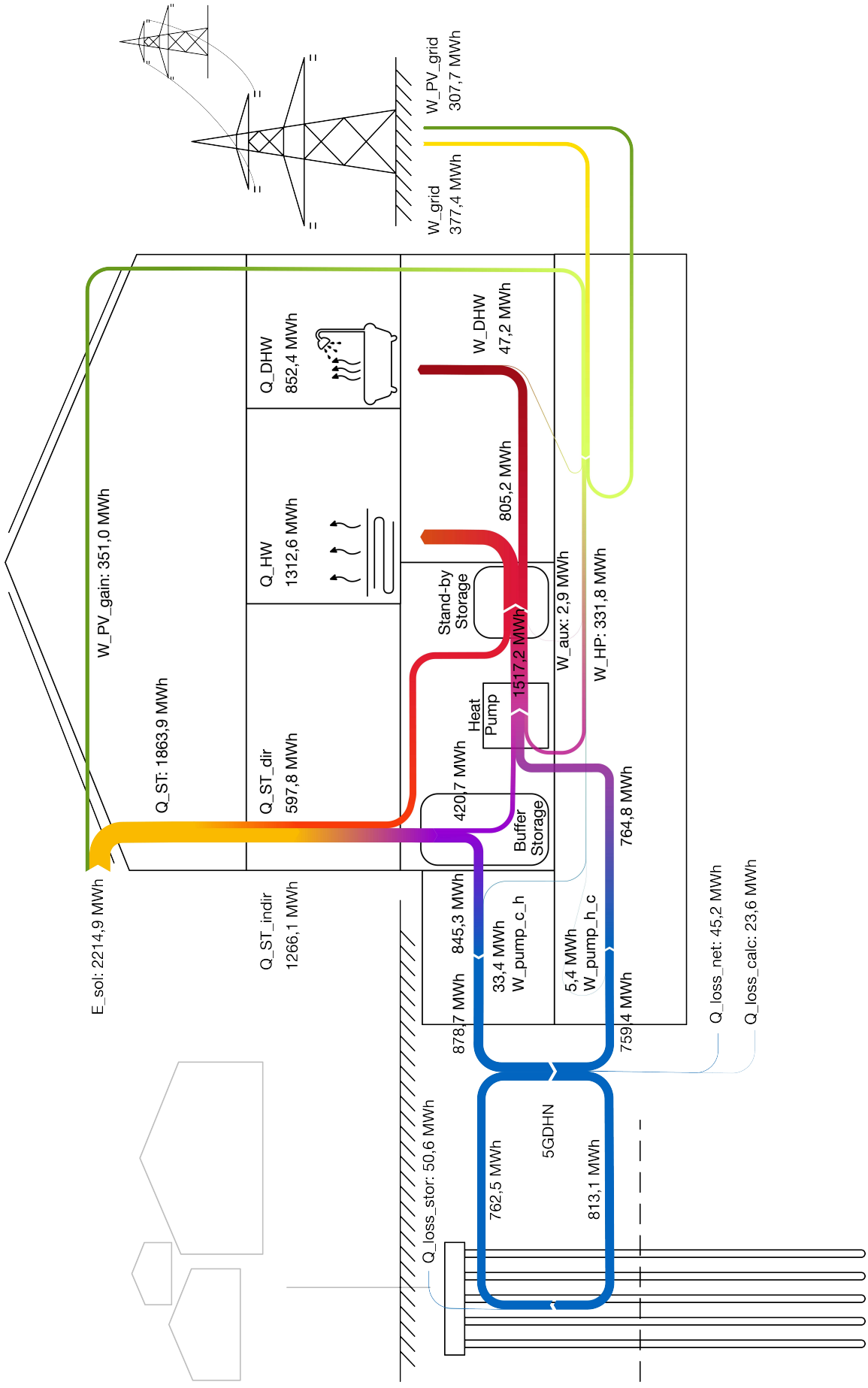

Figure 4-17: Sankey diagram of the energy flows through the system in the baseline scenario

4.4.2. Network Typology

As set out in 4.3.2, this section examines the performance of 5GDHCNs in three different network layouts: line network, ring network, and mesh network, at otherwise identical conditions (heat loads, distances, buildings, solar irradiation, etc.). In addition to the variation of the network layout, the pipe diameter of each network type is varied. The networks with a pipe diameter of 0.13 m are labelled as networks with small pipe diameter (NSD), and the networks with a pipe diameter of 0.26 m are labelled as networks with large pipe diameter (NLD). Figure 4-18 provides an overview and comparison of the performance of line, ring and mesh NSDs in baseline configuration.

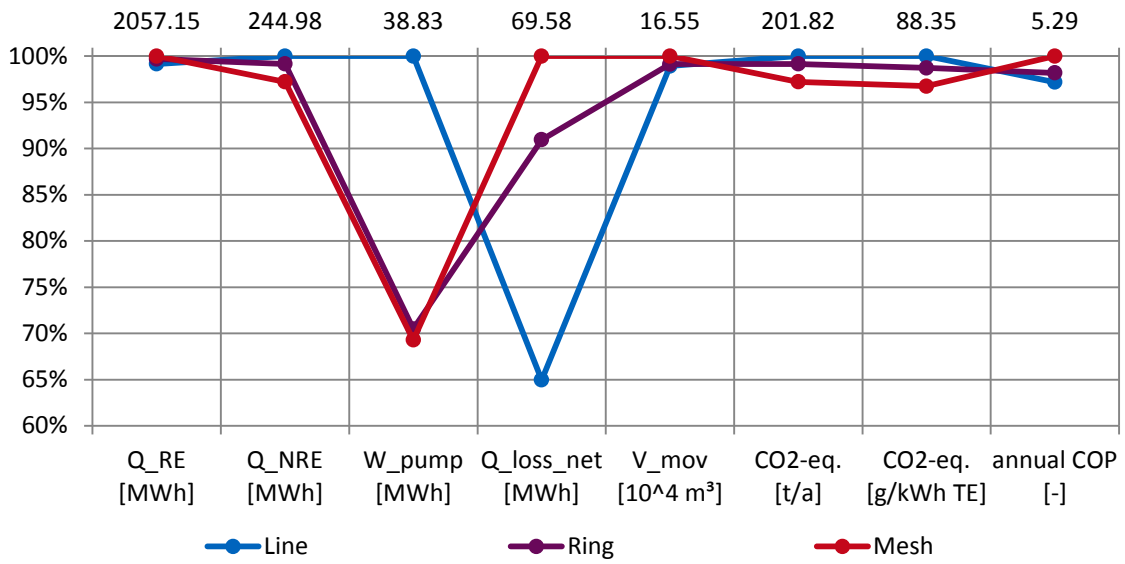

Figure 4-18: Performance comparison of line, ring and mesh NSD

The difference in the turnover of Q_{RE} and Q_{NRE} between line and ring or mesh networks (see also Table 4-8) can be traced back to a reduced W_{pump} and increased thermal losses Q_{loss_net} of the ring and mesh networks compared to the line network.

Table 4-8: Performance indicators of line, ring and mesh NSD

Type	Q_RE [MWh]	Q_NRE [MWh]	W_pump [MWh]	Q_loss_net [MWh]	V_mov [10^4 m³]	CO_2-eq. [t/a]	CO_2-eq. [g/kWh TE]	annual COP [-]
Line	2039.8	245.0	38.8	45.2	16.4	201.8	88.4	5.1
Ring	2050.7	242.9	27.4	63.3	16.4	200.1	87.2	5.2
Mesh	2057.1	238.2	26.9	69.6	16.6	196.2	85.5	5.3

While W_{pump} is decreased by 11.4 MWh or 11.9 MWh due to a reduced total hydraulic resistance compared to the line network, Q_{loss_net} is increased by 20.8 MWh or 24.4 MWh due to a larger pipe surface area. The CO_2-equivalent-minimising-effect of

a decreased W_pump outweighs the increase in Q_loss_net, due to the fact that these losses are mainly in renewably gained energy, while the decreased W_pump is made up of about two thirds non-renewable energy (electrical energy from the public distribution network). A closer look at the monthly values of W_pump of the three layouts is given in Figure 4-19. All three graphs follow the same pattern: low levels in the months from October to March, a steep rise from March to May, a plateau from May to June, peaking in August, and a steep decline from August to October.

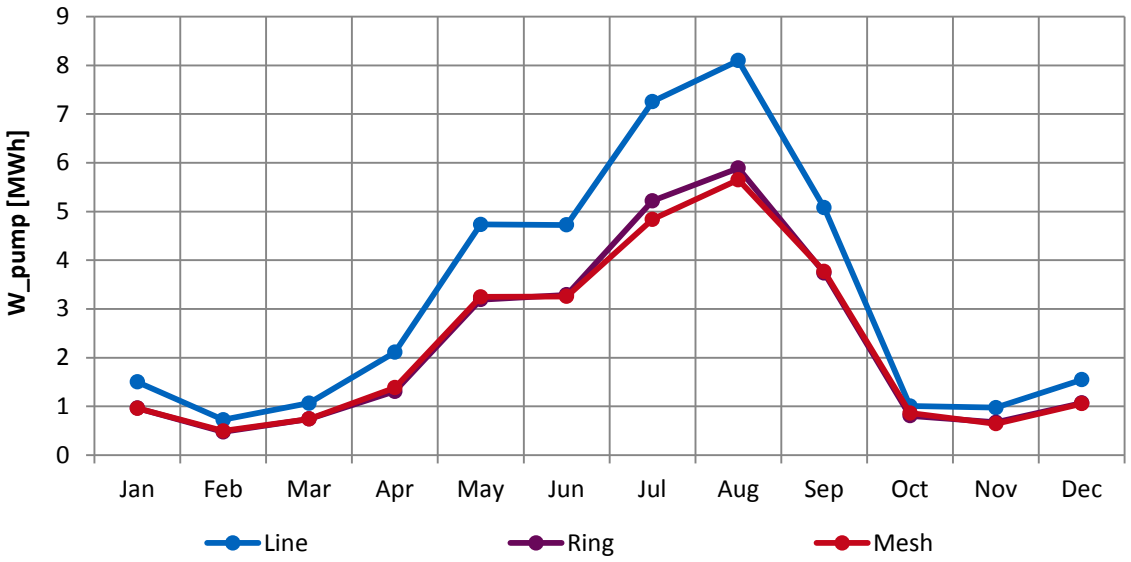

Figure 4-19: Monthly pump energy demand of line, ring and mesh NSD

As described in 4.4.1, this can be traced back to the pressure differences of the charging and discharging cycles of the networks. Noteworthy is the difference in performance during the summer months. At the time of the highest pressure difference between the warm and cold lines, due to the self-synchronizing effect of the discharging cycles into the networks, the ring and mesh networks perform significantly better because of their ability to split the flow in the pipes into two or more smaller flows, leading to a lower flow resistance. The minimal difference in performance between the ring and mesh networks in the months of July and August indicates this as well. The seasonal change of the thermal losses follows its driving force: the temperature difference between the pipes and the ground. Equation 4-5 presents the definition of the cumulative temperature differences (ΔT_cum) between warm and cold lines and ground for each network type which is displayed in Figure 4-20.

$$\Delta T_{cum} = \left(T_{net\_h} - T_{ground}\right) + \left(T_{net\_c} - T_{ground}\right) \tag{4-5}$$

With a ΔT_{cum} of only a few Kelvin in the winter months, the losses remain low until the increasing solar gains heat up the network. With the ground still cold from winter, ΔT_{cum} is largest in May, leading to the highest thermal losses, independently of the network layout.

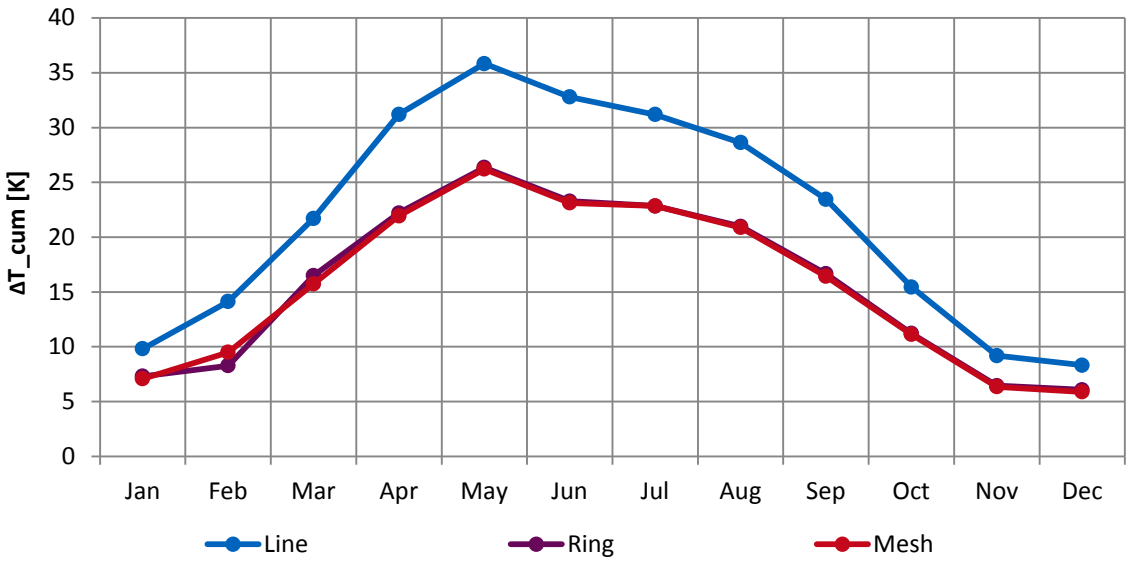

Figure 4-20: Cumulative temperature differences of line, ring and mesh NSD

The resulting thermal losses of the three layouts are displayed in Figure 4-21 on a monthly basis.

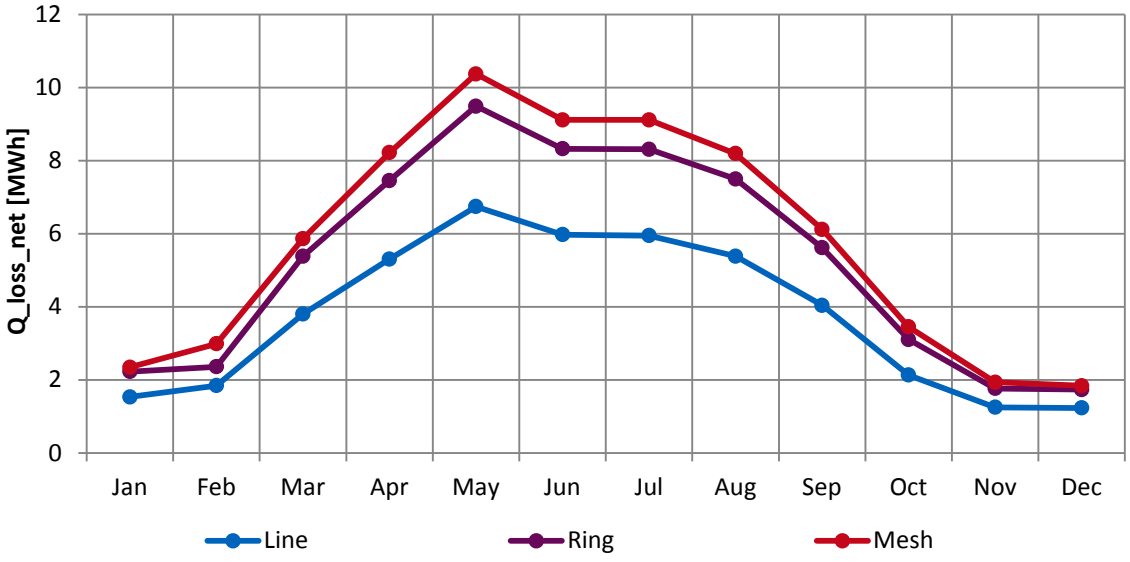

Figure 4-21: Monthly thermal losses of line, ring and mesh NSD

The total thermal losses of the line network are the lowest of the three network types, despite having the highest temperature difference between the pipes and the ground (cf. Figure 4-20), due to a significantly lower surface area. The ring and mesh layouts

perform quite similarly, with the difference traceable to the slightly different surface areas of the two, since the temperature difference is very similar (cf. Figure 4-20).

Up to this point the comparison of the network types is limited to the three different network types of NSD. Widening the focus to the influence of different pipe diameters on the various network types, the examination moves to the thermal network losses, the pump energy demand and the solar-thermal gains.

For all three network layouts, the simulation results show a linear increase in thermal losses with the increasing diameter of the pipes while keeping the thickness of the insulation layer constant (Figure 4-22).

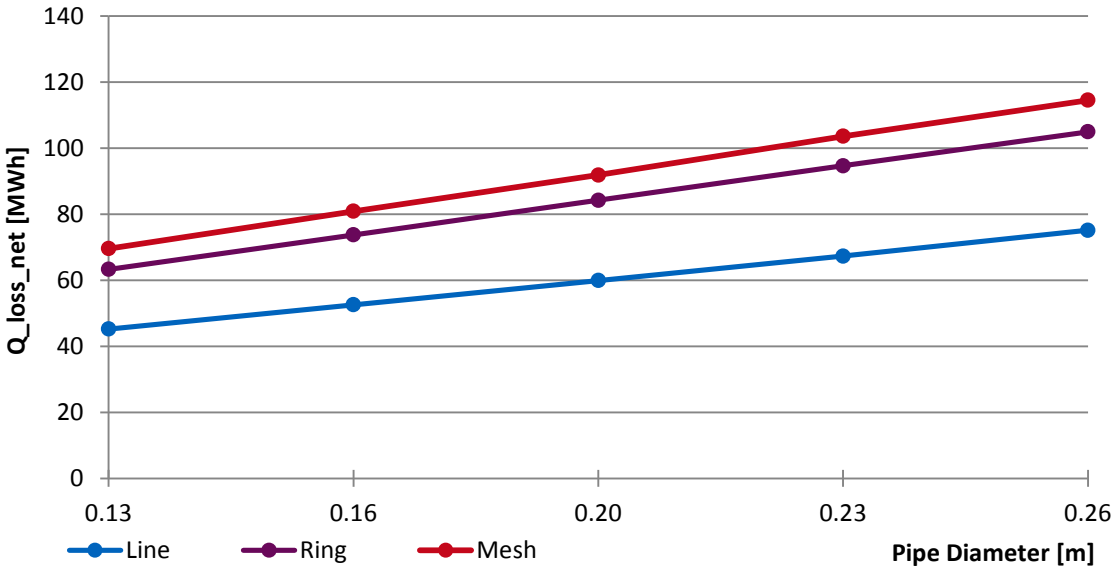

Figure 4-22: Thermal network losses of different network layouts for various pipe diameters

Figure 4-23 shows the specific thermal losses per meter of pipe. The difference in losses originating in the different network layouts is negligible compared to the effect of the increasing pipe diameter.

The effect of varying the pipe diameter on the thermal losses is quite clear: increasing the pipe diameter increases the surface area of the pipes, which leads to increased thermal losses. However, increased thermal losses are not the only effect of an increased pipe diameter. Increasing the pipe diameter not only increases the pipe surface but also the hydraulic cross-section of the pipe, resulting in fewer pressure losses due to reduced flow speeds at constant volume flows.

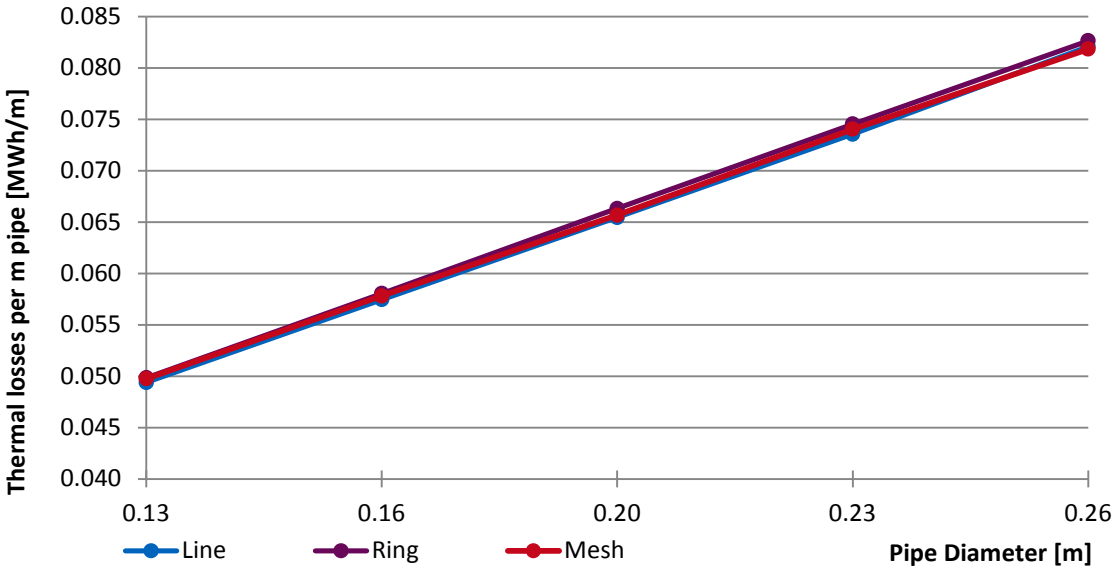

Figure 4-23: Specific thermal network losses per m pipe of different network layouts for various pipe diameters

This effect is displayed in Figure 4-24. Regardless of the network layout, the graph characteristics are very similar: high pump energy demands for small pipe diameters and subsequently fewer and fewer pump energy demands the larger the pipe diameter becomes.

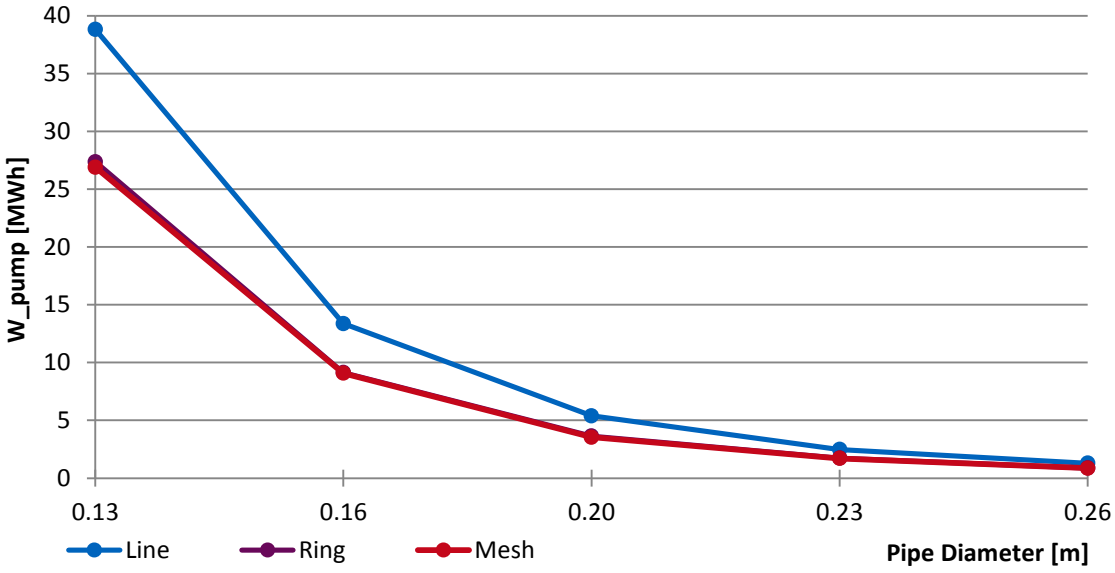

Figure 4-24: Pump energy demand of different network layouts for various pipe diameters

As described above, the pipe diameter used in the baseline case of 0.13 m leads to significantly lower pump energy demands of the ring and mesh layout compared to the line layout. With increasing pipe diameters this difference in performance is reduced to nearly zero with almost no difference in pump energy demand for the NLD. In terms of pump energy demand, the mesh and ring networks perform very similarly for all pipe diameters examined.

However, looking at the total CO_2-equivalents per year of the different network layouts, the line network is the one with the highest output (Figure 4-25). This can be explained through the different footprints of energy sources, which make up the differences in pump energy demand and thermal losses. With the thermal losses mostly covered by energy gained from solar-thermal collectors, the CO_2-equivalents of these losses are zero. The pump energy demand, however, is mainly covered by electrical energy from the public distribution network, of which about two thirds originates in non-renewable sources (see above). Therefore, the impact of the pump energy demand also governs the graph of CO_2-equivalents. Compared with Figure 4-24, the differences in the graph characteristics of the ring and mesh layouts originate in different shares of heat pump and auxiliary heater usage.

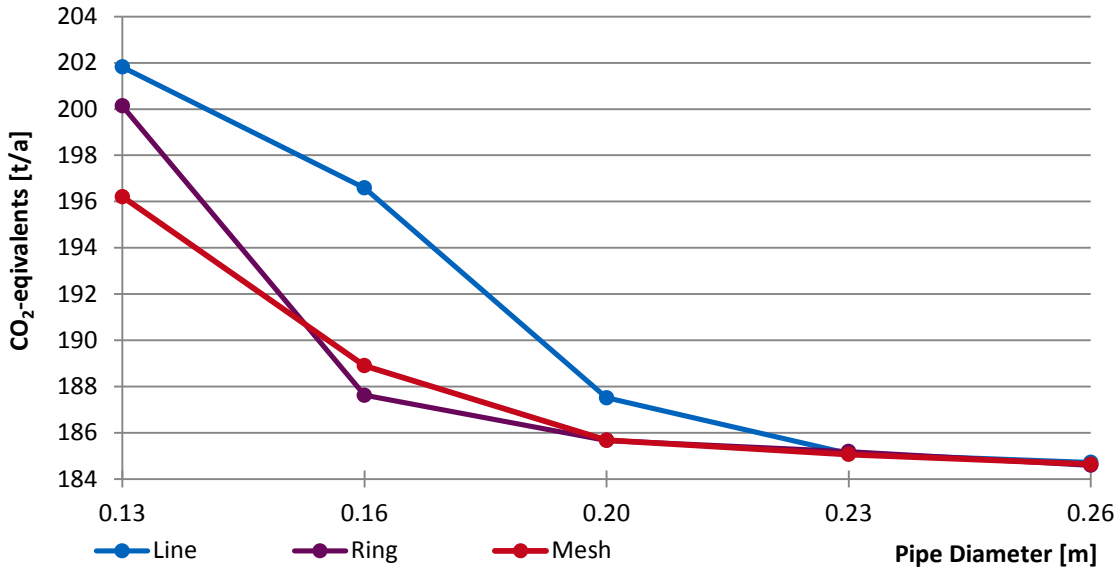

Figure 4-25: CO_2-equivalents of line, ring and mesh network layout for various pipe diameters

4.4.3. Network Heat-load Density

As set out in 4.3.3, this section examines the effects of a variation of the heat-load density within the network q_{net}. Figure 4-26 displays the decreasing heat-load density for the different network sizes obtained through the NSFs. The plot shows almost no difference in heat-load density of the networks between the two pipe diameters, since the difference in heat turnover is small compared to the total heat turnover.

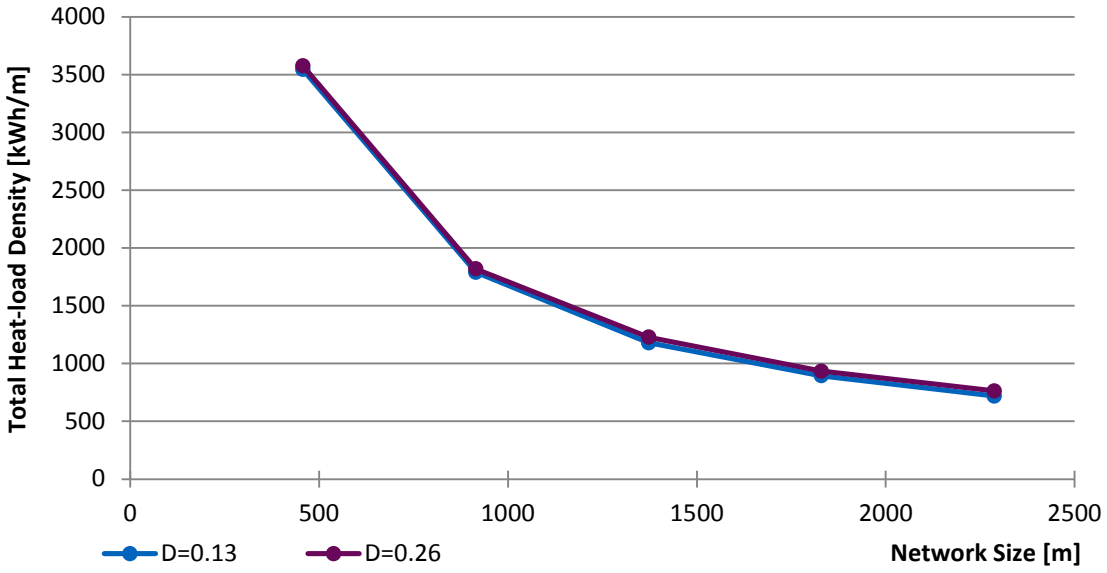

Figure 4-26: Total heat-load density of various network sizes for NSD and NLD

For NSD the different network sizes lead to the effects displayed in Figure 4-27: In the very large network (NSF 2.5), the turnover of Q_{RE} is 43.5 MWh higher than that of the very small network (NSF 0.5) for the same pipe diameter (Table 4-9).

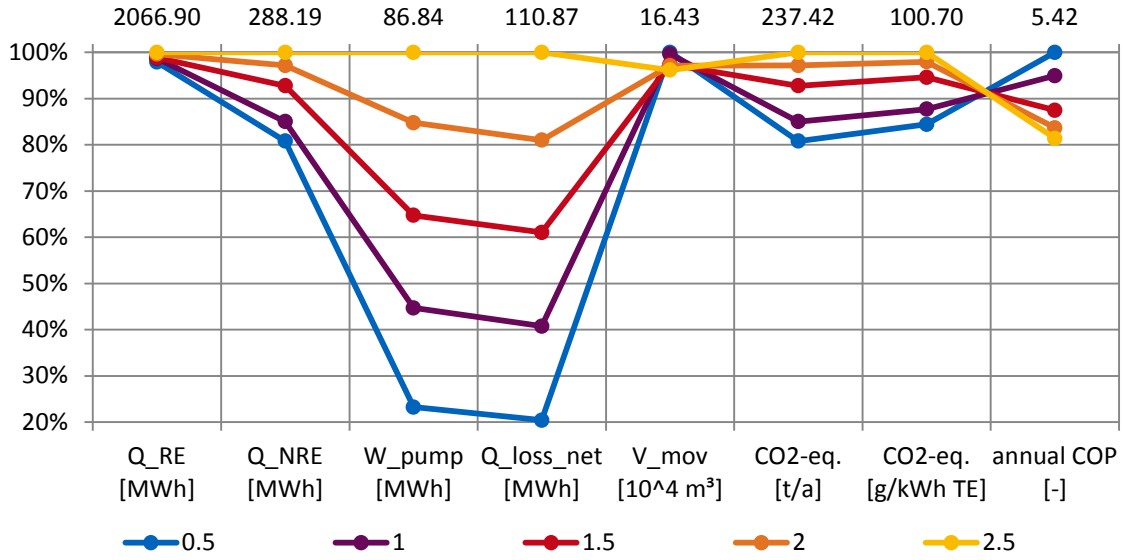

Figure 4-27: Performance indicators showing the simulation results for different NSFs of NSD

Also, the turnover of Q_{NRE} is increased by 55.3 MWh, Q_{loss_net} is increased by 88.3 MWh, and W_{pump} is increased by 66.6 MWh for the very large network compared to the very small network, leading to a reduction of the annual COP from 5.4 to 4.4. The total volume transported is slightly decreased by 6000 m³. However, the additional turnover of energy from non-renewable sources leads to an increase of the total and the specific CO_2-equivalents.

Table 4-9: Performance indicators for different NSFs of NSD

NSF [-]	Q_RE [MWh]	Q_NRE [MWh]	W_pump [MWh]	Q_loss_net [MWh]	V_mov [10^4 m³]	CO_2-eq. [t/a]	CO_2-eq. [g/kWh TE]	annual COP [-]
0.5	2023.4	232.9	20.2	22.6	16.4	191.9	85.0	5.4
1	2039.8	245.0	38.8	45.2	16.4	201.8	88.4	5.1
1.5	2043.4	267.4	56.2	67.7	16.0	220.3	95.3	4.7
2	2059.2	280.0	73.6	89.8	16.0	230.7	98.7	4.5
2.5	2066.9	288.2	86.8	110.9	15.8	237.4	100.7	4.4

The results of varying the network size of NLD show a similar behaviour of the network, but with a largely reduced pump energy turnover due to the increased hydraulic diameter (Figure 4-28). The turnover of energy from renewable sources is 97.9 MWh higher for the very large network (NSF 2.5) compared to the very small network (NSF 0.5) (Table 4-10).

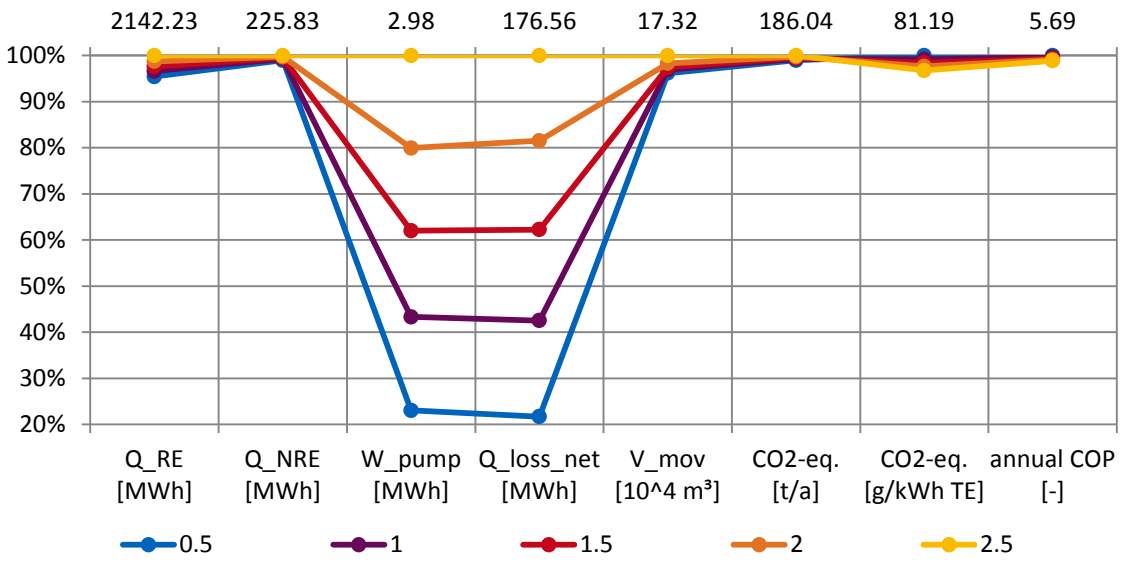

Figure 4-28: Performance indicators showing the simulation results for different NSFs of NLD

The turnovers of both non-renewable energy and pump energy are nearly constant, with a difference of 2.3 MWh between the very small (NSF 0.5) and the very large (NSF 2.5) network. However, for the pump energy this translates to a difference of 77% compared to the maximum pump energy turnover of 2.98 MWh of the very large network. The thermal losses of the very large network are increased by 138.3 MWh with an increase of 6000 m³ total volume transported compared to the very small net-

work. The total and specific CO_2-equivalents as well as the annual COP are nearly constant for the different network sizes.

Table 4-10: Performance indicators for different NSFs of NLD

NSF [-]	Q_RE [MWh]	Q_NRE [MWh]	W_pump [MWh]	Q_loss_net [MWh]	V_mov [10^4 m³]	CO_2-eq. [t/a]	CO_2-eq. [g/kWh TE]	annual COP [-]
0.5	2044.4	223.5	0.7	38.3	16.7	184.1	81.2	5.7
1	2070.1	224.2	1.3	75.1	16.8	184.7	80.5	5.7
1.5	2091.3	224.8	1.8	109.9	16.9	185.2	79.9	5.7
2	2114.9	225.3	2.4	143.9	17.0	185.6	79.3	5.6
2.5	2142.2	225.8	3.0	176.6	17.3	186.0	78.6	5.6
4	2222.8	236.0	4.9	293.2	17.7	194.4	79.1	5.4

The extremely large network with a NSF of 4 shows that the trends indicated in the variants of NSF 0.5 to 2.5 continue. Noteworthy is the trend of an increased turnover of energy from non-renewable sources and therefore an increase of total CO_2-equivalents, which barely show in the variants of NSF 0.5 to 2.5. Figure 4-29 displays the total heat loss density of different network sizes of NSD and NLD. The heat loss density of the NSD is nearly constant at a level of 50 kWh/m for the different network sizes. The heat losses of the NLD do not double compared to the NSD but reach a level of about 80 kWh/m, even though the surface area of the pipe does double compared to the pipe diameter of 0.13 m. This can be traced back to the heat flow through a hollow cylinder (Equation 3-2), which does not scale linearly with the diameter of the cylinder but through the natural logarithm of the ratio of outer and inner cylinder radius.

The heat loss density of the NLD also shows a higher difference of 6.5 kWh/m*a between the very large network and the very small network than the heat loss density of the NSD. One reason for this effect could be a higher cooling rate in the pipes in smaller networks due to the reduced flow speed, which leads with increasing network size to a reduction of the average losses and the heat loss density.

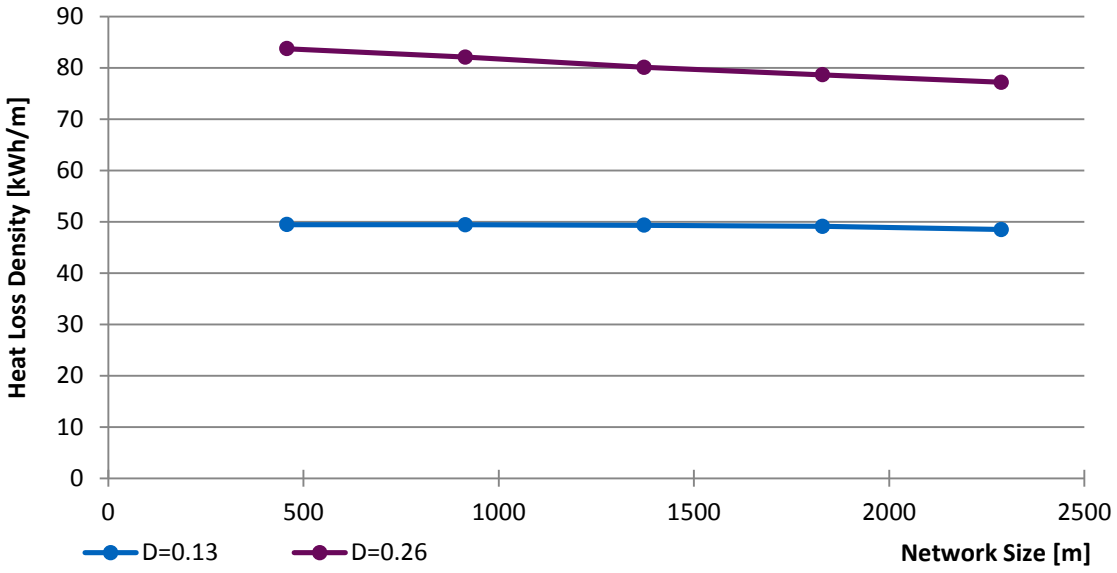

Figure 4-29: Total heat loss density of various network sizes for NSD and NLD

Figure 4-30 shows a comparison of the thermal losses of the differently sized networks (NSF 0.5 to 2.5) for NSD over the course of one year. The graph characteristics are very similar for all network sizes, with low thermal losses from November to February, a steep increase in the spring months with a maximum in May, a plateau in June and July, and a steep decrease during the months of August to October.

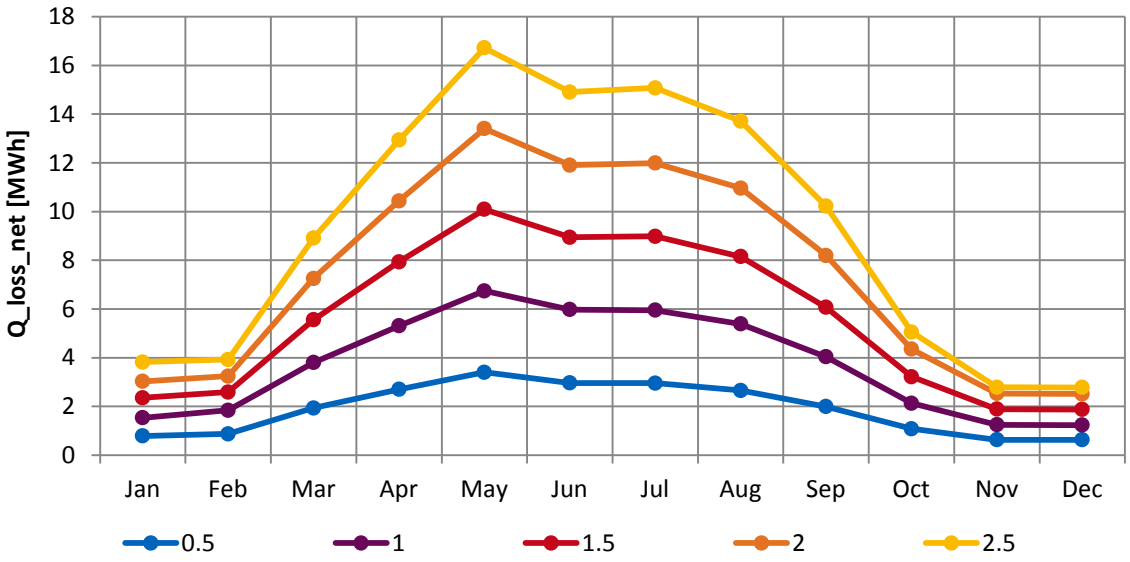

Figure 4-30: Thermal network losses of NSD with NSFs from 0.5 to 2.5

The total height of each graph is determined by the temperature difference between the network piping and the surrounding ground, as well as the total network piping surface. Since the network size is determined through NSFs, a proportional increase of the thermal losses as shown in Figure 4-30 is plausible. Similar to Figure 4-30, the thermal losses of the differently sized NLD are displayed in Figure 4-31. The absolute levels of the losses are significantly higher compared to the networks with a pipe diameter of 0.13 m, due to the increased pipe surface. However, the graph characteristics are very similar to the graphs in Figure 4-30 with low thermal losses during the winter months, maximum losses in the month of May, a plateau in June and July, and a steep decrease in the months from August to October.

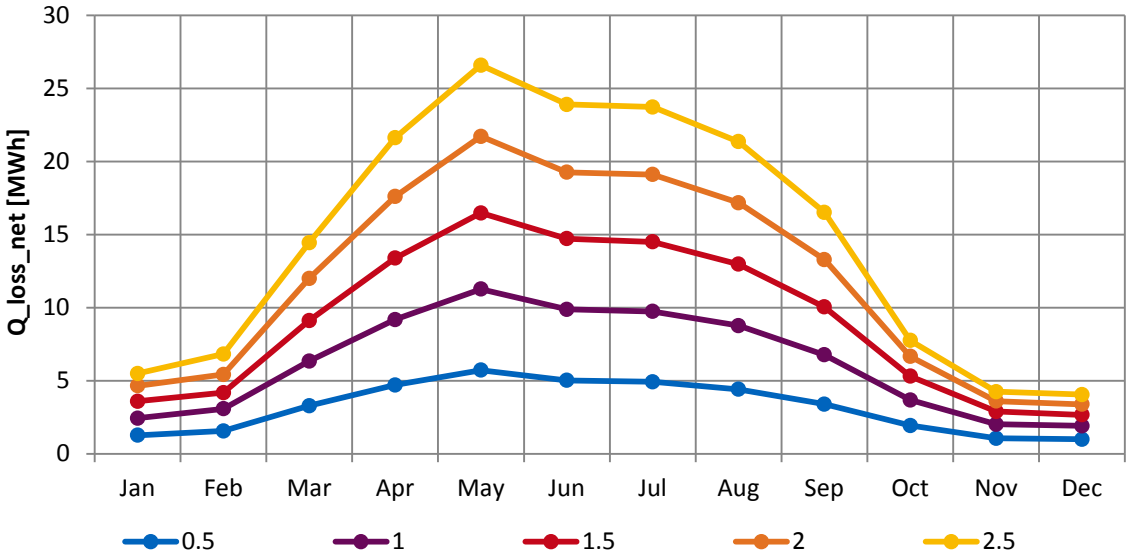

Figure 4-31: Thermal network losses of NLD with NSFs from 0.5 to 2.5

As described above, the variation of network size while keeping the heat demand constant leads to different heat densities in the networks. Table 4-11 displays the relationship of NSF, pipe diameter, $Q_{transported}$, Q_{loss_net} and q_{net}. Increasing the NSF from 0.5 to 2.5, the heat-load density decreases from 3.5 MWh/m.a to 0.7 MWh/m.a for both pipe diameters. At the same time the thermal losses Q_{loss_net} increase from 22.6 MWh to 110.9 MWh for NSD and from 38.3 MWh to 176.6 MWh for NLD.

Table 4-11: Q_transported, q_net, Q_loss_net and Q_loss of NSD and NLD

NSF [-]	Pipe diameter [m]	Q_transported [MWh]	q_net [MWh/m*a]	Q_loss_net [MWh]	Thermal losses of heat transp. [%]	Q_loss [MWh]	Total losses of heat transp. [%]
0.5	0.13	1621.5	3.54	22.6	1.4	91.9	5.7
1	0.13	1638.2	1.79	45.2	2.8	119.3	7.3
1.5	0.13	1620.1	1.18	67.7	4.2	146.0	9.0
2	0.13	1635.8	0.89	89.8	5.5	173.1	10.6
2.5	0.13	1643.3	0.72	110.9	6.7	192.3	11.7
0.5	0.26	1636.0	3.58	38.3	2.3	102.6	6.3
1	0.26	1663.9	1.82	75.1	4.5	129.0	7.8
1.5	0.26	1685.4	1.23	109.9	6.5	151.3	9.0
2	0.26	1709.9	0.93	143.9	8.4	175.7	10.3
2.5	0.26	1744.1	0.76	176.6	10.1	202.4	11.6

Figure 4-32 displays Q_{loss_net} as share of the total heat transported over the heat-load density of the networks. For the lowest heat-load density examined of 0.72 or 0.76 MWh/(m.a), NSD and NLD experience thermal losses of 6.7% or 10.1% of the total heat transported (Table 4-11).

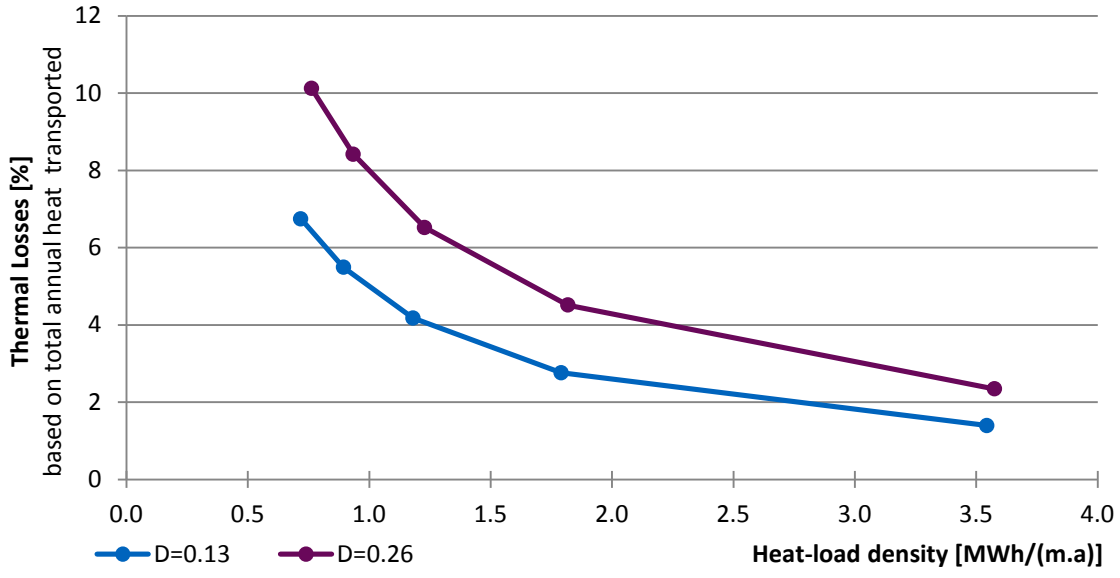

Figure 4-32: Thermal network losses over the network heat-load density of NSD and NLD

For higher heat densities, the shares of the thermal losses of the networks decrease and are below 10% of $Q_{transported}$. The graph displays a similar hyperbolic graph characteristic for both pipe diameters with higher thermal losses of the NLD (see also Figure 4-31). The storage losses of the seasonal storage for the different heat-load density networks are displayed in Figure 4-33. For low heat densities, the storage losses of the two different pipe diameters behave contrarily. For low heat densities, the NLD lose very little heat from the seasonal storage, less than 1% of the annual heat transported.

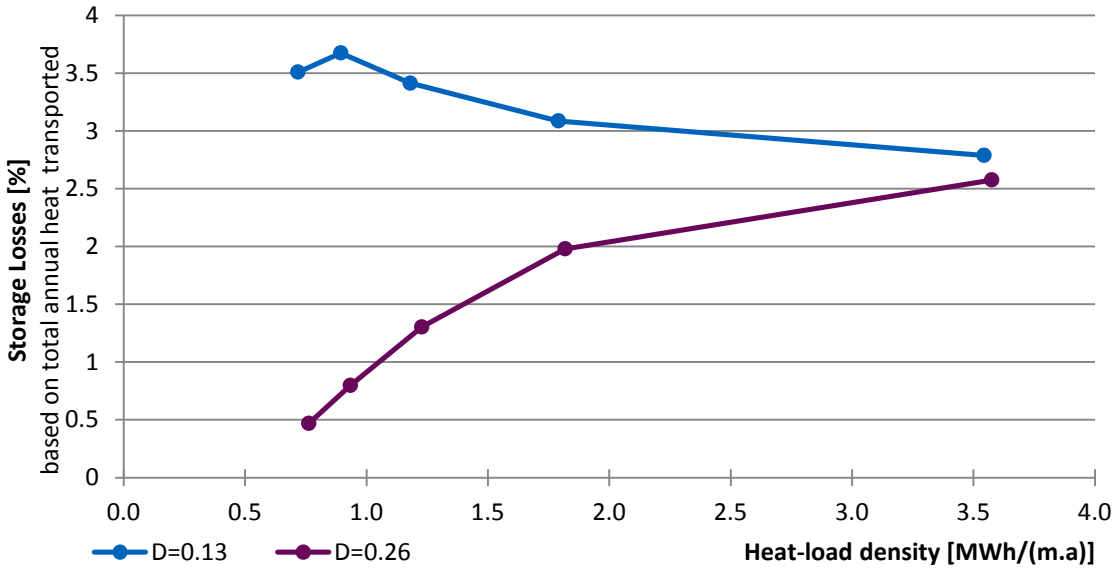

Figure 4-33: Network storage losses over the network heat-load density of NSD and NLD

However, the NSD lose up to 3.7% of the annual heat transported. For higher heat densities, both pipe diameters trend towards a seasonal storage loss of 2.6%.

One possible explanation for this behaviour could be a correlation to Q_{loss_net} of the different pipe sized networks displayed in Figure 4-32. The main driving force of thermal losses is temperature difference. With the significantly higher thermal losses for low heat densities in the NLD, the fluid temperature arriving at the seasonal storage is lower, resulting in lower losses. The behaviour of the NSD is the exact opposite: the lower thermal losses of the network itself lead to higher fluid temperatures when the fluid arrives at the seasonal storage, resulting in higher storage losses in the seasonal storage. For higher heat densities this divergent effect decreases, since the thermal losses decrease significantly, resulting in similar fluid temperatures of the two network types when they arrive at the seasonal storage. Shifting the focus to the total losses Q_{loss} (Figure 4-34), which combine as described above Q_{loss_net}, Q_{loss_stor} and the nearly constant Q_{loss_calc}, this explanation of behaviour is supported: the difference in

total losses between the two pipe diameters vanishes for low heat densities. For higher heat densities the difference in Q_{loss_net} is the dominant summand, resulting in slightly higher total losses of the NLD than the NSD. For heat densities higher than 1 MWh/m.a, the shares of the total losses of the networks are below 10% of the total heat transported.

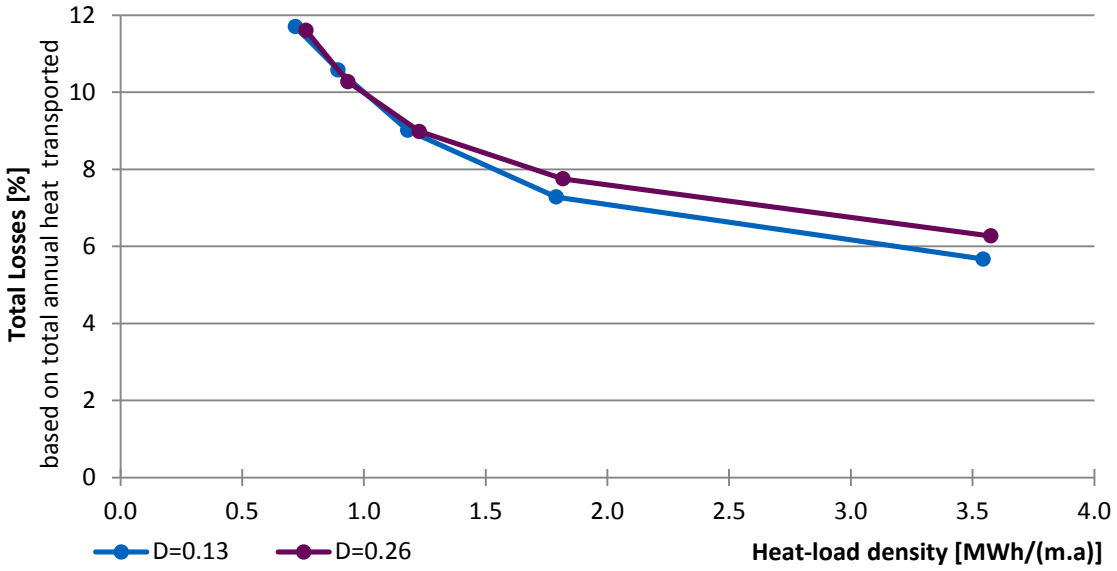

Figure 4-34: Total losses over the network heat-load density of NSD and NLD

Figure 4-35 sets the share of the pump energy demand W_{pump} in context with the total heat transported. The two graphs for NSD and NLD differ significantly in the range examined.

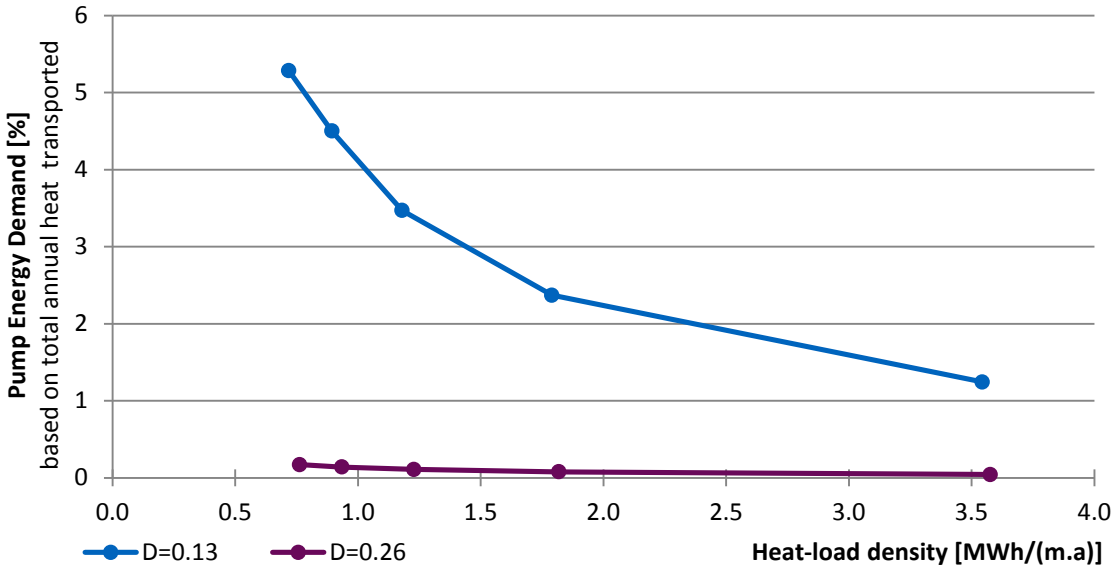

Figure 4-35: Pump energy demand of the network over the network heat-load density of NSD and NLD

While for the NSD a clear hyperbolic correlation of pump energy share and heat-load density can be identified, the NLD show very few changes of pump energy demand in the range observed and give the impression of an almost linear graph. However, the graph of the NLD also follows a hyperbolic pattern. The absolute level of pump energy needed is significantly higher for the NSD than for the NLD (cf. Table 4-9, Table 4-10). While the graphs converge for higher heat-load densities, the area of low heat-load density shows the potential for reduction of electrical pump energy demand of 5 percentage points.

4.4.4. Feed-in of Waste Heat

The input of heat from another heat source besides solar collectors changes the performance of the network. As set out in 4.3.4, the focus lies on the heat input from a pulsating waste heat source. Figure 4-36 provides an overview on some performance indicators of the network at 0%, 20%, 70% and 90% waste heat input. The seemingly random step size of waste heat input shares was chosen since at these values the extrema of the investigated range are reached.

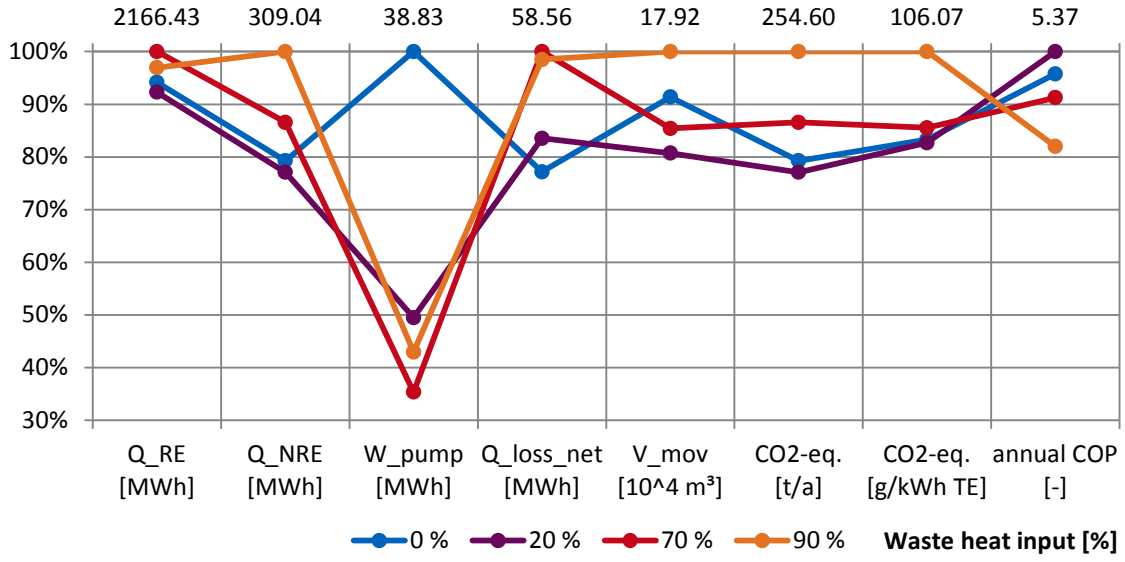

Figure 4-36: Performance comparison of networks with 0%, 20%, 70% and 90% feed-in of waste heat

While the values of most performance indicators range between 80% and 100%, the total pump energy demand W_{pump} varies between 35% and 100%, caused by the varying amount of feed-in of waste heat (see also Table 4-12). It includes the pump energy demand for the pump supplying the waste heat from the waste heat source into the network.

Table 4-12: Performance comparison of networks with 0%, 30%, 60% and 90% feed in of waste heat

Waste Heat [%]	Q_RE [MWh]	Q_NRE [MWh]	W_pump [MWh]	Q_loss_net [MWh]	V_mov [10^4 m³]	CO_2-eq. [t/a]	CO_2-eq. [g/kWh TE]	annual COP [-]
0%	2039.8	245.0	38.8	45.2	16.4	201.8	88.4	5.1
20%	1999.4	238.3	19.2	48.9	14.5	196.3	87.7	5.4
70%	2166.4	267.6	13.7	58.6	15.3	220.4	90.7	4.9
90%	2100.2	309.0	16.7	57.7	17.9	254.6	106.1	4.4

As depicted in Figure 4-37, an increase of waste heat put into the system leads to a decrease in the pump energy demand with a minimum at 50% waste heat input. From there the pump energy demand increases slightly. The decrease in pump energy demand originates in the reduced energy demand of the pumps discharging heat into the network (W_pump_c_to_h), since with reduced collector area the amount of heat to be discharged into the network also decreases. This decrease occurs up to the point where the higher additional electricity demand of the pump for waste heat input starts to dominate the graph.

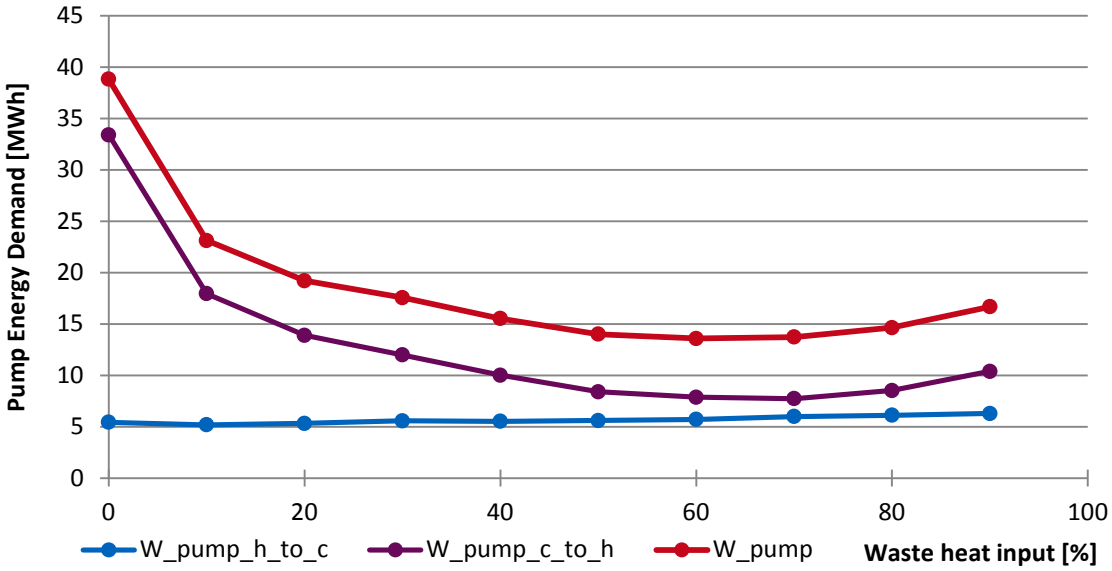

Figure 4-37: Pump energy demand of the network for different amounts of waste heat input

With a decrease in solar collector area, the pump energy demand for heat supply to the buildings from the network (W_pump_h_to_c) increases slightly due to the reduced direct and indirect local heat supply, which has to be made up for by heat pumps and heat supply from the network.

In the other performance indicator categories, for example, the input of non-renewable energy Q_{NRE}, Q_{loss_net} or CO_2-equivalents, the network with the highest waste heat input also shows the highest values. The performance indicators do not point to the origin of the increase in input of non-renewable energy. However, Figure 4-38 shows the source of the significant increase: the increasing energy demand of the heat pumps W_{HP} with increasing waste heat input. With less direct use of solar heat and less indirect local supply of the heat pumps with low temperature solar heat $Q_{ST\_indir\_HP}$, the heat pumps as well as W_{DHW} through the DHW electric heaters make up for the heat gap. The graph also distinctly shows the different orders of magnitude of the pump energy demand and the energy demand of the heat pumps. In combination with the decrease of the pump energy demand and an increase in the electricity demand for DHW electrical heaters, the total electricity demand of the system is lowest for a share of waste heat input of 20%.

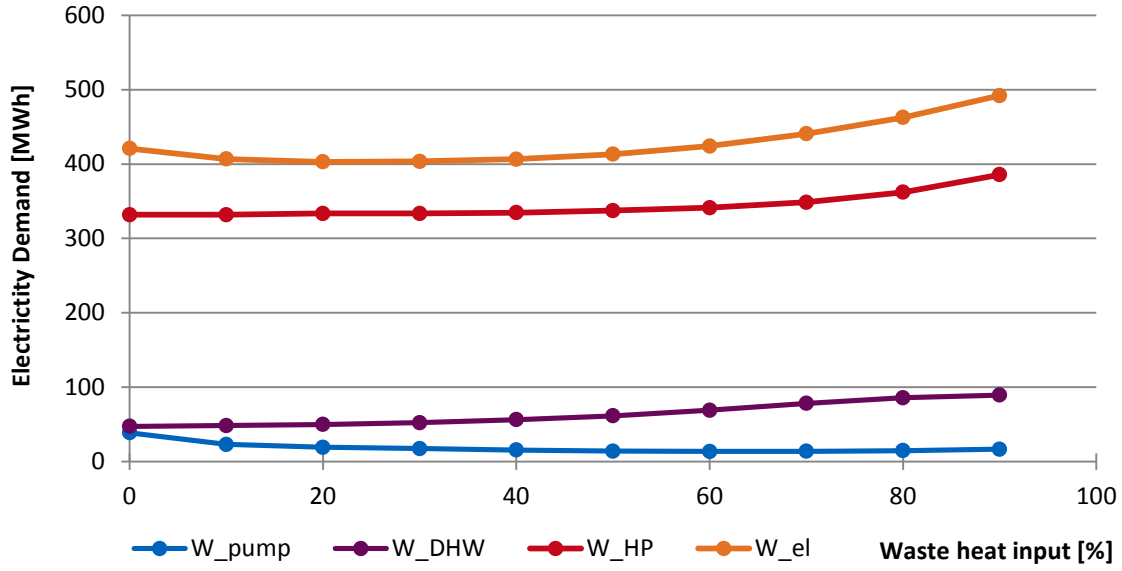

Figure 4-38: Electricity demand of the system for different amounts of waste heat input

Contrasting the electricity demand of the system with the electricity generation through the PVT panels, Figure 4-39 displays the effects of decreasing solar collector areas on photovoltaic energy generation and its direct usage.

With the linear decrease of solar collector area, the photovoltaic energy production W_{PV_gain} also decreases linearly. However, as described above, the total electric energy demand W_{el} only slightly decreases, and after levelling at a minimum, increases significantly. Noteworthy is that the amount of own consumption of the system W_{PV_use} does only slightly decrease compared to W_{PV_gain}.

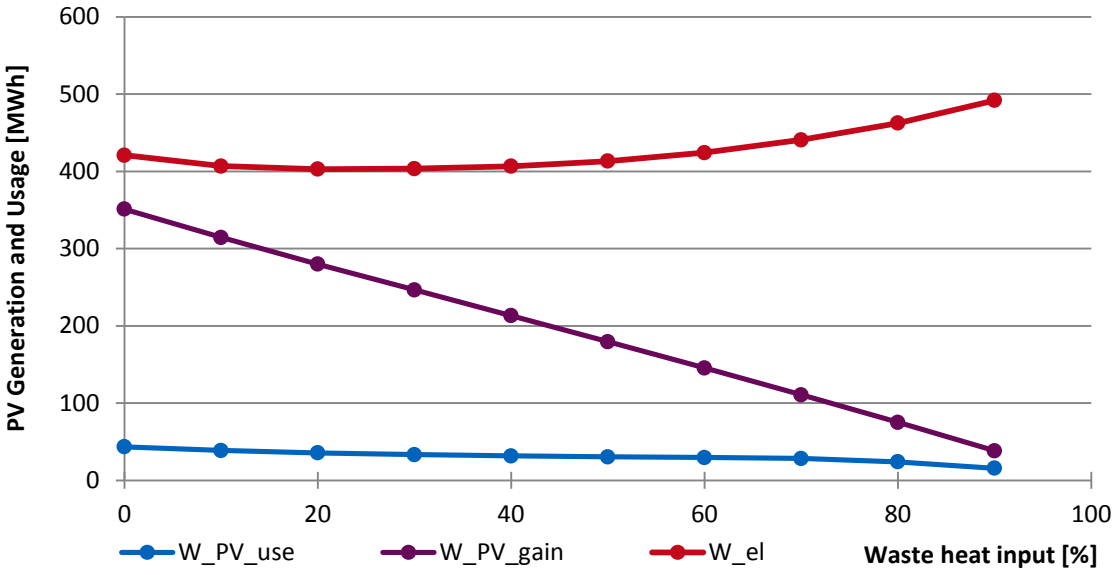

Figure 4-39: Photovoltaic generation and electricity demand and usage for different amounts of waste heat input

Furthermore, the direct correlation between the linear decrease of collector area and photovoltaic energy collected does not translate to the thermal energy collected by the PVT collectors. Figure 4-40 contrasts the direct and indirect solar-thermal energy gains, Q_{ST_dir} and Q_{ST_indir}, with the expected values, $Q_{ST\_dir\_exp}$ and $Q_{ST\_indir\_exp}$, of a linear decrease in collector area. The comparison is based on the direct and indirect solar-thermal energy gains at 0% waste heat input.

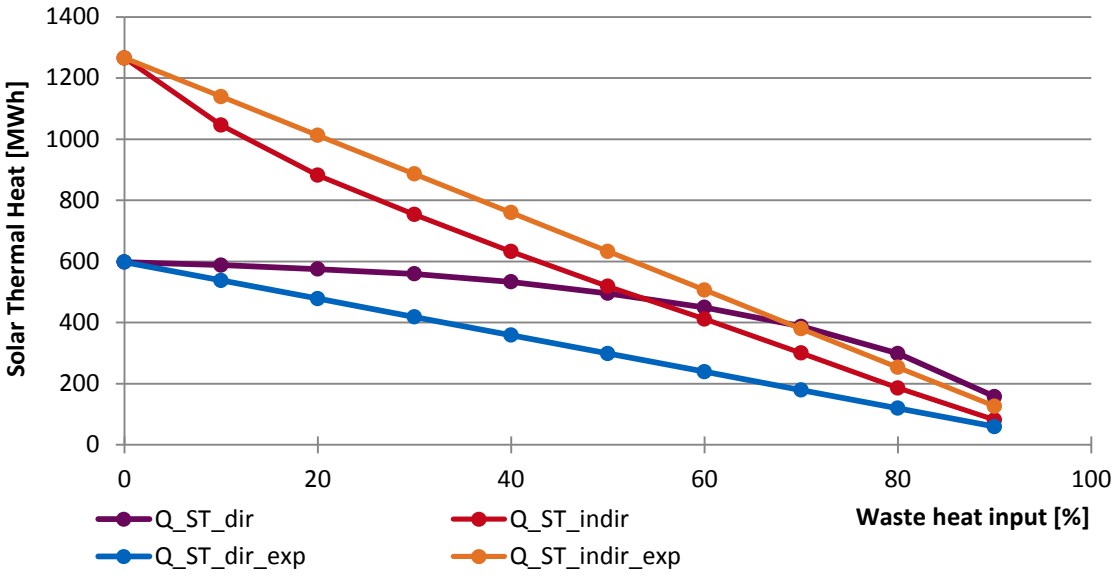

Figure 4-40: Actual and expected direct and indirect solar-thermal heat gains for different amounts of waste heat input

With increasing amounts of waste heat input into the system (decreasing solar collector area), the direct solar-thermal gains are significantly higher than expected. At the same time, the indirect solar-thermal gains are lower than expected. Above 55% waste heat input the direct gains surpass the indirect gains. This leads to a total solar-

thermal gain Q_ST of the system that does not correlate linearly with the input of waste heat (Figure 4-41). In combination with the linearly increasing input of waste heat (Q_waste), the sum of the two, the total thermal input into the system (Q_total) is therefore also not constant over the different amounts of waste heat input, and shows a minimum between 10% and 20% of waste heat input and a maximum at 70% of waste heat input. Noteworthy is the value of Q_ST of 239 MWh at 90% waste heat input, consisting of 81 MWh (Q_ST_indir) and 158 MWh (Q_ST_dir).

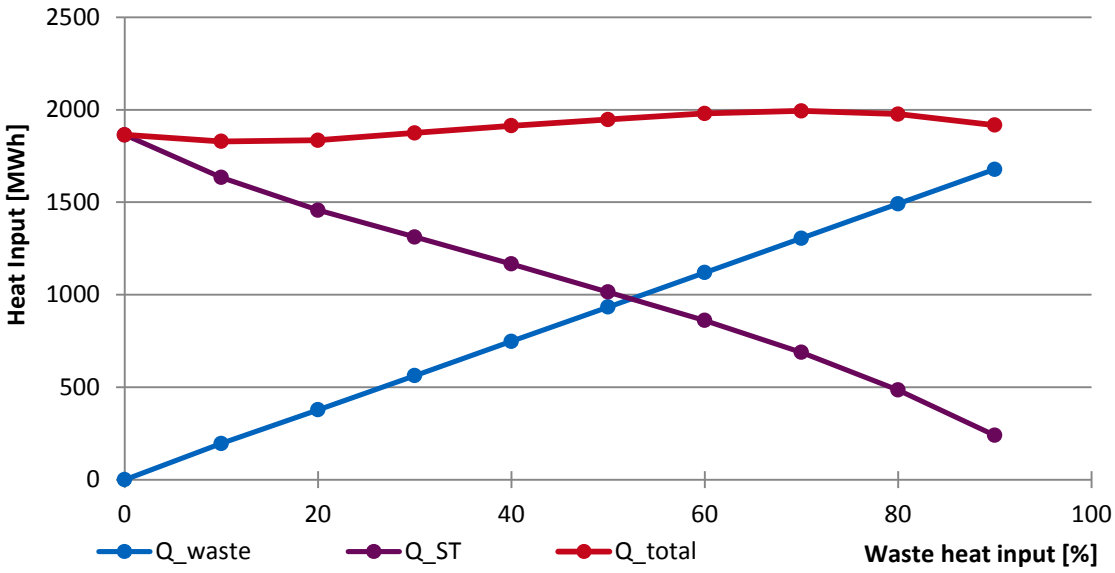

Figure 4-41: Total and solar-thermal heat input into the network for different amounts of waste heat input

As described above, Q_ST_dir refers to the solar-thermal heat coming directly to the stand-by storages from the solar collectors, while the indirect solar-thermal heat Q_ST_indir refers to the low-temperature solar-thermal heat passing through the buffer storages going either to the heat pumps as Q_ST_indir_HP or the network as Q_net_c. In this case the solar-thermal gains are very few, resulting in no indirect solar-thermal heat being discharged to the network and all 239 MWh being used locally. Figure 4-42 shows the monthly average network temperatures of the warm and cold lines (lines of same colour) for different amounts of waste heat input.

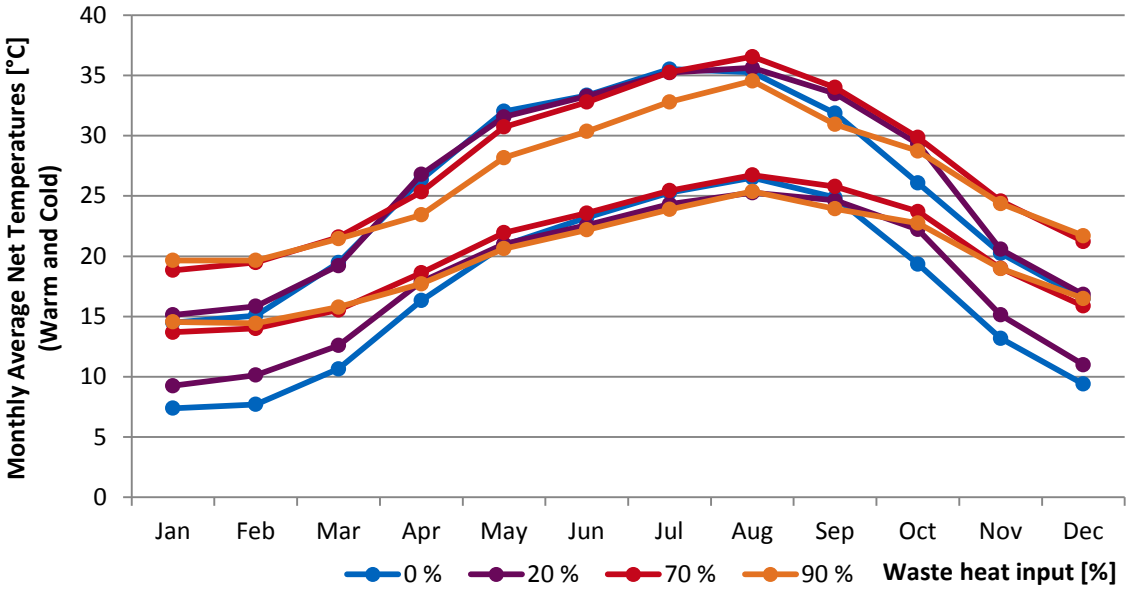

Figure 4-42: Overview of the monthly average network temperatures for different amounts of waste heat input

The effect of waste heat input on the average network temperatures is significant. For low amounts of waste heat input the monthly average network temperatures follow a sinusoidal pattern with a large amplitude. An increase in waste heat input leads to a reduction of the amplitude and a rise in the total average network temperature, especially in the winter months. This behaviour is directly linked to the waste heat source and its ability to maintain a temperature delta of 10 K between its input and output (4.3.4).

The higher average network temperature and the variation of Q_{total} over the different amounts of waste heat input reflects in Q_{loss}, the sum of the losses of the system (Figure 4-43). While Q_{loss_net} and Q_{loss_calc} vary little for the different amounts of waste heat input, Q_{loss_stor} experiences a broad change, mirroring the variation of the average network temperatures and Q_{total}. Here the seasonal storage acts as a heat overflow with an always positive Q_{loss_stor}, enabling a flow of excess heat to the storage surroundings.

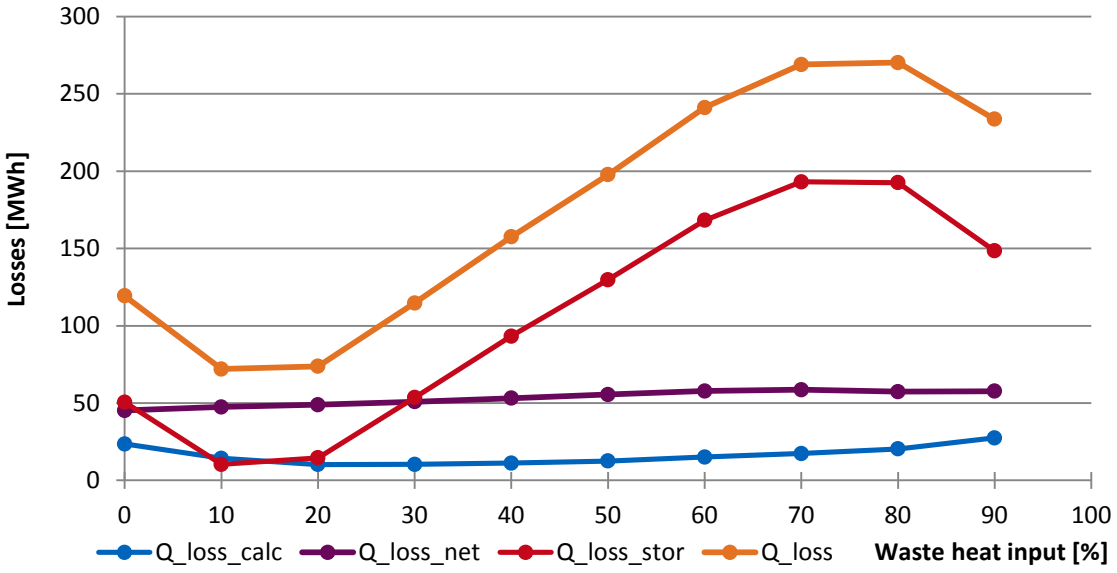

Figure 4-43: Overview of the losses of the system for different amounts of waste heat input

Figure 4-44 displays the heat input into the network Q_{net_c} and the heat taken from the network Q_{net_h} in combination with the indirect solar-thermal gains Q_{ST_indir} and their local usage in the corresponding heat pumps as $Q_{ST\_indir\_HP}$. With increasing amounts of waste heat input (and decreasing collector area), the local turnover of indirect solar-thermal heat decreases. At 90% waste heat input Q_{ST_indir} is equal to $Q_{ST\_indir\_HP}$ of 81 MWh, indicating only local turnover of indirect solar-thermal heat and no discharge into the network.

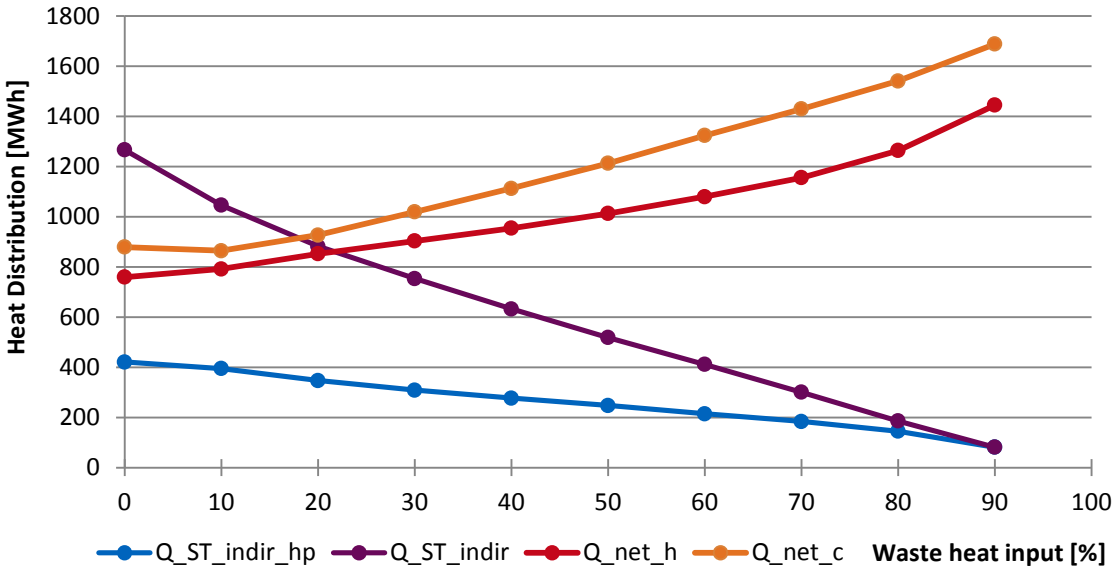

Figure 4-44: Overview of building performance of heat transferred to and from the network as well as local use of indirect solar-thermal heat for different amounts of waste heat input

With increasing waste heat input into the network and reduced local solar-thermal production by the buildings (cf. Figure 4-40), Q_net_h increases, substituting the missing local solar-thermal heat. Above 40% waste heat input the increase of Q_net_h steepens, complementing Figure 4-38 displaying the electricity demand due to increased heat pump activity as well as Figure 4-40 displaying a steep reduction in Q_ST_dir. This translates to an increase in CO_2-equivalents for waste heat inputs above 40% (Figure 4-45).

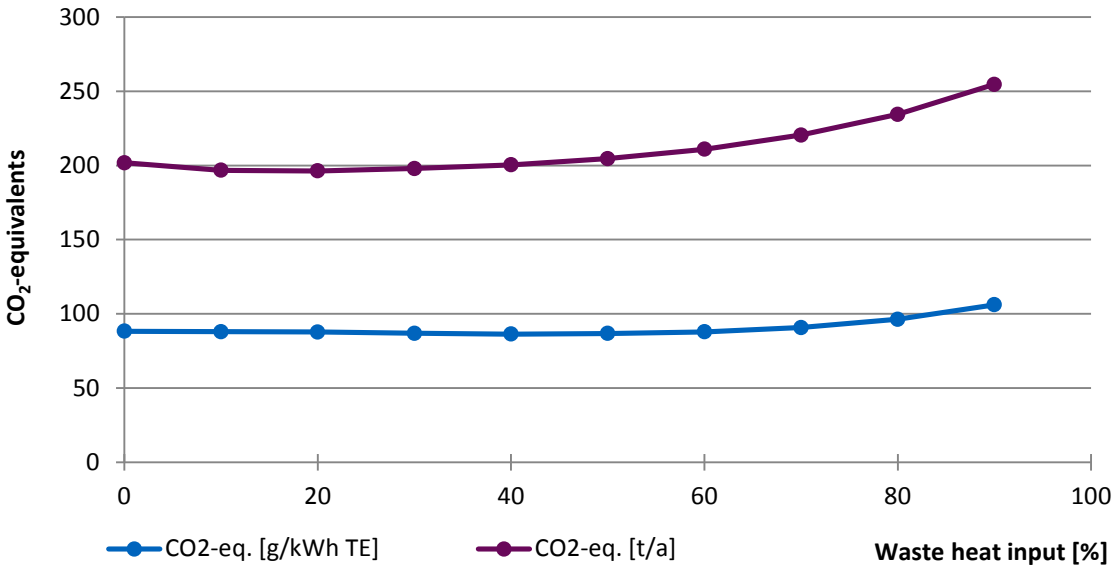

Figure 4-45: CO_2-equivalents of the system for different amounts of waste heat input

Here the total value of CO_2-equivalents in tons per year rises significantly more than the specific CO_2-equivalents in grams per kWh TE, since the total electricity demand also increases correspondingly to the total CO_2-equivalents (cf. Figure 4-39). With the increase of the total electricity demand and little change in turnover of energy from renewable sources Q_RE, the turnover of energy from non-renewable sources Q_NRE increases significantly with an increasing amount of waste heat in the network.

4.4.5. Network Pipe Insulation Thickness

This section examines the influence of different pipe insulation thicknesses (4.3.5) on the network performance. The thermal insulation of the network piping increases the thermal resistance between the pipes and the surrounding ground and thereby reduces heat transfer between the two. Figure 4-46 displays the performance indicators of the network for IFs from 0.25 to 2.

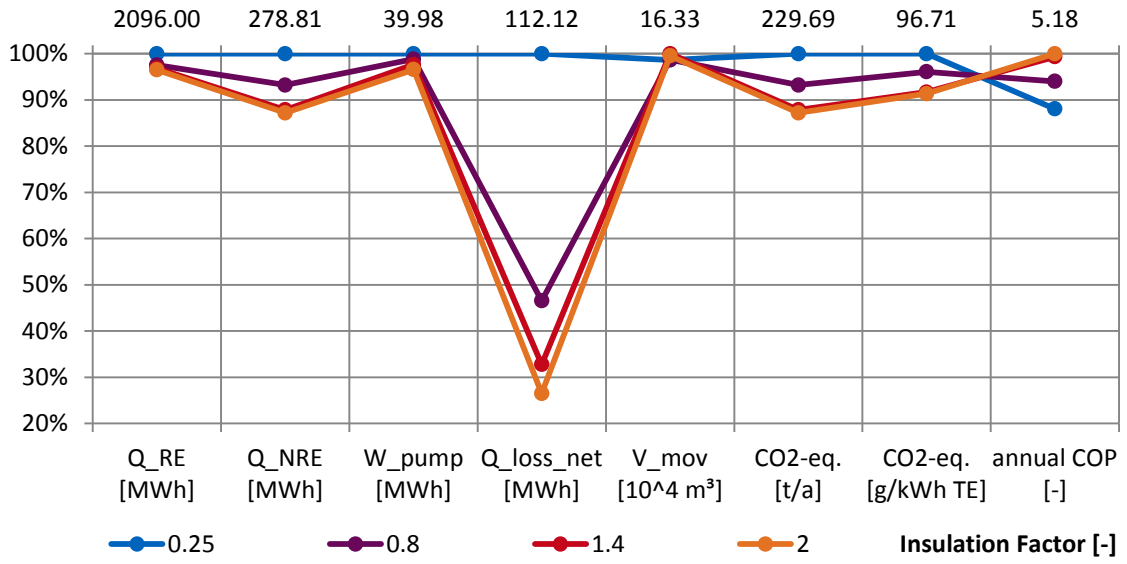

Figure 4-46: Performance comparison of networks with IFs of 0.25, 0.8, 1.4 and 2

The effect of additional pipe insulation is straightforward: the higher the IF, the thicker the pipe insulation, and the fewer the thermal losses Q_{loss_net}. Figure 4-47 displays the reduction of Q_{loss_net} of the networks for different IFs (pipe insulation thicknesses). The same graph shows the total volume moved through the networks, which is constant for all networks with different IFs. Lower thermal losses lead to a reduced electricity demand for the auxiliary heaters (W_{aux}) as displayed in Figure 4-48, which results in a reduced demand of Q_{RE} and Q_{NRE} (cf. Figure 4-46).

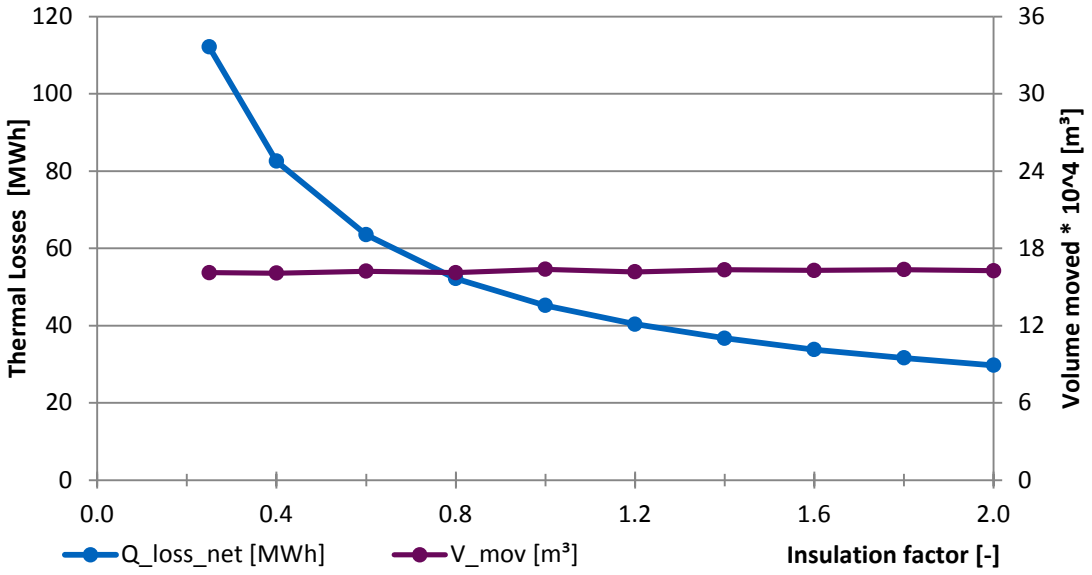

Figure 4-47: Thermal losses of networks with different IFs from 0.25 to 2

The high thermal losses at low IFs are compensated for by the auxiliary heaters which make up for the heat lost through the pipe walls during the transport of the network fluid.

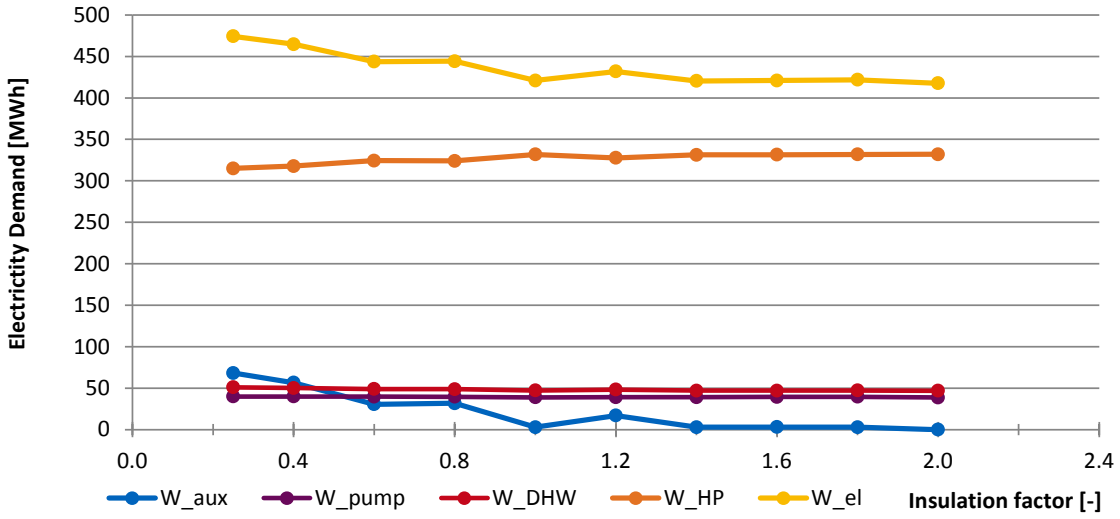

Figure 4-48: Electricity demand of networks with different IFs from 0.25 to 2

The electric energy required for pumping W_{pump} and reheating the DHW W_{DHW} is constant for networks with different IFs. With decreasing thermal losses of the network, the electric energy demand of the heat pumps W_{HP} increases slightly. Figure 4-49 also displays the increase of heat drawn from the networks with increasing IFs. One reason could be the higher temperatures at the building interfaces due to fewer thermal losses. With higher supply temperatures, the heat pumps have a higher temperature difference to use as a heat source and are able to run longer before shutting down due to undercooling. Figure 4-49 also shows a decrease of the indirect solar-thermal gains Q_{ST_indir} as well as Q_{net_c}. This also can be traced back to increasing temperatures in the network due to increasing IFs and therefore less capacity to buffer solar-thermal heat.

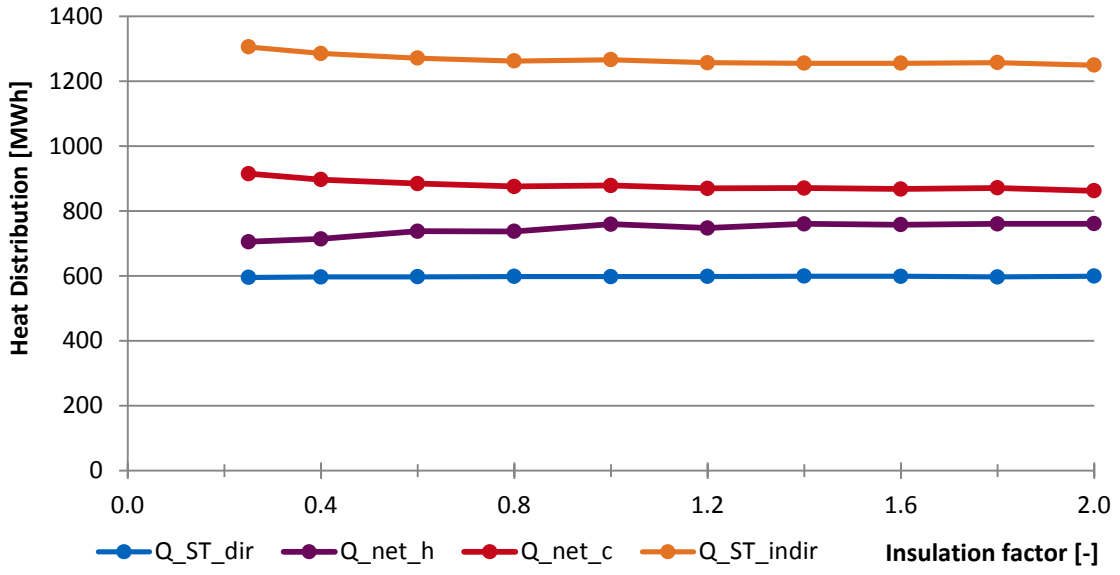

Figure 4-49: Overview of heat gains and distribution in networks with different IFs from 0.25 to 2

In total, an increase of the pipe insulation thickness leads to a decrease in the amount of Q_{NRE} required and a decrease in the total CO_2-equivalents (Figure 4-50) of more than 25 tons per year.

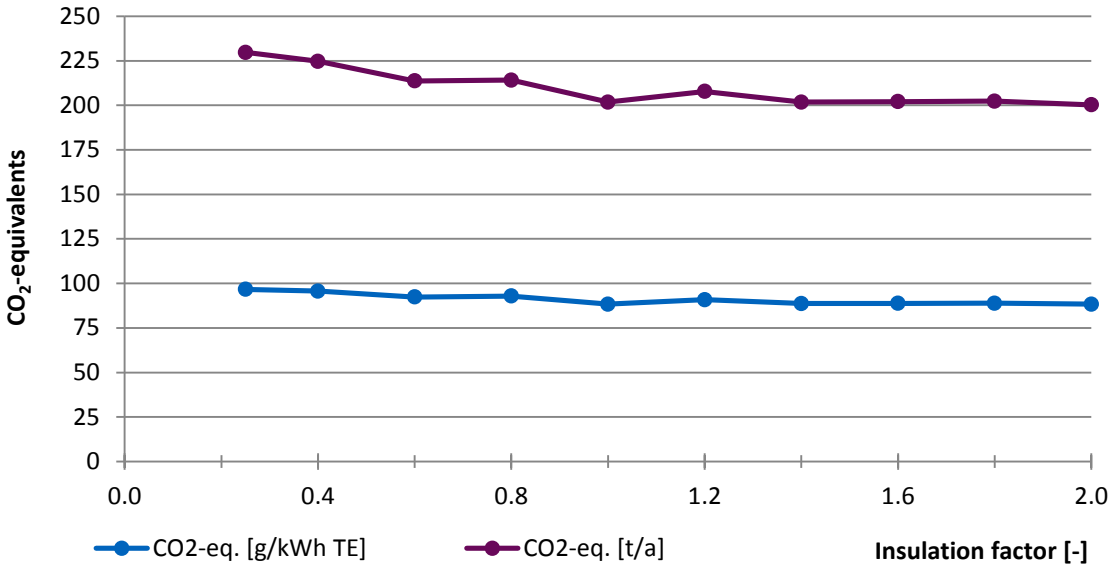

Figure 4-50: Overview of CO_2-equivalents in networks with different IFs from 0.25 to 2

4.4.6. Traditional District Heating Network

Of the traditional DHN simulation (4.3.6), the TE turnover of 2460 MWh can be divided into 2198 MWh useful energy and 262 MWh losses. Based on the parameters described in 4.3.6, 11.1% of the TE originate in renewable sources and 88.9% in non-renewable sources (Table 4-13). With the parameters described above (4.4), this leads to a total CO_2-equivalent of 643 t/a or 261.5 g/kWh TE.

The ratio of renewable energy to non-renewable energy in the DHN is reversed compared to the baseline case. Figure 4-51 displays this inversion as well as the increase of losses of the system Q_{loss}. With a nearly identical ratio of the outputs Q_{HW} and Q_{DHW}, compared to the baseline case, the reversed ratio of renewable and non-renewable energy on the side of the inputs is even more prominent. (Heissler et al. 2017b)

Table 4-13: Summary of the simulation results (Focus 6) (Heissler et al. 2017b)

2460	MWh Total Energy Turnover
consisting of	
2198	MWh Useful Energy
262	MWh Losses
or	
273	MWh Renewable Energy
2187	MWh Non-Renewable Energy
resulting in	
643	t CO_2-equivalent/a
262	g CO_2-equivalent/kWh Total Energy
—	annual COP

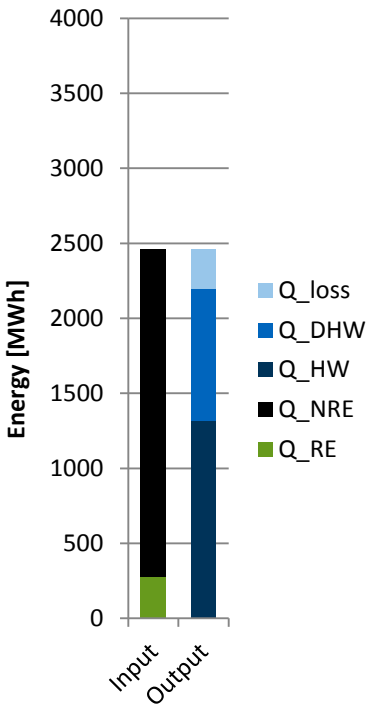

Figure 4-51: Energy In- and Output DHN (Heissler et al. 2017b)

Figure 4-52 shows the monthly HW and DHW demand which is met year-round by Q_{DHN}, the heat input into the DHN. During the summer months the heating demand Q_{HW} is very low and most of the energy demand comes from DHW preparation Q_{DHW} (Heissler et al. 2017b). The imbalance of supply and demand indicates the losses of the network.

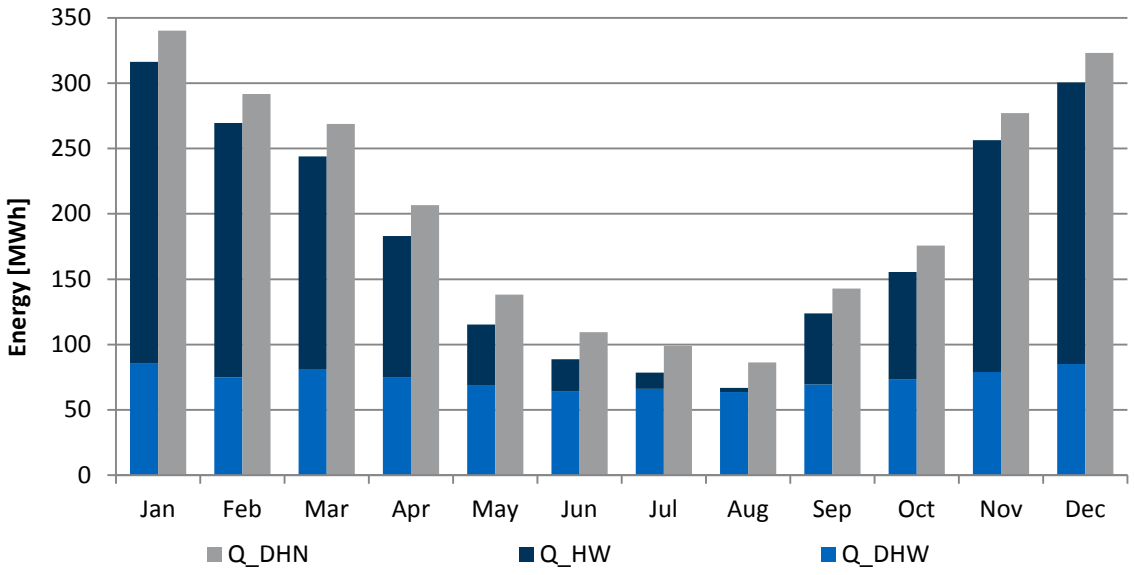

Figure 4-52: Monthly DHW and HW demand (Heissler et al. 2017b)

By design, the temperature graphs of the warm and cold lines of the DHN at the feeding point (Figure 4-53) of the heat source are very stable compared to the baseline case. The supply temperature measured at the feeding point is nearly 100 °C all year. With stable supply temperatures, the return temperature is also much more constant compared to the baseline case (Figure 4-13). Small temperature fluctuations in the return line occur in the summer months due to stagnation and controlled short-circuit measures. (Heissler et al. 2017b)

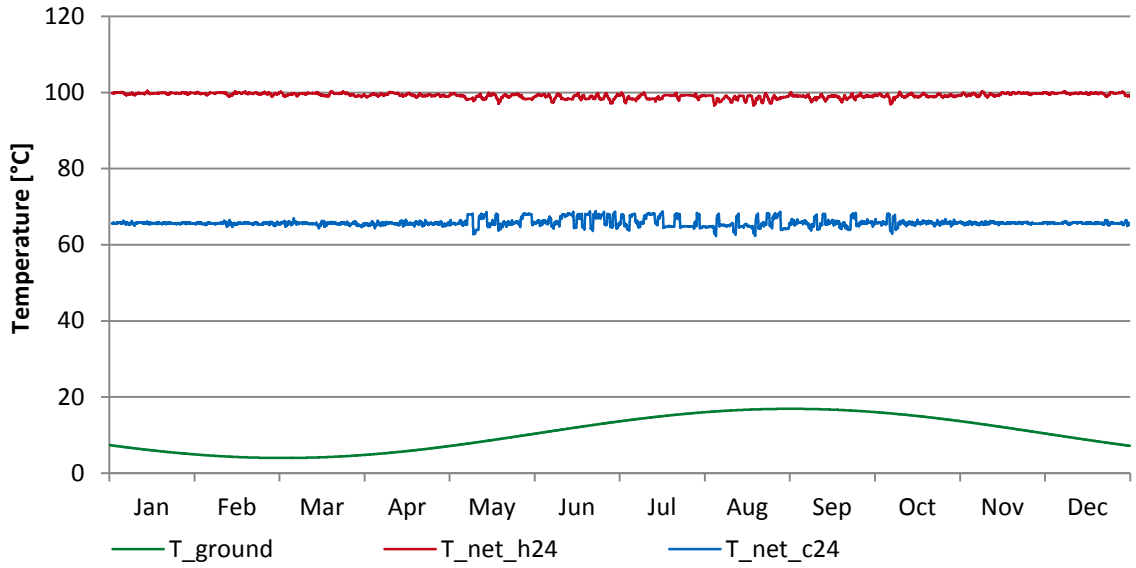

Figure 4-53: High and low temperatures of the DHN and undisturbed ground temperature (Heissler et al. 2017b)

All year round, supply and return line temperature lie significantly above the undisturbed ground temperature T_{ground}. During the course of one year the ground temperature oscillates between 4 °C and 17 °C (4.1). This oscillation is also visible in the thermal losses of the network (Q_{loss_net}) (Figure 4-54), which are lowest in the months of August and September when the temperature difference between the network and the undisturbed ground is lowest. The thermal losses of the DHN add up to 262 MWh over the course of one year, which is almost 6 times as high as the total thermal losses of the baseline case (cf. Figure 4-14). This amount of heat equals the total heat demand of the quarter in the month of February. (Heissler et al. 2017b)

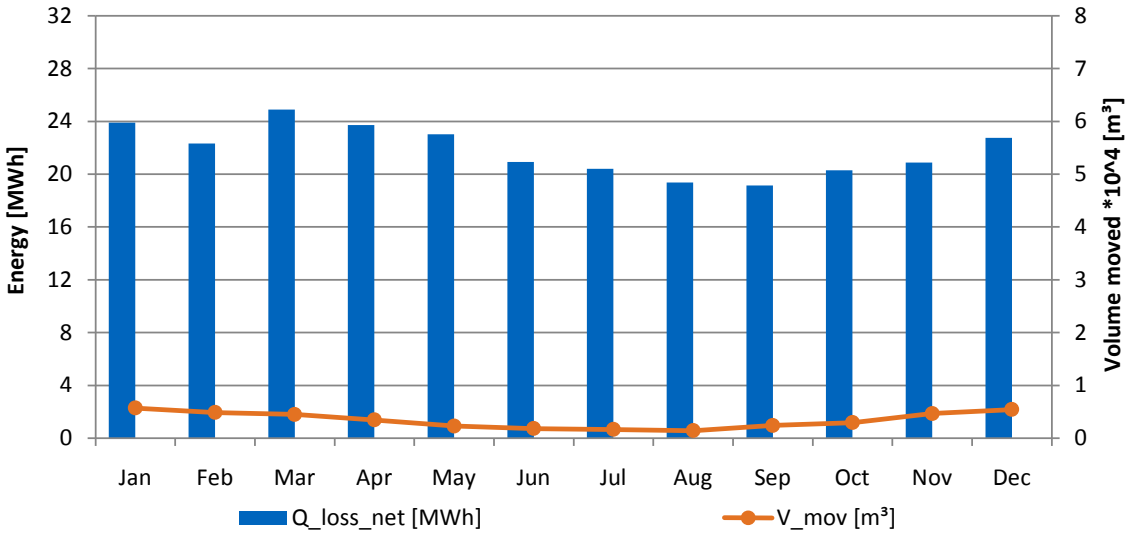

Figure 4-54: Thermal network losses and total volume moved in a traditional DHN

Compared to the baseline (4.4.1), V_{mov} is significantly lower, with not only lower monthly values but also a different graph characteristic. During the summer months a distinct correlation between lower heat demand and lower volume transported is visible. In the baseline case there are two peaks of flow, one in summer and one in winter. There is no maximum of flow here during the summer, since no heat is collected locally which would have to be discharged to the network. (Heissler et al. 2017b)

With the low total energy demand of the buildings in summer (Figure 4-52) and the high thermal losses, the drop of the supply temperature is most extensive at the critical path, the line to building interface 12. The temperature profiles of the warm and cold lines of the DHN at building interface 12 are T_{12_h} and T_{12_c}. For the benefit of readability, Figure 4-55 displays the 24h moving averages of T_{12_h} (T_{12_h24}) and T_{12_c} (T_{12_c24}) as well as T_{ground} (see 4.1). As described in 3.4, a drop of the supply temperature below 68 °C is prevented by controlled short-circuiting of the supply and return lines.

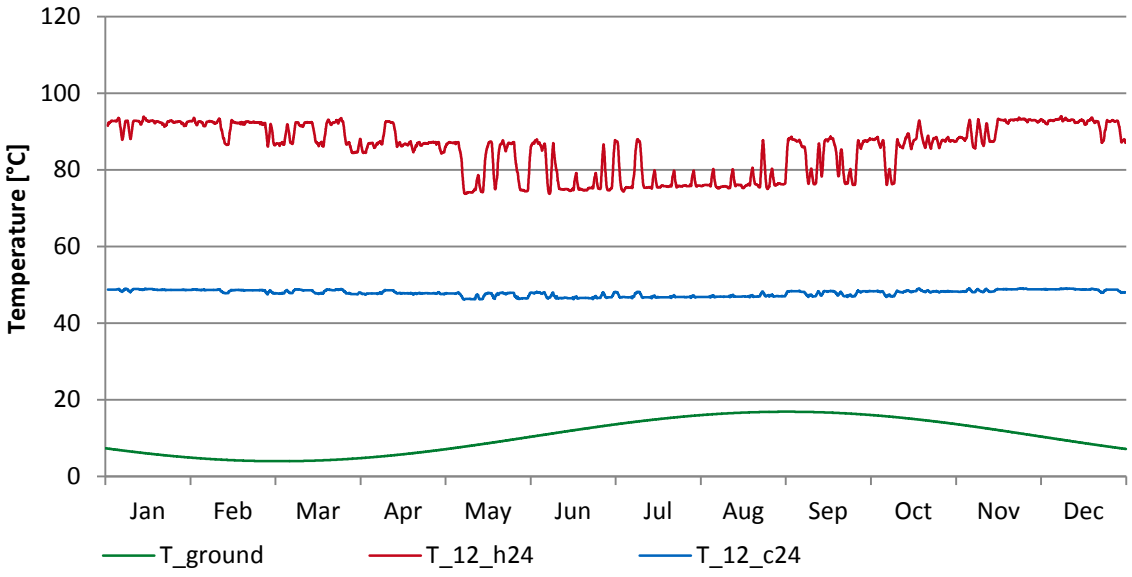

Figure 4-55: High and low temperatures of the DHN at the end of the critical path (building 12) and undisturbed ground temperature

The mean hourly values of the total pressure at the critical hydraulic path in the warm line, at the T-junction to building interface 12, are displayed in Figure 4-56. Similar to the NSM, the DHN Model is extremely sensitive to pressure levels below saturation vapour pressure. Therefore, a pressure level of 90 bar was chosen as zero level, to rule out any possibility of any single pressure peak reaching saturation vapour pressure. As described above (3.4), the pressure difference applied by the heat source is 10 bar. The pressure peaks in Figure 4-56 range from 89.35 bar to 90 bar, with an average pressure level in winter of 89.8 bar and in summer of 89.9 bar.

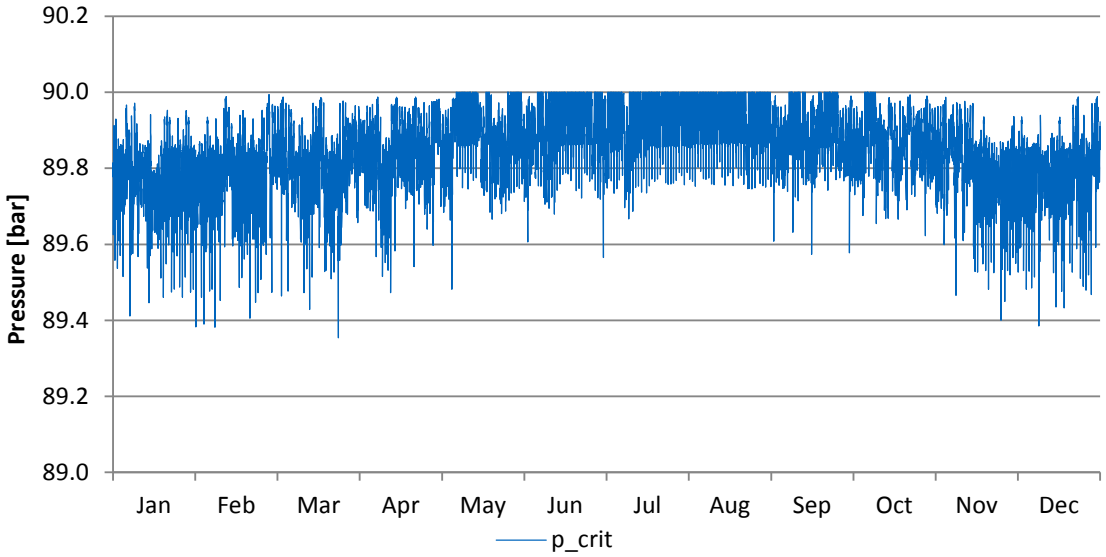

Figure 4-56: Total pressure at the critical path (Focus 6)

Figure 4-57 displays an overview of the energy flows of the DHN case with the cumulative energy flows for all buildings of the district over the time period of one year.

Similar to the visualization of the energy flows in the baseline case (Figure 4-17), the building shown in Figure 4-57 represents all the buildings in the system and serves to visualize the cumulated energy flows between the components of every building in the system at once. In sum, the buildings draw 2459.2 MWh from the feeding point of the DHN. On the way to the buildings, 261.6 MWh are lost to the surroundings. 2197.6 MWh reach the buildings and are used for heating (1312.5 MWh) and DHW preparation (885.2 MWh). Not included are the pump energy demand for the network and the thermal losses of any storage on the supply side.

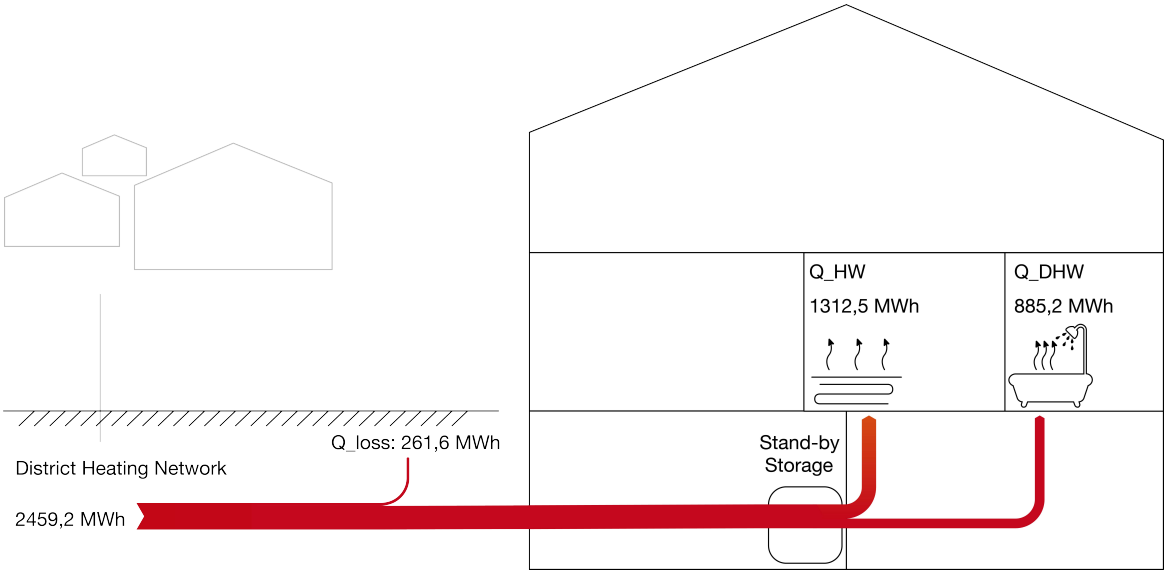

Figure 4-57: Sankey diagram of the energy flows through the system (Traditional DHN)

4.5. Previous study and results

As described in 2.2, a previously conducted study with a similar model structure (Heissler et al. 2017b) examines the influence of several different energy demand scenarios (Table 4-14) not examined in 4.4. With different boundary conditions to the results displayed in 4.4, the study does not look at the TE turnover, but at Q_{use} of the system, and does not encompass the pump energy demand. It follows that the values in this section are not comparable to the values displayed in 4.4. Still, the influence of different demand scenarios is made visible by comparison to the standard HW and DHW scenario in 4.5.1.

The standard HW and DHW demand here is equal to the demand defined in 4.2. The high HW demand scenario represents the energy demand of buildings with constructions based on WärmeschutzV of 1982, while the low HW demand scenario represents the energy demand of buildings with constructions based on passive house components. The high DHW demand of 35 l/pers.d is roughly based on DIN 4708-2 which defines 36 l/pers.d. The low DHW demand of 22.5 l/pers.d is based on EnEV, revised by Article 1 of the Ordinance of 11/18/2013 (BGBl. I p. 3951). (Heissler et al. 2017b)

Table 4-14: Scenarios of various HW and DHW demands investigated in (Heissler et al. 2017b)

	HW demand MFH [kWh/m²a]	HW demand SFH [kWh/m²a]	DHW demand [l/pers.d]
Standard HW and DHW demand	23	35	30
Low HW demand	14	25	30
High HW demand	50	90	30
Low DHW demand	23	35	22.5
High DHW demand	23	35	35

The results of these different demand scenarios are displayed briefly in the following sections.

4.5.1. Standard HW and DHW Demand

The standard scenario of the previous study shows a turnover of Q_use, the sum of Q_HW and Q_DHW, of 2166 MWh (Table 4-15). 88.7% of this energy is provided by renewable sources and 11.3% by non-renewable sources (Figure 4-58). (Heissler et al. 2017b)

Table 4-15: Summary of the simulation results (Standard HW and DHW demand) (Heissler et al. 2017b)

2166	MWh Useful Energy
consisting of	
1921	MWh Renewable Energy
245	MWh Non-Renewable Energy
resulting in	
196.5	t CO_2-equivalent/a
90.73	g CO_2-equivalent/kWh Useful Energy
5.44	annual COP (System)

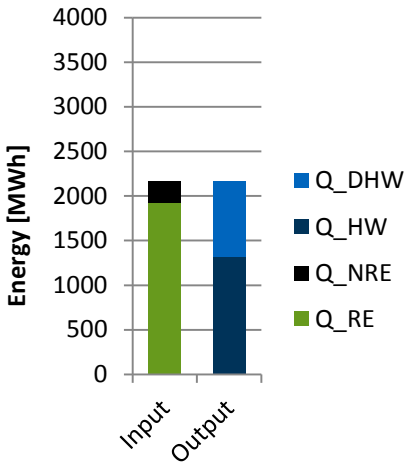

Figure 4-58: Energy In- and Output (Heissler et al. 2017b)

On the basis of Ökobaudat 2016 (BMI 2016b), the total CO_2-equivalent adds up to 196.5 t/a or 90.73 g CO_2-equivalent per kWh of Q_use. Q_loss_net adds up to 41 MWh/a (Figure 4-59). (Heissler et al. 2017b)

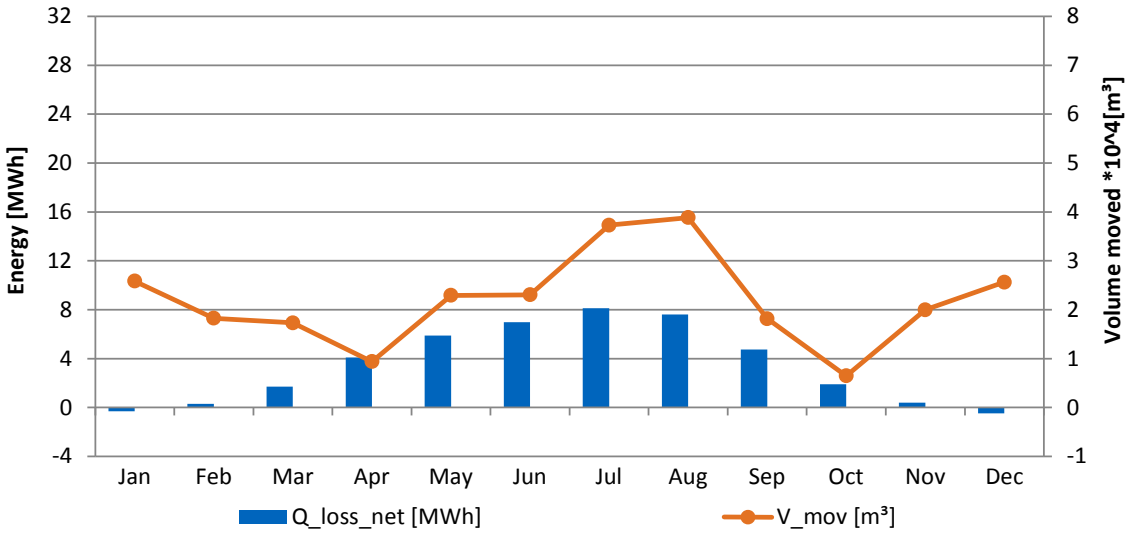

Figure 4-59: Thermal network losses and total volume transported (Standard HW and DHW demand) (Heissler et al. 2017b)

4.5.2. Low HW Demand

With a low Q_HW, Q_use adds up to 1703 MWh (Table 4-16). 89.2% of this energy is renewable and 10.8% is non-renewable (Figure 4-60). (Heissler et al. 2017b)

Table 4-16: Summary of the simulation results (Low HW demand) (Heissler et al. 2017b)

1703	MWh Useful Energy
consisting of	
1520	MWh Renewable Energy
183	MWh Non-Renewable Energy
resulting in	
147	t CO_2-equivalent/a
87	g CO_2-equivalent/kWh Useful Energy
5.61	annual COP (System)

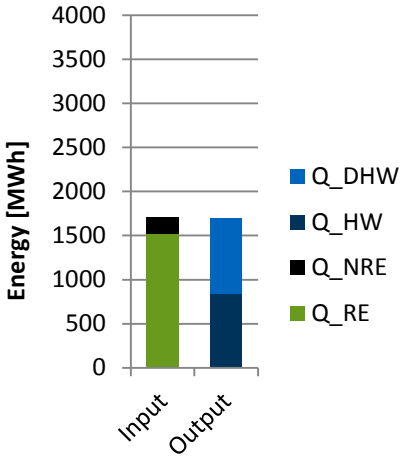

Figure 4-60: Energy In- and Output (Heissler et al. 2017b)

This leads, on the basis of Ökobaudat 2016 (BMI 2016b), to a total CO_2-equivalent of 147.4 t/a or 86.5 g CO_2-equivalent per kWh of Q_use. Q_loss_net (41.2 MWh/a) and V_mov are displayed in Figure 4-61. (Heissler et al. 2017b)

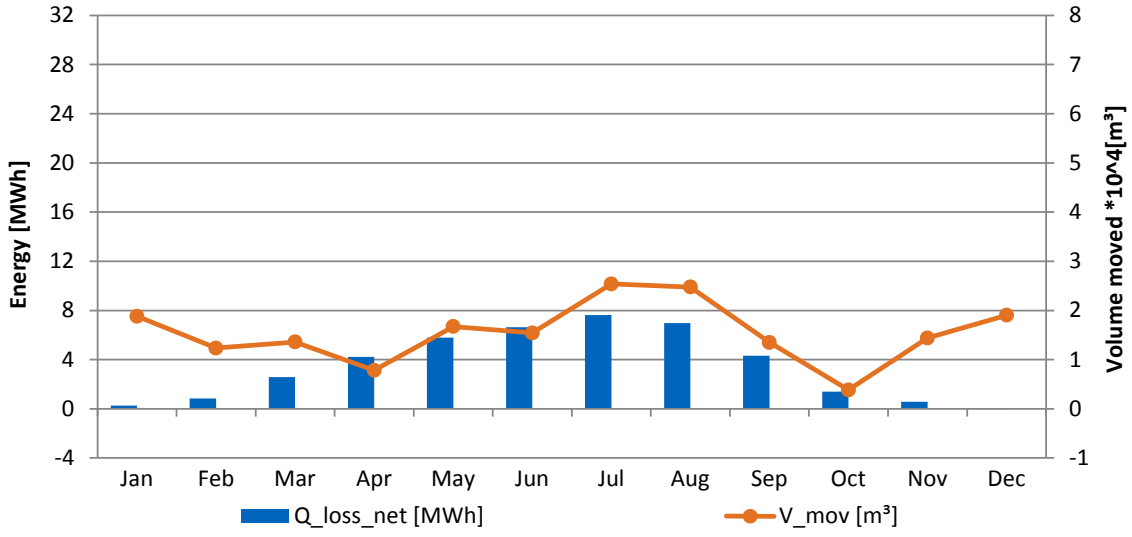

Figure 4-61: Thermal network losses and total volume transported (Low HW demand) (Heissler et al. 2017b)

In this scenario the electric auxiliary heaters of the stand-by storages start several times in the winter months, which indicates a slight undersizing of the local stand-by storages or the heat pumps, since the installed heating capacities are insufficient to fully supply the heat at times of very high demand. (Heissler et al. 2017b)

4.5.3. High HW Demand

With a high Q_{HW}, Q_{use} of 3821 MWh (Table 4-17) is significantly higher than that of current constructions. 88.2% of this demand is covered by energy from renewable sources and 11.8% from non-renewable sources (Figure 4-62). (Heissler et al. 2017b)

Table 4-17: Summary of the simulation results (High HW demand) (Heissler et al. 2017b)

3821	MWh Useful Energy
consisting of	
3369	MWh Renewable Energy
452	MWh Non-Renewable Energy
resulting in	
371	t CO_2-equivalent/a
97	g CO_2-equivalent/kWh Useful Energy
5.18	annual COP (System)

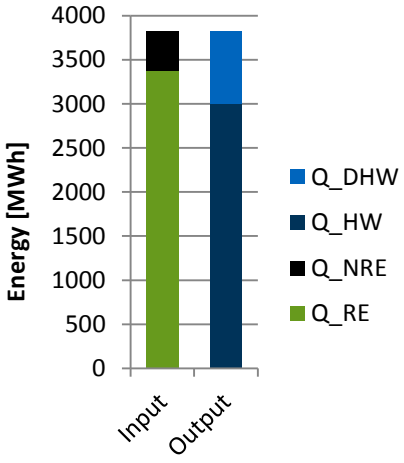

Figure 4-62: Energy In- and Output (Heissler et al. 2017b)

The energy demand results in a CO_2-equivalent of 371 t/a. Q_{loss_net} of the network is 46 MWh/a (Figure 4-63). (Heissler et al. 2017b)

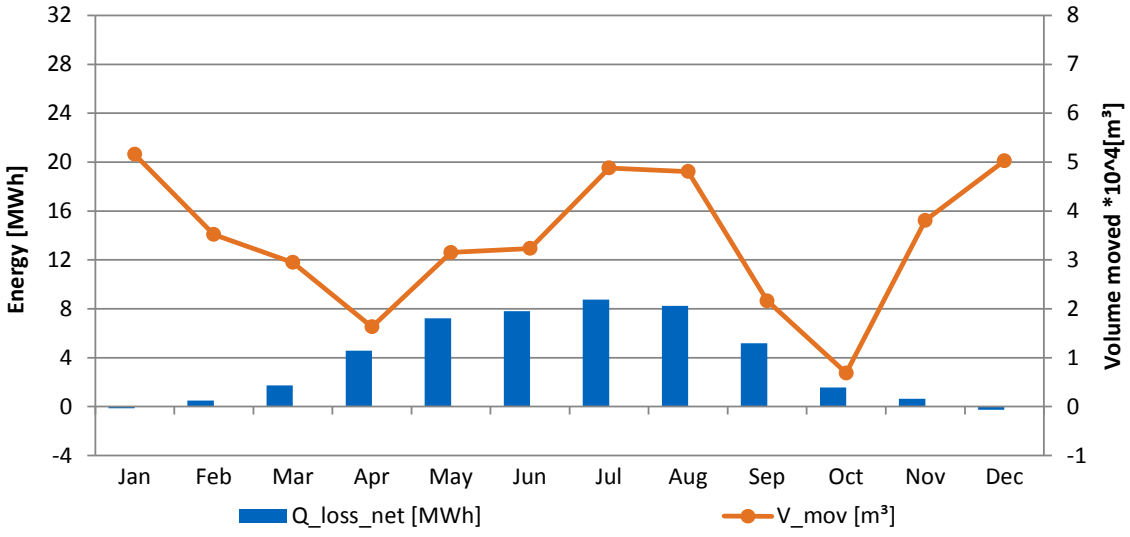

Figure 4-63: Thermal network losses and total volume transported (High HW demand) (Heissler et al. 2017b)

This scenario shows the systems' abilities to provide large quantities of low-temperature heat without a significant drop in the annual COP or an exhaustion of the available roof area for solar collector installation. The system is limited by the uneconomical sizes of the local buffer storages for a Q_{HW} this high. (Heissler et al. 2017b)

4.5.4. Low DHW Demand

A low DHW demand results in a Q_use of 1945 MWh (Table 4-18) with 1724 MWh renewable and 221 MWh non-renewable energy (Figure 4-64). (Heissler et al. 2017b)

Table 4-18: Summary of the simulation results (Low DHW demand) (Heissler et al. 2017b)

1945	MWh Useful Energy
consisting of	
1724	MWh Renewable Energy
221	MWh Non-Renewable Energy
resulting in	
176	t CO_2-equivalent/a
90	g CO_2-equivalent/kWh Useful Energy
5.47	annual COP (System)

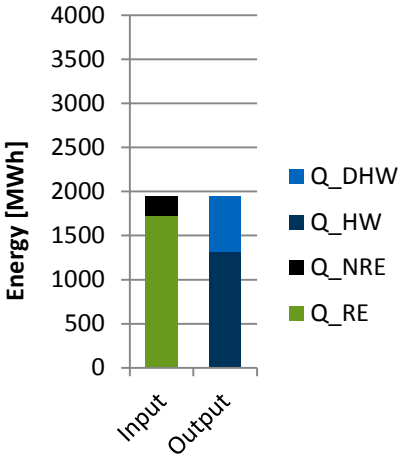

Figure 4-64: Energy In- and Output (Heissler et al. 2017b)

This leads to a total CO_2-equivalent of 176 t/a or 90 g CO_2-equivalent per kWh of Q_use. The thermal losses of the network Q_loss_net add up to 48 MWh/a (Figure 4-65). (Heissler et al. 2017b)

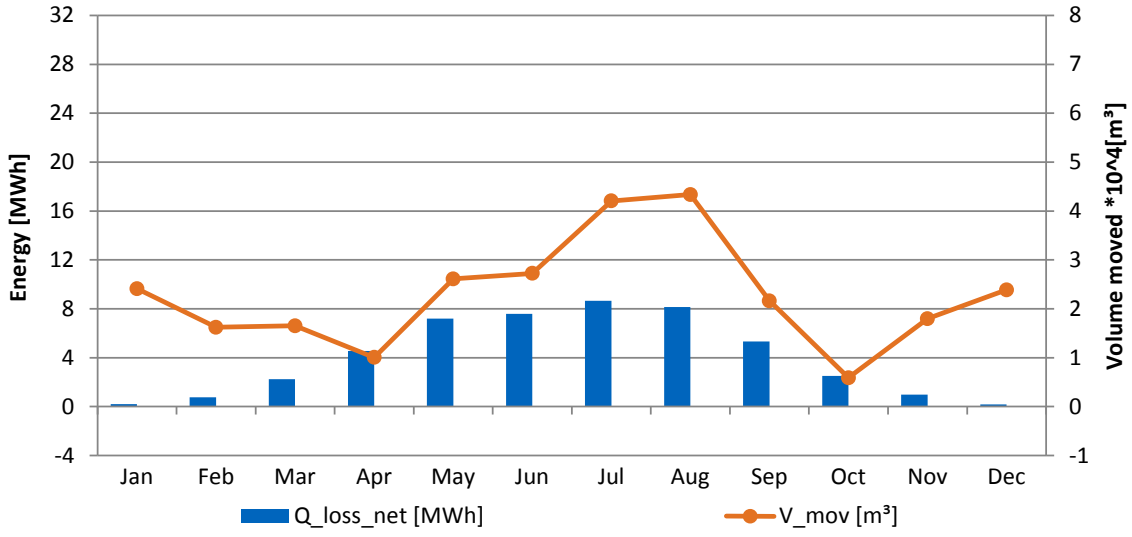

Figure 4-65: Thermal network losses and total volume transported (Low DHW demand) (Heissler et al. 2017b)

With this scenario's low DHW demand, the unchanged sizes of collector areas and seasonal storage lead to a rise of the system temperatures. With the temperature rise two opposite effects come into place: a higher efficiency of the heat pumps and higher thermal losses of the network. (Heissler et al. 2017b)

4.5.5. High DHW Demand

An increased DHW demand as examined in this scenario leads to a turnover of Q_use of 2312 MWh (Table 4-19) which consists 88.7% of renewable energy and 11.3 % of non-renewable energy (Figure 4-66). (Heissler et al. 2017b)

Table 4-19: Summary of the simulation results (High DHW demand) (Heissler et al. 2017b)

2312	MWh Useful Energy
consisting of	
2051	MWh Renewable Energy
261	MWh Non-Renewable Energy
resulting in	
211	t CO_2-equivalent/a
91	g CO_2-equivalent/kWh Useful Energy
5.4	annual COP (System)

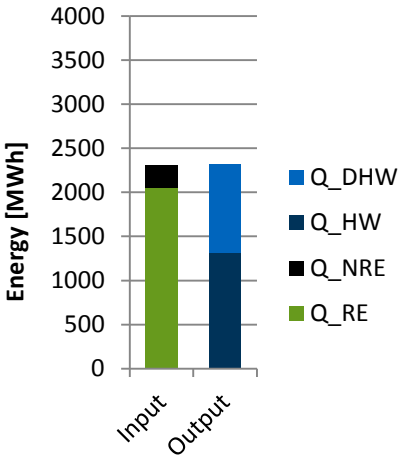

Figure 4-66: Energy In- and Output (Heissler et al. 2017b)

This results in a total CO_2-equivalent of 211 t/a or 91 g CO_2-equivalent per kWh of Q_use. Q_loss_net accumulates to 36 MWh (Figure 4-67). (Heissler et al. 2017b)

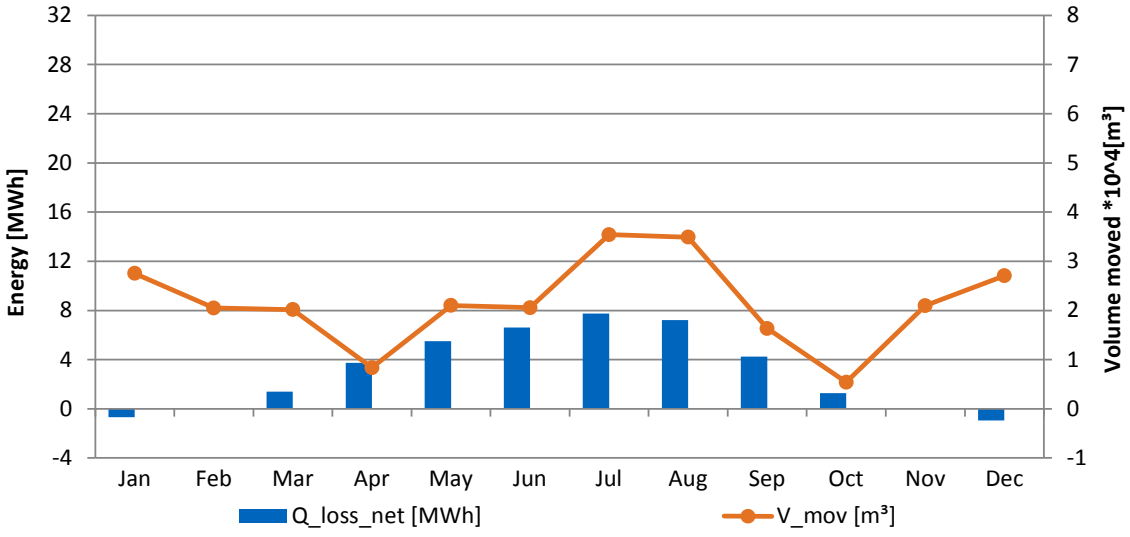

Figure 4-67: Thermal network losses and total volume transported (High DHW demand) (Heissler et al. 2017b)

The high DHW demand leads to less thermal input into and a higher thermal output from the 5GDHCN, leading to a decrease of the network temperatures and therefore fewer thermal losses. Compared to the low DHW demand scenario (4.5.4), the yearly COP is slightly decreased. (Heissler et al. 2017b)

5. Economics

This chapter investigates the profitability of the 5GDHCN at hand and is based on Schweiger (2018). The cost parameters are determined under the limits of the case study (4.1), the pipe sizing (Figure A-5, Figure A-6 and Figure A-7), and the three different network layouts as described in 4.3.1 and 4.3.2., and serve as the basis of the profitability analysis following the annuity method as described in VDI 2067.

5.1. Cost Parameter Calculation

To determine the profitability of the system, the dimensions and amounts of components, the cost parameters, and the characteristic cost curves are required. The real costs usually result from quotations or billings of the implementing companies. However, since the network design is not completed to its full extent, the real costs cannot be determined. Therefore, the approach is to determine the cost through cost parameters via literature research, manufacturer quotations, and expert opinions. The approach distinguishes between cost parameters for capital-related, demand-related, operation-related, and other costs, as well as proceeds. The cost parameters for investment costs of single components are combined to linear, potential or exponential trend lines, characteristic cost curves. On the basis of these characteristic cost curves and the dimensions of the respective component, a corresponding cost parameter is determined. These cost parameters are used for determining the investment costs. For example: a characteristic cost curve of DH piping can be created through the method described above from the varying costs for DH piping with different nominal diameters. The variable of the characteristic cost curve is the nominal diameter in mm. The result is the specific costs in €/m piping. Factoring in the length of the DH piping, the investment costs can be determined. (Schweiger 2018)

5.2. Profitability Calculation

The profitability calculation follows VDI 2067 in using the annuity method. According to VDI 2067 an annuity is defined as

> “Repeated payments of equal amount; usually the annual instalments required to pay off the principal and interest on a debt.” (VDI 2067)

This method enables a comparison of projects with high initial investment and low variable cost to projects with low initial investment and high variable cost, since all cost and interest is spread through the annuity over an observation period. In this investigation an observation period of 20 years is defined for all options examined. Four cost groups which together form the total costs are differentiated: capital-related (including replacement), demand-related, operation-related (including repair), and other costs. Each cost group is further divided into cost types. The annuity of each cost group ($A_{N,K}$, $A_{N,V}$, $A_{N,B}$, and $A_{N,S}$) is calculated separately. Subsequently, the annuity of total annual payments (A_N) is determined by subtracting the annuities of each cost group from the annuity of the proceeds ($A_{N,E}$) (VDI 2067). It follows that, for a profitable operation of a system, $A_N > 0$. For $A_N = 0$, the minimum cost of heat production for the observation period (K_{WG}) can be determined. (Schweiger 2018)

$$K_{WG} = \frac{\left(A_{N,K} + A_{N,V} + A_{N,B} + A_{N,S} - A_{N,E}\right)}{Q_W} \tag{5-1}$$

In this equation, Q_W is the annual heat demand in MWh. K_{WG} then serves as a basis for comparison with other systems. (Schweiger 2018)

The parameters displayed in Table 5-1 are the factors of the profitability analysis and are based on Schweiger 2018.

Table 5-1: Parameters of the profitability analysis (Schweiger 2018)

observation period t [a]	20	annuity factor ANF	0.0736
interest-rate factor q	1.04	price of electricity [Ct/kWh]	16.97
price change factor capital costs r_K	1.0296	price-dynamic cash value factor for capital costs b_K	17.5
price change factor demand-related costs r_V	1.0368	price-dynamic cash value factor for demand-related costs b_V	18.7
price change factor operation-related costs r_B	1.0268	price-dynamic cash value factor for operation-related costs b_B	17.1
price change factor miscellaneous costs r_S	1.0158	price-dynamic cash value factor for miscellaneous costs b_S	15.5
price change factor maintenance r_I	1.0268	price-dynamic cash value factor for maintenance b_I	17.1
price change factor proceeds r_E	1.0368	price-dynamic cash value factor for proceeds b_E	18.7

5.3. Results Profitability Analysis

The following sections display the results of the profitability analysis performed on the three different network layouts (line, ring and mesh) described in 4.3.1 and 4.3.2 as well as a waste heat scenario as described in 4.3.4.

5.3.1. Line Network

The investment costs of the line network as described in 4.3.1 (Figure A-5) add up to 4.3 Million € (Table 5-2). Figure 5-1 displays the shares of the single components in the total investment costs. (Schweiger 2018)

Table 5-2: Component-based investment costs (Line Network) (Schweiger 2018)

PVT modules	1.524.061 €
stratified storage tanks	719.118 €
heat pumps	619.812 €
borefield heat exchanger	532.437 €
network piping	435.935 €
pumps	156.330 €
valves	88.734 €
heat exchangers	87.821 €
electric heaters	85.489 €
other	45.337 €
Total	4.295.073 €

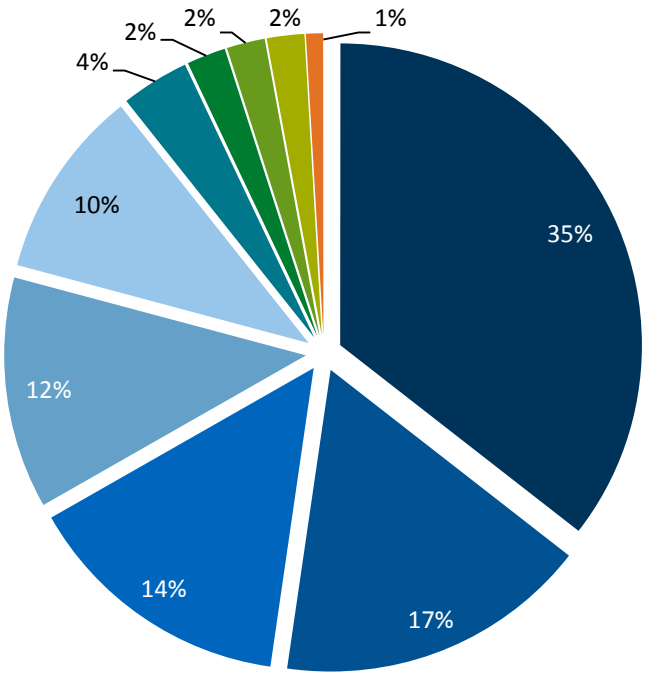

Figure 5-1: Percentage shares of the components in the investment costs of the line network (Schweiger 2018)

The PVT modules account for 35%, the largest share of the total investment costs, followed by the stratified storage tanks at 17%, the heat pumps at 14%, and the borefield heat exchanger at 12%. Other costs include heating pipes and heat meters. The annuities and the cost of heat production are displayed in Table 5-3 (see also Table B-11). (Schweiger 2018)

Table 5-3: Annuities and cost of heat production (Line Network) (Schweiger 2018)

Annuity	[€/a]
Capital-related cost	518.714
Demand-related cost	99.609
Operation-related cost	171.387
Other cost	38.129
Proceeds	49.515
Total	778.324

Energy demand	[MWh/a]
Useful Energy	2165

Cost of heat production	[€/MWh]	[ct/kWh]
Net Cost	359	35.9
VAT 19%	68	6.8
Gross Cost	427	42.7

The annuity of the capital-related costs is 518.714 €/a, which is 67% of the total annuity. The demand-related costs, 13% of the total annuity, mainly originate in the electricity demand of system, in which the heat pumps have the largest share of 87%. The proceeds arise from the sale and the own consumption of the PV energy collected. In total the net cost of heat production of the line network is 35.9 Ct/kWh or 42.7 Ct/kWh after tax. (Schweiger 2018)

5.3.2. Ring Network

The total cost of investment of the ring network (Figure A-6) of 4.31 Million €, as well as the investment cost of the network components, is displayed in Table 5-4. Figure 5-2 shows the percentage share of the components in the total investment costs. While the total cost is marginally higher than that of the line network, the percentage shares are identical with 35% as the largest share of the total investment costs for the PVT modules, followed by the stratified storage tanks with 17%, the heat pumps with 14% and the borefield heat exchanger with 12%. (Schweiger 2018)

Table 5-4: Component-based investment costs (Ring Network) (Schweiger 2018)

PVT modules	1.524.326 €
stratified storage tanks	719.118 €
heat pumps	621.063 €
borefield heat exchanger	532.437 €
network piping	437.186 €
pumps	158.634 €
valves	90.550 €
heat exchangers	89.484 €
electric heaters	85.691 €
other	50.201 €
Total	4.308.689 €

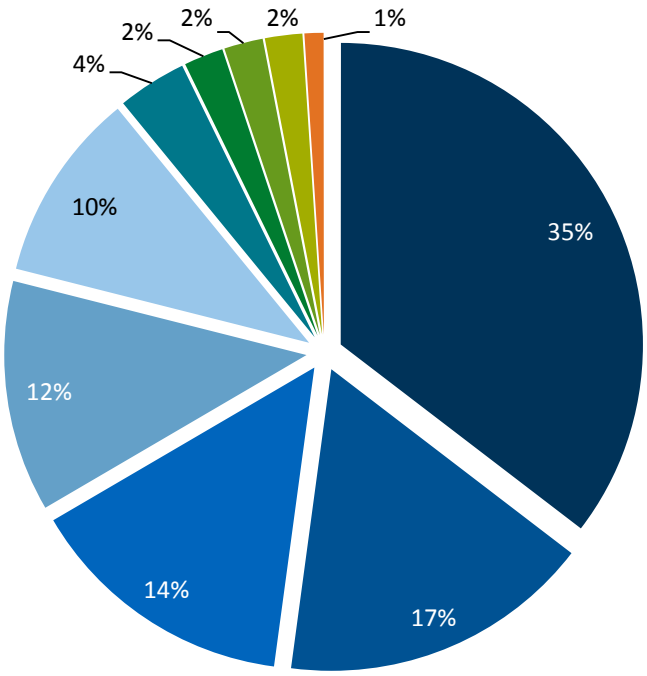

Figure 5-2: Percentage shares of the components in the investment costs of the ring network (Schweiger 2018)

The annuities and the cost of heat production of the ring network are shown in Table 5-5 (see also Table B-12). The annuity of the capital-related costs is 520.246 €/a, which is 67% of the total annuity. (Schweiger 2018)

Table 5-5: Annuities and cost of heat production (Ring Network) (Schweiger 2018)

Annuity	[€/a]
Capital-related cost	520.246
Demand-related cost	100.529
Operation-related cost	172.111
Other cost	38.250
Proceeds	49.652
Total	781.483

Energy demand	[MWh/a]
Useful Energy	2165

Cost of heat production	[€/MWh]	[ct/kWh]
Net Cost	361	36.1
VAT 19%	69	6.9
Gross Cost	430	43.0

The demand-related costs, 13% of the total annuity, mainly originate in the electricity demand of system in which the heat pumps have the largest share, 87%. The proceeds arise from the sale and the own consumption of the PV energy collected. In total, the net cost of heat production of the ring network is 36.1 Ct/kWh or 43.0 Ct/kWh after tax. (Schweiger 2018)

5.3.3. Mesh Network

The cost of investment of the mesh network (Figure A-7) is, at 4.5 Million €, the highest of the three different network types investigated. Table 5-6 shows the component-based investment costs as well as the total cost. The shares of the components in the total investment costs of the mesh network are displayed in Figure 5-3. (Schweiger 2018)

Table 5-6: Component-based investment costs (Mesh Network) (Schweiger 2018)

PVT modules	1.524.282 €
stratified storage tanks	719.118 €
network piping	638.729 €
heat pumps	623.072 €
borefield heat exchanger	532.437 €
pumps	154.690 €
valves	90.722 €
heat exchangers	89.233 €
electric heaters	85.776 €
other	50.294 €
Total	4.508.352 €

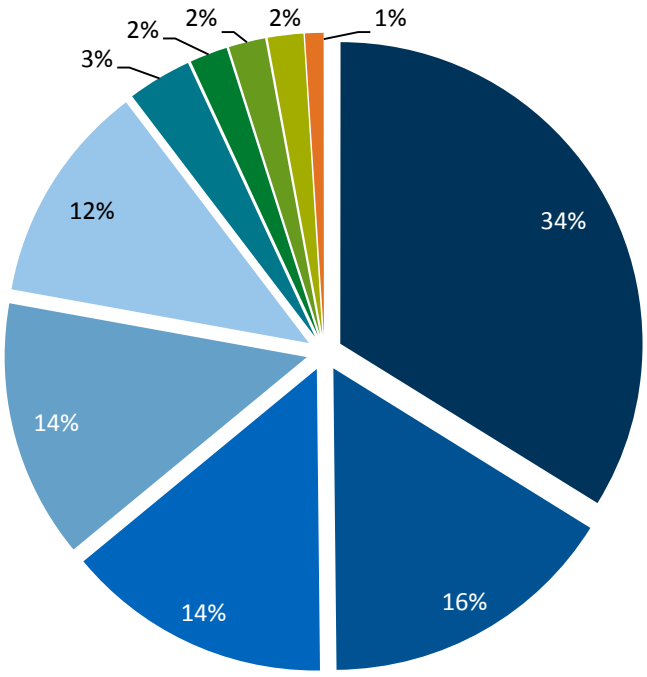

Figure 5-3: Percentage shares of the components in the investment costs of the mesh network (Schweiger 2018)

Compared to the other two network types the percentage shares are slightly shifted, with 34% as the largest share of the total investment costs for the PVT modules, followed by the stratified storage tanks at 16%, the network piping at 14%, and the heat pumps at 14%. The costs of heat production and the annuities of the different cost types are displayed in Table 5-7 (see also Table B-13). Here the annuity of the capital-related costs amounts to 535.067 €/a, which is 66% of the total annuity. 13% of the total annuity can be allocated to the demand-related costs where the electricity supply of the heat pumps has the largest share, 88%. The net cost of heat production amounts to 37.4 Ct/kWh or 44.5 Ct/kWh after tax. (Schweiger 2018)

Table 5-7: Annuities and cost of heat production (Mesh Network) (Schweiger 2018)

Annuity	[€/a]
Capital-related cost	535.067
Demand-related cost	108.514
Operation-related cost	176.848
Other cost	40.022
Proceeds	49.615
Total	810.836

Energy demand	[MWh/a]
Useful Energy	2165

Cost of heat production	[€/MWh]	[ct/kWh]
Net Cost	374	37.4
VAT 19%	71	7.1
Gross Cost	445	44.5

5.3.4. Waste Heat Network

On the basis of the profitability and cost calculation of the line network (5.3.1, Figure A-5), a waste heat scenario was examined by replacing the collectors with a waste heat supply of 100%, resulting in a unidirectional, undirected network. The investment costs of the waste heat network (WHN) as described in 4.4.4 add up to 2.1 Million € (Table 5-8). Figure 5-4 displays the shares of the single components in the total investment costs. (Schweiger 2018)

Table 5-8: Component-based investment costs (WHN) (Schweiger 2018)

heat pumps	619.812 €
borefield heat exchanger	532.437 €
network piping	435.935 €
stratified storage tanks	249.325 €
pumps	89.906 €
electric heaters	85.489 €
valves	47.837 €
heat exchangers	26.529 €
other	22.230 €
Total	2.109.500 €

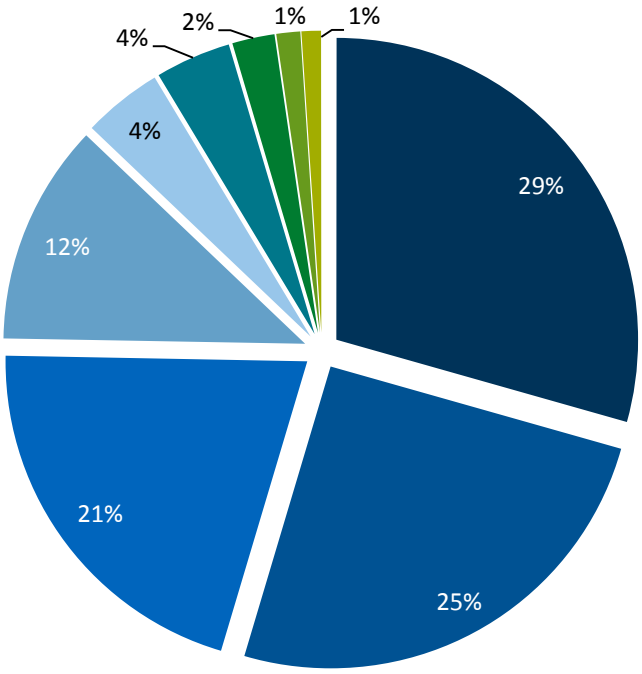

Figure 5-4: Percentage shares of the components in the investment costs of the WHN (Schweiger 2018)

Of the total investment costs the heat pumps account for the largest share with 29%, followed by the borefield heat exchanger at 25%, the network piping at 21%, and the stratified storage tanks at 12%. The annuities and the cost of heat production are displayed in Table 5-9 (see also Table B-14). (Schweiger 2018)

Table 5-9: Annuities and cost of heat production (WHN) (Schweiger 2018)

Annuity	[€/a]
Capital-related cost	189.727
Demand-related cost	99.609
Operation-related cost	95.895
Other cost	18.727
Proceeds	46.625
Total	357.333

Energy demand	[MWh/a]
Useful Energy	2165

Cost of heat production	[€/MWh]	[ct/kWh]
Net Cost	165	16.5
VAT 19%	31	3.1
Gross Cost	196	19.6

53% of the total annuity is capital-related costs, which have an annuity of 189.727 €/a. The demand-related costs, 28% of the total annuity, mainly originate in the electricity demand of system in which the heat pumps have the largest share, 87%. The proceeds arise from the sale of cooling capacity for a working price of 25 €/MWh (Ewendt and Bäckeralf 2005) without factoring in a base price. In total, the net cost of heat production of the WHN is 16.5 Ct/kWh or 19.6 Ct/kWh after tax. (Schweiger 2018)

5.4. Discussion

Comparing the effects of different network layouts on the cost and profitability calculation, the results show very few differences between the three different 5GDHCN types supplied by PVT collectors (Figure 5-5). While the total annuity of the mesh network is 4.18% higher than that of the line network, the total annuity of the ring network is only 0.41% higher. (Schweiger 2018)

A comparison of the cost of investment of the network piping of line and ring networks shows the ring network costs only 0.3% more, even though the total length of the ring network piping is increased by 36%. This effect originates in the reduced pipe diameters of the ring network compared to the line network (Figure A-5, Figure A-6). (Schweiger 2018)

However, when the heat supply is changed to waste heat, the capital and operation-related costs are reduced significantly, by 63% and 44% compared to the line network. The demand-related costs remain unchanged while the other costs are significantly reduced due to the decrease of the capital-related costs. The proceeds of the

collector-supplied networks through own consumption and the sale of surplus electric energy are slightly higher compared to the WHN, since there the proceeds only originate in the sale of cooling capacity.

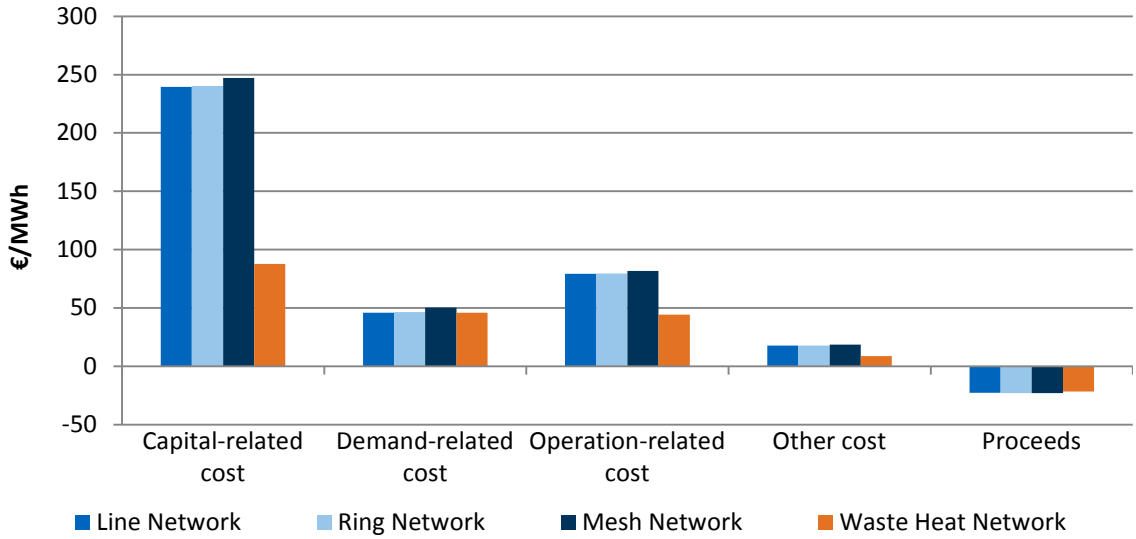

Figure 5-5: Costs of heat production in €/MWh of line, ring, mesh and WHN (Schweiger 2018)

Comparing the demand-related cost of the collector-supplied networks, the line and ring networks differ marginally by 0.42 €/MWh, while the difference between the line and mesh networks is 4.11 €/MWh. The proceeds of the collector-supplied networks do not differ since they are based on identical collector areas and identical amounts of own consumption. In total, the cost of heat production of the line and ring networks is similarly high, and the cost of heat production of the mesh network is even higher. This originates in the high capital-related costs and the low lifespans of some components such as the PVT collectors (Table B-11, Table B-12 Table B-13). (Schweiger 2018)

The waste-heat-based 5GDHCN, on the other hand, a system not based on the cost-driving PVT collectors and stratified storage tanks, shows significant potential for lower capital-related and operation-related costs. The total cost of the WHN in line configuration (5.3.4) is only 46% of the total cost of line network (5.3.1). Table 5-10 and Figure 5-6 display the cost of heat production of various networks and network types and enable a comparison with the results obtained in this work.

Table 5-10: Cost of heat production of various network types (Schweiger 2018)

No.	Name	Cost [€/MWh]	Heat source	Seasonal storage	Heat pumps	Source
[1]	Dollnstein	151	Solar, Ground, Gas	-	+	(Moises 2015; Pehnt et al. 2017)
[2]	München Ackermannbogen	197	Solar, DH	+	+	(Dallmayer et al. 2010; Pehnt et al. 2017)
[3]	Solar Network A	172	Solar	+	-	(Pehnt et al. 2017)
[4]	Solar Network B	115	Solar	-	-	(Pehnt et al. 2017)
[5]	Solar Network C	118	Solar	-	+	(Pehnt et al. 2017)
[6]	Trad. DHN	110	Combustion	-	-	(Statistisches Bundesamt 2019)
[7]	Waste Heat Network A	76	Waste heat	-	-	(Pehnt et al. 2017)
[8]	Line Network	359	Solar	+	+	5.3.1, (Schweiger 2018)
[9]	Ring Network	360	Solar	+	+	5.3.2, (Schweiger 2018)
[10]	Mesh Network	374	Solar	+	+	5.3.3, (Schweiger 2018)
[11]	Waste Heat Network B	165	Waste heat	+	+	5.3.4, (Schweiger 2018)

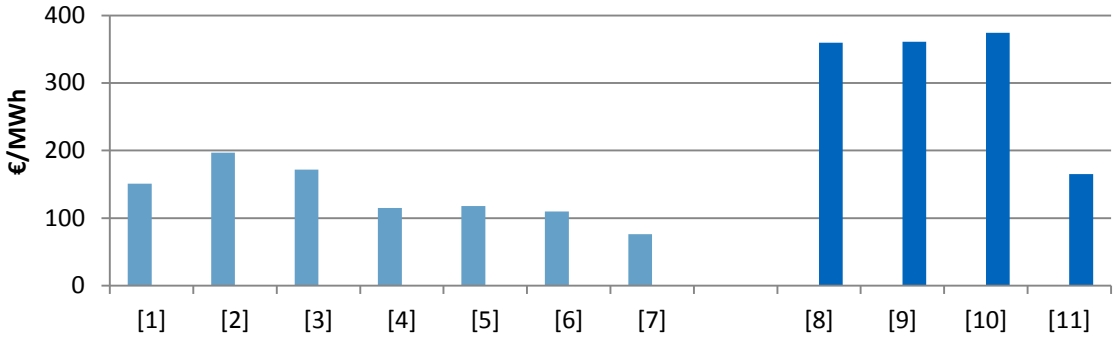

Figure 5-6: Comparison of the cost of heat production of various heating networks based on Schweiger (2018)

A comparison of the different network types shows the cost of energy production of 5GDHCNs in line [8], ring [9] and mesh [10] layout investigated in this work are significantly higher than all other network types examined. However, these costs do not reflect the capability and adaptability of the respective networks. Therefore, a general comparability on the basis of cost of heat production cannot be assumed.

The cost of energy production of WHN B [11] investigated in this work lies within the range of energy production costs of the other networks found in literature. Public subsidies available through national or international incentive programmes are not accounted for.

Another method to compare the economic and ecological advantages of technical systems is based on CO_2 abatement costs. These are used to compare cost and impact of different CO_2-saving measures (Conrad 2020) and describe the cost per ton CO_2 saved, relative to a defined basis. Here, the DHN simulation results (4.4.6) and the DHN cost of heat production (Statistisches Bundesamt 2019) serve as basis. On this basis the CO_2 abatement costs of the Line Network [8] result in 1435 €/t CO_2 and the CO_2 abatement costs of the WHN B [11] amount to 354 €/t CO_2. For existing systems the CO_2 abatement costs add up to 307 €/t CO_2 for the Dollnstein system [1] while the costs for the Ackermannbogen system [2] amount to 865 €/t CO_2 (Pehnt et al. 2017).

In summary, the investigation shows the financial differences between the line, ring and mesh network layouts are negligible compared to the differences found in literature to other network types and layouts. However, a waste-heat based 5GDHCN with seasonal storage [8], also examined here, lies well within the range of cost of heat production found in literature and within the range of CO_2 abatement cost of existing systems. The main reason for the significant difference is the removal of the cost driver solar collectors, which leads in turn to a complete reduction of the solar loops, large parts of the stratified storages, as well as pumps and heat exchangers. In turn, this reduces the bidirectional functionality of the network.

This chapter shows that an undirected network itself does not lead to a significant rise in the cost of heat production. The cost drivers are buildings with bidirectional functionality through local solar-thermal heat production. Buildings with bidirectional functionality which does not arise from local solar-thermal heat production but instead from local waste heat production (for example chillers, etc.), or any local heat production which occurs anyway, therefore also do not significantly add to the cost of heat production, if the local stratified storage capacities and additional infrastructure investments are kept small.

6. Discussion

This chapter examines the results obtained through simulations and profitability calculations and discusses them in terms of effects, plausibility and feasibility. Also general constraints or limitations intrinsic to the simulation model or the simulation are addressed again to indicate the boundaries of the validity of the results obtained. Table B-15 in the appendix presents an overview of the most relevant simulation results.

The acronyms used in Table B-15 and Section 6.2 are explained below in Table 6-1.

Table 6-1: Acronyms for different network types and specifications

Acronym	Network type and specification
DHN/0.13	Traditional DHN with a pipe diameter of 0.13 m
IF 0.2/0.13	Baseline-based network with a pipe diameter of 0.13 m and an IF of 0,2
IF 2/ 0.13	Baseline-based network with a pipe diameter of 0.13 m and an IF of 2
Line/0.13	Baseline scenario
Line/0.26	Baseline-based network with a pipe diameter of 0.26 m
Mesh/0.13	Baseline-based network in mesh layout with a pipe diameter of 0.13 m
Mesh/0.26	Baseline-based network in mesh layout with a pipe diameter of 0.26 m
Ring/0.13	Baseline-based network in ring layout with a pipe diameter of 0.13 m
Ring/0.26	Baseline-based network in ring layout with a pipe diameter of 0.26 m
NSF 0.5/ 0.13	Baseline-based network with a pipe diameter of 0.13 m and a NSF of 0.5
NSF 0.5/0.26	Baseline-based network with a pipe diameter of 0.26 m and a NSF of 0.5
NSF 2.5/0.13	Baseline-based network with a pipe diameter of 0.13 m and a NSF of 2.5
NSF 2.5/0.26	Baseline-based network with a pipe diameter of 0.26 m and a NSF of 2.5
WH20/0.13	20% waste heat supplied network with a pipe diameter of 0.13 m
WH50/0.13	50% waste heat supplied network with a pipe diameter of 0.13 m
WH90/0.13	90% waste heat supplied network with a pipe diameter of 0.13 m

6.1. Impact of parameters

One of the most important research questions is whether this system and its variants can function, and if the answer is yes, what the impact of its system parameters is. The simulation results show that the system does work, but with a widely varying performance depending on the system design as laid out in Section 4.3. The influence of the major design parameters on the functioning and the performance of the system as observed in 4.4 and 4.5 are summarized below.

6.1.1. DHW demand

The influence of the DHW on the performance of the system was examined regarding the DHW demand, which mirrors the behaviour of different types of users who handle the resource DHW economically, to an average degree or freely. Since Q_{HW} is identical for all three scenarios (c.f. Table 4-14), the results indicated only originate in the different Q_{DHW} demands. Table 6-2 outlines the system effects of these different DHW demands. (Heissler et al. 2017b)

Table 6-2: System effects of different DHW demands (Heissler et al. 2017b)

	Q_DHW [MWh]	Q_ST_dir [MWh]	Q_ST_indir [MWh]	W_DHW [MWh]	Q_HP_tot [MWh]	COP [-]
Low DHW demand	632.5	474.4	1315.5	36.2	1434.5	5.47
Standard DH and DHW demand	853.1	555.6	1242.8	49.5	1560.5	5.44
High DHW demand	999.6	603.5	1194.9	59.1	1649	5.4

Since the collector area is kept constant for all three scenarios, the sum of Q_{ST_dir} and Q_{ST_indir} of the collectors is constant. However, the share of Q_{ST_dir}, directly used in the stand-by storages, increases significantly, resulting in a decrease of solar heat Q_{ST_indir} sent to the buffer storages. Considering the expectation that a higher direct use of solar-thermal heat leads to an improved COP, the slightly decreasing trend of the COP surprises. This can be explained by the increase in total heat provided by the heat pumps Q_{HP_tot}, the sum of Q_{HP} and W_{HP}, and by the electric heaters W_{DHW}. In combination with the decrease of the indirect solar-thermal output and the resulting lower heat flow to the network, a negative heat balance at the seasonal storage is the result, which leads to cooling of the seasonal storage. An increase in heat input into the network (for example, an increase in collector area or an integration of additional heat sources) can counteract this effect. (Heissler et al. 2017b)

The comparison of the three different DHW scenarios shows the effect of the user on the system through the different amounts of DHW used. A similar result can be expected through user behaviour which leads to an increased HW demand (for example incorrect ventilation, window opening, heating behaviour, etc.). The effects of the user on the long-term functioning of the system as a whole show and prove the need to inform the user, prior to and during use, of the consequences of their actions regarding DHW use and ventilation habits. (Heissler et al. 2017b)

6.1.2. Network Typology

The effects of different network layouts of NSD on the functioning of the network as a whole are apparent in the pump energy demand and the thermal losses. Both change with the network type, but for different reasons.

The pump energy demand is dependent on the flow resistance of the network. The flow resistance decreases with increasing alternative flow paths available for pressure equalization. Thus, a mesh network offers the lowest flow resistance, followed by a ring network. The line network, with a single path available for pressure equalization, offers the highest flow resistance, leading to the highest pump energy demand of the three (Table 4-8).

The thermal losses of the network only indirectly depend on the network type, since the total surface area changes with the type of network. Due to increasing pipe surface area from line to ring to mesh network (Table 4-3) the thermal losses also increase. The network type itself has almost no influence on the thermal losses (Figure 4-23).

Noteworthy is the influence of the thermal losses on the temperature in the network. Due to the higher losses, the temperature difference of ring and mesh networks to the surroundings is lower than that of the line network (Figure 4-20), leading to an unbalanced seasonal storage. One consequence is, therefore, a higher heat input required for ring and mesh networks to deliver equal amounts of thermal energy to the buildings as the line network.

At first glance, weighing the two counteracting effects seems obvious: pump energy in MWh vs. thermal energy in MWh. However, since the thermal energy of the systems observed originates mostly in renewable sources, the impact of thermal loss does not weigh as much as the increase in pump energy, which is only made up to about one third of renewable sources. This leads to the result displayed in the total CO_2-

equivalents of the three network types (Table 4-8): the lowest impact during the use of the system originates from the mesh network.

6.1.3. Pipe Size

As displayed in Figure 4-23, the thermal losses are unspecific to the type of network when normalized over the total pipe length of the network. In an addition to Figure 4-23, Figure 6-1 shows a data row "Theory" which displays the defining geometrical factor $\frac{1}{\ln r_a - \ln r_i}$ of Equation 3-2 for the heat flow through a hollow cylinder of pipe insulation with the respective diameters, normalized to the y-intercept of the simulation results of line, ring and mesh networks of 0.05.

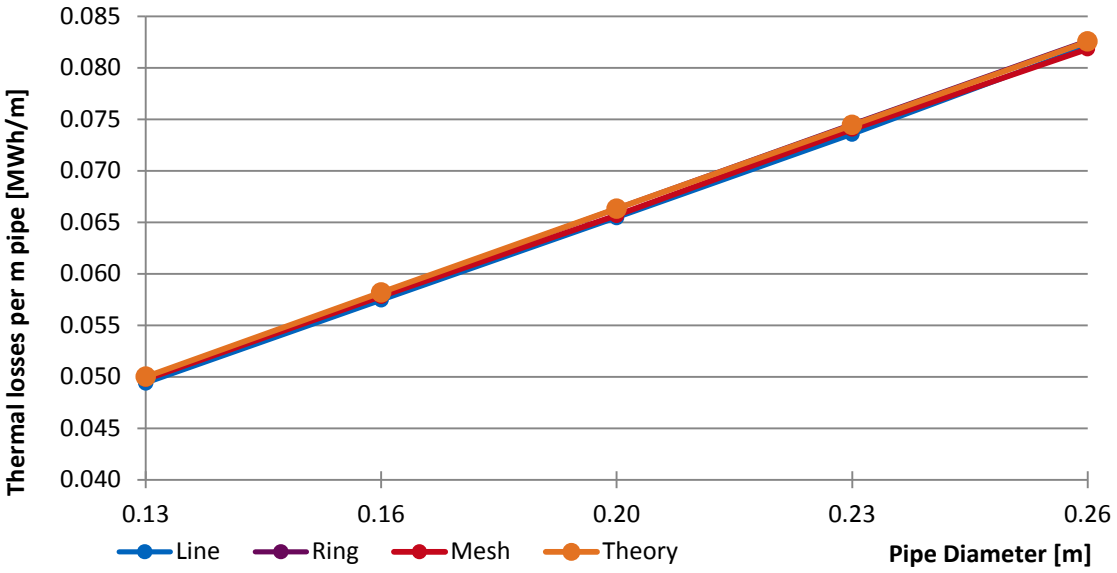

Figure 6-1: Specific thermal network losses per m pipe of different network layouts, simulated for line, ring and mesh network as well as calculated for specific diameters according to Equation 3-2

The "Theory" graph is congruent to the graphs of line, ring and mesh networks over the range of pipe diameters examined, and shows a linear behaviour. This displays the adherence of the thermal losses in the simulations to the law of heat flow through a hollow cylinder. Other effects impacting the heat flow caused by network geometry, ground, or other influences are not observed.

With increasing pipe diameter, the effects on pump energy demand of the different network layouts as described above (6.1.2) diminish. At the same time the thermal losses increase.

6.1.4. Network Heat-load Density and Network Size

Increasing the network size while keeping the heat turnover constant is a means of varying the heat-load density of the network. The effect of an increased network size, is as mentioned above (6.1.2), twofold: increased pipe surface areas and therefore higher thermal and total losses, as well as increased pump energy demands. And while, for the two pipe diameters examined, the thermal and total losses have the same hyperbolic characteristics for increasing heat–load densities (Figure 4-32), the characteristic of the pump energy demand changes significantly. The graph of the smaller diameter also follows a clear hyperbolic correlation. However, the hyperbolic graph for the larger pipe diameter is shifted to the left and gives a linear impression (Figure 4-35).

As a result, the total CO_2-equivalents of the NLD, except for the NSF 4 network, are reduced by up to 5 t/a compared to the best-performing network of the NSD. This also reflects in the annual system COPs of the NLD of 5.6 or 5.7, which outperform the best-performing network of the NSD and its annual system COP of 5.4 (Table 4-9 and Table 4-10).

For increasing sizes of NLD, the increase in pump energy demand is marginal compared to the increase in thermal and total losses. Higher total losses lead to lower feed temperatures of the solar-thermal collectors which result in higher solar-thermal gains that compensate for the additional thermal network losses from the increased surface area. Therefore, no negative consequences in terms of network performance or increased CO_2-equivalents are observed, as long as the higher total losses are compensated for through additional renewable heat input.

However, as soon as the system is no longer able to compensate for the additional thermal losses, the output of heat pumps and the auxiliary heaters increases, which leads to a rise of the electric energy demand and subsequently a higher turnover of non-renewable energy. This can be observed in the performance of the extremely large network with a NSF of 4 (Table 4-10). The additional electric input also has a negative impact on the system COP as well as the total CO_2-equivalents of the system, as is shown by the extremely large network.

Therefore, keeping the heat-load density as high as possible improves the energy performance. If necessary, the system is flexible, to buffer a decrease in heat-load density for NLD as long as the additional thermal losses are covered by additional renewable energy input. However, the increase in electric energy demand for pumps, heat

pumps, and auxiliary heaters limits the reducibility of the heat-load density in the network.

The extent and definite limit of this effect are not within the scope of this work. Since the network size is also economically limited, a doubling of the network pipe diameter leads to an increase in cost between factors 3 and 4 per m piping depending on the type of surface (sealed or natural surface) (Schweiger 2018), so keeping the network as small as possible is also economically advantageous.

Figure 6-2 shows the total thermal losses in % of the annual heat transported through the network, over the heat-load density of the network for different specific thermal losses. The graphs of 5.6 and 9.2 W/m are taken from Figure 4-32 and display the thermal losses of the NSD (5.6 W/m) and of the NLD (9.2 W/m). The data of the specific thermal losses of 20, 25, 30, and 35 W/m is based on regular DHNs (C.A.R.M.E.N e.V. 2013). The data points of C.A.R.M.E.N e.V. (2013) were taken from continuous graphs to fit the specific heat-load densities examined in this work.

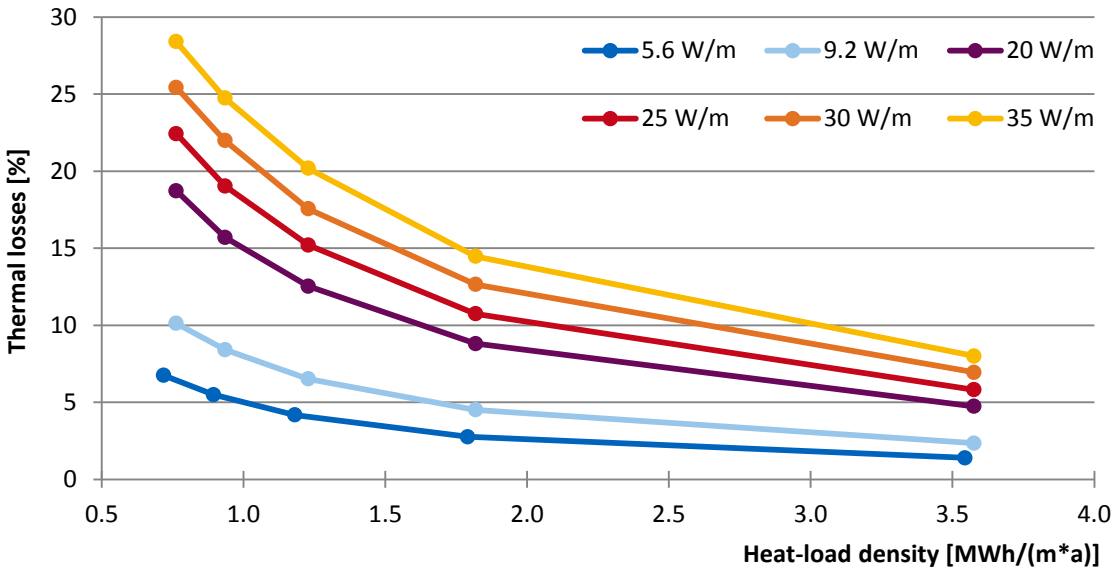

Figure 6-2: Thermal losses of the networks over the network heat-load density for different specific thermal losses – 20 W/m to 35 W/m data from C.A.R.M.E.N e.V. (2013)

Comparing the graph characteristics, both data sources follow the same hyperbolic pattern with the DHN graphs showing significantly higher thermal losses. These higher thermal losses originate mainly in the higher system temperatures (cf. 4.4.6). As described in C.A.R.M.E.N e.V. (2013), the design aim for traditional bio-mass-supplied DHNs are specific thermal losses below 10%. Both graphs of the 5GDHCN almost completely fulfil this aim, with only the first of the 9.2 W/m networks (NSF 2.5, d=0.26 m; Table 4-11) not reaching this target. Even more, for higher heat densities

the 5GDHCNs outperform the traditional DHNs, with thermal losses below 5% for heat densities above 1.7 MWh/(m.a).

Therefore, the lower system temperatures not only lead to fewer thermal losses but also present an opportunity for the construction of 5GDHCNs in areas with low heat-load density, where traditional DHNs are not built.

6.1.5. Waste Heat Share

The effect of increasing the share of waste heat input into the system while reducing the solar-thermal input is opposite to the original expectations. The original expectation was that less solar-thermal input leads to less pump energy needed for the heat transport, which leads to a lower electric energy demand resulting in a lower turnover of non-renewable energy. However, the exact opposite can be observed: the higher the waste heat input share, the higher the turnover of non-renewable energy.

As discussed above in 4.4.4, the increased electric energy demand of the heat pumps, due to decreasing direct and indirect local solar heat gains, outweigh the effect of reduced pump energy demand. However, since the effect of decreasing pump energy demand and increasing heat pump energy demand happen simultaneously, the optimum in terms of electric energy demand is at a share of 20% of waste heat input (Figure 4-38).

Knowing the optimum electric energy demand, and the impact it has on the total system performance, a direct comparison of the baseline case to the 20% waste heat input case shows a potential for reduction of 40 MWh of renewable and 6 MWh of non-renewable energy, saving 6 t/a of CO_2-equivalents. However, with the optimum at 20% waste heat input, a steady increase from there and an even higher increase above 60% waste heat input, the exact metric used for comparison is important. Examining the specific CO_2-equivalents in g/kWh TE, the increase above 60% (Figure 4-41) does not seem substantial due to the also-increasing amount of total energy input into the system. However, comparing the total CO_2-equivalents in t/a, the increase and its magnitude are visible. Therefore, a comparison on the basis of the total CO_2-equivalents in t/a is most suitable for the comparison of different systems.

In conclusion, the examination of the performance of WHNs with different shares of waste heat input shows that the supply of a network with waste heat only is not the most climate-efficient. A balanced mixture of solar or otherwise locally gained heat and waste heat supply offers the best option in terms of total CO_2-equivalents in t/a.

6.1.6. Pipe Insulation Thickness

The low network temperatures of 5GDHCNs and the subsequent low temperature differences between network piping and surroundings lead to the question whether pipe insulation is necessary or can be omitted. With simulation runs of IFs from 0.25 to 2, a range of no insulation to double the baseline insulation thickness is covered. Besides the obvious result that with thicker pipe insulation the thermal losses decrease (Figure 4-47), the investigation also shows the influence of the pipe insulation thickness on the electricity demand. At low IFs, the high thermal losses lead to increased heating through the auxiliary heaters and therefore an increased total electricity demand (Figure 4-48). The non-renewable share of this increased electricity demand leads in turn to an increase of the total CO_2-equivalents in t/a (Figure 4-50). As before, the specific CO_2-equivalents do not show the same pattern, since with the increase in total CO_2-equivalents the electricity input into the system also increases, levelling the impact.

The scope of this work is very limited in terms of life-cycle focused investigations. However, knowing the impact of varied pipe insulation thicknesses on the CO_2-equivalents during the use of the system, an obvious step is to compare it to the difference following in the production of these varied pipe insulation thicknesses. Figure 6-3 therefore contrasts the total CO_2-equivalents resulting from the use of the different pipe insulation thicknesses with the total CO_2-equivalents resulting from the production of the different pipe insulation thicknesses. All values are displayed relative to the baseline case with IF 1.

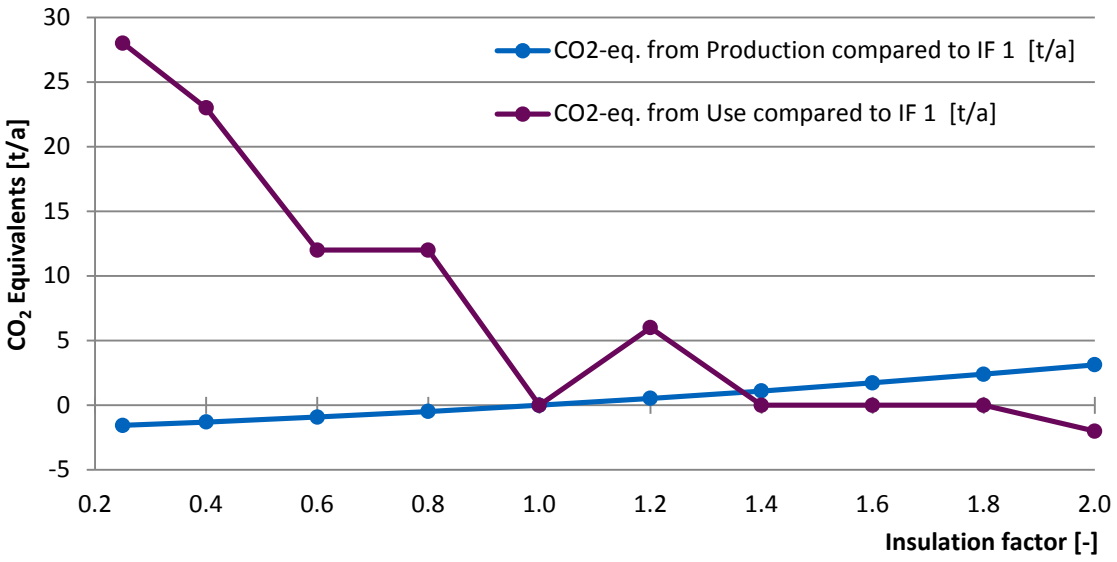

Figure 6-3: Impact of different IFs on the CO_2-eq. of the system of production and use phases relative to the baseline scenario

The total life span of the system is assumed to be 50 years, the same life span as the polyurethane insulation material (BMI 2017). The CO_2-equivalents of the production include phases A1-A3, C2, C4, and D of the polyurethane pipe insulation data set of Oekobaudat 2019 (BMI 2019). Retaining the assumption that, because of its thin dimensions, the thickness of the pipe wall can be discounted as its own material (3.3.3), the pipe wall thickness is counted instead as additional insulation material thickness.

For an IF of 0.25, the thinnest pipe insulation thickness examined in this work, the CO_2-equivalents for production are 1.6 t/a lower than those of the baseline case. At the same time, the CO_2-equivalents of its use are 28 t/a higher due to the high thermal losses. Therefore, a reduced network pipe insulation thickness results in a net increase in CO_2-equivalents of up to 26 t/a (Figure 4-50, Figure 6-3). However, if the additional thermal network losses are made up for by additional renewable thermal energy input, the negative impact on the total CO_2-equivalents can be avoided. Still, increasing the heat input into the network for the prevention of additional CO_2 output does seem strange when the same heat could also be used for heating in a network with better insulation. The answer to the original question of whether any insulation is needed is yes, if the otherwise additionally-needed thermal energy to cover the higher losses does not come for free without any surplus energy required that has a share of NRE.

6.1.7. Pump Energy Demand

As described in 4.4.1, the main parameter determining the pump energy demand is the pressure loss of the network. A large influence on the pressure losses of the different networks are simultaneity, parametric modelling, pipe layout, and network layout.

Simultaneity

In this work, two types of heat sources are examined: solar-thermal collectors and waste heat input. With the decentralized PVT collectors as heat sources, the pump energy demand is very much determined by the simultaneity of the heat input into the network. Figure 6-4 displays the pump energy demand of the baseline scenario (4.4.1) for both pumping directions, heat input and output of the network.

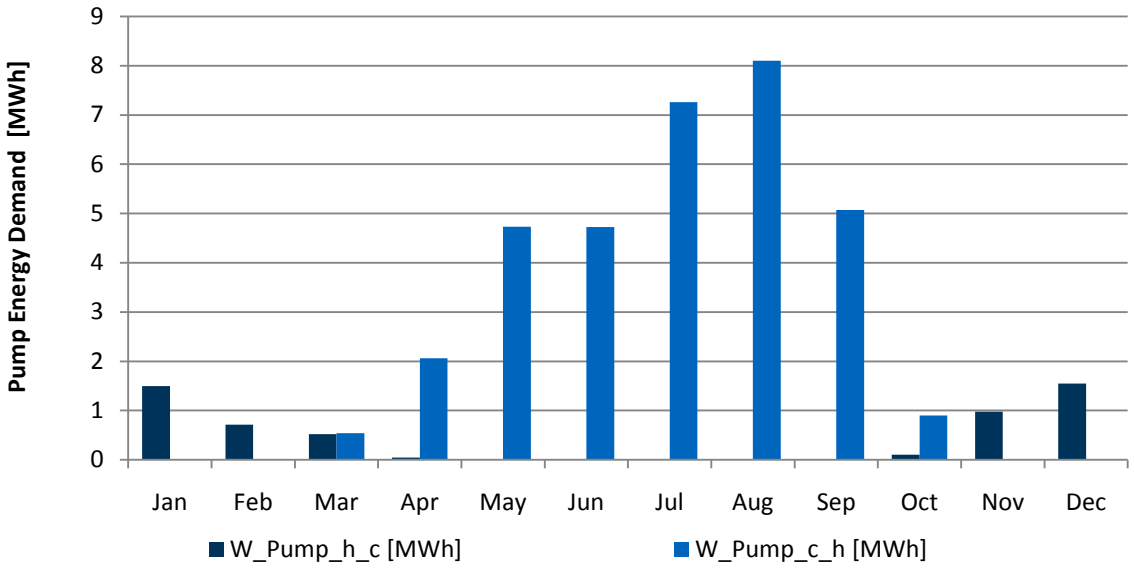

Figure 6-4: Pump energy demand for heat input and output of the baseline network

As described in 4.4.1, the high concurrence of the solar-thermal input into the network (W_Pump_c_h) through the simultaneity of the solar irradiation leads to high pressure differences and a significantly higher pump energy demand than the opposite direction, the heat discharge from the network (W_Pump_h_c).

With another heat source, the pump energy demand characteristic is entirely different. Figure 6-5 displays the pump energy demand for heat input and output of the 90% waste heat scenario (4.4.4). This includes the central pump for waste heat transport by which the waste heat is supplied to the system.

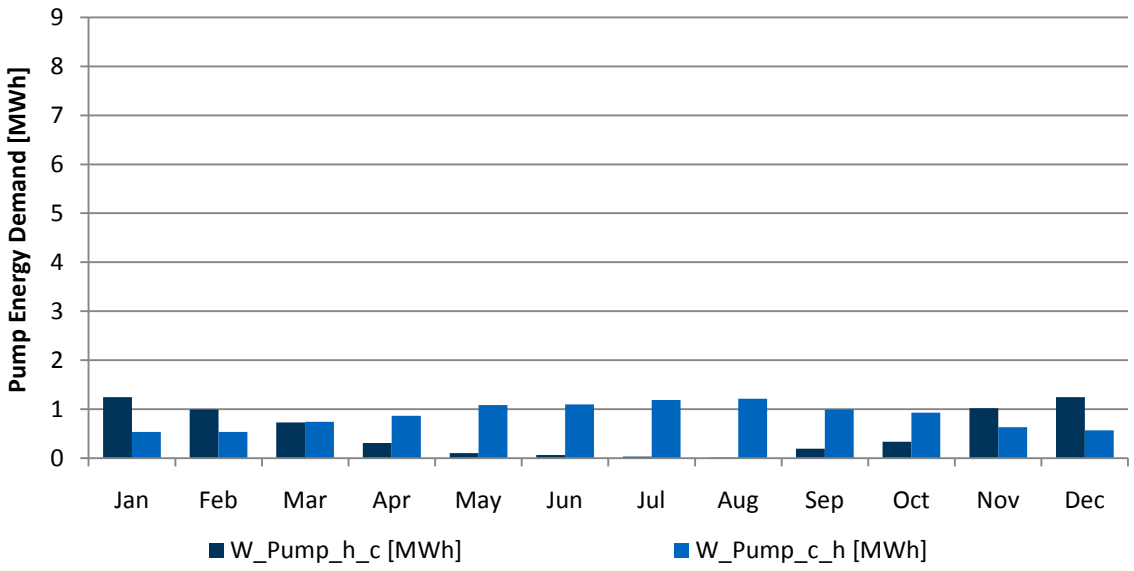

Figure 6-5: Pump energy demand for heat input and output of the WHN with 90% waste heat input

Compared to the baseline scenario, the pump energy demand is reduced for both pumping directions. During the winter months $W_{Pump\_h\_c}$ is similar to the baseline case of 5.4 MWh and adds up to 6.3 MWh. However $W_{Pump\_c\_h}$, the pump energy demand of the central pump supplying the waste heat to the network, is, due to the pulsating characteristic of the pump, very different to the baseline case (33.4 MWh), with a total electric energy demand of 10.4 MWh. With no thermal input from the buildings into the network, there is no effect of self-synchronization and therefore no increased pressure loss.

Parametric Modelling

To assess the influence of parametric modelling (linear scaling of buildings, storage tanks, and PVT collector areas) on the pressure losses, the individual buffer storage sizes in the BSMs of the baseline scenario were arbitrarily varied around the range of their design sizes while keeping the buffer storage volume of the system as a whole constant. Figure 6-6 displays the effect of this storage size variation.

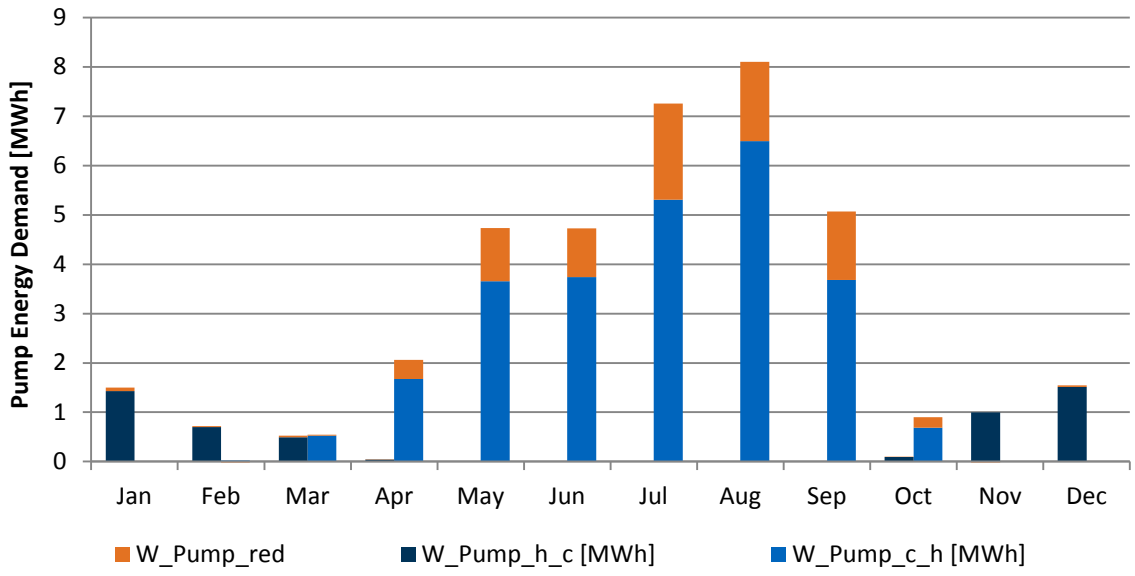

Figure 6-6: Pump energy demand for heat input and output of the network in baseline configuration with varied buffer storage sizes

The reduced pump energy compared to the baseline pump energy demand (W_{Pump_red}) is shown in orange colour. During the months of highest simultaneity, the effects of parametric modelling are significant. These effects lead to similar charging and discharging times, and increase the self-synchronizing behaviour and subsequently the pump energy demand up to 27% compared to the scenario with arbitrarily varied buffer storage sizes.

However, even considering this effect, the highest pump energy demand during the summer months is still up to 4.3 times higher than the highest pump energy demand in winter. Additionally, the arbitrary variation of buffer storage sizes leads in total to a less efficient system: Compared to the original baseline model, the model modification leads to a total reduction of 7.8 MWh in pump energy demand in summer, but also to a 23 MWh loss of low-temperature solar heat gains.

Pipe Layout (diameter, pipe length)

The influence of the pipe layout on the pump energy demand is straightforward and as expected: for larger hydraulic cross-sections (pipe diameters) (Figure 4-24) and shorter pipe lengths (Figure 4-35) the pressure losses decrease.

Network Layout (mesh, ring, line)

The influence of different network typologies of line, ring and mesh networks on the pump energy demand is displayed in Figure 4-24. For the same hydraulic cross-section, ring and mesh layouts perform significantly better and have a lower pump energy demand. The ring and mesh network layouts allow the fluid stream to split into two or more streams, reducing the flow speed in each stream by half or more. This leads to lower pressure losses and subsequently a lower pump energy demand.

A dependency between pipe insulation and pump energy demand cannot be detected (Figure 4-48). In total, the influence of the pump energy demand on the performance of the system and its turnover of non-renewable energy is small compared to the electric energy demand of the system as a whole and the heat pumps in particular (cf. Figure 4-16, Figure 4-38, Figure 4-48).

6.2. Which system is best?

When comparing different systems, the intuitive question to ask is “Which system is best?” However, of course there is no straightforward, universally valid answer to this question. The answer to this question will inevitably have to start with “It depends.” In this case it depends on the focus set: specific losses, ratio of RE to NRE, tons CO_2-equivalent per year, annual System COP, profitability, or heat source topology. Not accounted for in this work are further factors such as construction effort, embedded energy, expandability, or flexibility. In the following, the question is addressed for the focus areas set above.

6.2.1. Specific Thermal Losses

Comparing the specific thermal losses of the systems examined, all 5GDHCNs have significantly lower thermal losses than the traditional DHNs (Figure 6-7). Even the network with almost no pipe insulation (IF 0.2/0.13) loses less heat per m piping than the DHN with 60 mm pipe insulation. The lower system temperatures in the 5GDHCNs are the main reason for this behaviour.

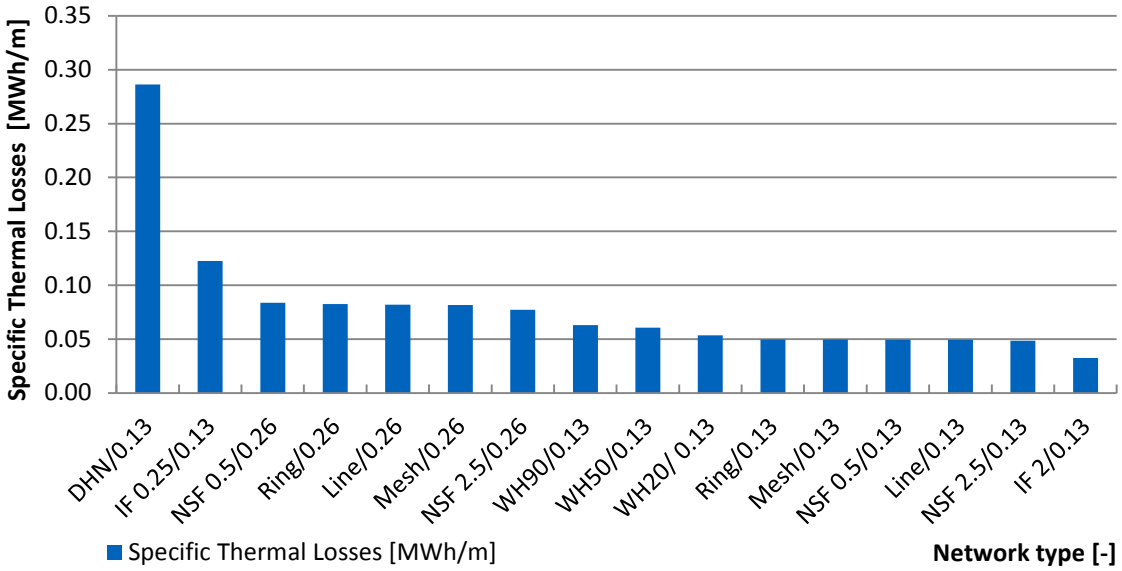

Figure 6-7: Specific thermal losses of different network types

Another trend also visible in Figure 6-7 are the higher specific thermal losses of the NLD, ascribable to the larger surface area of the piping. Not surprisingly, the network with the best performance in terms of thermal losses is the network with double the pipe insulation compared to the baseline case (IF 2/0.13).

6.2.2. Specific Total Losses

Figure 6-8 displays a comparison of the specific total losses, which include thermal losses, storage losses, and calculatory losses, and paints a slightly different picture than the thermal losses of Figure 6-7: the traditional DHN still performs worse than all other networks, but the differences to the other networks are significantly smaller. The main reason for this effect is the thermal losses of the seasonal storage, which do not occur in the DHN scenario. Here, the networks with higher network temperatures in the winter months (see also 4.4.4) experience additional losses. The best-performing network with the least specific total losses is the WHN, with 20% waste heat input (WH20/0.13).

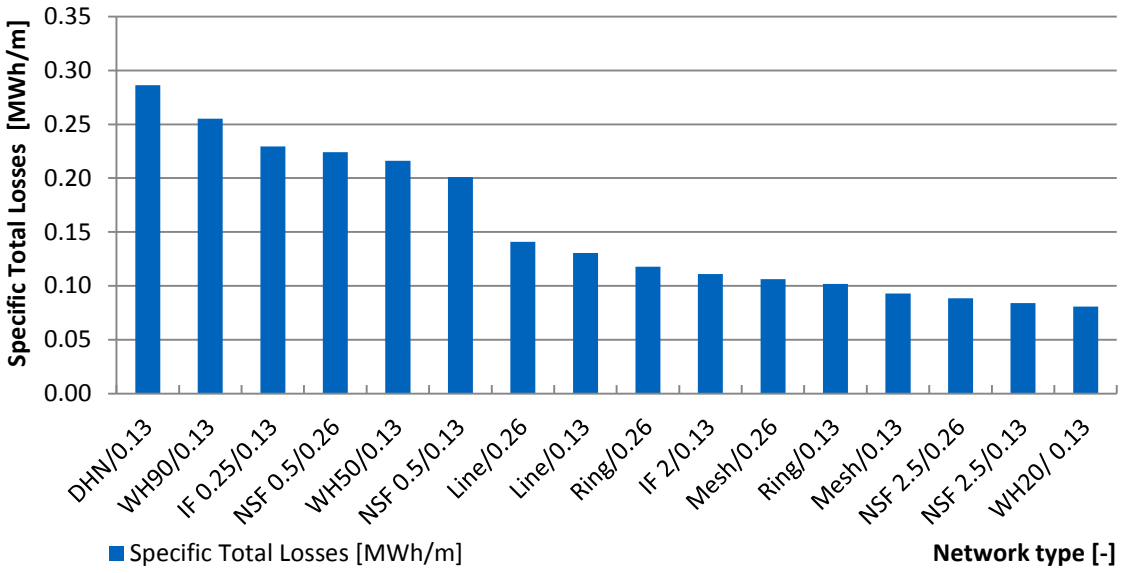

Figure 6-8: Specific total losses of different network types

6.2.3. Ratio of Turnover of Renewable Energy to Non-Renewable Energy

For a comparison of the turnover of energy from renewable sources versus non-renewable sources, the ratio of renewable energy input to total energy input into the system is displayed in Figure 6-9.

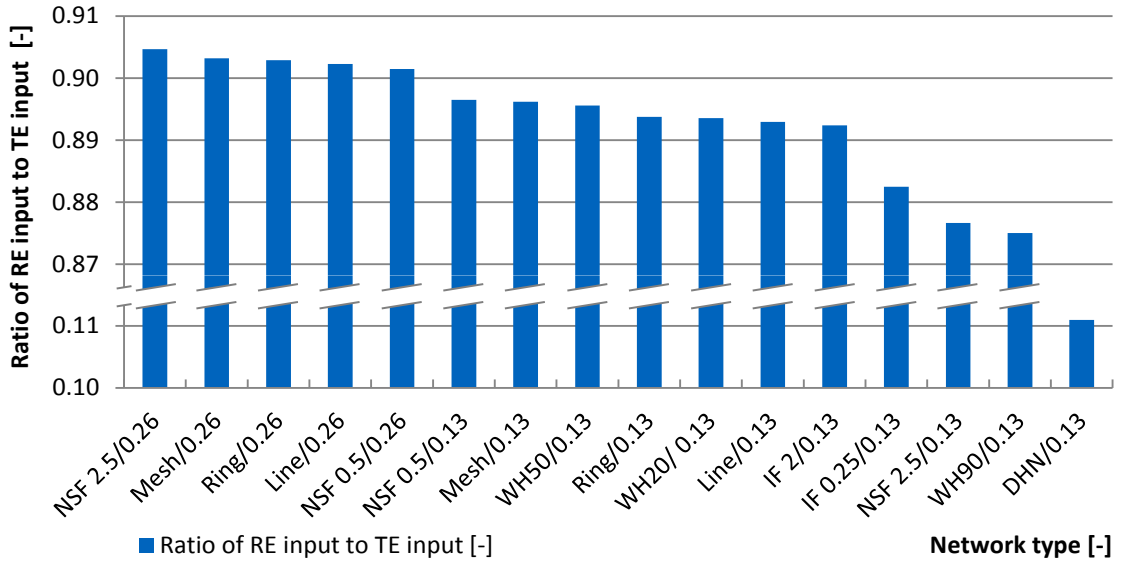

Figure 6-9: Ratio of renewable energy input to total energy input into the system of different network types

Here, the network with the lowest heat-load density and a large pipe diameter (SF 2.5/0.26) shows the best ratio of renewable to total energy turnover, with the other NLD in close pursuit with ratios of renewable to total energy turnover of above 0.9.

6.2.4. CO_2-equivalent per year

The total CO_2-equivalent in tons per year of the different networks is displayed in Figure 6-10. The network with the lowest annual CO_2-equivalent is the very small network with a large pipe diameter (NSF 0.5/0.26), and the one with the highest annual CO_2-equivalent is the traditional DHN (DHN/0.13).

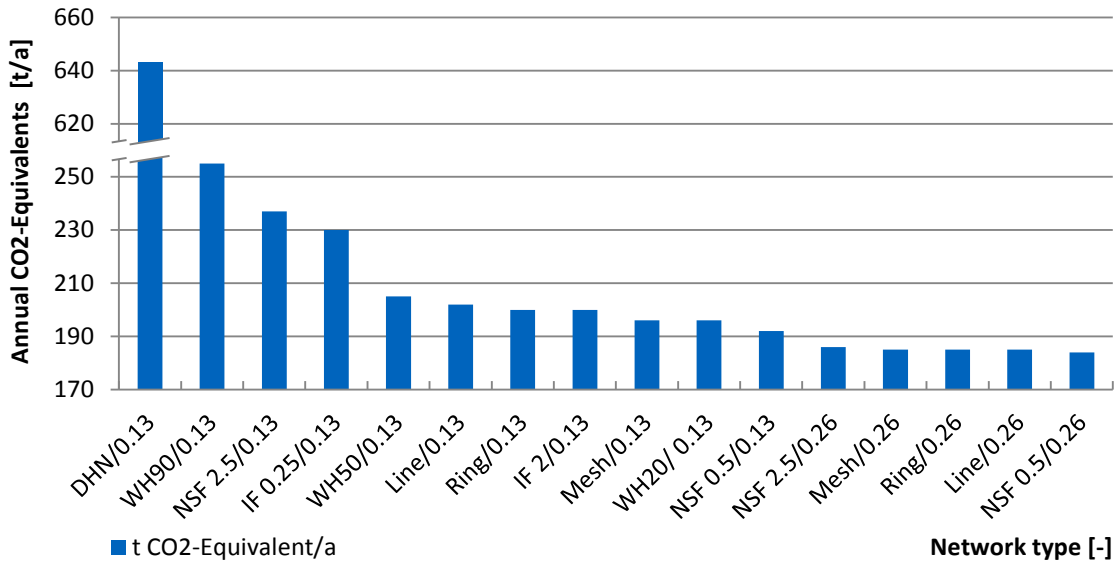

Figure 6-10: Annual CO_2-equivalents of different network types

6.2.5. Annual System COP

Since the systems all have the purpose of heat supply, a figure available for comparing the different system configurations is the annual coefficient of performance of the system as a whole (including solar gains). It is defined as the ratio of useful energy output to electrical energy required (4.4). Figure 6-11 displays the simulation results where the network with the highest annual COP of 5.69 is the very small network with a large pipe diameter (NSF 0.5/0.26). The network with a waste heat input of 90% (WH90/0.13) is the network with the lowest COP due to the high electrical energy demand for pumps and heat pumps. No annual COP is assigned to the DHN, since the electrical energy demand of the DHN (e.g. pumping power) is not within the scope of this work (4.3.6).

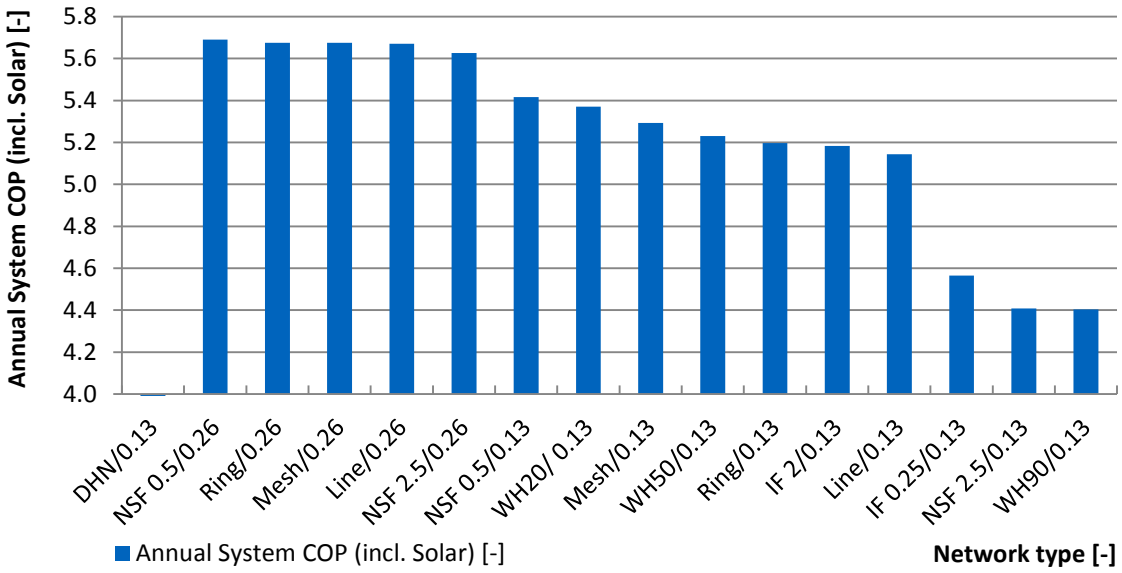

Figure 6-11: Annual System-COPs of different network types (including solar gains)

6.2.6. Profitability

In terms of profitability, a WHN with 100% waste heat supply is the most profitable network of the networks compared in 5.4, with a cost of heat production of 19.6 Ct/kWh. It outperforms the solar-supplied 5GDHCNs in line, ring and mesh configurations as well as other already-constructed networks (Table 5-10).

Compared to traditional DHNs (Table 5-10, [6]) with a gross cost of heat production of 11.1 Ct/kWh in 2018 (Statistisches Bundesamt 2019), the difference in gross cost to a WHN with 100% waste heat supply is 8.5 Ct/kWh.

However, this price difference does not reflect system efficiency, the different amounts of thermal losses on the way to the user, or the origin of the energy lost.

6.2.7. Centralized versus Decentralized Heat Sources

Another important question is whether the type of heat source reflects on the performance and the footprint of the network as a whole. Figure 6-12 displays energy input, output and CO_2-equivalents of three types of network which are supplied by different heat sources:

- The traditional DHN (DHN/0.13; 4.4.6) is centrally supplied and heated, and transports the warm heat carrier with a temperature above demand-level to the buildings.

- The WHN (W90/0.13, 4.4.4) is 90% centrally supplied by a low-temperature waste heat source, and transports the low-temperature heat carrier to the buildings where electric heat pumps raise the temperature to demand level.

- The Solar-thermal Network (STN) (Line/0.13, 4.4.1) is decentrally supplied by low-temperature solar heat sources, and transports the low-temperature heat carrier to the buildings where electric heat pumps raise the temperature to demand level.

The energy input is divided into Q_{RE} and Q_{NRE}, the energy output into Q_{loss} and the useful energy Q_{use}.

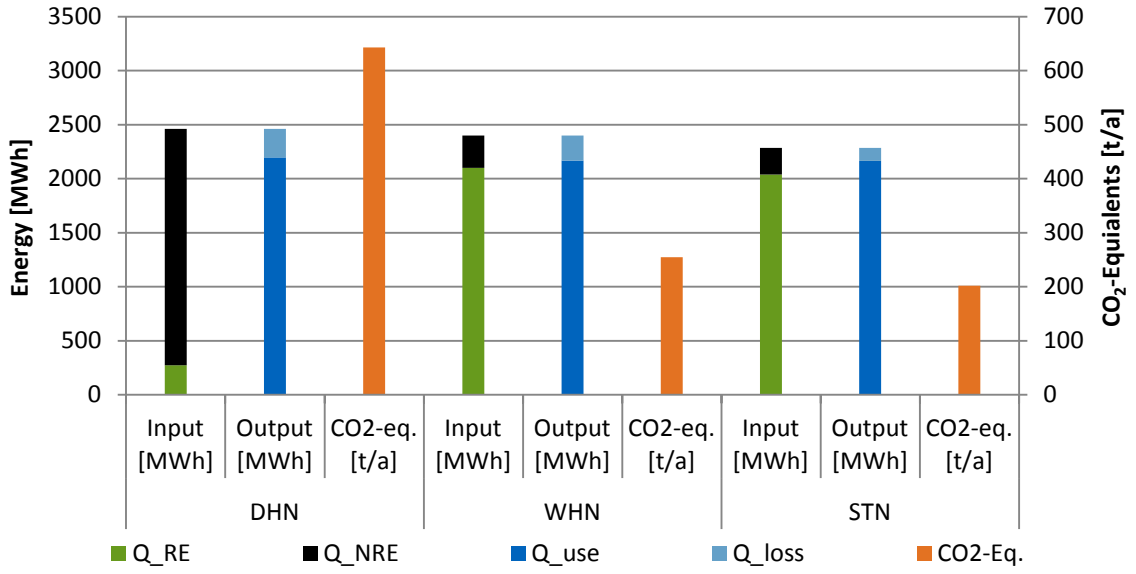

Figure 6-12: Energy input, output and CO_2-equivalents of three types of networks with different heat sources

The DHN and WHN share the system property of one central heat source in the network. However, the temperature levels of the heat sources are quite different: the high-temperature DHN heat source contrasts with the low-temperature WHN heat source.

The WHN and STN share the system property of a low-temperature heat carrier in the network and a decentralized heating to demand level through heat pumps. However, the heat sources in the STN are decentralized, while there is only one central heat source in the WHN.

The losses of the systems Q_{loss} differ significantly. While the losses of the centrally supplied DHN and WHN amount to 262 MWh and 234 MWh, the losses of the STN add up to 119 MWh. However, the substantially higher losses of the centrally supplied

networks have different origins: the losses of the DHN can be traced back to higher thermal losses of the network itself, while the higher losses of the WHN originate in higher storage losses of the seasonal storage due to higher network temperatures (Figure 4-42, Figure 4-43).

Comparing the input amounts of Q_{RE} and Q_{NRE} of the three networks, the traditional DHN has by far the highest turnover of non-renewable energy, with 2187 MWh. This is nine times the level of the STN of 245 MWh, and more than seven times the level of the WHN of 300 MWh. These values are mirrored in the CO_2-equivalents of the three networks, but not in the same ratio as Q_{NRE}, since the calculation of the CO_2-equivalents is based not only on Q_{NRE} but also the form of energy (heat, electricity, etc.): the CO_2-equivalents of the STN amount to 202 t/a, the WHN to 255 t/a, while the DHN comes to 643 t/a, three times the level of the STN. The main reason for this behaviour is the calculation as described in 4.4: the CO_2-equivalent per kWh electrical energy obtained from the public distribution network is weighed with 0.5345 kg/kWh (BMI 2016b), while the CO_2-equivalent per kWh thermal energy obtained from a DHN is weighed with 0.2614 kg/kWh (BMI 2016a).

In total, the footprint of the use phase of the traditional, centrally heated DHN is significantly higher regarding the turnover of energy from non-renewable sources, and also substantially higher in the CO_2-equivalents involved, compared to the decentrally heated WHN or STN.

In conclusion, both centrally supplied networks do not perform as well, concerning thermal losses, turnover of NRE and CO_2 emissions, as the decentrally supplied STN. However, a simple comparison of central and decentral heat supply for thermal networks falls one step short of one important factor: the temperature level of its heat carrier.

Worse than either, WHN or STN, performs the DHN with a high-temperature heat carrier, which leads to significantly higher thermal losses, a higher non-renewable energy demand, and a higher CO_2 footprint during the use phase, than a central or a decentral low-temperature heat supply. The effects of the additional pump energy demand in a decentral, low-temperature heat supplied network is very small compared to the thermal losses of a traditional DHN. In conclusion, the type of heat supply, central or decentral, is not the major factor determining the level of heat losses. The temperature level of the heat supply to the network is.

6.3. Hypothesis Revisited: Carbon-neutral district

In Section 1.2 the hypothesis - *A district heating network at low temperature levels with seasonal heat storage is able to provide a CO_2-neutral heat supply in residential districts with urban density* – was postulated. With the results discussed above for an FAR of 1.34, this hypothesis is not admissible without changes. Due to the electricity demand of the system for pumps and heat pumps, the system cannot function entirely on locally produced, CO_2-neutral electricity. With the electricity obtained from the public distribution network, a share of non-renewable energy enters the system and leads to CO_2 emissions for the system. However, an active load management of the heat pumps or an addition of electricity storage capacities can reduce this surplus electricity needed from the public distribution network, for example in the baseline case, to 70 MWh/a which is a reduction of 81%. Additionally, ensuring the purchased surplus electricity from the public distribution network comes from renewable sources, the system can provide a CO_2-neutral heat supply for a residential district.

6.4. Critique

During the course of every work, experience and knowledge are gained. This process of learning leads inevitably to questioning the choices made at an earlier, less informed state. This section looks at these choices and discusses the topics in question.

Pressure and Pressure Peaks

The network and storage model is a digital model, controlled by digital controls which are more or less ideal. It therefore suffers from pressure peaks due to very fast control mechanisms and pumps with less inertia than real pumps would have. This leads to very fast pump responses, positive and negative pressure spikes, and in turn to higher pump energy demands. It also makes the network and storage simulation unstable, since any pressure point in the system falling below saturation vapour pressure for even one single time step leads to an error, which aborts the simulation of the NSM and leads to a total simulation failure. However, due to the interconnectedness, the interdependency and the independence of control of the various simulation models, a prediction of the pressure range to be expected prior to a simulation run is impossible. The workaround chosen in this work was to set the default pressure level of the whole system to the unrealistic level of 90 bar. With 90 bar as zero level, the simulation does

run and finish, and the pressure peaks can be examined afterwards (as for example in Figure 4-15). With the decision for the medium of water to be incompressible and have only a linear dependency on temperature for the internal energy U and the enthalpy H, this default pressure level has no consequences on the performance of the pumps or the pump energy demand. However, it is of course not a desirable feature.

Simulation runtime

The benefit of a co-simulation is, as described earlier, the chance to use specific modelling tools for each problem, specifically tailored to tackle each type of problem. However, the connection of different modelling and simulation tools, in this work achieved by BCVTB, comes at a price: mostly reduced simulation speed. The simulation framework used in this work, a co-simulation of 16 TRNSYS instances, one Dymola instance and one BCVTB instance, takes, for a 2-year simulation with a simulation time step of one minute, between seven and nine days. With a large variety of simulation parameters as in this work, a parametric study or an optimization for a single parameter is nearly to impossible. To achieve anything close, either a significant simplification of the model or a remodelling in one single, multithread-optimized tool would be necessary. One significant simplification could be a larger simulation time step, for example of 15 minutes, which could reduce the total simulation time needed and increase the simulation stability regarding the pressure peaks described above. However, this would also blur the simulation, especially the network and storage simulation, since pressure change and wave propagation have a high change rate in reality.

Ground Temperature

As described above (4.1), the ground temperature used in this work was measured in Potsdam, although the location of the case study is Munich. The temperature range of both locations is similar, since the conductivities of the ground and the air temperatures are similar; however, the medium ground temperature of Potsdam is higher than that of Munich, resulting in a better performance during the winter months due to warmer ground temperatures and a worse performance in the summer months due to overheating of the ground with regard to the seasonal storage. However, in hindsight a better approach would have been to use the sinus pattern of the measured Potsdam temperatures, shifting the medium level to match the medium ground temperature of Munich. Based on the IWEC data for Berlin and Munich, the average yearly dry bulb temperature of Munich is 1.84 K lower than that of Berlin (ASHRAE 2001). This temperature difference was applied to the ground temperature described in Equation 4-2.

To check its influence on the simulation model as a whole, a simulation run of the baseline case (4.3.1) with the altered ground temperature was performed. Table 6-3 and Figure 6-13 display a short summary of the simulation results.

Table 6-3: Summary of the simulation results (lower ground temperature)

2305	MWh Total Energy Turnover
consisting of	
2165	MWh Useful Energy
140	MWh Losses
or	
2046	MWh Renewable Energy
259	MWh Non-Renewable Energy
resulting in	
214	t CO_2-equivalent/a
93	g CO_2-equivalent/kWh Total Energy
4.9	annual COP (System)

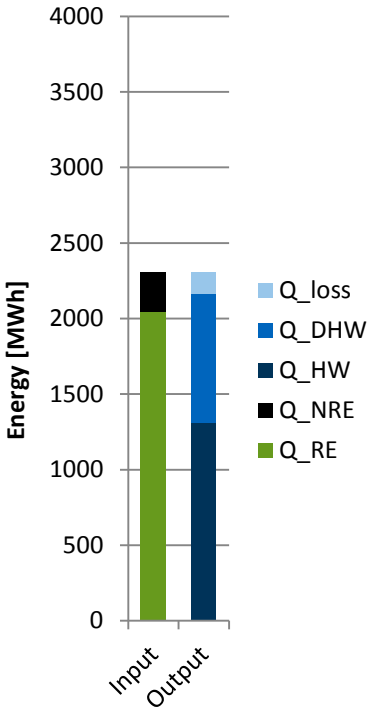

Figure 6-13: Energy In- and Output

The TE turnover of 2305 MWh is 21 MWh higher than that of the baseline case. Figure 6-14 displays Q_{loss_net} with a yearly total of 53 MWh, the origin of the increase.

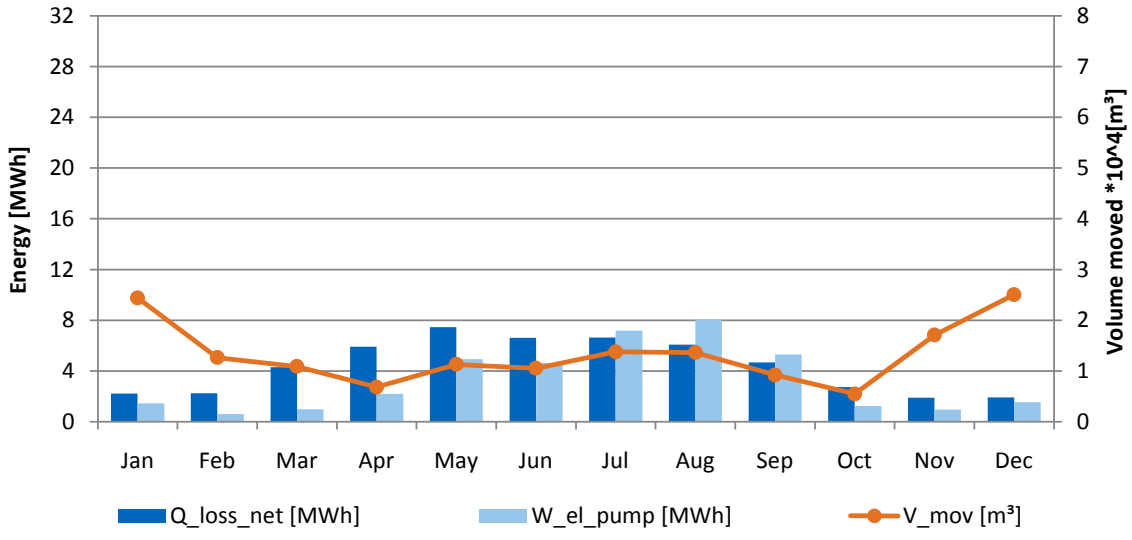

Figure 6-14: Thermal network losses, electric pump energy demand and total volume moved (lower ground temperature)

Figure 6-15 shows the lower T_ground and the associated network temperatures. The higher thermal losses are met by an increase in NRE turnover of 15 MWh and increase in RE turnover of 6 MWh. This is reflected in the increased CO_2-equivalents and the reduced annual COP compared to the baseline case. This effect can be counteracted by a larger solar collector area.

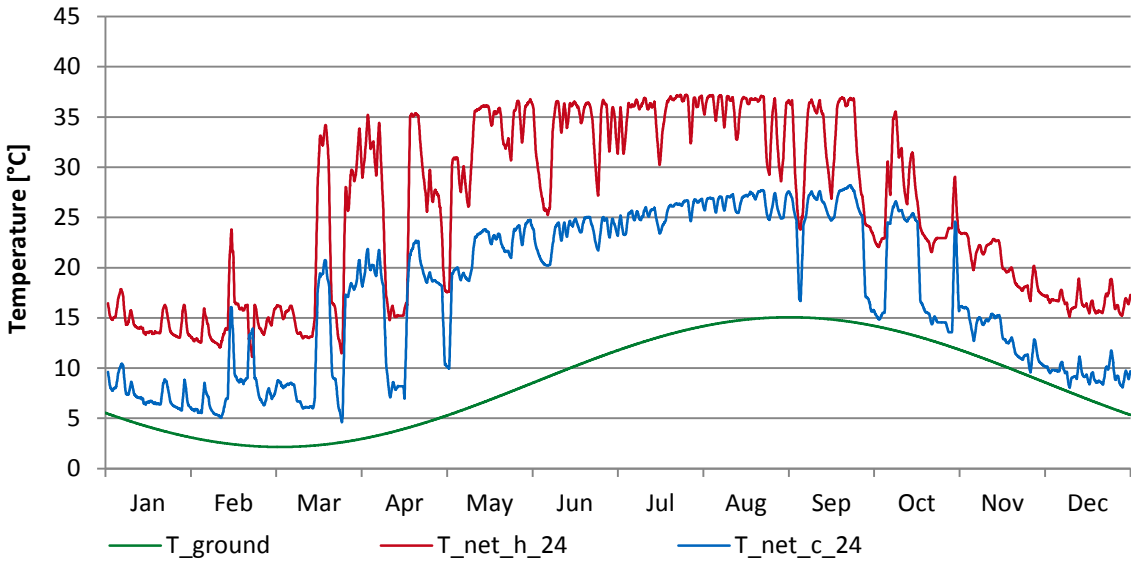

Figure 6-15: High and low temperatures of the 5GDHCN with lower ground temperature

In summary, the higher ground temperature of the systems described in 4.3 leads to a slightly better system performance or a slightly smaller collector area requirement than would be the case with the adjusted ground temperature.

Weather Data

The weather data used in this work is the data for the location Munich, provided by the American Society of Heating, Refrigerating and Air-Conditioning Engineers Research Project 1015 which led to the IWEC program. It is based on hourly measured weather data of a time period of up to 18 years, originally published in 2001. (ASHRAE 2001)

The weather data is therefore historic and is not taking into account the globally increasing temperatures due to global warming. However, since this work focusses on heating networks, the performance of 5GDHCNs in a slightly colder climate than that of today shows the robustness of the system. Further research on the cooling performance of these types of networks, however, should base the simulations on current or even future weather data which include the general increase in temperature.

7. Conclusion and Outlook

The approach of a simulation framework and several adaptable, task-oriented models makes the simulation flexible and adaptable to different local requirements and boundary conditions. With the input data set by the “Ecological Model Settlement” in Munich, the application of the developed simulation framework provides a variety of simulation results, giving insights about the behaviour and profitability of 5GDHCNs with different network typologies and sizes, demands of HW and DHW, pipe sizes, pipe insulation thicknesses, and varying heat sources.

The 5GDHCNs examined in this work performed best at low simultaneities of network charging or discharging actions. Random discharging actions as observed during the winter months do not lead to significant effects on network performance. The highest simultaneity was observed in the summer months when several buildings charged the network at the same time. This led to an increase in pump pressure and subsequently in pump energy demand.

For areas solely supplied by solar heat, the applicability of this system to high-rise buildings is obviously limited, since there is only a finite roof area on each building which can be equipped with solar-thermal collectors. However, the aim of this technology is not to reach energy autarky of single buildings, but to closely cross-link buildings and heat sources within a quarter, enabling a heat transfer from areas with excess heat to areas with increased heat demand.

This system, as with any other heating system based on low supply temperatures, is limited in the amount of heat it can transfer into a room. Therefore, increased areas of heat transfer are needed in radiators, heating panels, or underfloor heating surfaces. In conclusion, the supply of buildings with a very high heat demand is possible with this system but it is not reasonable from an economic or a comfort point of view.

A 5GDHCN presents an opportunity for areas with low heat-load density, where traditional DHNs are not built. It can provide its highest benefit in quarters with a large low-temperature waste heat potential or additional cooling requirements. There, this network type is not only capable of recycling the waste heat, but it can also compete economically with other network types which are state of the art.

7.1. Summary

Following the hypothesis stated at the outset, this work shows the development of a simulation framework for 5GDHCN simulations, which allows the coupling of different simulation and modelling tools to a co-simulation environment. It enables the user to benefit from different specified tools simultaneously in one simulation to answer the complex research questions posed.

For this simulation framework several models, among them a BSM, an Interlink Zone and a NSM, are constructed. With parameters based on a case study, several simulation runs for different scenarios are conducted, which encompass different network typologies, heat densities, types of heat supply, or pipe insulation thicknesses.

The different DHW demands examined show the impact of different user behaviour on the system and its functioning. A comparison of the three network typologies, line, ring and mesh networks, points to the counteracting effects of additional piping: alternate flow paths result in lower pump energy demand and at the same time an increased pipe surface area results in higher thermal losses.

Similar to traditional DHNs, high heat densities in 5GDHCNs are more efficient. However, due to fewer thermal losses, even heat densities as low as 1 MWh/m.a achieve thermal losses of less than 10%, one of the design aims of traditional DHNs. This is one potent argument for the construction of 5GDHCNs in areas with low heat densities.

A variation of the waste heat input in the system as substitute for solar heat input reveals an optimum in terms of CO_2 emissions: a 20% waste heat input reduces the additional electric energy demand of the system and saves up to six tons of CO_2-equivalents per year compared to the baseline scenario fully supplied by solar heat. This result is based on the datasets for CO2-equivalents per kWh electrical energy obtained from the public distribution network by BMI 2016b.

Even though 5GDHCNs run at very low temperature levels, the systems examined in this work show thermal insulation cannot be omitted. The effect measured in additional CO_2-equivalents per year caused by too little insulation is higher than the benefit in CO_2-equivalents from reduced production effort.

The influence of the pump energy demand, mainly dependent on the pressure losses of the system, is little compared to the overall electric energy demand of the system which is mainly caused by the electric energy demand of the heat pumps. However, one avoidable effect is the simultaneity of storage charging and discharging processes, due to parametric design, leading to an increased pump energy demand.

In addition to the simulations, a cost and profitability analysis is conducted for selected scenarios of different network typologies and types of heat supply. It shows the networks supplied with PVT collectors have significantly higher capital and operation-related costs than a network supplied by waste heat, due to the cost-driving solar collectors.

In a final step, the results from the profitability analysis and the simulations are discussed and put into context.

7.2. Outlook

This work mainly focusses on 5GDHCNs in a residential quarter, mostly omitting the potential a use of 5GDHCNs for cooling could unlock. This technology is only implemented halfway if it is only used for heating purposes, since one of its largest benefits is its ability to recycle low-temperature heat, which could come from the implementation in mixed quarters, with heating and cooling demand.

Any surplus heat from a cooling process (for example, air conditioning, food storage, or industrial waste heat) is a potential heat source which, once connected to the network, can reduce the need for other more costly heat sources such as solar collectors, and even gain additional revenue through the selling of cooling capacity. The extent of the cooling capacity of 5GDHCNs, the network interaction with heating and cooling demand, the effect of a cooling demand on the network hydraulics, and the resulting pump energy demand offer a broad variety of questions for further examination.

Therefore, this technology is in principle not only suitable for the temperate Middle-European climate, but also for regions which have a cooling and a heating requirement, like North America or Southern Europe. Further research examining the potential and the transferability to other climates and boundary conditions should therefore be the next step.

With the results of this work the influence of the parameters determining the heat losses in a 5GDHCN are identified. In future networks, for which cooling is the main application, these parameters could be used as a starting point to design the network accordingly and complete the investigation started by this work.

Also not covered in this thesis is the examination of the modularity and flexibility of 5GDHCNs. What are the effects of a modular network construction and expansion, and is there is a maximum advisable distance to the seasonal storage?

This work also shows a high seasonal surplus in photovoltaic energy generation in the summer, met by a slightly higher electric energy demand in the winter months. In this work the offset is compensated by the public distribution network. However, this only shifts the problem of electricity storage to a higher level. The effect of an implementation of local electricity storage capacities or active load balancing on the system in conjunction with addressing the seasonal electrical imbalance of the system shown in this work also opens a field for further research. For 5GDHCNs to become a generally applicable solution, the challenge of this seasonal electricity offset has to be addressed and managed.

In Germany, the future development of 5GDHCNs is not a matter of technology but a matter of politics. In the current legal setting, which favours central, company- or public-owned over decentral, cooperatively-owned supply structures, and does not encompass the ramifications of its taxation effects (Heissler et al. 2017b), district-based 5GDHCN solutions which cross public ground and include integrated energy approaches are close to impossible to build. Even though the ecological and environmental benefits are straightforward with CO_2 abatement costs of 354 €/t CO_2 (5.4) for the WHN, the economic feasibility strongly depends on the current general economic situation, which is dominated by a cheap non-renewable heat supply through fossil fuels. As long as fossil fuels are the cheapest, go-to solution, no area-wide installation of renewable heat supply structures can be established.

One approach to make renewable heat supply structures economically feasible could be a CO_2 price which, as mentioned above, has been adopted by the German Federal Government in the Climate Action Programme 2030 and made into law by the Bundestag. Figure 7-1 displays the prices per ton of CO_2 emission suggested by the German Institute for Economic Research (DIW) (Stefan Bach et al. 2019), the Mercator Research Institute on Global Commons and Climate Change, together with the Potsdam Institute for Climate Impact Research (MCC/PIK) (Edenhofer et al. 2019). The CO_2

prices of the German Federal Government, as shown in Figure 7-1, are provisional prices that anticipate a planned amendment to the Fuel Emission Trading Act BEHG, as decided by the Mediation Committee of the Bundestag and Bundesrat (Geschäftsstelle des Vermittlungsausschusses 2019).

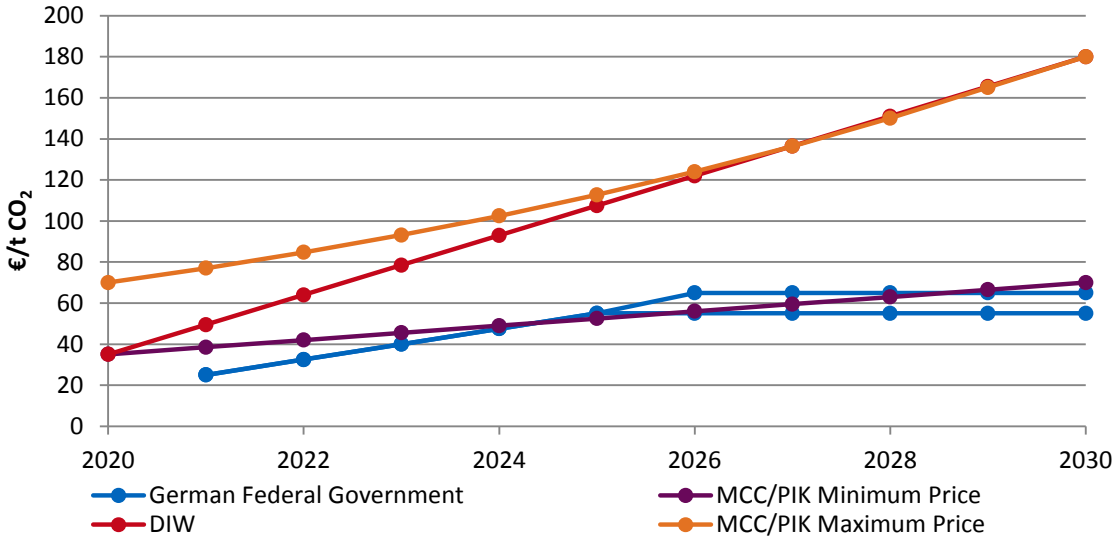

Figure 7-1: Prices in € per ton CO_2 emission suggested by various institutions (Bundesregierung 2019; Edenhofer et al. 2019; Stefan Bach et al. 2019)

The direct opposition of the different price curves shows that the price curve adopted by the German Federal Government starts lower than any of the recommended minimum price curves, with the aim of a self-regulating CO_2 price between 55 € and 65 € from 2026 onwards (Bundesregierung 2019). This pricing decision comes at a time at which the German Institute for Economic Research states that a CO_2 price of 80 €/t will not suffice to reach the German Climate Goals in 2030, especially not in the building and traffic sector (Stefan Bach et al. 2019).

A study commissioned by the Federal Ministry for the Environment, Nature Conservation and Nuclear Safety to examine the effectiveness of the measures of the Climate Action Programme 2030 also concludes that the measures do not suffice to reach a reduction of CO_2 emissions of 55% (Harthan et al. 2020). Another study investigating the same topic, commissioned by the Federal Ministry for Economic Affairs and Energy, comes to the same conclusion (Kremmler et al. 2020). The main sectors that fail to reach the reduction goals are the traffic and building sectors (Harthan et al. 2020).

Figure 7-2 displays a comparison of the cost per kWh heat in a traditional DHN and a WHN with 100% waste heat supply, based on the cost of heat per kWh determined in 5.3.4, with the upper border of the CO_2 price range of the German Federal Government (GFG) as well as the other price curves as basis.

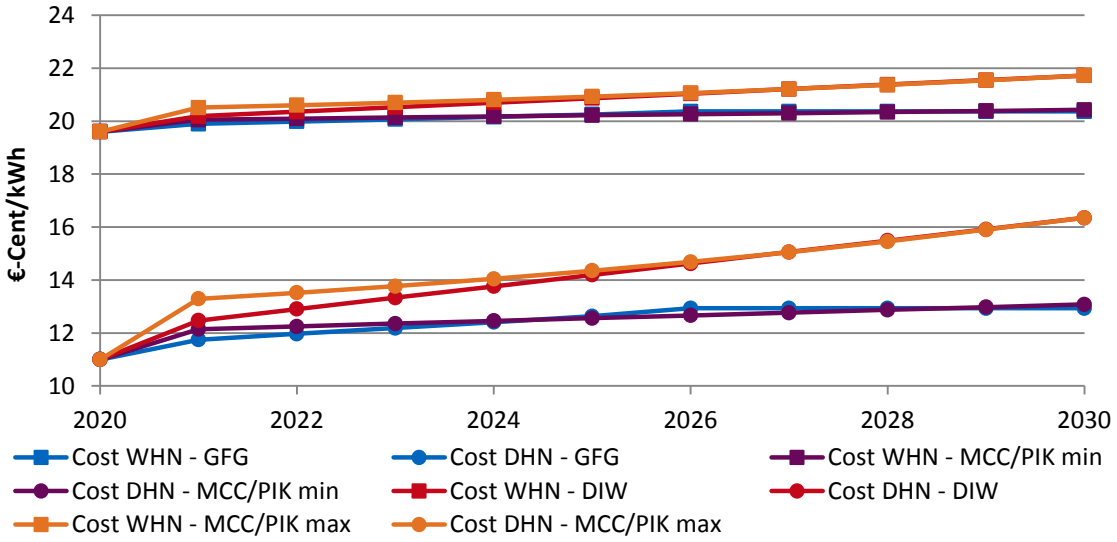

Figure 7-2: Cost in €-Cent per kWh heat over time for a DHN and WHN based on various CO_2 prices depicted in Figure 7-1

The graphs show that, for all CO_2 prices displayed in Figure 7-1, the resulting price per kWh heat is cheaper in the DHN than in the WHN. Even with the maximum price suggested by the MCC/PIK, the two technologies do not reach economic competitiveness within the next ten years. Also, the upper border of the price range of the GFG's CO_2 pricing policy, marking the absolute minimum of the price curves suggested, does not promote the implementation of this new technology and keeps the price difference even bigger than a pricing based on the lowest recommended CO_2 price by MCC/PIK.

The insufficiency of the CO_2 prices shown in Figure 7-1 is further exposed by the CO_2 price recommendation of the German Environment Agency (GEA), a state agency of the Federal Ministry for the Environment, Nature Conservation and Nuclear Safety, which proposes a CO_2 price of 649 €/t in 2020. This price recommendation is based on the damage costs caused to society by greenhouse gas emissions and the resulting climate change. (Matthey and Bünger 2019)

Central to the calculation of these damage costs is that present and future damages are equally weighted to account for equal values of today's and future generations' benefit. This means that the damage that will occur for a future generation is weighted equally to damage that occurs in the present (Matthey and Bünger 2019). Today none of these damage costs are accounted for in the determination of energy prices.

Bearing this in mind, Figure 7-3 again displays the prices per ton CO_2 emission as displayed in Figure 7-1 above, complemented by the price curve suggested by the GEA.

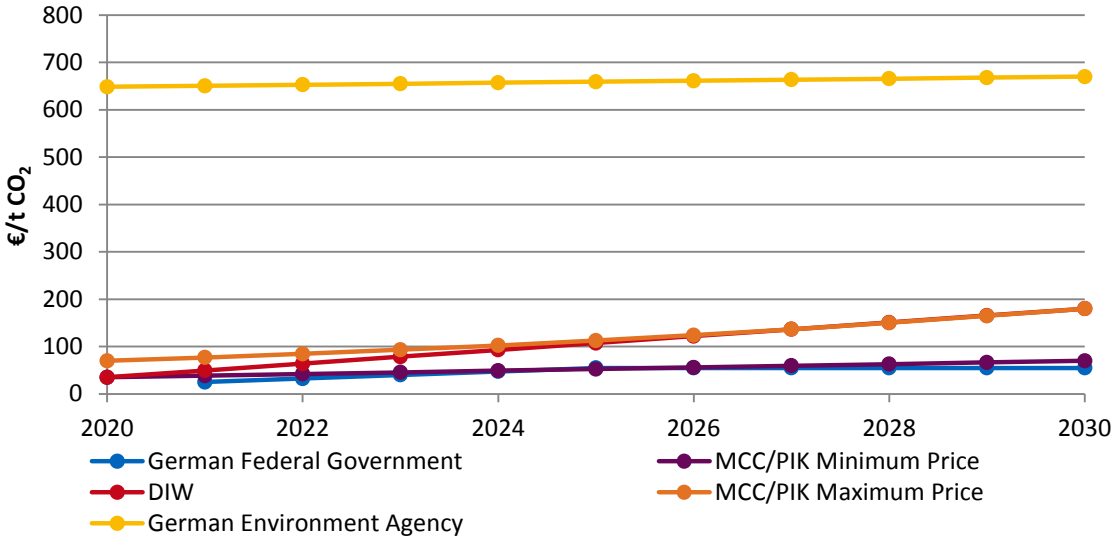

Figure 7-3: Prices in € per ton CO_2 emission suggested by various institutions and the German Environment Agency (Bundesregierung 2019; Edenhofer et al. 2019; Stefan Bach et al. 2019; Matthey and Bünger 2019)

With the GEA's recommended CO_2 price per kWh, heat from a WHN would already be 3 €-Ct/kWh cheaper than heat from a DHN. To achieve economic viability of a WHN, a CO_2 price of 480 €/t would suffice. A price that is not high considering that, according to the GEA, it should actually be 649 €/t.

However, under the current CO_2 and fossil fuel price policy of the GFG, WHNs are currently not economically viable, even though they are highly advantageous systems and an effective instrument for the reduction of CO_2 emissions and NRE use in the building sector.

Yes, it is our freedom to shape CO_2 pricing. But our freedom to do little, to aim low, to postpone, is paid for by the freedom and the quality of life of future generations.

List of References

Alary, Michael; Joly, Rean R. (1991): Risk factors for contamination of domestic hot water systems by legionellae. In *Applied and Environmental Microbiology* 57 (8), pp. 2360–2367, checked on 5/2/2018.

Amstein + Walthert (Ed.) (2010): Energiekonzept ETH Zürich Hönggerberg. Available online at http://www.energieinstitut.at/wp-content/uploads/2015/04/A-W_Poster_Energiekonzept_ETHZ_Hoenggerberg.pdf, checked on 3/23/2018.

Amstein + Walthert (Ed.) (2015): allreal Richti Wallisellen. Energiekonzept Richti Wallisellen. Available online at http://www.richti.ch/downloads/Energiekonzept-Richti-Wallisellen.pdf, checked on 3/23/2018.

ASHRAE (2001): International Weather for Energy Calculations. IWEC Weather Files. Users Manual and CD-ROM. Edited by ASHRAE. Atlanta. Available online at https://energyplus.net/weather/sources#IWEC, checked on 3/1/2018.

Baetens, R.; Coninck, R. de; van Roy, J.; Verbruggen, B.; Driesen, J.; Helsen, L.; Saelens, D. (2012): Assessing electrical bottlenecks at feeder level for residential net zero-energy buildings by integrated system simulation. In *Applied Energy* 96, pp. 74–83. DOI: 10.1016/j.apenergy.2011.12.098.

Bausch-Gall, Ingrid (2012): Kurs zur Einführung in Dymola/Modelica. Dymola Multi-Engineering Modeling and Simulation. Edited by Bausch-Gall GmbH. München, checked on 5/24/2018.

Bayerisches Landesamt für Umwelt (2013): Übersichtsbodenkarte von Bayern. 1:25.000. DEBY_f110733a-e136-4004-a5c3-546219a9a9ed. Augsburg: Bayernatlas, checked on 2/24/2020.

Behnisch, Joachim (2018): Ohrbergsiedlung. Rohrleitungsplan Kaltwassernetz. Edited by Energieservice Westfalen Weser, checked on 4/12/2018.

Bestenlehner, Dominik; Drück, Harald; Stübler, Andrea (2014): Energetisches Einsparpotential eines kalten Nahwärmenetzes zur Wärmeversorgung eines Stadtquartiers im Vergleich zu einem konventionellen Nahwärmenetz. Edited by OTTI - 24. Symposium Thermische Solarenergie. Bad Staffelstein, checked on 4/4/2018.

BINE Informationsdienst (Ed.) (2015): Neckarpark Stuttgart: Wärme aus Abwasser. Available online at http://www.bine.info/themen/energiesysteme/waerme-kaelte netze/news/neckarpark-stuttgart-waerme-aus-abwasser/, checked on 3/23/2018.

Blocon AB (Ed.) (2018): Earth Energy Designer (EED). Blocon AB. Available online at https://buildingphysics.com/eed-2/, checked on 5/25/2018.

Bloomquist, R. Gordon (2001): Geothermal District Energy System Analysis, Design and Development. European Summer School on Geothermal Energy Applications. Edited by International Geothermal Association. Oradea, checked on 4/17/2018.

BMI (2016a): Fernwärme Mix - Ökobaudat 2016 I. Informationsportal nachhaltiges Bauen - Fernwärme Mix. Edited by Bundesministerium des Innern, für Bau und Heimat (BMI), checked on 6/7/2017.

BMI (2016b): Strom Mix 2015 - Ökobaudat 2016 I. Informationsportal nachhaltiges Bauen - Strom Mix 2015. Edited by Bundesministerium des Innern, für Bau und Heimat (BMI) (9.2.05), checked on 6/7/2017.

BMI (2017): Nutzungsdauern von Bauteilen für Lebenszyklusanalysen nach Bewertungssystem Nachhaltiges Bauen (BNB). Edited by Bundesministerium des Innern, für Bau und Heimat (BMI). Bundesinstitut für Bau-,Stadt- und Raumforschung im Bundesamt für Bauwesen und Raumordnung. Berlin. Available online at https://www.nachhaltigesbauen.de/fileadmin/pdf/baustoff_gebauededaten/BNB_Nutzungsdauern_von_Bauteilen_2017-02-24.pdf, updated on 2/24/2017, checked on 11/22/2019.

BMI (2019): Polyurethan Hartschaum (Rohrisolierung) - Ökobaudat 2019 III. Informationsportal nachhaltiges Bauen - Polyurethan Hartschaum (Rohrisolierung). Edited by Bundesministerium des Innern, für Bau und Heimat (BMI) (8.1.02). Available online at https://www.oekobaudat.de/datenbank/browser-oekobaudat/daten/db1/8.1.02/Geb%C3%A4udetechnik/Heizung/W%C3%A4rmeverteilung%20und%20Abgabe.html#bereich1, checked on 11/22/2019.

BMU (2016): Klimaschutzplan 2050. Klimaschutzpolitische Grundsätze und Ziele der Bundesregierung. Edited by Bundesministerium für Umwelt, Naturschutz und nukleare Sicherheit (BMU). Berlin. Available online at https://www.bmu.de/themen/klima-energie/klimaschutz/nationale-klimapolitik/klimaschutzplan-2050/, updated on Februar 2019, checked on 1/27/2020.

Bolle, Michael (2015): Vorstellung Berliner Stadtwerke und Wärmenetz (Low-Exergie) im Industriegebiet. Edited by Berliner Wasserbetriebe. Berlin. Available online at http://www.motzener-strasse.de/system/files/8Vorstellung%20Berliner%20Stadtwerke%20und%20Low-Exergie-Netz.pdf, checked on 3/27/2018.

Brand, Marek; Svendsen, Svend (2013): Renewable-based low-temperature district heating for existing buildings in various stages of refurbishment. In *Energy* 62, pp. 311–319. DOI: 10.1016/j.energy.2013.09.027.

Braungardt, Simon; Günther, Danny; Miara, Marek; Wapler, Jeannette (2013): Electrically driven heat pumps. Themeninfo 1/2013. Edited by BINE Informationsdienst. FIZ Karlsruhe GmbH; Leibniz Institute for Information Infrastructure. Karlsruhe. Available online at http://www.bine.info/fileadmin/content/Publikationen/Themen-Infos/I_2013/themen_0113_engl _Internetx.pdf, checked on 10/4/2019.

Brooks, Christopher; Lee, Edward A.; Liu, Xiaojun; Neuendorffer, Stephen; Zhao, Yang; Zheng, Haiyang (2008): Ptolemy II. Heterogeneous concurrent modeling and design in Java. Edited by Department of Electrical Engineering and Computer Sciences. University of California, Berkeley. Berkeley (Technical Report No. UCB/EECS-2007-7), checked on 5/18/2018.

Buffa, Simone; Cozzini, Marco; D'Antoni, Matteo; Baratieri, Marco; Fedrizzi, Roberto (2019): 5th generation district heating and cooling systems. A review of existing cases in Europe. In *Renewable and Sustainable Energy Reviews* 104, pp. 504–522. DOI: 10.1016/j.rser.2018.12.059.

Bundesregierung (2019): Klimaschutzprogramm 2030. Bundesregierung. Berlin. Available online at https://www.bundesregierung.de/breg-de/themen/klimaschutz/klimaschutzprogramm-2030-1673578, checked on 12/19/2019.

Bünning, Felix; Wetter, Michael; Fuchs, Marcus; Müller, Dirk (2018): Bidirectional low temperature district energy systems with agent-based control. Performance comparison and operation optimization. In *Applied Energy* 209, pp. 502–515. DOI: 10.1016/j.apenergy.2017.10.072.

BVerwG, Decision of 9/8/2016, case number [ECLI:DE:BVerwG:2016:080916U10CN1.15.0].

C.A.R.M.E.N e.V. (Ed.) (2013): Nahwärmenetze und Bioenergieanlagen. Ein Beitrag zur effizienten Wärmenutzung und zum Klimaschutz. Merkblatt. C.A.R.M.E.N e.V. Straubing, checked on 4/26/2018.

Caratsch, Marie-Theres; Hangartner, Diego; Ködel, Joachim; Sfeir, Joseph; Sulzer, Matthias (2015): Projekt „Thermische Vernetzung". Konzeptvorschlag. Schweizer Bundesamt für Energie (BFE). Available online at http://www.bfe.admin.ch/php/modules/publikationen/stream.php?extlang=de&name=de_392869086.pdf &endung=Projekt, checked on 3/23/2018.

Carbonell, D.; Philippen, D.; Haller, M. Y.; Brunold, S. (2016): Modeling of an ice storage buried in the ground for solar heating applications. Validations with one year of monitored data from a pilot plant. In *Solar Energy* 125, pp. 398–414. DOI: 10.1016/j.solener.2015.12.009.

Carli, Michele de; Galgaro, Antonio; Pasqualetto, Michele; Zarrella, Angelo (2014): Energetic and economic aspects of a heating and cooling district in a mild climate based on closed loop ground source heat pump. In *Applied Thermal Engineering* 71 (2), pp. 895–904. DOI: 10.1016/j.applthermaleng.2014.01.064.

Christiansen, Christian Holm; Olsen, Peter Kaarup; Gudmundsson, Oddgeir; Hofmeister, Morten (2014): New Guideline for Low Temperature District Heating. Increasing Efficiency. In *EuroHeat&Power* (11), pp. 46–50.

Codony, F.; Alvarez, J.; Oliva, J. M.; Ciurana, B.; Company, M.; Camps, N. et al. (2002): Factors promoting colonization by legionellae in residential water distribution systems. An environmental case-control survey. In *European journal of clinical microbiology & infectious diseases : official publication of the European Society of Clinical Microbiology* 21 (10), pp. 717–721. DOI: 10.1007/s10096-002-0789-y.

Conrad, Jochen (2020): Modellierung und Bewertung von Maßnahmen zur kosteneffizienten CO2-Verminderung im Sektor private Haushalte. Dissertation. Technische Universität München, München. Lehrstuhl für Energiewirtschaft und Anwendungstechnik. Available online at https://mediatum.ub.tum.de/download/1525924/1525924.pdf, checked on 10/20/2020.

Cosmo GmbH (2016): Flachheizkörper. Technische Information 1/2016. Edited by Cosmo GmbH. Hamburg. Available online at https://www.cosmo-info.de/mehr/katalogregal/cosmo-technische-informationen, checked on 5/4/2018.

Crawley, Drury B.; Hand, Jon W.; Kummert, Michaël; Griffith, Brent T. (2008): Contrasting the capabilities of building energy performance simulation programs. In *Building and Environment* 43 (4), pp. 661–673. DOI: 10.1016/j.buildenv.2006.10.027.

Dallmayer, W.; Kuckelkorn, Jens M.; Radspieler, M.; Reuß, Manfred; Schölkopf, W.; Schweigler, C.; Staudacher, L. (2010): Begleitforschung Solare Nahwärme am Ackermannbogen in München - SNAB. Abschlussbericht. [Laufzeit: 04/2004 - 09/2009]. Edited by Bayerisches Zentrum für Angewandte Energieforschung e.V.

Dassault Systèmes: Dymola. Vélizy-Villacoublay. Available online at https://www.3ds.com/de/produkte-und-services/catia/produkte/dymola/.

Destatis (Ed.) (2018): Fernwärmeversorgung 2017: Abgegebene Wärmemenge leicht gesunken. Available online at https://www.destatis.de/DE/Presse/Pressemitteilungen/2018/11/PD18_434_434.html, checked on 3/23/2020.

Doetsch, Christian; Bargel, Stefan (2009): Theoretische Betrachtung zur idealen Netztemperatur. Edited by Fraunhofer UMSICHT. Available online at https://www.lowex.info/Kassel_2009/17b_2009_10_29_LowEx_Symposium_Kassel_UMSICHT.pdf, checked on 3/27/2018.

Drück, Harald (2006): Multiport Store - Model for TRNSYS - Type 340. Stratified fluid storage tank with four internal heat exchangers, ten connections for direct charge and discharge and an internal electric heater. Version 1.99F. Edited by Institut für Thermodynamik und Wärmetechnik (ITW). Universität Stuttgart. Stuttgart.

Edenhofer, Ottmar; Flachsland, Christian; Kalkuhl, Matthias; Knopf, Brigitte; Pahle, Michael (2019): Optionen für eine CO2 -Preisreform. With assistance of Potsdam-Institut für Klimafolgenforschung, Mercator Research Institute on Global Commons and Climate Change. Edited by Sachverständigenrat zur Begutachtung der gesamtwirtschaftlichen Entwicklung. Berlin. Available online at https://www.sachverstaendigenrat-wirtschaft.de/fileadmin/dateiablage/Arbeitspapiere/Arbeitspapier_04_2019.pdf, updated on Juli 2019, checked on 12/19/2019.

Elmqvist, Hilding (2014): Modelica Evolution - From My Perspective. In : Proceedings of the 10th International Modelica Conference, March 10-12, 2014: Linköping University Electronic Press (Linköping Electronic Conference Proceedings), pp. 17–26, checked on 5/18/2018.

Energi Alpina (2015): Start des Projektes „CO2-freies Tujetsch aus Berg- und Tunnelwärme“ mit der ersten Etappe. Ciril Deplazes, ciril.deplazes@energia. Available online at http://www.energia-alpina.ch/fileadmin/user_upload/Docs/2._Pressemitteilung_2015.08.12.pdf, checked on 3/23/2018.

Energi Alpina (Ed.) (2016): Anergienetz Sedrun. Available online at http://www.energia-alpina.ch/fileadmin/user_upload/Docs/Flyer_ea_anergienetz_definitiv_senza_passkreuz.pdf, checked on 3/23/2018.

EQUA Simulation AB (Ed.) (2018): IDA Indoor Climate and Energy (IDA ICE) - Simulation Software. EQUA Simulation AB. Available online at https://www.equa.se/de/ida-ice, checked on 5/25/2018.

ETH Zürich (Ed.) (2015): Energiekonzept Anergienetz Hönggerberg. Infrastrukturbereich Immobilien, checked on 3/23/2018.

Ewendt, Robert; Bäckeralf, Marco (2005): Technische Machbarkeitsstudie und Wirtschaftlichkeitsbetrachtung einer Kraft-Wärme-Kälte-Kopplungsanlage für das Klinikum Lippe-Detmold. Studienarbeit. Fachhochschule Bielefeld, Bielefeld. Fachbereich Eletrotechnik und Informationstechnik, checked on 9/19/2019.

Fish, Garron (2017): The Dymola Compilation Process in Action. Edited by Claytex Tech Blog. Claytex. Leamington Spa. Available online at http://www.claytex.com/blog/dymola-compilation-process/, checked on 5/24/2018.

Forschungsinitiative EnergiewendeBauen (Ed.) (2017): Neckarpark Stuttgart gewinnt Nahwärme und -kälte aus dem Abwasserkanal. EnEff:Wärme - Neckarpark Stuttgart. Landeshauptstadt Stuttgart. Available online at https://projektinfos.energiewendebauen.de/projekt/neckarpark-stuttgart-gewinnt-nahwaerme-und-kaelte-aus-dem-abwasserkanal/, checked on 3/23/2018.

Geschäftsstelle des Vermittlungsausschusses (Ed.) (2019): Vermittlungsausschuss erzielt Kompromiss zum Klimapaket. Vermittlungsausschuss von Bundestag und Bundesrat. Available online at https://www.vermittlungsausschuss.de/SharedDocs/pm/2019/015.html, checked on 2/12/2020.

BEHG (2019): Gesetz über einen nationalen Zertifikatehandel für Brennstoffemissionen (Brennstoffemissionshandelsgesetz). In *BGBl. I* (50), 2728-2737, checked on 1/28/2020.

KSG (2019): Gesetz zur Einführung eines Bundes-Klimaschutzgesetzs und zur Änderung weiterer Vorschriften. In *BGBl. I* (48), pp. 2513–2521, checked on 1/28/2020.

EEWärmeG, revised by Article 9 of the Act of 10/20/2015 (BGBl. I p. 1722) (2008): Gesetz zur Förderung Erneuerbarer Energien im Wärmebereich (Erneuerbare-Energien-Wärmegesetz). In *BGBl. I* (36), pp. 1658–1665, checked on 2/18/2020.

Harthan, R.; Repenning, J.; Blanck, R.; Böttcher, H.; Bürger, V.; Emele, L. et al. (2020): Treibhausgasminderungswirkung des Klimaschutzprogramms 2030. Available online at https://www.umweltbundesamt.de/publikationen/treibhausgasminderungswirkung-klimaschutzprogramm-2030, checked on 3/12/2020.

Heissler, Karl Martin; Franke, Laura; Nemeth, Isabell; Auer, Thomas (2016): Modeling low temperature district heating networks for the utilization of local energy potentials. In *Bauphysik* 38 (6), pp. 372–377. DOI: 10.1002/bapi.201610038.

Heissler, Karl Martin; Metz, Jakob; Auer, Thomas; Nemeth, Isabell (2017a): Increasing the Utilization of Local Energy Potentials through Low Temperature District Heating Networks. Design to Thrive. Edited by PLEA 2017. Edinburgh, checked on 2/27/2018.

Heissler, Karl Martin; Metz, Jakob; Lang, Werner; Auer, Thomas; Nemeth, Isabell (2017b): Potenziale von Niedrigtemperaturnetzen zur Steigerung des Anteils erneuerbarer Energien in Quartieren. Niedrigtemperaturnetze in Quartieren. TUM. München.

Hillel, Daniel (1982): Introduction to soil physics. New York: Acad. Press.

Holstenkamp, Lars; Meisel, Marcus; Neidig, Phillip; Opel, Oliver; Steffahn, Jens; Strodel, Nikolai et al. (2017): Interdisciplinary Review of Medium-deep Aquifer Thermal Energy Storage in North Germany. In *Energy Procedia* 135, pp. 327–336. DOI: 10.1016/j.egypro.2017.09.524.

IBC Energie Wasser Chur (Ed.) (2014): Das Anergienetz – ein guter Entscheid (IBC Power das Kundenmagazin der IBC). Available online at https://ibc-chur.ch/wp-content/uploads/2016/04/1461226333-9cc85cef27b2f7834377c11bbfc3af37.pdf, checked on 3/23/2018.

Kermi GmbH (2016): therm-x2 Flachheizkörper. Edited by Kermi GmbH. Plattling. Available online at https://portal.kermi.de/DownloadCenter2/kermi_de/de/de/h/s/heating/documents/11, checked on 5/4/2018.

Klein, S. A.; Duffie, J. A.; Beckman, W. A. (1976): TRNSYS – a transient simulation program. In *ASHRAE Transactions* 1976 (82(1)), pp. 623–633.

Krames, Helmut (2013): Thermische Großspeicher. Arten - Anwendung - Auslegung. Edited by Institut für angewandtes Stoffstrommanagement. Birkenfeld, checked on 4/13/2018.

Kräuchi, Philipp; Kolb, Matthias (2012): Simulation thermischer Arealvernetzung mit IDA-ICE. BauSim 2012. Edited by Fourth German-Austrian IBPSA Conference, checked on 4/13/2018.

Kräuchi, Philipp; Kolb, Matthias; Gautschi, Thomas; Menti, Urs-Peter; Sulzer, Matthias (2014): Modellbildung für thermische Arealvernetzung mit IDA-ICE. BauSim 2014. Edited by Fifth German-Austrian IBPSA Conference. Available online at http://www.ibpsa.org/proceedings/bausimPapers/2014/ p1130_final.pdf, checked on 5/15/2018.

Kremmler, Andreas; Kirchner, Almut; Maur, Alex auf der; Ess, Florian; Kreidelmeyer, Sven; Piégsa, Alexander et al. (2020): Energiewirtschaftliche Projektionen und Folgeabschätzungen 2030/2050. Comissioned by the Bundesministerium für Wirtschaft und Energie. Prognos AG; Fraunhofer ISI; GWS; iinas. Available online at https://www.bmwi.de/Redaktion/DE/Publikationen/Wirtschaft/klimagutachten.pdf?__blob=publicationFile&v=6, updated on 3/10/2020, checked on 3/12/2020.

Lämmle, Manuel; Oliva, Axel; Hermann, Michael; Kramer, Korbinian; Kramer, Wolfgang (2017): PVT collector technologies in solar thermal systems. A systematic assessment of electrical and thermal yields with the novel characteristic temperature approach. In *Solar Energy* 155, pp. 867–879. DOI: 10.1016/j.solener.2017.07.015.

Lauber IWISA AG: Ringleitung Anergienetz ETH Zürich. Edited by ETH Zürich, Lauber IWISA AG. Available online at https://studylibde.com/doc/8606552/brosch%C3%BCre-anergienetz-eth, checked on 3/27/2020.

Lauber IWISA AG (Ed.) (2008): Anergienetz Visp-West. Eine erdölunabhängige Energieversorgung. Available online at http://www.lauber-iwisa.ch/data/Ressources/1353872213-Projektblatt_Anergienetz_fix_Low.pdf, checked on 3/23/2018.

Linder, Arthur; Berchtold, Willi (1982): Statistische Methoden II Varianzanalyse und Regressionsrechnung. Basel: Birkhäuser, checked on 2/6/2018.

Lund, Henrik; Werner, Sven; Wiltshire, Robin; Svendsen, Svend; Thorsen, Jan Eric; Hvelplund, Frede; Mathiesen, Brian Vad (2014): 4th Generation District Heating (4GDH). Integrating smart thermal grids into future sustainable energy systems. In *Energy* 68, pp. 1–11. DOI: 10.1016/j.energy.2014.02.089.

Matthey, Astrid; Bünger, Björn (2019): Methodenkonvention 3.0 zur Ermittlung von Umweltkosten – Kostensätze. Stand 02/2019. Edited by Umweltbundesamt. Dessau-Roßlau. Available online at https://www.umweltbundesamt.de/ sites/default/files/medien/1410/publikationen/2019-02-11_methodenkonvention-3-0_kostensaetze_korr.pdf, updated on 2/11/2019, checked on 1/8/2020.

Maurer Hartmann, Jeannette (2013): Anergienetz ETH Hönggerberg. Informationen und Zahlen. Stand Sommer 2013. Edited by ETH Zürich. Zürich, checked on 3/23/2018.

Mercker, O.; Arnold, O. (2017): Abschlussbericht zum Vorhaben Ansätze zur Reduktion der konventionell erzeugten Wärmeverteilverluste in solar unterstützten Mehrfamilienhäusern. Institut für Solarenergieforschung Hameln GmbH (ISFH). Hameln/Emmerthal, checked on 3/6/2018.

Mesquita, L.; Faktor, B.; Conn, D.; Couronne, B.; Paget, K.: Drake Landing Solar Community. The District Heating System. Edited by Drake Landing Solar Community. Available online at http://dlsc.ca/district.htm, checked on 6/30/2019.

Modelica Association (Ed.) (2015): Modelica Version 3.2.1. Build 4. Available online at https://modelica.org/, checked on 5/18/2018.

Moises, Wolfgang (2015): Kombinierte Kalt-/Warme-Nahwärmenetze im Vergleich zu Standard-Nahwärmenetzen. Projektbeispiel „Dollnstein“. Edited by Team für Technik. Team für Technik. Available online at https://www.tftgmbh.de/projekte/ regenerative-energie/dollnstein/, checked on 9/23/2019.

Müller, D.; Lauster, M.; Constantin, A.; Fuchs, M.; Remmen, P. (2016): AixLib - An open-source Modelica library within the IEA-EBC Annex 60 framework. In John Grunewald (Ed.): Proceedings CESBP 2016/BauSIM 2016. Central European Symposium on Building Physics 2016. Dresden, 14.-16.09.2016. Technische Universität Dresden. Stuttgart: Fraunhofer IRB Verlag, pp. 3–9, checked on 5/24/2018.

Nageler, P.; Schweiger, G.; Pichler, M.; Brandl, D.; Mach, T.; Heimrath, R. et al. (2018): Validation of dynamic building energy simulation tools based on a real test-box with thermally activated building systems (TABS). In *Energy and Buildings* 168, pp. 42–55. DOI: 10.1016/j.enbuild.2018.03.025.

Novo, A. V.; Bayon, J. R.; Castro-Fresno, D.; Rodriguez-Hernandez, J. (2010): Review of seasonal heat storage in large basins. Water tanks and gravel–water pits. In *Applied Energy* 87 (2), pp. 390–397. DOI: 10.1016/j.apenergy.2009.06.033.

Nussbaumer, Thomas (2017): Planungshandbuch Fernwärme. Ittingen: Energie-Schweiz, Bundesamt für Energie, checked on 4/16/2018.

Ommen, Torben; Thorsen, Jan Eric; Markussen, Wiebke Brix; Elmegaard, Brian (2017): Performance of ultra low temperature district heating systems with utility plant and booster heat pumps. In *Energy* 137, pp. 544–555. DOI: 10.1016/j.energy.2017.05.165.

Open Street Map Foundation (2019): Open Street Map. With assistance of Open Street Map Contributers. Available online at https://www.openstreetmap.org/.

Østergaard, Dorte; Svendsen, Svend (2017): Space heating with ultra-low-temperature district heating – a case study of four single-family houses from the 1980s. In *Energy Procedia* 116, pp. 226–235. DOI: 10.1016/j.egypro.2017.05.070.

Østergaard, Poul Alberg; Andersen, Anders N. (2016): Booster heat pumps and central heat pumps in district heating. In *Applied Energy* 184, pp. 1374–1388. DOI: 10.1016/j.apenergy.2016.02.144.

Pajarola, Jano Felice (2017): Ein Bau für Sport, Events und Wärme. In *Bündner Tagblatt*, 12/18/2017. Available online at http://www.energia-alpina.ch /file-admin/user_upload/Docs/Tagblatt_2017.12.18.pdf, checked on 3/23/2018.

Pehnt, Martin; Nast, Michael; Götz, Christian; Blömer, Sebastian; Barckhausen, Anton; Schröder, David et al. (2017): Wärmenetzsysteme 4.0. Endbericht - Kurzstudie zur Umsetzung der Maßnahme „Modellvorhaben erneuerbare Energien in hocheffizienten Niedertemperaturwärmenetzen“. ifeu - Institut für Energie- und Umweltforschung Heidelberg GmbH. Available online at https://www.ifeu.de/wp-content/uploads/W%C3%A4rmenetze-4.0-Endbericht-final.pdf, checked on 9/18/2019.

Perrot, Pierre (1998): A to Z of thermodynamics. Oxford: Oxford University Press.

Perschk, A. (2012): TRNSYS-TUD Entwicklung. Symposium "Integrale Planung und Simulation in Bauphysik und Gebäudetechnik". Edited by Professur für Gebäudetechnik und Wärmeversorgung. Technische Universität Dresden. Dresden. Available online at https://tu-dresden.de/bu/architektur/ibk/ressourcen/dateien/institute/events/2012_EnOB_Symposium/06_trnsys_tud_entwicklung_perschk.pdf?lang=de, checked on 5/25/2018.

Pfnür, Andreas; Winiewska, Bernadetta; Oschatz, Bert; Mailach, Bettina (2016): Studie "Dezentrale vs. zentrale Wärmeversorgung im deutschen Wärmemarkt". Edited by Institut für Wärme- und Öltechnik (IWO). Darmstadt, Dresden. Available online at https://www.zukunftsheizen.de/fileadmin/user_upload/3_Technik/3.6_Projekte_und_Studien/3.6.3_Nah-_und_Fernwaermenetze/Studie_Dezentrale_vs_zentrale_Waermeversorgung_IWO.pdf, checked on 4/4/2018.

Picard, Damien; Helsen, Lieve (Eds.) (2014): Advanced Hybrid Model for Borefield Heat Exchanger Performance Evaluation, an Implementation in Modelica. the 10th International Modelica Conference, March 10-12, 2014, Lund, Sweden, March 10-12, 2014: Linköping University Electronic Press (Linköping Electronic Conference Proceedings).

Pietruschka, Dirk (2016): Vision 2020. Die Plusenergiegemeinde Wüstenrot. Stuttgart: Fraunhofer IRB Verlag (Schriftenreihe EnEff:Stadt). Available online at http://www.irbnet.de/daten/rswb/16099004074.pdf, checked on 3/23/2018.

Potsdam-Institut für Klimafolgenforschung (Ed.) (2018): Bodentemperatur — PIK Research Portal. Available online at https://www.pik-potsdam.de/services/klima-wetter-potsdam/klimazeitreihen/bodentemperatur/index_html, checked on 2/6/2018.

Python Software Foundation (Ed.) (2018): Python. Python Software Foundation. Available online at https://www.python.org, checked on 5/25/2018.

VDI 4655, 2008: Referenzlastprofile von Ein- und Mehrfamilienhäusern für den Einsatz von KWK-Anlagen, checked on 6/7/2018.

Rehau (2011): Rauthermex - Mit Sicherheit mehr Wärme. Technische Informationen 817600. Edited by Rehau. Available online at https://www.rehau.com/download/886126/technische-information-rauthermex.pdf, checked on 2/7/2018.

Robbi, Steffen (2013): LowEx-Fernwärme. Vergleichende Bewertung von Maßnahmen für eine effiziente, multifunktionale Fernwärmeversorgung. Dissertation. Technische Universität Dresden, Dresden, checked on 4/13/2018.

Schluck, T.; Kräuchi, Philipp; Sulzer, Matthias (2015): Non-linear thermal networks - How can a meshed network improve energy efficiency? In *Proceedings of international conference CISBAT 2015 Future buildings and districts sustainability from nano to urban scale*, pp. 779–784, checked on 4/16/2018.

Schmidt, Dietrich; Kallert, Anna; Blesl, Markus; Svendsen, Svend; Li, Hongwei; Nord, Natasa; Sipilä, Kari (2017): Low Temperature District Heating for Future Energy Systems. In *Energy Procedia* 116, pp. 26–38. DOI: 10.1016/j.egypro.2017.05.052.

Schmidt, Dietrich; Schurig, Marlen (2013): Wärmeversorgungskonzept für die Siedlung "Zum Feldlager". Kassel. Available online at https://www.ibp.fraunhofer.de/content/dam/ibp/de/documents/Kompetenzen/Energiesysteme/Projekte/Niedrigexergiesysteme/20131104_Feldlager.pdf, checked on 3/27/2018.

Schmirler, Rudolf (2018): Kurzschlussregelungen Fernwärmenetze im Münchener Stadtgebiet. Call to Karl Martin Heissler. München, 6/29/2018.

Schweiger, Jakob (2018): Wirtschaftlichkeit von Niedrigtemperaturnetzen. Unter Betrachtung verschiedener Netztypologien. Master Thesis. TUM, München. Chair of Building Technology and Climate Responsive Design, checked on 12/14/2018.

Sibbitt, Bruce; McClenahan, Doug; Djebbar, Reda; Thornton, Jeff; Wong, Bill; Carriere, Jarrett; Kokko, John (2012): The Performance of a High Solar Fraction Seasonal Storage District Heating System – Five Years of Operation. In *Energy Procedia* 30, pp. 856–865. DOI: 10.1016/j.egypro.2012.11.097.

VDI 6002, März 2014: Solare Trinkwassererwärmung - Allgemeine Grundlagen - Systemtechnik und Anwendung im Wohnungsbau, checked on 6/7/2018.

Spescha, Sandro (2014): Technische Bestimmungen (TB) für den Anschluss an ein Anergienetz. Edited by IBC Energie Wasser Chur. Chur. Available online at https://ibc-chur.ch/wp-content/uploads/2016/04/1461306229-020e5b03283499960a766d1acbe739cd.pdf, checked on 3/23/2018.

Stadtwerke München (Ed.) (2015): Fernwärme und Rücklauftemperatur in modernen Niedertemperaturnetzen. Available online at https://www.swm.de/dam/jcr:7821c04d-9a95-44bf-9edb-2792c8c89f28/broschuere-fernwaerme-ruecklauftemperatur.pdf, checked on 3/27/2018.

Statistisches Bundesamt (2019): Daten zur Energiepreisentwicklung. Lange Reihen von Januar 2005 bis Oktober 2019. Edited by Statistische Bundesamt. Destatis, updated on 11/27/2019, checked on 12/13/2019.

Stefan Bach; Niklas Isaak; Claudia Kemfert; Uwe Kunert; Wolf-Peter Schill; Nicole Wägner; Aleksandar Zaklan (2019): Für eine sozialverträgliche CO_2-Bepreisung. Forschungsvorhaben „CO2-Bepreisung im Wärme- und Verkehrssektor: Diskussion von Wirkungen und alternativen Entlastungsoptionen“ im Auftrag des Bundesministeriums für Umwelt, Naturschutz und nukleare Sicherheit (BMU). Politikberatung kompakt 138. Edited by Deutsches Institut für Wirtschaftsforschung. DIW. Berlin. Available online at https://www.diw.de/documents/publikationen/73/diw_01.c.635193.de/diwkompakt_2019-138.pdf, checked on 12/19/2019.

Sulzer, Matthias (2011): Effizienzsteigerung mit Anergienetze. Potentiale - Konzepte - Beispiele. Edited by Inretis Energie- und Gebäudetechnik. Available online at http://www.lauber-iwisa.ch/data/Ressources/1329729930-Effizienzsteigerung_mit_Anergienetze_Nov._2011.pdf, checked on 3/23/2018.

Sulzer, Matthias; Hangartner, Diego (2014): Kalte Fernwärme (Anergienetze). Grundlagen-/Thesenpapier. Horw. Available online at https://www.researchgate.net/profile/Matthias_Sulzer/publication/262418798_Grundlagen-Thesen_Kalte_Fernwarme_Anergienetze/links/0c960537b26bf21731000000/Grundlagen-Thesen-Kalte-Fernwaerme-Anergienetze.pdf, checked on 12/13/2017.

Swisspower AG (Ed.) (2014): Report 2014. Masterplan 2050 der Swisspower Stadtwerke. Available online at https://swisspower.ch/content/files/publications/ Masterplan-PDF/Masterplan-Report-2014.pdf, checked on 3/23/2018.

DIN 1988-200, Mai 2012: Technische Regeln für Trinkwasser-Installationen – Teil 200: Installation Typ A (geschlossenes System) – Planung, Bauteile, Apparate, Werkstoffe; Technische Regel des DVGW.

Technisches Handbuch Fernwärme. Technik und Normung (2009). 2nd ed. Frankfurt am Main: AGFW-Projektg. für Rationalisierung, Information und Standardisierung.

TESS, L. L.C. (Ed.) (2018): TRNSYS: Transient System Simulation Tool. Trnsys Version: 17.02.0004. Thermal Energy System Specialists, LLC. Available online at http://www.trnsys.com/, checked on 5/24/2018.

VDI 4640, Juni 2010: Thermische Nutzung des Untergunds, checked on 2/7/2018.

Thorsen, Jan Eric; Lund, Henrik; Mathiesen, Brian Vad (2018): Progression of District Heating – 1st to 4th generation. Aalborg Universitet. Aalborg. Available online at https://vbn.aau.dk/ws/portalfiles/portal/280710833/1_4GDH_progression_revised_May2018.pdf, checked on 10/4/2019.

Transsolar Energietechnik GmbH (Ed.) (2014): A Transient System Simulation Program. Seminar I - Einführung in die Arbeit mit TRNSYS. Transsolar Energietechnik GmbH. Stuttgart.

Umweltbundesamt (2018): Energieverbrauch privater Haushalte. Dessau-Roßlau. Available online at https://www.umweltbundesamt.de/daten/private-haushalte-konsum/wohnen/energieverbrauch-privater-haushalte#textpart-1, updated on 10/10/2018, checked on 1/29/2020.

United Nations (2015): The Paris Agreement. Edited by United Nations. Paris. Available online at https://treaties.un.org/Pages/ViewDetails.aspx?src=TREATY&mtdsg_no=XXVII-7-d&chapter=27&clang=_en, checked on 1/27/2020.

University of Wisconsin, Madison (Ed.) (2017): TRNSYS - Official Website. TRNSYS Frequently Asked Questions. University of Wisconsin, Madison. Available online at http://sel.me.wisc.edu/trnsys/faq/faq.htm, checked on 5/25/2018.

Vanoli, Klaus; Christoffers, Dirk; Rockendorf, Gunter; Kranz, Reinhard (1997): Solarsiedlung am Ohrberg. In *Forschungsverbund Sonnenenergie Themen 97/98*, pp. 18–24. Available online at http://www.fvee.de/fileadmin/publikationen/ Themenhefte/th1997/th1997.pdf, checked on 3/23/2018.

VDI-Wärmeatlas. Berechnungsblätter für den Wärmeübergang (2002). 9. [überarb.] Aufl. Berlin: Springer (VDI-Buch).

EnEV, revised by Article 1 of the Ordinance of 11/18/2013 (BGBl. I p. 3951) (2007): Verordnung über den energiesparenden Wärmeschutz und energiesparende Anlagentechnik bei Gebäuden (Energieeinsparverordnung). In *BGBl. I* 2007 (34), 1519-1563, checked on 2/18/2020.

WärmeschutzV (1982): Verordnung über einen energiesparenden Wärmeschutz bei Gebäuden (Wärmeschutzverordnung). In *BGBl. I* (7), pp. 209–219, checked on 9/10/2019.

Vetterli, Nadège; Thaler, Eveline; Sulzer, Matthias; Ryser, Pascal (2017): Suurstoffi - Monitoring, Auswertung und Betriebsoptimierung eines thermisch vernetzten Areals. Edited by Hochschule Luzern. Zentrum für Integrale Gebäudetechnik ZIG. Horw. Available online at https://www.novatlantis.ch/wp-content/uploads/2017/01/ZIG_20170117_Suurstoffi_Poster_ryp.pdf, checked on 3/23/2018.

Viessmann Eis-Energiespeicher GmbH (2017): Eis-Energiespeichersysteme für Großanlagen. Innovative Energiequelle für Sole/Wasser-Wärmepumpen. Edited by Viessmann Eis-Energiespeicher GmbH. Ludwigsburg. Available online at https://www.viessmann.de/content/dam/vi-brands/DE/Produkte/Eisspeicher/tt-Eis-Energiespeicher_ab_21%20kW.pdf/_jcr_content/renditions/original.media_file.download_attachment.file/tt-Eis-Energiespeicher_ab_21%20kW.pdf, checked on 5/7/2018.

Vivian, Jacopo; Emmi, Giuseppe; Zarrella, Angelo; Jobard, Xavier; Pietruschka, Dirk; Carli, Michele de (2018): Evaluating the cost of heat for end users in ultra low temperature district heating networks with booster heat pumps. In *Energy. DOI:* 10.1016/j.energy.2018.04.081.

DIN V 4108-6, 2003: Wärmeschutz und Energie-Einsparung in Gebäuden - Teil 6: Berechnung des Jahresheizwärme- und des Jahresheizenergiebedarfs, checked on 6/7/2018.

Weber, Reinhart (2007): Klassische Physik. Experimentelle und theoretische Grundlagen. 1. Aufl. Stuttgart: Teubner (Physik, 1).

Wetter, Michael (2011): Co-simulation of building energy and control systems with the Building Controls Virtual Test Bed. In *Journal of Building Performance Simulation* 4 (3), pp. 185–203. DOI: 10.1080/19401493.2010.518631.

Wetter, Michael; Zuo, Wangda; Nouidui, Thierry S.; Pang, Xiufeng (2014): Modelica Buildings library. In *Journal of Building Performance Simulation* 7 (4), pp. 253–270. DOI: 10.1080/19401493.2013.765506.

VDI 2067, September 2012: Wirtschaftlichkeit gebäudetechnischer Anlagen - Grundlagen und Kostenberechnung, checked on 9/11/2019.

Yang, Xiaochen; Li, Hongwei; Svendsen, Svend (2016): Evaluations of different domestic hot water preparing methods with ultra-low-temperature district heating. In *Energy* 109, pp. 248–259. DOI: 10.1016/j.energy.2016.04.109.

Yang, Xiaochen; Svendsen, Svend (2017): Achieving low return temperature for domestic hot water preparation by ultra-low-temperature district heating. In *Energy Procedia* 116, pp. 426–437. DOI: 10.1016/j.egypro.2017.05.090.

Zarin Pass, R.; Wetter, M.; Piette, M. A. (2018): A thermodynamic analysis of a novel bidirectional district heating and cooling network. In *Energy* 144, pp. 20–30. DOI: 10.1016/j.energy.2017.11.122.

DIN 4708-2, April 1994: Zentrale Wassererwärmungsanlagen - Regeln zur Ermittlung des Wärmebedarfs zur Erwärmung von Trinkwasser in Wohngebäuden, checked on 6/7/2018.

Zvingilaite, E.; Ommen, Torben; Elmegaard, Brian; Franck, M. L. (2012): Low temperature district heating consumer unit with micro heat pump for domestic hot water preparation. In : 13th International Symposium on District Heating and Cooling. 3rd of September-4th of September, Copenhagen, Denmark: District Energy Development Center, checked on 5/28/2018.

List of Figures

List of Tables

A. Appendix of Figures

Figure A-1: Line Network Topology, total pipe length: 915.1 m, not to scale, based on Heissler et al. (2017b)

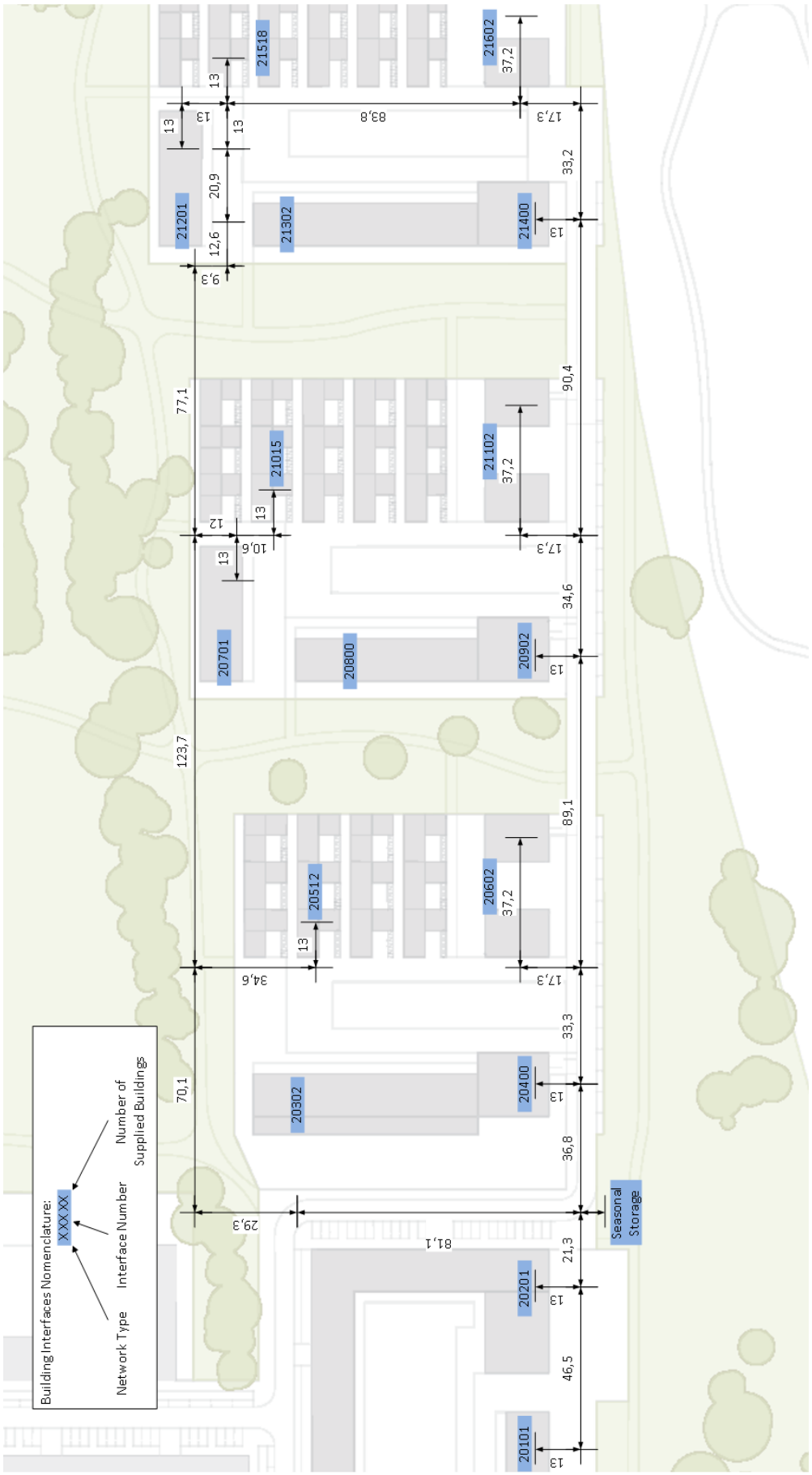

Figure A-2: Ring Network Topology, total pipe length: 1269.8 m, not to scale, based on Heissler et al. (2017b)

Figure A-3: Mesh Network Topology, total pipe length: 1398.8 m, not to scale, based on Heissler et al. (2017b)

Figure A-4: Line Network Topology with waste heat input, total pipe length: 915.1 m, not to scale, based on Heissler et al. (2017b)

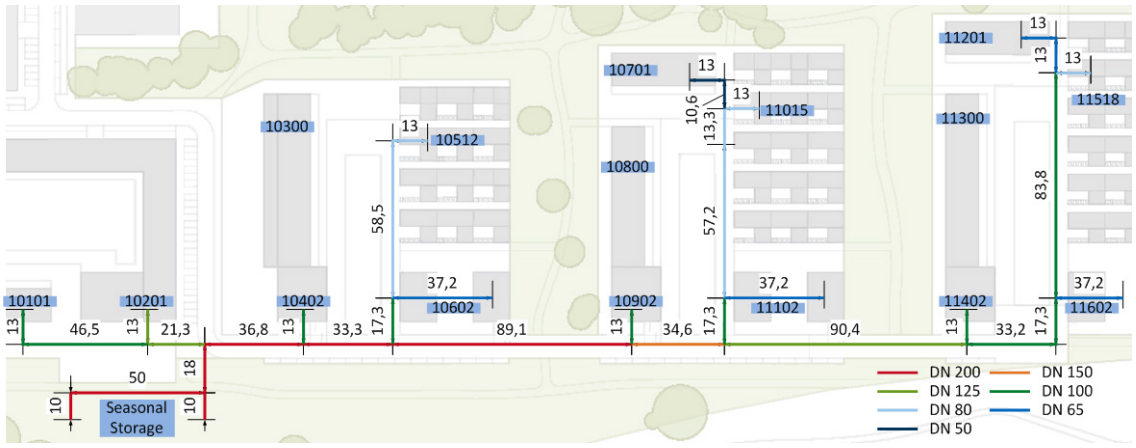

Figure A-5: Line network piping dimensions as basis of the profitability calculation (Schweiger 2018)

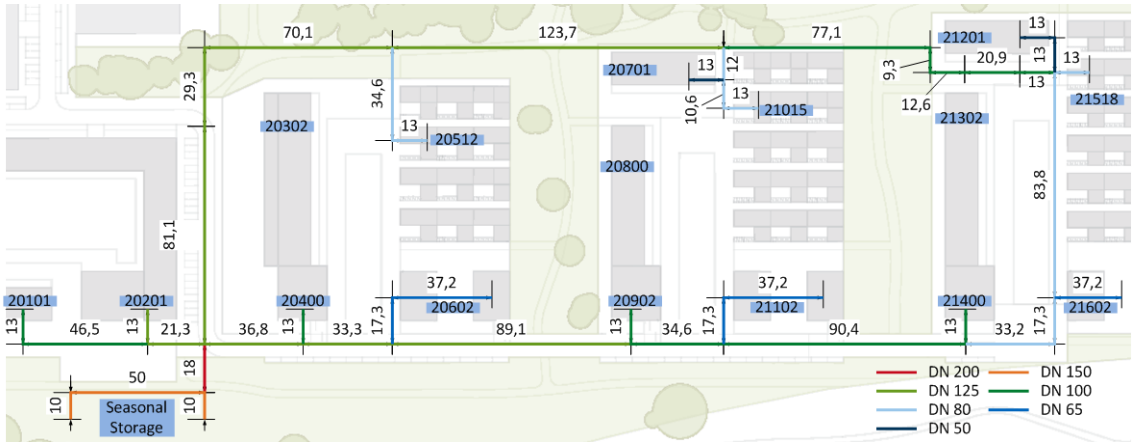

Figure A-6: Ring network piping dimensions as basis of the profitability calculation (Schweiger 2018)

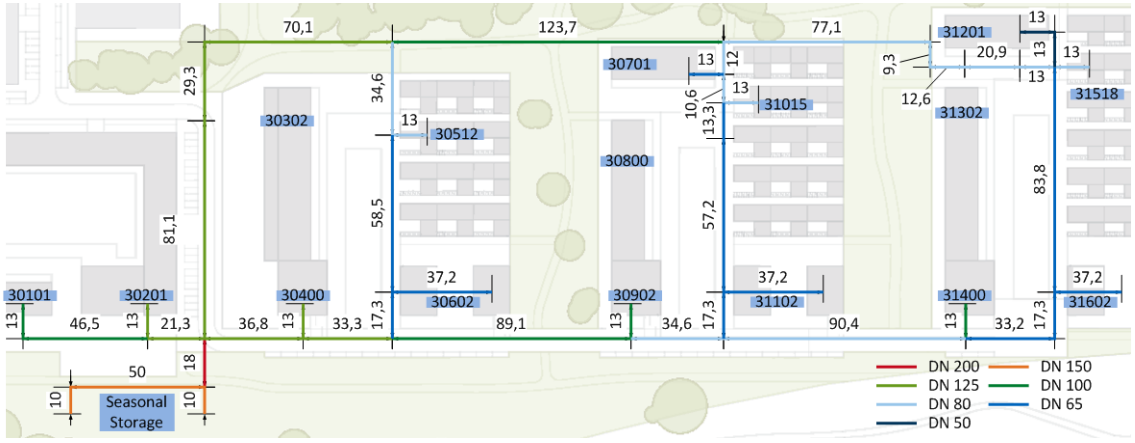

Figure A-7: Mesh network piping dimensions as basis of the profitability calculation (Schweiger 2018)

A. Appendix of Figures

B. Appendix of Tables

Table B-1: TRNSYS Types used in the Solar Loop of the BSM

Component	Type	Comment
PVT-Collector	Type 50a	TRNSYS 17 Library
Weather Data Generator	Type 15-3	TRNSYS 17 Library
Collector Array Shading	Type 30a	TRNSYS 17 Library
Piping	Type 31	TRNSYS 17 Library
Diverter	Type 11f	TRNSYS 17 Library
Mixer	Type 11d	TRNSYS 17 Library
Controller	Type 2b	TRNSYS 17 Library
Controller	Type 22	TRNSYS 17 Library
Heat Exchanger	Type 91	TRNSYS 17 Library
Pump	Type 3d	TRNSYS 17 Library
Multiport Storage Model	Type 340	Stratified fluid storage tank (Drück 2006)
Storage Tank	Type 4c	TRNSYS 17 Library

B. Appendix of Tables

Table B-2: PVT-Collector parameters (TESS 2018)

Name	Value	Unit
Collector Fin Efficiency Factor	0.96	-
Fluid Thermal Capacitance	4.19	kJ/kg.K
Collector Plate Absorptance	0.92	-
Collector Loss Coefficient	16	kJ/hr.m².K
Cover Transmittance	0.89	-
Temperature Coefficient of Solar Cell Efficiency	0.0032	-
Reference Temperature for Cell Efficiency	25	°C
Packing factor	0.8	-

Table B-3: TRNSYS Types used in the Heating Loop of the BSM

Component	Type	Comment
Heating and Cooling Loads Imposed on a Flow Stream	Type 682a	TESS
Auxiliary Heater	Type 6	TRNSYS 17 Library
Data Reader For Generic Data Files	Type 9e	TRNSYS 17 Library
Piping	Type 31	TRNSYS 17 Library
Heat Exchanger	Type 91	TRNSYS 17 Library
Multiport Storage Model	Type 340	Stratified fluid storage tank (Drück 2006)

Table B-4: TRNSYS Types used in the Secondary Loop

Component	Type	Comment
2-Stage Water-to-Water Heat Pump	Type 1221	TESS
Pump	Type 3d	TRNSYS 17 Library
Controller	Type 2b	TRNSYS 17 Library
Controller	Type 22	TRNSYS 17 Library
Piping	Type 31	TRNSYS 17 Library
Multiport Storage Model	Type 340	Stratified fluid storage tank (Drück 2006)

Table B-5: TRNSYS Types used in the Primary Loop

Component	Type	Comment
2-Stage Water-to-Water Heat Pump	Type 1221	TESS
Piping	Type 31	TRNSYS 17 Library
Diverter	Type 11f	TRNSYS 17 Library
Mixer	Type 11d	TRNSYS 17 Library
Mixer	Type 11h	TRNSYS 17 Library
Five-stage Room Thermostat	Type 108	TRNSYS 17 Library
Controller	Type 2b	TRNSYS 17 Library
Controller	Type 22	TRNSYS 17 Library
Heat Exchanger	Type 91	TRNSYS 17 Library
Pump	Type 3d	TRNSYS 17 Library
Input Value Recall	Type 93	TRNSYS 17 Library
Storage Tank	Type 4c	TRNSYS 17 Library
BCVTB Communication	Type 6666	TESS

Table B-6: TRNSYS Types used in the DHN BSM

Component	Type	Comment
Heating and Cooling Loads Imposed on a Flow Stream	Type 682a	TESS
Auxiliary Heater	Type 6	TRNSYS 17 Library
Data Reader For Generic Data Files	Type 9e	TRNSYS 17 Library
Piping	Type 31	TRNSYS 17 Library
Heat Exchanger	Type 91	TRNSYS 17 Library
Multiport Storage Model	Type 340	Stratified fluid storage tank (Drück 2006)
Controller	Type 22	TRNSYS 17 Library
Thermostat	Type 108	TRNSYS 17 Library
Pump	Type 3d	TRNSYS 17 Library
BCVTB Communication	Type 6666	TESS

Table B-7: Overview of construction phases, building types, floors per building and living area per building (Heissler et al. 2017b)

Construction Phase	Building Type	Amount of Buildings	Amount of Floors per Building	Living Area per Building (total) [m²]
1	A	1	5	5800
	B	1	5	10600
2	D	1	5	3800
	E	1	7	2500
	F	15	2	220 (3300)
	G	2	4	970 (1940)
3	C	1	3	1370
	D	1	5	3800
	E	1	7	2500
	F	15	2	220 (3300)
	G	2	4	970 (1940)
4	C	1	3	1370
	D	1	5	3800
	E	1	7	2500
	F	15	2	220 (3300)
	G	2	4	970 (1940)

Table B-8: Usable floor area, roof area, collector area, buffer storage volume, and stand-by storage volume per building interface based on Heissler et al. (2017b)

Building interface	Usable floor area[m²]	Roof area [m²]	Collector area [m²]	Buffer storage volume [m³]	Stand-by storage volume [m³]
1	5850	1170	497	47	22
2	10410	2082	885	84	38
4	6300	1116	536	51	23
5	3330	1665	283	27	12
6	1944	486	169	16	7
7	1368	456	116	11	5
9	6300	1116	536	51	23
10	3330	1665	283	27	12
11	1944	486	169	16	7
12	1368	456	116	11	5
14	6300	1116	536	51	23
15	3330	1665	283	27	12
16	1944	486	169	16	7
Sum	53718	13965	4578	435	196

Table B-9: Minimal sum of the suared residuals of the average ground temperature Tm (Potsdam-Institut für Klimafolgenforschung 2018) and the function T(t)

Month	Hour t	T_m	T(t)	$(T_m - T(t))^2$
January	744	5.33	5.03	0.09
February	1416	4.29	4.01	0.08
March	2160	4.45	4.62	0.03
April	2880	6.55	6.77	0.05
May	3624	10.03	10.00	0.00
June	4344	13.55	13.25	0.09
July	5088	15.93	15.83	0.01
August	5832	17.07	16.89	0.03
September	6552	16.19	16.19	0.00
October	7296	13.61	13.88	0.07
November	8016	10.26	10.72	0.21
December	8760	7.29	7.38	0.01
			Sum	0.67

Table B-10: Parameters of the sinusoid function of the ground temperature

Parameter	Value
A	6.45711
B	-0.04132
C	-26.26886
D	10.44180

Table B-11: Detailed profitability calculation of the 5GDHCN in line layout (Schweiger 2018)

5GDHCN Line Layout	Observation Period [a]	20
Capital-related Cost		
	Lifespan [a]	Annuity [€/a]
PVT-Modules	10	254.140
Heat Pumps	20	54.272
Borefield Heat Exchanger	50	33.855
Network Piping	40	29.461
Stratified Storage Tanks	40	48.599
Valves	10	14.797
Pumps	10	26.068
Heat Exchangers	20	7.690
Heating Piping	40	2.681
Electric Heaters	15	10.396
Heat Meters	10	945
Other	10	35.811
Total		518.714
Demand-related Cost		
	Energy Demand [MWh/a]	Annuity [€/a]
Electricity Demand HP	372	86.857
Auxiliary Power - Network	13.8	3.210
Auxiliary Power - Buildings	40.9	9.542
Total	427	99.609
Operation-related Cost		
		Annuity [€/a]
PVT-Modules		34.377
Heat Pumps		23.362
Borefield Heat Exchanger		23.888
Network Piping		6.519
Stratified Storage Tanks		13.443
Valves		15.924
Pumps		7.014
Heat Exchangers		2.627
Heating Piping		593
Electric Heaters		2.557
Heat Meters		2.542
Other		38.540
Total		171.385
Other Cost		
		Annuity [€/a]
Planning Costs		19.745
Insurance, General Charges, Pro Rata Administrative Cost etc.		18.384
Total		38.129
Proceeds		
	Energy Production [MWh/a}	
Electricity Sales	252	27.462
Own Consumption (Electricity)	71	22.053
Total	323	49.515
Summary		
Total Annuity [€/a]		778.324
Heat Delivered [MWh/a]		2.165
Net Cost of Heat Production [€/MWh]		359
Value Added Tax 19%		68
Gross Cost of Heat Production [€/MWh]		427

Table B-12: Detailed profitability calculation of the 5GDHCN in ring layout (Schweiger 2018)

5GDHCN Ring Layout	Observation Period [a]	20
Capital-related Cost		
	Lifespan [a]	Annuity [€/a]
PVT-Modules	10	254.184
Heat Pumps	20	54.382
Borefield Heat Exchanger	50	33.855
Network Piping	40	29.545
Stratified Storage Tanks	40	48.599
Valves	10	15.099
Pumps	10	26.453
Heat Exchangers	20	7.835
Heating Piping	40	3.014
Electric Heaters	15	10.420
Heat Meters	10	934
Other	10	35.924
Total		520.246
Demand-related Cost		
	Energy Demand [MWh/a]	Annuity [€/a]
Electricity Demand HP	373	87.080
Auxiliary Power - Network	10.3	2.409
Auxiliary Power - Buildings	47.3	11.040
Total	427	100.529
Operation-related Cost		
		Annuity [€/a]
PVT-Modules		34.383
Heat Pumps		23.409
Borefield Heat Exchanger		23.888
Network Piping		6.538
Stratified Storage Tanks		13.443
Valves		16.250
Pumps		7.117
Heat Exchangers		2.676
Heating Piping		667
Electric Heaters		2.563
Heat Meters		2.514
Other		40.824
Total		172.111
Other Cost		
		Annuity [€/a]
Planning Costs		19.807
Insurance, General Charges, Pro Rata Administrative Cost etc.		18.443
Total		38.250
Proceeds		
	Energy Production [MWh/a}	
Electricity Sales	253	27.538
Own Consumption (Electricity)	71	22.114
Total	324	49.652
Summary		
Total Annuity [€/a]		781.483
Heat Delivered [MWh/a]		2.165
Net Cost of Heat Production [€/MWh]		361
Value Added Tax 19%		69
Gross Cost of Heat Production [€/MWh]		430

Table B-13: Detailed profitability calculation of the 5GDHCN in mesh layout (Schweiger 2018)

5GDHCN Mesh Layout	Observation Period [a]	20
Capital-related Cost		
	Lifespan [a]	Annuity [€/a]
PVT-Modules	10	254.177
Heat Pumps	20	54.558
Borefield Heat Exchanger	50	33.855
Network Piping	40	43.166
Stratified Storage Tanks	40	48.599
Valves	10	15.128
Pumps	10	25.795
Heat Exchangers	20	7.813
Heating Piping	40	3.019
Electric Heaters	15	10.431
Heat Meters	10	937
Other	10	37.589
Total		535.067
Demand-related Cost		
	Energy Demand [MWh/a]	Annuity [€/a]
Electricity Demand HP	410	95.572
Auxiliary Power - Network	10.0	2.332
Auxiliary Power - Buildings	45.5	10.610
Total	474	108.514
Operation-related Cost		
		Annuity [€/a]
PVT-Modules		34.382
Heat Pumps		23.484
Borefield Heat Exchanger		23.888
Network Piping		9.552
Stratified Storage Tanks		13.443
Valves		16.281
Pumps		6.940
Heat Exchangers		2.669
Heating Piping		668
Electric Heaters		2.566
Heat Meters		2.521
Other		40.454
Total		176.848
Other Cost		
		Annuity [€/a]
Planning Costs		20.725
Insurance, General Charges, Pro Rata Administrative Cost etc.		19.297
Total		40.022
Proceeds		
	Energy Production [MWh/a}	
Electricity Sales	252	27.462
Own Consumption (Electricity)	71	22.053
Total	323	49.515
Summary		
Total Annuity [€/a]		810.836
Heat Delivered [MWh/a]		2.165
Net Cost of Heat Production [€/MWh]		374
Value Added Tax 19%		71
Gross Cost of Heat Production [€/MWh]		445

Table B-14: Detailed profitability calculation of the waste heat 5GDHCN (Schweiger 2018)

5GDHCN Waste Heat	Observation Period [a]	20
Capital-related Cost		
	Lifespan [a]	Annuity [€/a]
Heat Pumps	20	54.272
Borefield Heat Exchanger	50	33.855
Network Piping	40	29.461
Stratified Storage Tanks	40	16.850
Valves	10	7.977
Pumps	10	14.992
Heat Exchangers	20	2.323
Heating Piping	40	1.154
Electric Heaters	15	10.396
Heat Meters	10	859
Other	10	17.588
Total		189.727
Demand-related Cost		
	Energy Demand [MWh/a]	Annuity [€/a]
Electricity Demand HP	372	86.857
Auxiliary Power - Network	13.8	3.210
Auxiliary Power - Buildings	40.9	9.542
Total	427	99.609
Operation-related Cost		
		Annuity [€/a]
Heat Pumps		23.362
Borefield Heat Exchanger		23.888
Network Piping		6.519
Stratified Storage Tanks		4.661
Valves		8.585
Pumps		4.034
Heat Exchangers		793
Heating Piping		255
Electric Heaters		2.557
Heat Meters		2.312
Other		18.929
Total		95.895
Other Cost		
		Annuity [€/a]
Planning Costs		9.698
Insurance, General Charges, Pro Rata Administrative Cost etc.		9.029
Total		18.727
Proceeds		
	Energy Sales [€/MWh}	
Cooling Capacity Sales	25	46.625
Total	25	46.625
Summary		
Total Annuity [€/a]		357.333
Heat Delivered [MWh/a]		2.165
Net Cost of Heat Production [€/MWh]		165
Value Added Tax 19%		31
Gross Cost of Heat Production [€/MWh]		196

Table B-15: Overview of the simulation parameters and simulation results of the major simulation runs

	Line		Ring		Mesh		NSF 0.5		NSF 2.5		WH 20	WH 50	WH 90	IF 0.25	IF 2	DHN
Simulation Parameter	**96**	**97**	**104**	**105**	**106**	**107**	**92**	**99**	**95**	**101**	**152**	**149**	**145**	**154**	**144**	**9**
Chapter	4.4.1	4.4.2	4.4.2	4.4.2	4.4.2	4.4.2	4.4.3	4.4.3	4.4.3	4.4.3	4.4.4	4.4.4	4.4.4	4.4.5	4.4.5	4.4.6
Pipe Diameter [m]	0.13	0.26	0.13	0.26	0.13	0.26	0.13	0.26	0.13	0.26	0.13	0.13	0.13	0.13	0.13	0.13
Total Pipe Length [m]	915	915	1270	1270	1399	1399	457.5	457.5	2287.5	2287.5	915	915	915	915	915	915
Total Collector Area [m²]	4564	4564	4564	4564	4564	4564	4564	4564	4564	4564	0.8*4564	0.5*4564	0.1*4564	4564	4564	-
Thickness of Pipe Insulation [cm]	6	6	6	6	6	6	6	6	6	6	6	6	6	1.2	12	6
Amount of Waste Heat Input [MWh]	-	-	-	-	-	-	-	-	-	-	373	932	1678	-	-	-
Simulation Results																
Total Energy Turnover [MWh]	2284	2294	2295	2315	2295	2314	2257	2268	2358	2368	2238	2358	2400	2375	2267	2460
Useful Energy [MWh]	2165	2165	2165	2165	2165	2166	2165	2165	2165	2166	2164	2161	2167	2165	2165	2198
Total Losses [MWh]	119	129	129	150	130	149	92	103	192	202	74	198	234	210	102	262
Thermal Grid Losses [MWh]	45	75	63	105	70	114	23	38	111	177	49	55	58	112	30	262
Renewable Energy [MWh]	2040	2070	2051	2090	2057	2090	2023	2044	2067	2142	1999	2112	2100	2096	2023	273
Non-Renewable Energy [MWh]	245	224	244	225	238	224	234	223	291	226	238	246	300	279	244	2187
Tons of CO_2-equivalent per year [t/a]	202	185	200	185	196	185	192	184	237	186	196	205	255	230	200	643
Grams of CO_2-equivalent per kWh Total Energy [g/kWh]	88	81	87	80	85	80	85	81	101	79	88	87	106	97	88	262
Annual COP (System incl. Solar) [-]	5.1	5.7	5.2	5.7	5.3	5.7	5.4	5.7	4.4	5.6	5.4	5.2	4.4	4.6	5.2	-
Total Solar-thermal Gains [MWh]	1864	1912	1877	1933	1886	1933	1857	1887	1864	1983	1457	1014	239	1900	1848	-
Direct Solar-thermal Gains [MWh]	598	596	595	596	596	596	597	598	596	595	575	495	158	595	599	-
Indirect Solar-thermal Gains [MWh]	1266	1316	1282	1337	1290	1337	1259	1290	1268	1388	882	519	81	1305	1249	-
Heat input into Network [MWh]	879	896	883	916	892	916	857	869	917	973	926	1213	1688	915	862	2460
Heat output from Network [MWh]	759	767	754	766	762	767	765	767	727	771	852	1013	1445	705	761	2198
Electric Energy Demand [MWh]	421	382	417	382	409	382	400	381	491	385	403	413	492	474	418	-
Pump Energy Demand [MWh]	38.8	1.3	27.4	0.9	26.9	0.9	20.2	0.7	86.8	3	19.3	13.6	16.3	40	38.6	-
Photovoltaic Solar Gains [MWh]	351	353	27	354	352	354	351	352	351	356	280	179	38	353	350	-
Electric input from Public Distribution Network [MWh]	378	346	374	345	367	345	359	344	444	348	367	383	476	430	375	-
Electric output to Public Distribution Network [MWh]	308	317	309	318	310	318	310	316	304	319	244	149	22	308	307	-

C. Acknowledgments

Many different people have contributed significantly to the successful completion of this work. My first and foremost thanks are directed to Prof. Dipl.-Ing. Thomas Auer for his supervision, support, his critical questions, and the opportunity to pursue a research topic which is slightly off the beaten path of research mainly taken at the Chair of Building Technology and Climate-Responsive Design. I would also like to thank Prof. Dr.-Ing. Werner Lang of the Chair of Energy Efficient and Sustainable Design and Building for his friendly guidance, support, and encouragement.

My profound thanks go

- to Prof. Dr.-Ing. Frank Petzold for chairing the examination committee,
- to Prof. Dr.-Ing. Isabell Nemeth for putting me on track and sending me off in the right direction,
- to Dr.-Ing. Klaus Klimke for taking on the task of mentoring me,
- to Jochen Lam for his invaluable support in trying times of simulation errors and cryptic error codes,
- to Jakob Metz for his analytic and structured modelling contributions and his selfless help when it was needed,
- to Jakob Schweiger for his contribution to the economic assessment,
- and to Ryan S. Stickney for proofreading this thesis and helping me express myself.

I am very grateful to all my colleagues at the Chair of Building Technology and Climate-Responsive Design and the Chair of Energy Efficient and Sustainable Design and Building for a very pleasant, friendly and appreciative working environment, for many fruitful discussions and constructive pinballing of ideas and concepts. I was lucky to belong to the families of both chairs.

Many parts of this work would not exist if not for my friends who put up with me, who share their lives with me, and keep me company. Thank you for your encouragement and for countless hours of mutual listening and understanding.

Last but not least my biggest thanks go to my family. Thank you for all the opportunities you have provided me with in my life. Without your unlimited support this work would not have been possible. Thank you for your patience and your encouragement, your positivity, your help, and for always being there when needed.